Journal of Applied Mechanics

(*Contributions of the ASME Applied Mechanics Division*)

Performance of the Viscously Damped Vibration Absorber Applied to Systems Having Frequency-Squared Excitation . . . . . *F. M. Sauer and C. F. Garland* 109

Thermal Stresses in a Rectangular Plate Clamped Along an Edge . . . *B. J. Aleck* 118

Polygonal Approximation Method in the Hodograph Plane . . . . *H. Poritsky* 123

The Shape of a Piston Ring in Its Unrestrained State . . . . . *Che-Tyan Chang* 134

Numerical Solution of Elastoplastic Torsion of a Shaft of Rotational Symmetry . . . . . *R. P. Eddy and F. S. Shaw* 139

Stress Concentration Around a Triaxial Ellipsoidal Cavity . . . . . *M. A. Sadowsky and E. Sternberg* 149

Stability of Linear Oscillating Systems With Constant Time Lag . . . *H. I. Ansoff* 158

Dynamic Capacity of Rolling Bearings . . . *Gustaf Lundberg and Arvid Palmgren* 165

Slow-Motion Pictures of Impact Tests by Means of Photoelasticity . *Ludwig Foeppl* 173

Fracture of Gray-Cast-Iron Tubes Under Biaxial Stresses . . *R. C. Grassi and I. Cornet* 178

A Strain-Energy Expression for Thin Elastic Shells . . . . . *H. L. Langhaar* 183

The Use of the Centrifugal Pendulum Absorber for the Reduction of Linear Vibration . . . . . *F. E. Reed* 190

Supersonic Diffusers for Wind Tunnels . . . . . *E. P. Neumann and F. Lustwerk* 195

Vibration of Slender Bars With Discontinuities in Stiffness . . . . *W. T. Thomson* 203

Correlation of Tension Creep Tests With Relaxation Tests . . . . *Irving Roberts* 208

Note on the Bending of Circular Plates of Variable Thickness . . . *H. D. Conway* 209

Stresses and Displacements in a Semi-Infinite Elastic Body With Parabolic Cross Section Acted on by Its Own Weight Only . . . . . *R. J. Hank and F. H. Scrivner* 211

Discussion on Previously Published Papers by *G. A. Nothmann; W. R. Leopold; W. Prager; M. P. White and LeVan Griffis; R. B. Green; J. R. Weske; J. E. Brock* 213

Book Reviews 223

JUNE, 1949

VOL. 16, NO. 2

Transactions of The American Society of Mechanical Engineers

Performance of the Viscously Damped Vibration Absorber Applied to Systems Having Frequency-Squared Excitation

By F. M. SAUER[2] and C. F. GARLAND,[3] BERKELEY, CALIF.

The effectiveness of the viscously damped vibration absorber is presented for the case in which the magnitude of the periodic exciting force acting upon the main system is proportional to the square of its frequency. Dimensionless expressions for the amplitudes of the main mass and absorber mass and for their phase relationships are derived as functions of frequency for three cases, namely, one in which the absorber is tuned to the natural frequency of the main system, one in which the absorber is tuned for maximum effectiveness over a wide range of forcing frequencies, and one in which the absorber is coupled to the main system by a viscous fluid only (the viscous Lanchester damper). The influence of main-system damping upon the amplitude of vibration of the main mass is shown for each case. Diagrams are presented showing the optimum damping, the maximum amplitude of the main mass, and the maximum relative amplitude between the main mass and absorber mass, as functions of the mass ratio. The performance of the absorber when applied to the system having velocity-squared excitation is compared with its performance when applied to the system having constant exciting force, published previously (1, 2).[4] The tuning and damping for optimum performance are found to be different in the two cases. A model absorber with controllable tuning and damping, constructed for experimental work, is described and experimental data are presented for the case of most favorable tuning.

Nomenclature

The following nomenclature is used in the paper:

ω = exciting frequency, radians per sec
M = main mass, lb-sec²/ft
K = spring constant of main system, lb/ft
$\Omega_n = \sqrt{\frac{K}{M}}$ = natural frequency of main system, radians per sec
C = main system damping constant, lb-sec/ft
$\Gamma = \frac{C}{M\Omega_n}$ = main system damping coefficient, dimensionless
m = absorber mass, lb-sec²/ft
k = absorber spring constant, lb per ft
$\omega_n = \sqrt{\frac{k}{m}}$ = natural frequency of absorber, radians per sec
c = absorber damping constant, lb-sec/ft
$\gamma = \frac{c}{m\Omega_n}$ = absorber damping coefficient, dimensionless
$\mu = \frac{m}{M}$ = mass ratio, dimensionless
$f = \frac{\omega_n}{\Omega_n}$ = natural-frequency ratio or "tuning," dimensionless
$R = \frac{\omega}{\Omega_n}$ = frequency ratio, dimensionless
y_1 = instantaneous displacement of main mass, ft
$\frac{dy_1}{dt}$ = instantaneous velocity of main mass, fps
$\frac{d^2y_1}{dt^2}$ = instantaneous acceleration of main mass, ft/sec²
y_2 = instantaneous displacement of absorber mass, ft
$\frac{dy_2}{dt}$ = instantaneous velocity of absorber mass, fps
$\frac{d^2y_2}{dt^2}$ = instantaneous acceleration of absorber mass, ft/sec²
a_1 = amplitude of vibration of main mass, ft
a_2 = amplitude of vibration of absorber mass, ft
$a_2 - a_1$ = relative amplitude of vibration between main and absorber masses, ft
m_r = mass causing rotational unbalance, lb-sec²/ft
e = eccentricity of the unbalanced mass, ft
ϕ_1 = phase angle by which displacement of main mass lags behind exciting force, deg
ϕ_2 = phase angle by which displacement of absorber mass lags behind exciting force, deg
ϕ_{21} = phase angle by which relative displacement of main and absorber masses lags behind exciting force, deg
$X = \sqrt{\frac{2\mu}{1+\mu}}$

Introduction

The practicability of reducing vibration amplitudes in mechanical systems by means of the dynamical absorber, with and without damping, has been demonstrated previously (1) for cases in which the magnitude of the exciting force is independent of frequency. Many vibration problems encountered in machinery installations, however, are caused by unbalanced rotating

[1] The theoretical work is based upon a thesis prepared by F. M. Sauer under the supervision of C. F. Garland and submitted in June, 1947, to the University of California in partial satisfaction of the requirements for the M.S. degree.

[2] Instructor in Mechanical Engineering, University of California. Jun. ASME.

[3] Associate Professor of Engineering Design, University of California. Mem. ASME.

[4] Numbers in parentheses refer to the Bibliography at the end of the paper.

Contributed by the Applied Mechanics Division for presentation at the Semi-Annual Meeting, San Francisco, Calif., June 27–30, 1949, of The American Society of Mechanical Engineers.

Discussion of this paper should be addressed to the Secretary, ASME, 29 West 39th Street, New York, N. Y., and will be accepted until July 11, 1949, for publication at a later date. Discussion received after the closing date will be returned.

Note: Statements and opinions advanced in papers are to be understood as individual expressions of their authors and not those of the Society. Paper No. 49—SA-5.

or reciprocating parts which generate periodic disturbing forces whose magnitudes vary with the square of their frequencies. The performance of a viscously damped absorber attached to a system excited in this manner is found to differ markedly from its performance in the presence of an exciting force of constant amplitude. Hence the tuning and damping of the absorber must be different in the first case from that in the second if it is to function effectively over the full range of operating frequencies. In the present paper the theory of the damped vibration absorber published previously (1, 2) is extended to the case of frequency-squared excitation, and the results of the theoretical analysis are compared with experimental data obtained in working with a laboratory model.

Response of the Coupled Mass and Absorber System to a Velocity-Squared Exciting Force

For purposes of analysis the idealized spring-mass system, Fig. 1, is assumed to approximate the more complex structure of a machine, its mounting, and an absorber. The large mass M represents the machine whose motion is to be controlled, connected to its foundation by the spring mounting K. The small mass m, represents the absorber coupled to the main mass through a spring-damper system. In this analysis viscous damping and linear springs are assumed. The motion is limited to one axis.

The component of the exciting force in the vertical direction, caused by the rotational unbalance, is $m_r e\omega^2 \sin \omega t$, where m_r is the unbalanced mass with eccentricity e, and ω is the rotational velocity. The $m_r e$ product is a constant of the main system, and any case of rotational unbalance may be reduced to an equivalent term of this nature.

The equations of motion for the two masses are

$$M\frac{d^2y_1}{dt^2} + c\left(\frac{dy_1}{dt} - \frac{dy_2}{dt}\right) + k(y_1 - y_2) + Ky_1 = m_r e\omega^2 \sin \omega t \quad [1]$$

and

$$m\frac{d^2y_2}{dt^2} - c\left(\frac{dy_1}{dt} - \frac{dy_2}{dt}\right) - k(y_1 - y_2) = 0 \quad [2]$$

The solution of these simultaneous equations yields the following nondimensional expressions for the amplitudes and phase relationships for the steady state

$$\frac{a_1}{\frac{m_r e}{M}} = R^2\sqrt{\frac{(f^2 - R^2)^2 + \gamma^2R^2}{[(1 - R^2)(f^2 - R^2) - \mu f^2R^2]^2 + \gamma^2R^2[1 - (1 + \mu)R^2]^2}} \quad [3]$$

$$\frac{a_2}{\frac{m_r e}{M}} = R^2\sqrt{\frac{f^4 + \gamma^2R^2}{[(1 - R^2)(f^2 - R^2) - \mu f^2R^2]^2 + \gamma^2R^2[1 - (1 + \mu)R^2]^2}} \quad [4]$$

$$\frac{a_2 - a_1}{\frac{m_r e}{M}} = R^2\sqrt{\frac{R^4}{[(1 - R^2)(f^2 - R^2) - \mu f^2R^2]^2 + \gamma^2R^2[1 - (1 + \mu)R^2]^2}} \quad [5]$$

$$\tan \phi_1 = \frac{-\mu\gamma R^5}{(f^2 - R^2)[(1 - R^2)(f^2 - R^2) - \mu f^2R^2] + \gamma^2R^2[1 - (1 + \mu)R^2]} \quad [6]$$

$$\tan \phi_2 = \frac{-\gamma R^3(1 - R^2)}{f^2[(1 - R^2)(f^2 - R^2) - \mu f^2R^2] + \gamma^2R^2[1 - (1 + \mu)R^2]} \quad [7]$$

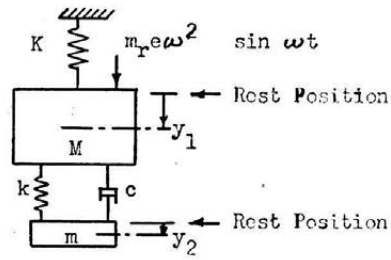

Fig. 1 Idealized System

$$\tan \phi_{21} = \frac{-\gamma R[1 - (1 + \mu)R^2]}{(1 - R^2)(f^2 - R^2) - \mu f^2R^2} \quad [8]$$

$$\tan (\phi_1 - \phi_2) = \frac{\gamma R^3}{f^2(f^2 - R^2) + \gamma^2R^2} \quad [9]$$

From Equation [3] it is seen that the amplitude of motion of the main mass at a given frequency is a function of three properties of the absorber, namely, its mass, its spring constant, and the amount of damping. These three properties can be varied independently. For any selected value of absorber mass, the optimum damper performance is realized only when both the tuning and damping are set at their most favorable (i.e., "optimum") values.

Absorber With Optimum Tuning and Damping

The most desirable absorber would reduce the amplitude of the main mass to zero over the entire range of frequencies. This is impossible, however, and the best absorber obtainable in the practical case minimizes the amplitudes.

For any given mass ratio μ, and tuning f, there are two frequency ratios R_P and R_Q (see Fig. 2), at which the amplitude of the main mass is independent of damping (1, 2). If Equation [3] is written in the form

$$\frac{a_1}{\frac{m_r e}{M}} = \sqrt{\frac{A + \gamma^2B}{C + \gamma^2D}}$$

the amplitude a_1 is seen to be independent of damping when $A/C = B/D$, i.e., when

$$\frac{f^2 - R^2}{(1 - R^2)(f^2 - R^2) - \mu f^2 R^2} = \pm\left[\frac{1}{1 - (1 + \mu)R^2}\right]$$

With the minus sign this yields

$$\mu R^4 = 0 \quad \text{so that} \quad R^4 = 0$$

With the plus sign the equation becomes

$$R^4 - \frac{2(f^2 + \mu f^2 + 1)R^2}{2 + \mu} + \frac{2f^2}{2 + \mu} = 0 \ldots\ldots [10]$$

Equation [10] defines the two values R_P and R_Q as functions of μ and f. If arbitrary values for μ and f be substituted into Equation [10], the frequency ratios R_P and R_Q can be evaluated and, from Equation [3], the amplitudes at these two frequencies can be determined. For a given value of μ the relative amplitudes at R_P and R_Q vary as f is changed, one increasing as the other decreases. Hence there is a particular value of f for which these amplitudes are equal. This value is

$$f_{opt} = \sqrt{\frac{1}{1 + \mu}} \ldots\ldots [11]$$

and is the best or optimum tuning for a given size of absorber mass. For a damper tuned to this value the expression for the amplitude at P and Q, Fig. 2, becomes

$$\frac{a_1}{\frac{m_r e}{M}} = \sqrt{\frac{2}{\mu(1 + \mu)}} \ldots\ldots [12]$$

and the corresponding frequencies are given by the expressions

$$R_P^2 = \frac{2 - \sqrt{\frac{2\mu}{1 + \mu}}}{2 + \mu} \quad \text{and} \quad R_Q^2 = \frac{2 + \sqrt{\frac{2\mu}{1 + \mu}}}{2 + \mu} \ldots [13]$$

The values of amplitude and frequency at points P and Q

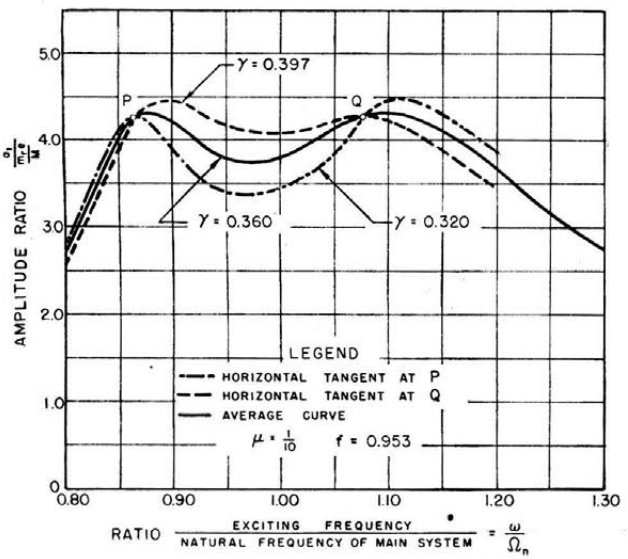

FIG. 2 COMPARISON OF THE OPTIMUM DAMPING COEFFICIENTS FOR OPTIMUM TUNING

having been established for the condition of optimum tuning, the question of optimum damping must next be considered. Referring to Equation [3], it is seen that the shape of the amplitude-frequency curve, Fig. 2, depends upon the value of γ. If γ is large, the amplitude curve has a single peak at a frequency between R_P and R_Q; if γ is quite small, two peaks appear, one at a frequency less than R_P and the other at a frequency greater than R_Q. It can be demonstrated that no one value of damping will produce an amplitude curve with peaks at P and Q simultaneously. A value of damping can be determined, however, which approximates this condition very closely, yielding peaks with nearly equal amplitudes at points near P and Q. This process may be summarized as follows:

Solving Equation [3] for the damping coefficient and substituting

$$f^2 = \frac{1}{1 + \mu} \quad \text{and} \quad \frac{a_1}{\frac{m_r e}{M}} = \sqrt{\frac{2}{\mu(1 + \mu)}}$$

the resulting expression for γ^2 has the form

$$\gamma^2 = \frac{R^4 f^4 - 2f^2 R^6 + R^8 - \frac{2}{\mu(1 + \mu)}[R^8 - 4R^6 + (2f^2 + 4)R^4 - 4f^2 R^2 + f^4]}{\frac{2R^2}{\mu(1 + \mu)} - \frac{4R^4}{\mu} + \frac{2(1 + \mu)R^6}{\mu} - R^6} \ldots\ldots [14]$$

In order for the amplitude curve to pass horizontally through point P it must pass through a neighboring point P' of the same amplitude but of frequency[5]

$$R^2 = \frac{2 - \sqrt{2\mu/1 + \mu} \pm \delta}{2 + \mu} = \frac{2 - X \pm \delta}{2 + \mu} = R_P^2 \pm \frac{\delta}{2 + \mu}$$

Substituting this expression for R^2 into Equation [14], the resulting equation is of the form

$$\gamma^2 = \frac{A_0 + A_1\delta + A_2\delta^2 + \ldots.}{B_0 + B_1\delta + B_2\delta^2 + \ldots.} \ldots\ldots [15]$$

Equation [15] assumes the indeterminate from 0/0 if $\delta = 0$, since point P is independent of damping; hence $A_0 = B_0 = 0$. Therefore

$$\gamma^2 = \operatorname*{Limit}_{\delta \to 0} \frac{A_0 + A_1\delta + A_2\delta^2 + \ldots.}{B_0 + B_1\delta + B_2\delta^2 + \ldots.} = \frac{A_1}{B_1}$$

Since the terms in δ of higher order than the first become zero when δ approaches zero, these terms may be dropped as soon as they appear. Hence

$$R^4 = R_P^4 \pm \frac{2(2 - X)\delta}{(2 + \mu)^2}$$

$$R^6 = R_P^6 \pm \frac{3(2 - X)^2\delta}{(2 + \mu)^3}$$

$$R^8 = R_P^8 \pm \frac{4(2 - X)^3\delta}{(2 + \mu)^4}$$

Evaluating the numerator (N) and denominator (D) of the right-hand member of Equation [14] separately

[5] This method is employed in reference (3).

$$N = R_P{}^4f^4 - 2f^2R_P{}^6 + R_P{}^8 - \frac{2}{\mu(1+\mu)}[R_P{}^8 - 4R_P{}^6 + (2f^2+4)R_P{}^4 - 4f^2R_P{}^2 + f^4] \pm \delta\left\{\frac{2(2-X)}{(1+\mu)^2(2+\mu)^2} - \frac{6(2-X)^2}{(1+\mu)(2+\mu)^3} + \frac{4(2-X)^3}{(2+\mu)^4} - \frac{2}{\mu(1+\mu)}\left[\frac{4(2-X)^3}{(2+\mu)^4} - \frac{12(2-X)^2}{(2+\mu)^3} + \frac{4(3+2\mu)(2-X)}{(1+\mu)(2+\mu)^2} - \frac{4}{(2+\mu)(1+\mu)}\right]\right\}$$

The sum of the first four terms equals zero since both the numerator and denominator are zero when R has the particular value R_P; hence

$$N = \frac{\pm 6\delta[4\mu - X(2+3\mu)]}{(1+\mu)^2(2+\mu)^3}$$

Similarly

$$D = \pm\frac{4\delta[\mu - X(1+\mu)]}{\mu(1+\mu)(2+\mu)^2}$$

Therefore

$$\gamma^2 = \frac{N}{D} = \frac{3\mu(2-X)}{2(1+\mu)(2+\mu)} = \frac{3\mu\left(2-\sqrt{\frac{2\mu}{1+\mu}}\right)}{2(1+\mu)(2+\mu)} \quad \ldots [16]$$

To obtain the curve with zero slope at Q the frequency

$$\sqrt{\frac{2+\sqrt{2\mu/1+\mu} \pm \delta}{2+\mu}}$$

is substituted into Equation [14]. This yields the expression

$$\gamma^2 = \frac{3\mu\left(2+\sqrt{\frac{2\mu}{1+\mu}}\right)}{2(1+\mu)(2+\mu)} \quad \ldots [17]$$

The average of the two values of the damping coefficient defined by Equations [16] and [17] is

$$\gamma^2 = \frac{3\mu}{(1+\mu)(2+\mu)} \quad \ldots [18]$$

The amplitude-frequency curves for these three values of the damping coefficient are plotted in Fig. 2, for $\mu = 1/10$. It is noted that the curve which is horizontal at P attains a larger amplitude to the right of Q, while the curve which is horizontal at Q attains a larger amplitude to the right of P. The average curve is only slightly higher at these points and represents a convenient and practicable solution. Equation [18] then defines the optimum damping for the case of optimum tuning.

In the design of the absorber it is necessary to know the maximum relative amplitude between the main mass and the absorber, since large deflections of the absorber spring may result in excessively large stresses. Differentiation of Equation [5] leads to a complex third-order equation in R^2 which can be solved only numerically for various values of μ. A simple but approximate method is to equate the work done per cycle by the exciting force to the energy dissipated per cycle by damping. This yields[6]

$$\pi P_0 a_1 \sin\phi_1 = \pi c\omega(a_2 - a_1)^2 \quad \ldots [19]$$

where $P_0 = m_r e\omega^2$. Assuming $\sin\phi_1 = 1.0$, and solving for the relative amplitude ratio

$$\left(\frac{a_2 - a_1}{\frac{m_r e}{M}}\right)^2 = \left(\frac{a_1}{\frac{m_r e}{M}}\right) \times \frac{M\omega}{c} = \left(\frac{a_1}{\frac{m_r e}{M}}\right) \times \frac{M}{m} \times \frac{m\Omega_n}{c} \times \frac{\omega}{\Omega_n}$$

or, since

$$\mu = \frac{m}{M}, \quad \gamma = \frac{c}{m\Omega_n}, \quad \text{and} \quad R = \frac{\omega}{\Omega_n}$$

this becomes

$$\left(\frac{a_2 - a_1}{\frac{m_r e}{M}}\right)^2 = \frac{a_1}{\frac{m_r e}{M}} \cdot \frac{R}{\mu\gamma} \quad \ldots [20]$$

The relative amplitudes obtained by the energy method, and those obtained from the solution of Equation [5] are compared in Fig. 3. The two solutions are seen to be in close agreement in

[6] Reference (2), p. 127.

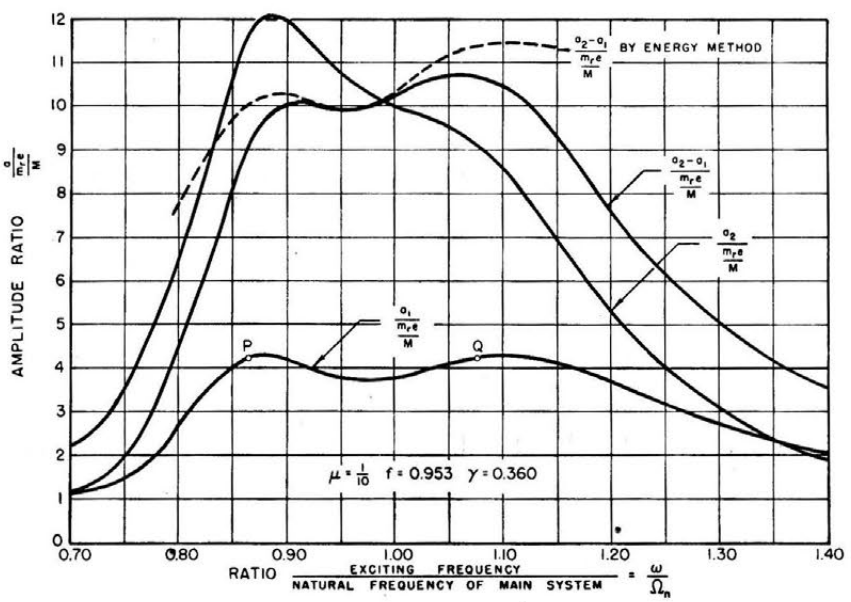

FIG. 3 AMPLITUDE RATIOS FOR OPTIMUM TUNING AND DAMPING

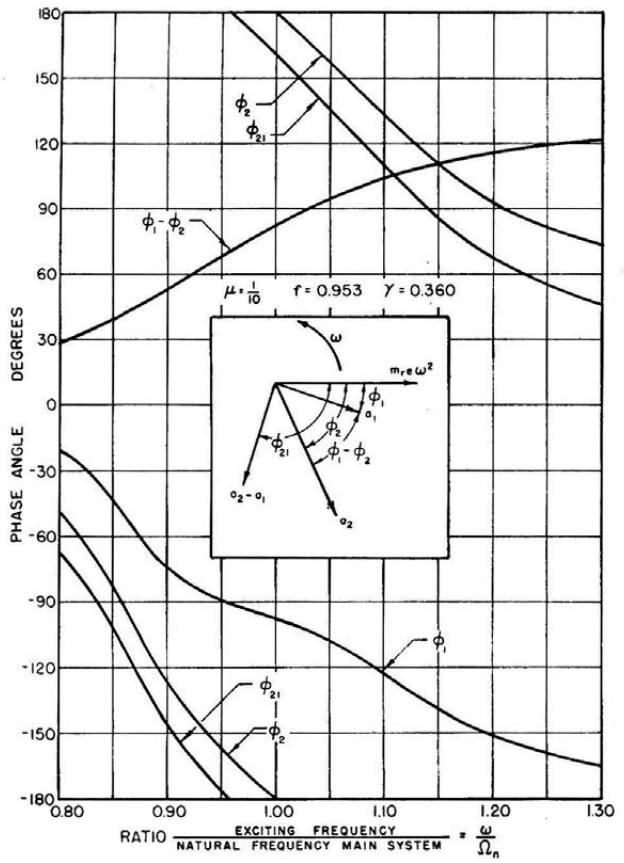

FIG. 4 PHASE RELATIONSHIPS FOR OPTIMUM TUNING AND DAMPING

the region of maximum amplitude, the discrepancy between the two curves at other frequencies being due to the deviation of the value of sin ϕ_1 from unity (see Fig. 4). By substituting the amplitude and frequency of point Q into Equation [20], the following approximate expression for the maximum relative amplitude is obtained

$$\left(\frac{a_2 - a_1}{\frac{m_r e}{M}}\right)^4 = \left(\frac{a_1}{\frac{m_r e}{M}}\right)^2 \cdot \frac{R_Q^2}{\mu^2\gamma^2} = \frac{2\left(2 + \sqrt{\frac{2\mu}{1+\mu}}\right)}{3\mu^4} \quad \ldots [21]$$

The maximum relative amplitude determined by Equation [21] will always be slightly greater than the true value because at frequency R_Q the value of sin ϕ_1 is less than unity.

ABSORBER TUNED TO FREQUENCY OF MAIN SYSTEM

In the earlier work (1) on the dynamical absorber, it was demonstrated that an absorber, tuned to the frequency of the main system (i.e., one in which $f = 1.0$) and damped very lightly, will reduce the amplitude of the main system to a minimum at its resonant frequency. This tuning results in unequal amplitudes at P and Q, however, and hence it is not the best if the damper is to operate effectively over a wide frequency range. It is of interest, nevertheless, to investigate the performance of the absorber, so tuned, when applied to the main system having velocity-squared excitation. For this case, $f = 1$ for all values of μ. Substituting $f = 1$ into Equation [10], the frequency equation becomes

$$R^4 - 2R^2 + \frac{2}{2+\mu} = 0 \quad \ldots [22]$$

which has the roots

$$R_P^2 = 1 - \sqrt{\frac{\mu}{2+\mu}} \quad \text{and} \quad R_Q^2 = 1 + \sqrt{\frac{\mu}{2+\mu}} \quad \ldots [23]$$

The amplitude ratio at P becomes

$$\left(\frac{a_1}{\frac{m_r e}{M}}\right)_P = \sqrt{\frac{2+\mu}{\mu}} + 1 \quad \ldots [24]$$

Similarly, the amplitude ratio at Q becomes

$$\left(\frac{a_1}{\frac{m_r e}{M}}\right)_Q = \sqrt{\frac{2+\mu}{\mu}} - 1 \quad \ldots [25]$$

The amplitude at point P is seen to be always larger than that at Q, as shown in Fig. 5. Hence the amplitude curve with the lowest peak value over the frequency range must have zero slope at P. This curve represents the most favorable damping obtainable for the arbitrary tuning $f = 1$. By substituting

$$R = \sqrt{1 - \sqrt{\frac{\mu}{2+\mu}}} \pm \delta, \quad \left(\frac{a_1}{\frac{m_r e}{M}}\right)_P = \sqrt{\frac{2+\mu}{\mu}} + 1$$

and $f = 1$ into Equation [14], and letting δ approach zero as before, the following expression for the optimum damping is obtained

$$\gamma^2 = \frac{\mu}{2}\left(3 - \sqrt{\frac{\mu}{2+\mu}}\right) \quad \ldots [26]$$

The maximum value of the relative amplitude, found by substituting the expressions for amplitude and frequency at point

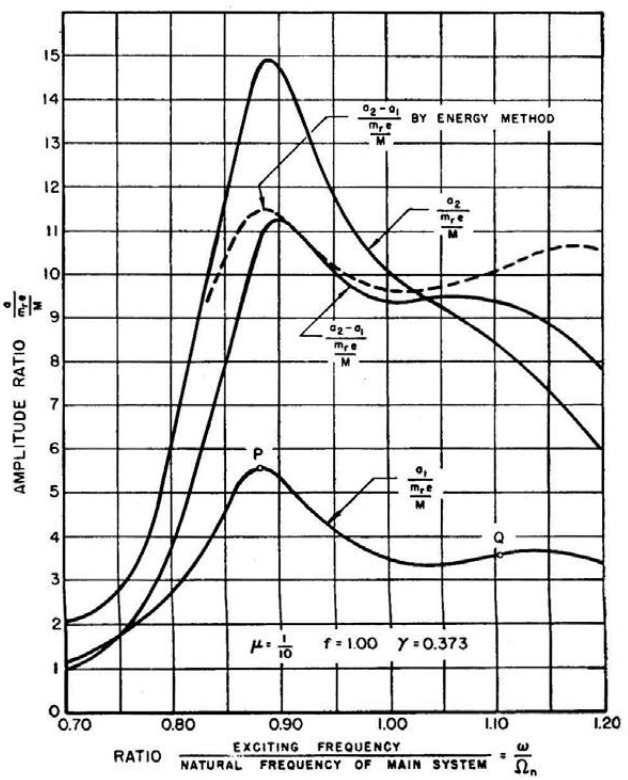

FIG. 5 AMPLITUDE RATIOS FOR ABSORBER TUNED TO FREQUENCY OF MAIN SYSTEM, OPTIMUM DAMPING

P into Equation [20], is

$$\left(\frac{a_2 - a_1}{\frac{m_r e}{M}}\right)^4 = \frac{\left(\sqrt{\frac{2+\mu}{\mu}} + 1\right)^2 \left(1 - \sqrt{\frac{\mu}{2+\mu}}\right)}{\frac{\mu^3}{2}\left(3 - \sqrt{\frac{\mu}{2+\mu}}\right)}$$

Hence

$$\left(\frac{a_2 - a_1}{\frac{m_r e}{M}}\right)^4 = \frac{4\left[(3 + 2\mu) + 2\sqrt{\mu(2+\mu)}\right]}{\mu^4(9 + 4\mu)} \quad \ldots\ldots [27]$$

From the plot of the several amplitude ratios in Fig. 5, the amplitude obtained by the energy method is seen to be considerably higher than the true value near point P. Hence Equation [27] yields a conservative approximation to the value of the maximum relative amplitude.

$$\left(\frac{a_2 - a_1}{\frac{m_r e}{M}}\right)^2 = \frac{2}{\mu} \cdot \frac{\sqrt{\frac{2}{2+\mu}}}{\mu\sqrt{\frac{2}{2+\mu}}} = \frac{2}{\mu^2} \quad \ldots\ldots [31]$$

Equation [31] represents a conservative approximation, as did Equations [21] and [27] in the cases discussed previously. The exact value of the maximum relative amplitude may be found by plotting the amplitude curve for a few values near R_Q using Equation [5].

Comparison of Optimum Tuning and Damping Coefficients for Systems Having Constant Excitation and Frequency-Squared Excitation

The values for optimum tuning and damping for the case of frequency-squared excitation are compared with those for the case of constant excitation in Table 1. The optimum tuning for the first case is nearer to unity; therefore, if the value $f = 1/(1 + \mu)$ were used for this case, the point Q would have a larger amplitude than point P. For optimum tuning, the system having frequency-squared excitation requires more damping than does the one having constant excitation; for tuning $f = 1$, the reverse is true.

TABLE 1 COMPARISON OF OPTIMUM TUNING AND DAMPING WITH CONSTANT EXCITATION

Squared excitation		Constant excitation	
Tuning	Optimum damping	Tuning	Optimum damping[a]
$f^2_{\text{opt}} = \frac{1}{1+\mu}$	$\gamma^2 = \frac{3\mu}{(1+\mu)(2+\mu)}$	$f_{\text{opt}} = \frac{1}{1+\mu}$	$\gamma^2 = \frac{3\mu}{2(1+\mu)^3}$
$f = 1$	$\gamma^2 = \frac{\mu}{2}\left(3 - \sqrt{\frac{\mu}{2+\mu}}\right)$	$f = 1$	$\gamma^2 = \frac{\mu(3+\mu)\left(1 + \sqrt{\frac{\mu}{2+\mu}}\right)}{2(1+\mu)}$
$f = 0$	$\gamma^2 = \frac{2}{2+\mu}$	$f = 0$	$\gamma^2 = \frac{2}{(1+\mu)(2+\mu)}$

[a] These expressions are presented in reference (3).

Lanchester-Type Absorber With Viscous Damping

The Lanchester absorber with viscous damping represents a special case of the foregoing system in which the damper spring is omitted, the absorber mass being coupled to the main system through the fluid only. In this case $k = 0$ and $f = 0$. Substituting these values into Equation [10]

$$R^4 - \frac{2}{2+\mu} R^2 = 0$$

from which $R_P^2 = 0$ and $R_Q^2 = \frac{2}{2+\mu}$ ..... [28]

The amplitude at Q then becomes

$$\left(\frac{a_1}{\frac{m_r e}{M}}\right)_Q = \frac{2}{\mu} \quad \ldots\ldots [29]$$

For the amplitude curve to pass horizontally through Q, the value of the optimum damping becomes

$$\gamma^2 = \frac{2}{2+\mu} \quad \ldots\ldots [30]$$

The value of the maximum relative amplitude may be found by the energy method if these values are substituted into Equation [20]. This yields

The effect of the mass ratio upon maximum amplitude of the main mass in systems with optimum damping is shown in Fig. 9, for the cases of $f = 0$, $f = 1$, and optimum tuning, respectively. In Fig. 10 a similar comparison is made of the relative amplitudes of the two masses. The influence of mass ratio upon the value of optimum damping for each of these three values of tuning is shown in Fig. 11.

Effect of Damping in Main System

With viscous damping present in the main system the equation for the amplitude of motion of the main mass may be shown to be

$$\frac{\frac{a_1}{m_r e}}{M} = \sqrt{\frac{R^4[(f^2 - R^2)^2 + \gamma^2 R^2]}{[(1 - R^2)(f^2 - R^2) - \mu f^2 R^2]^2 + \gamma^2 R^2[1 - (1+\mu)R^2]^2 + \Gamma^2 R^2[(f^2 - R^2)^2 + \gamma^2 R^2] + 2\mu\gamma\Gamma R^6}} \quad \ldots\ldots [32]$$

Comparing Equation [32] with Equation [3], the two additiona terms, $\Gamma^2 R^2[(f^2 - R^2)^2 + \gamma^2 R^2] + 2\mu\gamma\Gamma R^6$, are seen to appear in the denominator. These are due to main-system damping. The amplitude at P decreases faster with increasing Γ than does the amplitude at Q since $(f^2 - R^2)$ is positive at P and negative at Q. Figs. 12, 13, and 14 show the effects of main-system damping upon the amplitude coefficient for the three cases of tuning considered, with optimum damping in the absorber. For opti-

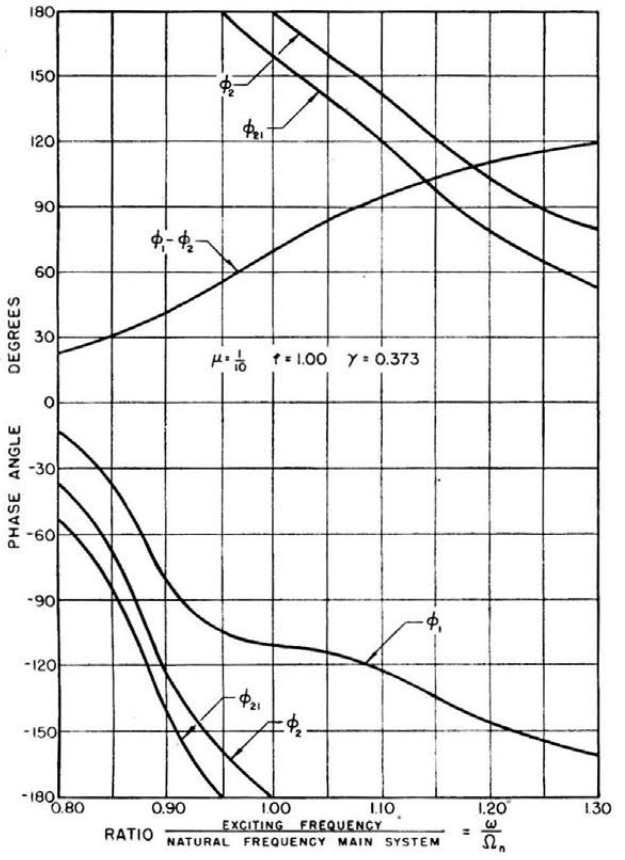

FIG. 6 PHASE RELATIONSHIPS FOR ABSORBER TUNED TO FREQUENCY OF MAIN SYSTEM, OPTIMUM DAMPING

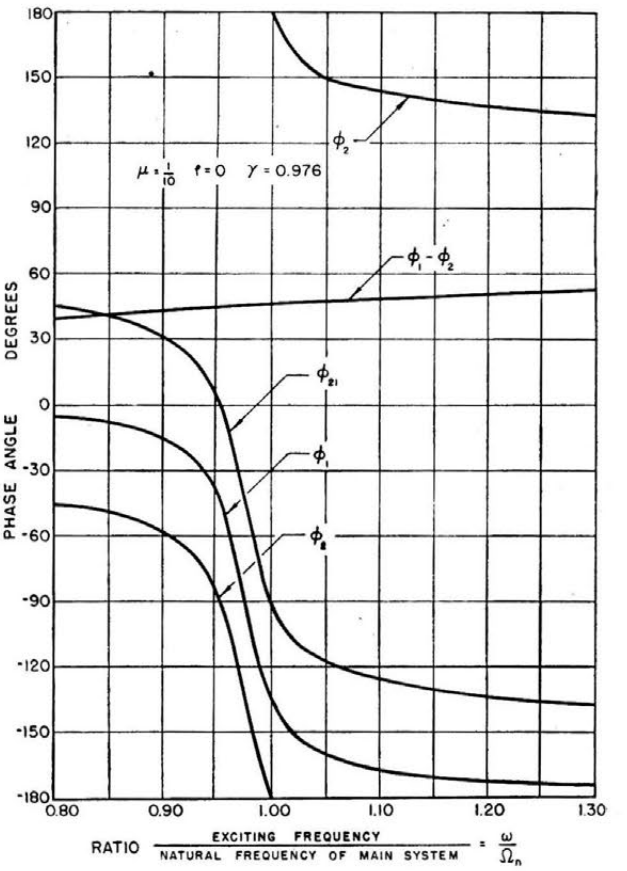

FIG. 8 PHASE RELATIONSHIPS FOR LANCHESTER DAMPER

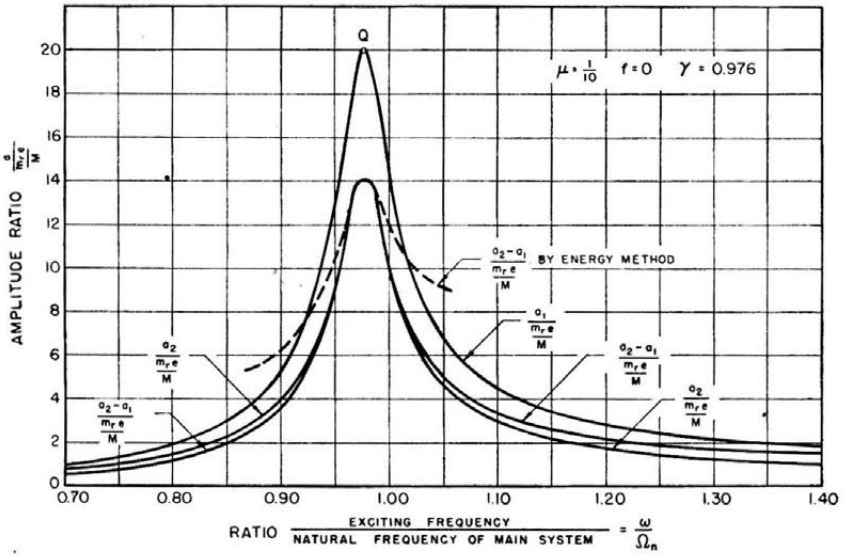

FIG. 7 AMPLITUDE RATIOS FOR VISCOUS LANCHESTER DAMPER, OPTIMUM DAMPING

mum tuning, the amplitude at P becomes lower than that at Q as Γ is increased while, for $f = 1$, the amplitude at P is higher at first and then gradually decreases below Q as the damping in the main system is increased.

The effectiveness of the absorber diminishes as the main-system damping is increased, but even for the rather large value of main-system damping illustrated in Fig. 12, ($\Gamma = 0.100$), the main-system amplitude is reduced to approximately one third of that without the absorber.

EXPERIMENTAL WORK

Experiments were conducted using a laboratory model, Fig. 15, consisting of a flexibly supported table A, excited by a vibration generator B, which employs two unbalanced shafts rotating in opposite directions. The vibration absorber C was attached to the framework of the table as shown. The speed of the vibration generator was varied by means of potentiometers in the armature and field circuits of its driving motor. The steady-state vibrations of the table structure were recorded by means of the Geiger torsiograph D. The absorber unit is shown in more detail in Fig. 16. It consists of a cylinder filled with SAE No. 10 oil and is fitted with a diaphragm, or piston, attached to a rod extending in both directions along the axis of the cylinder. The diaphragm has adjustable ports for controlling the damping, and seals between the vertical shaft and the cylinder are effected by bellows, eliminating the dry friction which would be present if stuffing boxes were used. The springs and weights can be changed to vary the mass ratio and tuning at will.

The physical constants of the main system were as follows: $M = 4.38$ lb-sec^2/ft; $K = 6240$ lb per ft; $\Omega_n = 37.8$ radians per

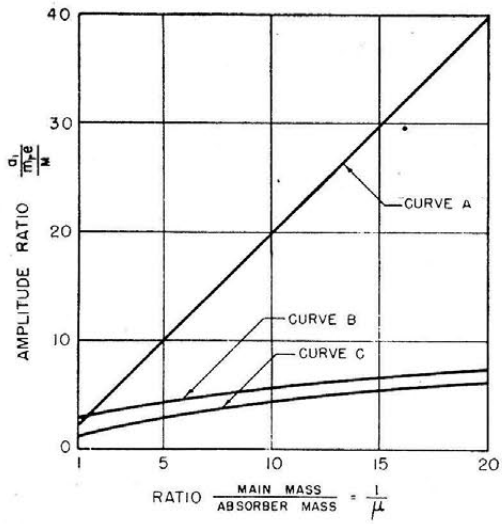

FIG. 9 MAXIMUM AMPLITUDE OF MAIN MASS WITH OPTIMUM DAMPING IN ABSORBER

(Curve A, Lanchester damper; curve B, absorber tuned to natural frequency of main system; curve C, optimum tuning.)

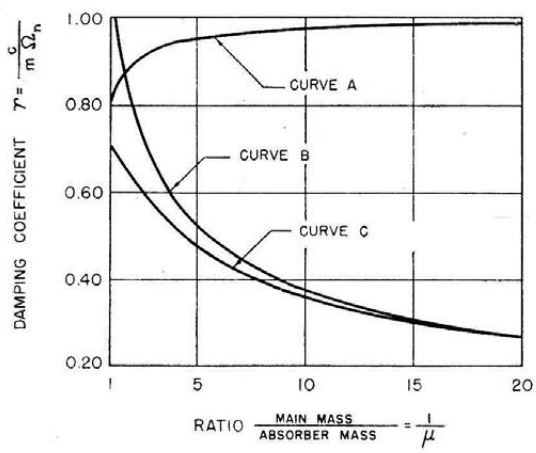

FIG. 11 OPTIMUM DAMPING COEFFICIENT

(Curve A, Lanchester damper; curve B, absorber tuned to natural frequency of main system; curve C, optimum tuning.)

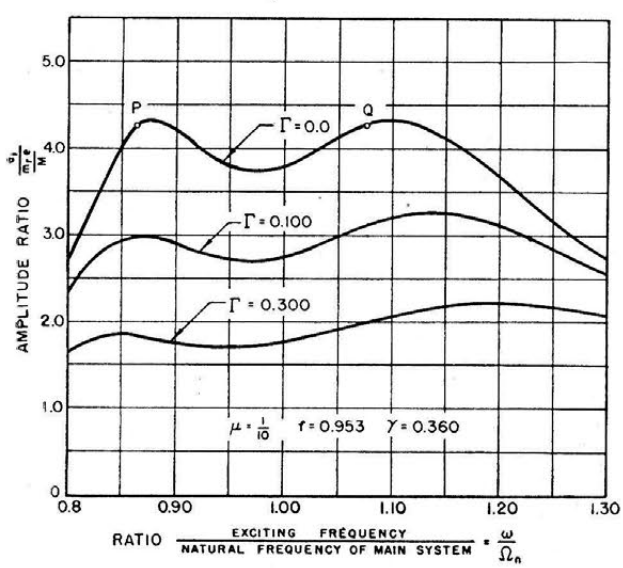

FIG. 12 EFFECT OF DAMPING IN MAIN SYSTEM WITH OPTIMUM TUNING AND DAMPING IN ABSORBER

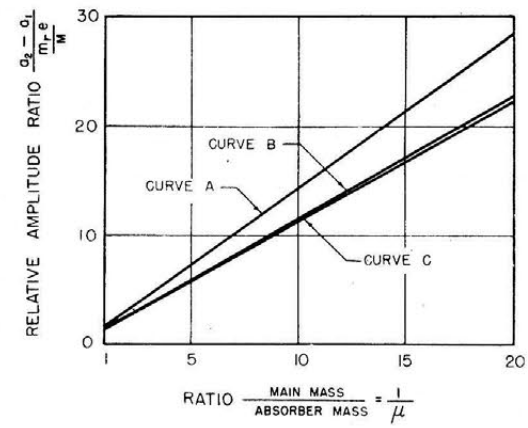

FIG. 10 MAXIMUM RELATIVE AMPLITUDE BY ENERGY METHOD

(Curve A, Lanchester damper; curve B, absorber tuned to natural frequency of main system; curve C, optimum tuning.)

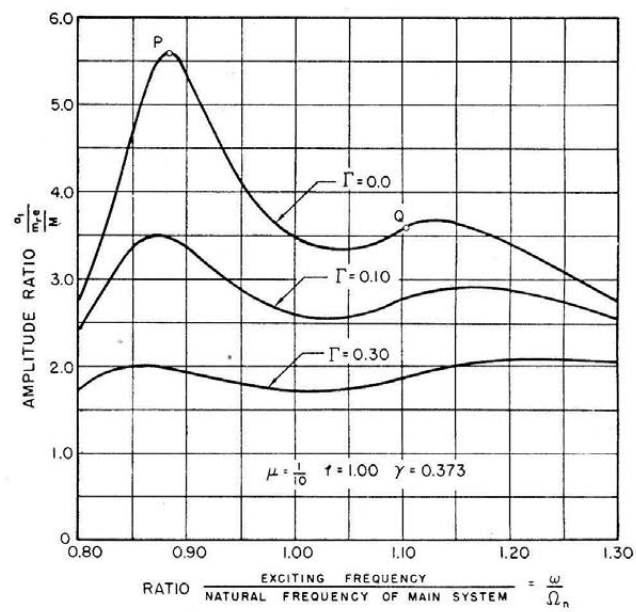

FIG. 13 EFFECT OF DAMPING IN MAIN SYSTEM FOR ABSORBER TUNED TO FREQUENCY OF MAIN SYSTEM

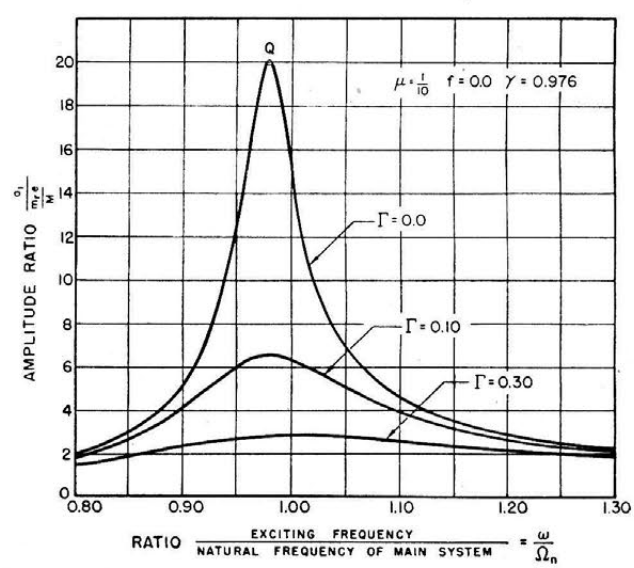

FIG. 14 EFFECT OF DAMPING IN MAIN SYSTEM FOR VISCOUS LANCHESTER DAMPER

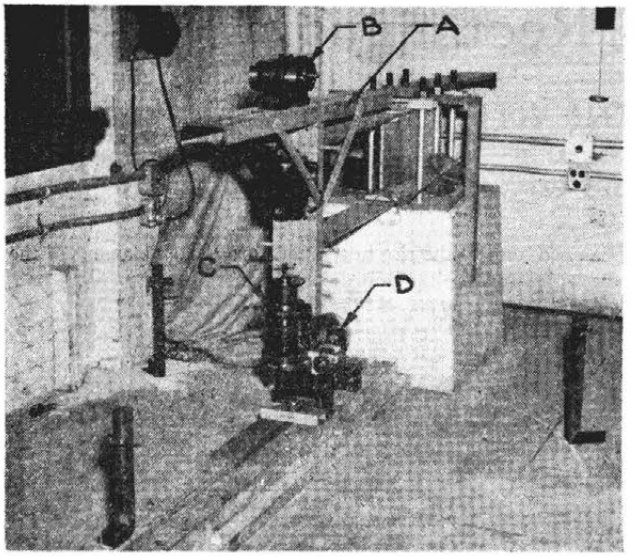

FIG. 15 LABORATORY MODEL

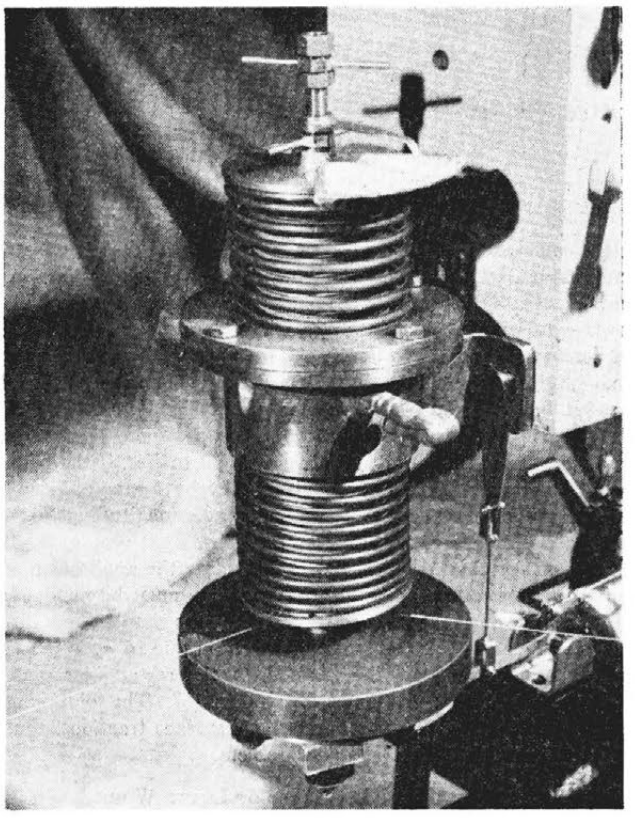

FIG. 16 VIBRATION ABSORBER

sec; $\Gamma = 0.038$. The constants of the vibration generator were $m_r = 0.0406$ lb-sec²/ft; $e = 0.855$ in. The constants for the absorber unit were $k = 473$ lb per ft; $m = 0.360$ lb-sec²/ft; $\omega_n = 36.3$ radians per sec. (The value of m was adjusted to give optimum tuning after k was determined.) The dimensionless coefficients derived from the foregoing coefficients were: $\mu = 0.0823$; $f_{opt} = 0.961$.

Amplitudes and frequencies were measured directly from the vibrograph records. The results of three damper settings are presented in Fig. 17.

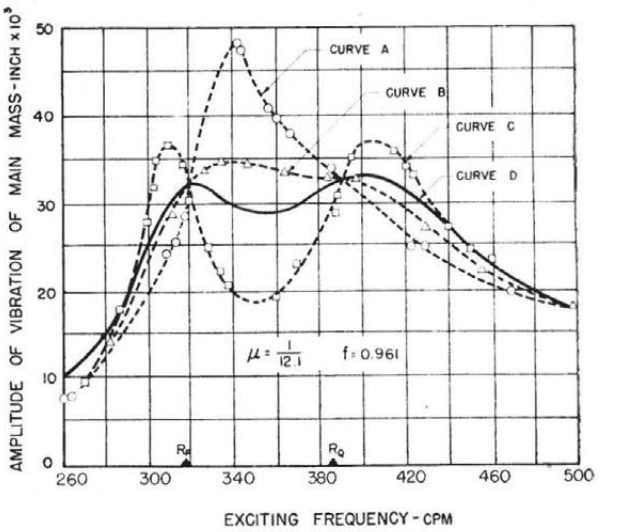

FIG. 17 FREQUENCY RESPONSE FOR LABORATORY MODEL WITH OPTIMUM TUNING

(Curve A, damping greater than optium; curve B, most favorable experimental damping; curve C, damping less than optimum; curve D, theoretical optimum damping, $\gamma = 0.331$.)

Excellent agreement was found between the experimental results and the theory, as indicated. The theoretical curve computed from the physical constants was adjusted so that the amplitude of points P and Q corresponded to the experimental values. This necessitated an adjustment in the $m_r e$ product of 3 per cent. The computed values of R_p and R_Q are shown on the frequency scale in Fig. 17.

SUMMARY AND CONCLUSIONS

Dimensionless theoretical expressions for the amplitudes and phase relationships, as functions of frequency, tuning, and absorber damping, have been derived and are presented in Equations [3] to [9], inclusive. These relationships are presented graphically in Figs. 2 to 8, inclusive.

The optimum tuning for the most effective absorber that can be applied to this system is expressed by Equation [11] as a function of the mass ratio (the mass ratio is chosen arbitrarily in the practical case).

The optimum amounts of damping for the cases of optimum tuning, tuning $f = 1$, and tuning $f = 0$, are expressed as functions of μ in Equations [18], [26], and [30], respectively, and are shown graphically in Fig. 11. A comparison of the optimum tuning and damping coefficients for systems having velocity-squared excitation and constant excitation is summarized in Table 1.

The theoretical expressions were found to be in excellent agreement with the experimental results. Therefore it is considered practical, by means of a dynamical absorber, tuned and damped in accordance with the principles presented herein, to minimize vibration amplitudes in a structure when those vibrations are excited over a wide range of frequencies by rotating or reciprocating parts.

BIBLIOGRAPHY

1 "The Theory of the Dynamic Vibration Absorber," by J. Ormondroyd and J. P. Den Hartog, Trans. ASME, vol. 50, 1928, p. 9.

2 "Mechanical Vibrations," by J. P. Den Hartog, second edition, Mc Graw-Hill Book Company, Inc., New York, N. Y., 1940, p. 120.

3 "A Note on the Damped Vibration Absorber," by J. E. Brock, JOURNAL OF APPLIED MECHANICS, Trans. ASME, vol. 68, 1946, p. A-284.

Thermal Stresses in a Rectangular Plate Clamped Along an Edge[1]

By B. J. ALECK,[2] JERSEY CITY, N. J.

An approximate solution has been obtained for the stresses induced by a uniform change in temperature of a thin rectangular plate, clamped along an edge. The solution has been carried to completion for plates whose clamped edge is long, i.e., more than 5 times the length of the perpendicular free edge. The solution for smaller ratios of clamped to perpendicular lengths is expressed in terms of six determined functions whose coefficients are to be evaluated by satisfying two boundary conditions. The thermal-stress problem is first converted to one of specified boundary tractions. The normal stress, σ_x, parallel to the clamped edge is assumed of the form $\sigma_x = f_1(x) + y f_2(x) + y^2 f_3(x)$, where $f_i(x)$ are as yet undetermined functions, and where y is the co-ordinate at right angles to the clamped edge. Using the equations of equilibrium and the boundary conditions, τ_{xy} and σ_y are expressed in terms of powers of y and the derivatives of $f_i(x)$. The integral representing the strain energy is then expressed in terms of the expressions for σ_x, σ_y, and τ_{xy}. In accordance with the principle of least work, the integral representing the strain energy is minimized, using the calculus of variations. The resulting simultaneous differential equations for $f_i(x)$ are solved as a linear combination of twelve functions (six of which drop out, by symmetry). Given $f_1(x)$, then $f_2(x)$ and $f_3(x)$ are determinate by virtue of the simultaneous equations. The six coefficients in the expression for f_1 are evaluated by satisfying the boundary conditions along the free edges. The maximum normal stress concentration, over 10, occurs at the junction of the free and clamped edges.

Conversion of the Problem in Thermal Stress to One of Boundary Tractions

CONSIDER a rectangular plate of constant small thickness, whose height is h' and whose width is b. One of the edges of the plate, of length b, is clamped; all other edges are free. At temperature T the plate is free of stress. The plate material is elastic, obeys Hooke's law, is isotropic, and its coefficient of linear expansion is α. The sign convention and directions of the x, y co-ordinate system are indicated in Fig. 1. The problem is to determine in an approximate manner the stresses produced by the increase of temperature from T to $T + t$.

If the plate is imagined cut free, i.e., if the clamped edge were unclamped, due to the rise in temperature t, each element of the body would undergo the unit deformations

$$\left.\begin{aligned} \epsilon_x &= \alpha t \\ \epsilon_y &= \alpha t \\ \gamma_{xy} &= 0 \end{aligned}\right\} \quad \ldots\ldots\ldots\ldots\ldots\ldots [1]$$

Now suppose that compressive stress, $\sigma_x = -E\alpha t$ to be applied; it would be accompanied by the unit strains

$$\left.\begin{aligned} \epsilon_x &= -\alpha t \\ \epsilon_y &= -\nu(\alpha t) \\ \gamma_{xy} &= 0 \end{aligned}\right\} \quad \ldots\ldots\ldots\ldots\ldots\ldots [2]$$

Superposing strains, Equations [1] and [2]

$$\left.\begin{aligned} \epsilon_x &= 0 \\ \epsilon_y &= \alpha t(1 - \nu) \\ \gamma_{xy} &= 0 \end{aligned}\right\} \quad \ldots\ldots\ldots\ldots\ldots\ldots [3]$$

and the state of stress becomes

$$\left.\begin{aligned} \sigma_x &= -E\alpha t \\ \sigma_y &= 0 \\ \tau_{xy} &= 0 \end{aligned}\right\} \quad \ldots\ldots\ldots\ldots\ldots\ldots [4]$$

The effect of these operations has been to increase the plate temperature, to bring each point back to its original x-position, and to increase the height of the plate in a uniform manner. This new height will be called h. Since ϵ_x and γ_{xy} are zero, no clamping forces are required to force points along the clamped edge to their original relative position. The plate is then imagined cemented back to the clamping member. Therefore it is concluded that the stress distribution due to the increase in temperature t, would be pure compression equal to $E\alpha t$, if the plate is prevented from expanding longitudinally by means of lateral pressure, independent of the clamping along a longitudinal edge. The state of the plate is indicated in Fig. 1(a).

Since the original problem did not envisage the application of the lateral restraining pressure, that pressure must be removed. This is accomplished by superposition upon the simple stress distribution of Fig. 1(a), the stress distribution due to $\sigma_x = E\alpha T$, applied along the edges of height h of the rectangular plate clamped along one edge of length b (see Fig. 1b). The solution of the problem of Fig. 1(b), one of specified surface tractions, thus replaces the original thermal-stress problem.

Application of Principle of Least Work

When the reactions are fixed, the principle of least work states that the strain energy will be a minimum for that state of stress, among those satisfying the boundary-stress conditions and the equations of equilibrium, which also satisfies the conditions of compatibility.

The variational principle has been applied extensively by Dr. Eric Reissner (1, 2, 3, 4)[3] to obtain approximate solutions to difficult problems. His technique, adopted by the author, is to use the minimum principle to establish functional coefficients of arbi-

---

[1] Abstracted from a thesis submitted in partial fulfillment of the requirements for the degree of Master of Science at Cornell University, Ithaca, N. Y., September, 1947.

[2] Special Projects Department, The M. W. Kellogg Company. Jun. ASME.

Contributed by the Applied Mechanics Division and presented at the Annual Meeting, New York, N. Y., November 28–December 3, 1948, of The American Society of Mechanical Engineers.

Discussion of this paper should be addressed to the Secretary, ASME, 29 West 39th Street, New York, N. Y., and will be accepted until July 11, 1949, for publication at a later date. Discussion received after the closing date will be returned.

Note: Statements and opinions advanced in papers are to be understood as individual expressions of their authors and not those of the Society. Paper No. 48—A-28.

[3] Numbers in parentheses refer to the Bibliography at the end of the paper.

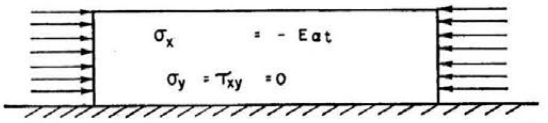

FIG. 1(a) PLATE WITH THERMAL STRESSES INTRODUCED BY UNIFORM INCREASE IN TEMPERATURE AND RESTRAINT TO LATERAL EXPANSION

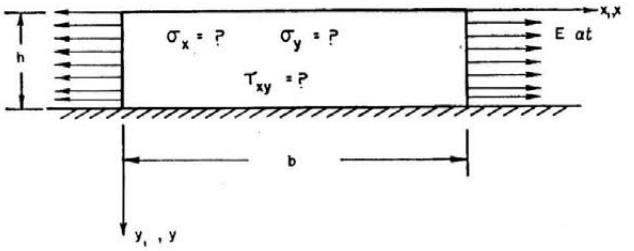

FIG. 1(b) PLATE CLAMPED ALONG A LONGITUDINAL EDGE SUBJECT TO UNIFORM TENSILE STRESS ON THE LATERAL EDGES

trary functions instead of parameters occurring in arbitrarily selected functions.

The procedure is to assume σ_x in the form

$$\sigma_x = f_1(x) + y f_2(x) + y^2 f_3(x) \quad \ldots\ldots [5]$$

where $f_i(x)$ are yet to be determined functions, and where the x, y are the nondimensionalized co-ordinates x_1/h, y_1/h, respectively. The omission of $f_1(x)$ in the foregoing expression for σ_x and replacement by $y^3 f_1(x)$, for example, would not be satisfactory, because σ_x could not then satisfy the boundary condition $\sigma_x = E\alpha t$. The decision to use $f_i(x)$ as coefficients of an ascending power series in y was arbitrary.

The equations of equilibrium are (5)

$$\frac{\partial \sigma_x}{\partial x} + \frac{\partial \tau_{xy}}{\partial y} = 0 \quad \ldots\ldots [6]$$

$$\frac{\partial \sigma_y}{\partial y} + \frac{\partial \tau_{xy}}{\partial x} = 0 \quad \ldots\ldots [7]$$

Substituting the expression for σ_x from Equation [5] in Equation [6], integrating $(\partial \tau_{xy}/\partial y)$ partially with respect to y, and using the boundary condition $\tau_{xy} = 0$ for $y = 0$, the following expression is obtained

$$-\tau_{xy} = y f_1' + \frac{1}{2} y^2 f_2' + \frac{1}{3} y^3 f_3' \quad \ldots\ldots [8]$$

where the primes indicate differentiation with respect to x. Substituting the expression for τ_{xy} from Equation [8] in Equation [7], integrating $(\partial \sigma_y/\partial y)$ partially with respect to y, and using the boundary condition $\sigma_y = 0$ for $y = 0$ then

$$\sigma_y = \frac{1}{2} y^2 f_1'' + \frac{1}{6} y^3 f_2'' + \frac{1}{12} y^4 f_3'' \quad \ldots\ldots [9]$$

Expressions for stresses satisfying the boundary stress conditions and the equations of equilibrium have been determined. These are now inserted in the expression for strain energy (6)

$$V = \frac{1}{2E} \int_0^{\frac{b}{h}} \int_0^1 [\sigma_x^2 + \sigma_y^2 + (2 + 2\nu)\, \tau_{xy}^2 - 2\nu \sigma_x \sigma_y]\, dx\, dy \quad \ldots\ldots [10]$$

After the substitution of Equations [5], [8], and [9], and upon integration with respect to y from 0 to 1, the expression for V contains only a sum of many products of functions of x, all terms in y having vanished during integration. Calculus of variations techniques are now applied to minimize V.

Thus if $f_1(x)$, $f_2(x)$, $f_3(x)$ are to produce a minimum value of V, the value of V should remain unchanged by a term to the first power in ϵ, an arbitrarily small number, if

$$f_1(x) \text{ is replaced by } f_1(x) + \epsilon \eta_1(x)$$

$$f_2(x) \text{ is replaced by } f_2(x) + \epsilon \eta_2(x)$$

and

$$f_3(x) \text{ is replaced by } f_3(x) + \epsilon \eta_3(x)$$

where

$$\eta_1(x), \ \eta_2(x), \text{ and } \eta_3(x)$$

are arbitrary functions of x.

Performing the substitution, subtracting the two values of V, ignoring terms in powers of ϵ greater than the first, and setting the result equal to zero, the following relation is obtained

$$\left.\begin{aligned}
&\int_0^{\frac{b}{h}} \epsilon \Bigg\{ \eta_1 \left[2f_1 + f_2 + \frac{2}{3} f_3 - \frac{2\nu}{6} f_1'' - \frac{2\nu}{24} f_2'' - \frac{2\nu}{60} f_3'' \right] \\
&+ \eta_1' \left[(2 + 2\nu) \right] \left[\frac{2}{3} f_1' + \frac{1}{4} f_2' + \frac{2}{15} f_3' \right] \\
&+ \eta_1'' \left[\frac{1}{10} f_1'' + \frac{1}{36} f_2'' + \frac{1}{84} f_3'' - \frac{2\nu}{6} f_1 - \frac{2\nu}{8} f_2 - \frac{2\nu}{10} f_3 \right] \\
&+ \eta_2 \left[f_1 + \frac{2}{3} f_2 + \frac{1}{2} f_3 - \frac{2\nu}{8} f_1'' - \frac{2\nu}{30} f_2'' - \frac{2\nu}{72} f_3'' \right] \\
&+ \eta_2' \left[(2 + 2\nu) \right] \left[\frac{1}{4} f_1' + \frac{1}{10} f_2' + \frac{1}{18} f_3' \right] \\
&+ \eta_2'' \left[\frac{1}{36} f_1'' + \frac{1}{126} f_2'' + \frac{1}{288} f_3'' - \frac{2\nu}{24} f_1 - \frac{2\nu}{30} f_2 - \frac{2\nu}{36} f_3 \right] \\
&+ \eta_3 \left[\frac{2}{3} f_1 + \frac{1}{2} f_2 + \frac{2}{5} f_3 - \frac{2\nu}{10} f_1'' - \frac{2\nu}{36} f_2'' - \frac{2\nu}{84} f_3'' \right] \\
&+ \eta_3' \left[2 + 2\nu \right] \left[\frac{2}{15} f_1' + \frac{1}{18} f_2' + \frac{2}{63} f_3' \right] \\
&+ \eta_3'' \left[\frac{1}{84} f_1'' + \frac{1}{288} f_2'' + \frac{1}{648} f_3'' - \frac{2\nu}{60} f_1 - \frac{2\nu}{72} f_2 - \frac{2\nu}{84} f_3 \right] \Bigg\} dx = 0
\end{aligned}\right\} \quad \ldots [11]$$

Integrating by parts to convert terms in η' and η'' to terms in η,

$$\left.\begin{aligned}
\int_0^{\frac{b}{h}} f \eta' dx &= -\int_0^{\frac{b}{h}} f' \eta dx \\
\int_0^{\frac{b}{h}} f \eta'' dx &= \int_0^{\frac{b}{h}} f'' \eta dx
\end{aligned}\right\} \quad \ldots\ldots [12]$$

if $\eta(0) = \eta(b/h) = \eta'(0) = \eta'(b/h) = 0$, which is permissible, since the η's are arbitrary. When Equations [12] are applied in relation to Equations [11], the equation becomes a sum of integrals in which η_1, η_2, and η_3 appear as factors of the respective integrands. Since the η_i are arbitrary, the condition that the sum of the integrals must vanish independent of the values of η_i is that the coefficients of η_i should vanish. On the basis of this argument, the following differential equations result

$$\left.\begin{aligned}
&\left[2f_1 - f_1''\left(\frac{4}{3} + 2\nu\right) + \frac{1}{10}f_1^{iv}\right] + \\
&\left[f_2 - f_2''\left(\frac{1}{2} + \frac{5}{12}2\nu\right) + \frac{1}{36}f_2^{iv}\right] + \\
&\left[\frac{2}{3}f_3 - f_3''\left(\frac{4}{15} + \frac{2\nu}{4}\right) + \frac{1}{84}f_3^{iv}\right] = 0 \\
&\left[f_1 - f_1''\left(\frac{1}{2} + \frac{5}{12}2\nu\right) + \frac{1}{36}f_1^{iv}\right] + \\
&\left[\frac{2}{3}f_2 - f_2''\left(\frac{1}{5} + \frac{2\nu}{6}\right) + \frac{1}{126}f_2^{iv}\right] + \\
&\left[\frac{1}{3}f_3 - f_3''\left(\frac{1}{9} + \frac{7}{72}2\nu\right) + \frac{1}{288}f_3^{iv}\right] = 0 \\
&\left[\frac{2}{3}f_1 - f_1''\left(\frac{4}{15} + \frac{2\nu}{4}\right) + \frac{1}{84}f_1^{iv}\right] + \\
&\left[\frac{1}{2}f_2 - f_2''\left(\frac{1}{9} + \frac{7}{72}2\nu\right) + \frac{1}{288}f_2^{iv}\right] + \\
&\left[\frac{2}{5}f_3 - f_3''\left(\frac{4}{63} + \frac{2\nu}{18}\right) + \frac{1}{648}f_3^{iv}\right] = 0
\end{aligned}\right\} \quad [13]$$

If $2\nu = 1/2$, these reduce to

$$\left.\begin{aligned}
&\left(2f_1 - f_1''\frac{11}{16} + \frac{1}{10}f_1^{iv}\right) + \left(f_2 - \frac{17}{24}f_2'' + \frac{1}{36}f_2^{iv}\right) \\
&\qquad + \left(\frac{2}{3}f_3 - \frac{47}{120}f_3'' + \frac{1}{84}f_3^{iv}\right) = 0 \\
&\left(f_1 - \frac{17}{24}f_1'' + \frac{1}{36}f_1^{iv}\right) + \left(\frac{2}{3}f_2 - \frac{17}{60}f_2'' + \frac{1}{126}f_2^{iv}\right) \\
&\qquad + \left(\frac{1}{2}f_3 - \frac{23}{144}f_3'' + \frac{1}{288}f_3^{iv}\right) = 0 \\
&\left(\frac{2}{3}f_1 - \frac{47}{120}f_1'' + \frac{1}{84}f_1^{iv}\right) + \left(\frac{1}{2}f_2 - \frac{23}{144}f_2'' + \right. \\
&\qquad \left. \frac{1}{288}f_2^{iv}\right) + \left(\frac{2}{5}f_3 - \frac{23}{252}f_3'' + \frac{1}{648}f_3^{iv}\right) = 0
\end{aligned}\right\} \quad [14]$$

The condition that a solution of the form

$$\left.\begin{aligned}
f_1 &= A\,e^{\lambda x} \\
f_2 &= B\,e^{\lambda x} \\
f_3 &= C\,e^{\lambda x}
\end{aligned}\right\} \quad [15]$$

exists is that the symmetrical determinant below vanishes

$$\begin{vmatrix}
2 - \frac{11}{6}\lambda^2 + \frac{1}{10}\lambda^4, & 1 - \frac{17}{24}\lambda^2 + \frac{1}{36}\lambda^4, & \\
& & \frac{2}{3} - \frac{47}{120}\lambda^2 + \frac{1}{84}\lambda^4 \\
1 - \frac{17}{24}\lambda^2 + \frac{1}{36}\lambda^4, & \frac{2}{3} - \frac{17}{60}\lambda^2 + \frac{1}{126}\lambda^4, & \\
& & \frac{1}{2} - \frac{23}{144}\lambda^2 + \frac{1}{288}\lambda^4 \\
\frac{2}{3} - \frac{47}{120}\lambda^2 + \frac{1}{84}\lambda^4, & \frac{1}{2} - \frac{23}{144}\lambda^2 + \frac{1}{288}\lambda^4, & \\
& & \frac{2}{5} - \frac{23}{252}\lambda^2 + \frac{1}{648}\lambda^4
\end{vmatrix} = 0 \quad [16]$$

As expansion of this determinant involves the repeated subtraction of nearly equal numbers, six significant figures are not adequate to obtain one-place accuracy of some coefficients. To avoid this difficulty, each term is multiplied by the least common denominator (90,720) and all operations are carried out exactly (without dropping any numbers) on the resulting whole numbers. Equation [16] rewritten in expanded form then becomes

$$\left.\begin{aligned}
&32{,}400\,w^6 - 17{,}554{,}320\,w^5 + 1{,}318{,}615{,}200\,w^4 \\
&- 52{,}203{,}771{,}648\,w^3 + 507{,}935{,}493{,}920\,w^2 \\
&- 3{,}219{,}622{,}318{,}080\,w + 2{,}765{,}319{,}782{,}400 = 0
\end{aligned}\right\} \quad [17]$$

where $\lambda^2 = w$

The roots of this equation are

$$\left.\begin{aligned}
w_1 &= 460.9306040 \\
w_2 &= 35.0691295 + i\,36.8670015 \\
w_2' &= 35.0691295 - i\,36.8670015 \\
w_3 &= 4.8642053 + i\,6.9119811 \\
w_3' &= 4.8642053 - i\,6.9119811 \\
w_4 &= 1.001159473
\end{aligned}\right\} \quad [18]$$

Associated with each root w, there exists a unique relation between the A, B, and C of Equations [15]. For each w, this relation is established using two of Equation [16] in conjunction with the value of w under consideration. The symbols for the coefficients A, corresponding to each w, and the simultaneous value of B/A and C/A are given in Table 1, where also is found the values of $\lambda = \pm\sqrt{w}$. The number of significant figures is

TABLE 1 SYMBOLS FOR COEFFICIENTS

w	A	$\frac{B}{A}$	$\frac{C}{A}$
w_1	A_1	(−9.25970701)	13.29296811
w_2	$A_2 + iA_2'$	(−8.33136777 + i 0.1589243793)	(11.188566696 − i 0.429955968)
w_2'	$A_2 - iA_2'$	(−8.33136777 − i 0.1589243793)	(11.188566696 + i 0.429955968)
w_3	$A_3 + iA_3'$	(−4.32764770 + i 0.456750600)	(3.24377169 − i 0.306407564
w_3'	$A_3 - iA_3'$	(−4.32764770 − i 0.456750600)	(3.24377169 + i 0.306407564)
w_4	A_4	−0.130826469	−0.778698640

w	$\pm\lambda = \sqrt{w}$
w_1	21.46929444
w_2	6.555611318 + 2.811922874 i
w_2'	6.555611318 − 2.811922874 i
w_3	2.58032807 + 1.339360912 i
w_3'	2.58032807 − 1.339360912 i
w_4	1.000579569

larger than needed for the particular problem solved; in other applications, this number may be required.

So far, the length of the plate has played no role. If the plate is short, it will be convenient to choose the y-axis so that it bisects the length of the plate. By virtue of symmetry, the $f_i(x)$ must be even functions and, in place of Equations [15], it will be more expedient to use the relations

$$\left.\begin{aligned} f_1 &= A\cosh\lambda x \\ f_2 &= B\cosh\lambda x \\ f_3 &= C\cosh\lambda x \end{aligned}\right\} \quad \ldots\ldots\ldots\ldots\ldots\ldots [19]$$

The coefficients of similar $\sinh \lambda x$ terms vanish. The relations between B/A and C/A for each λ will remain unchanged from the values given in Table 1. If, on the other hand, the plate is infinitely long, it is more convenient to place the y-axis at the free edge. The coefficients of terms $e^{\lambda x}$ must vanish if the real part of λ is positive. Since the differential Equations [14] are linear, the Equations [15] may be rewritten

$$f_1 = A_1 e^{\lambda_1 x} + (A_2 + i\,A_2')e^{\lambda_2 x} + (A_2 - i\,A_2')e^{\lambda' 2 x} + (A_3 + i\,A_3')e^{\lambda_3 x} + (A_3 - i\,A_3')e^{\lambda' 3 x} + A_4 e^{\lambda_4 x}$$

or

$$\left.\begin{aligned} f_1 &= \Sigma A_i\, e^{\lambda_i x} \\ f_2 &= \Sigma B_i\, e^{\lambda_i x} \\ f_3 &= \Sigma C_i\, e^{\lambda_i x} \end{aligned}\right\} \quad \ldots\ldots\ldots\ldots\ldots\ldots [20]$$

The six A_i coefficients are independent; the B_i and C_i are algebraically related to A_i, which are to be determined by the boundary conditions

$$\left.\begin{aligned} \sigma_x &= E\alpha t \quad \text{at} \quad x = 0 \\ \tau_{xy} &= 0 \quad \text{at} \quad x = 0 \end{aligned}\right\} \quad \ldots\ldots\ldots\ldots [21]$$

Translated into terms of A_i's, for the boundary conditions, the following are obtained

$$\left.\begin{aligned} \Sigma A_i &= E\alpha t \quad \Big| \quad \Sigma A_i\lambda_i = 0 \\ \Sigma B_i &= 0 \quad \Big| \quad \Sigma B_i\lambda_i = 0 \\ \Sigma C_i &= 0 \quad \Big| \quad \Sigma C_i\lambda_i = 0 \end{aligned}\right\} \quad \ldots\ldots\ldots [22]$$

These six equations are sufficient to determine the six A_i, which (for $E\alpha t = 1$) become fixed at

$$\begin{aligned} A_1 &= -0.53163 & 2A_3 &= -1.297 \\ 2A_2 &= 1.1768 & 2A_3' &= 2.153 \\ 2A_2' &= 2.9436 & A_4 &= 1.652 \end{aligned}$$

Using the foregoing, the values of f_1, f_2, and f_3 are established from Equations [20] and used in the Expressions [5], [8], [9] for σ_x, τ_{xy}, and σ_y. The results are superposed on those of Fig. 1(a) and plotted in Figs. 2, 3, and 4. As would be expected from Dr. J. N. Goodier's extension of the Saint Venant principle (7, 8), the effects of the applied stress do not extend more than several plate heights into the body. The significance of this statement is that the thermal stress is $\sigma_x = -E\alpha t$ for the full interior of the plate.

The stress concentration occurs at the junction of the free and clamped edge and is $\sigma_y = 10.2\,E\alpha t$. The stress normal to the clamped edge σ_y, falls off so rapidly as to suggest that a concentrated normal force would have been found for an exact solution. The shear stress τ_{xy}, reaches a maximum, $2.7\,E\alpha t$, more gradually, and does not seem to indicate the presence of a concentrated shearing force for the exact solution. Clamping conditions have not been satisfied completely since along $y = 1$, $E\epsilon_x = (\sigma_x - \nu\sigma_y) \neq$ constant for the approximate solution.

The treatment of this problem has been two-dimensional.

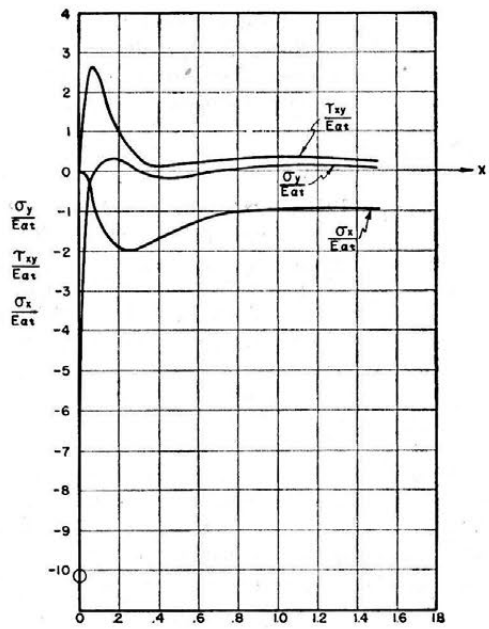

FIG. 2 STRESSES $\frac{\sigma_x}{E\alpha t}$, $\frac{\sigma_y}{E\alpha t}$, $\frac{\sigma_{xy}}{E\alpha t}$ ALONG CLAMPED EDGE

(Unit of abscissa is one wall height; origin is at free edge. Poisson's ratio = 0.25.)

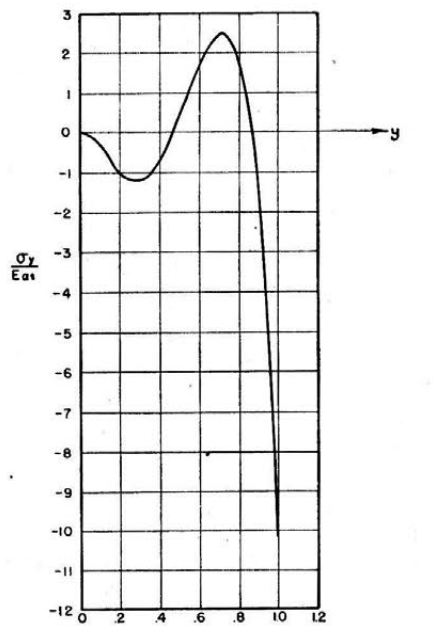

FIG. 3 STRESSES $\frac{\sigma_y}{E\alpha t}$ ALONG SHORT FREE EDGE; $\sigma_x = \tau_{xy} = 0$

(Unit of abscissa is one wall height; origin is at free edge. Poisson's ratio = 0.25.)

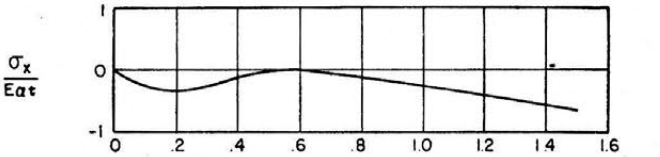

FIG. 4 STRESSES $\frac{\sigma_x}{E\alpha t}$ ALONG LONG FREE EDGE; $\sigma_y = \tau_{xy} = 0$

(Unit of abscissa is one wall height; origin is at free edge. Poisson's ratio = 0.25.)

Stresses and strains in the third direction have not been mentioned. By using Dr. J. N. Goodier's analysis (7, 8), it can be shown that three-dimensional effects will be important only in the region of the clamped edge for distances several plate thicknesses away from the clamped edge.

Conclusion

These results were derived originally to aid in the design of thin parapet walls on dams or possibly buildings. Other applications which suggest themselves fall in the category of bimaterial constructions, where the stiffnesses of the components are not of the same order of magnitude, and the coefficients of expansion are different. Examples are thin layers of plastic bonded to metal, and thin glazes on ceramic tiles. Cracked brittle lacquers in experimental stress-analysis applications are subjected to a similar state of stress, if the stress distribution is locally substantially constant. In conjunction with the economical design of walls and research into the crazing patterns of glazes, a study of the effect of plate length to height ratio on the stress concentrations would be valuable. It is anticipated that the end effects would tend to cancel as the plate length is reduced and thus indicate the optimum distance between parapet-wall expansion joints.

If one postulates the maximum stress theory to apply to glazed ceramics, the crack spacing of the glaze will be such as to permit stresses lower than the maximum allowable to exist. It has indeed been shown that as the glaze is cooled rapidly from successively higher temperatures, the crack spacing is reduced.

Acknowledgment

The author acknowledges the inspiration, help, and encouragement of Dr. J. N. Goodier in the preparation of the thesis from which this paper was abstracted.

BIBLIOGRAPHY

1 "Least Work Solutions of Shear Lag Problems," by E. Reissner, *Journal of the Aeronautical Sciences*, vol. 8, May, 1941, pp. 284–291.

2 "Distribution of Stresses in Built-In Beams of Narrow Rectangular Cross Section," by F. B. Hildebrande and Eric Reissner, Journal of Applied Mechanics, Trans. ASME, vol. 64, 1942, p. A-108.

3 "Analysis of Shear Lag in Box Beams by the Principle of Minimum Potential Energy," by Eric Reissner, *Quarterly of Applied Mathematics*, vol. 4, no. 3, 1946, pp. 268–278.

4 "On Bending of Elastic Plates," by Eric Reissner, *Quarterly of Applied Mathematics*, vol. 5, no. 1, 1947, pp. 55–68.

5 "Theory of Elasticity," by S. Timoshenko, McGraw-Hill Book Company, Inc., New York, N. Y., 1934, p. 21.

6 Ibid., p. 152.

7 "A General Proof of Saint Venant's Principle," by J. N. Goodier, *Philosophical Magazine*, series 7, vol. 23, April, 1937, pp. 607–609.

"A Supplementary Note.....," by J. N. Goodier, *Philosophical Magazine*, series 7, vol. 24, August, 1937, p. 325.

8 "An Extension of Saint Venant's Principle With Applications," by J. N. Goodier, *Journal of Applied Physics*, vol. 13, no. 3, March, 1942, pp. 167–171.

Polygonal Approximation Method in the Hodograph Plane

By H. PORITSKY,[1] SCHENECTADY, N. Y.

This paper extends the discussion of the approximate method of integrating the equations of compressible fluid flow in the hodograph plane first presented by the author before the Sixth International Congress of Applied Mechanics, Paris, France, September, 1948. As an introduction to the discussion of the polygonal approximation method, fundamental fluid-flow equations are reviewed briefly. Determination of the flow function ψ by the "Method of Reflections" is described and an application of the method illustrated. How flow in the physical plane can be determined by superposition of solutions discussed is shown for the simpler incompressible case.

1 Introduction

VERY little progress has been made in the direct solution of the nonlinear equations of steady two-dimensional flow of a compressible fluid in the physical plane, Equations [5] and [7]. More success has attended the solution of the linear equations of flow in the hodograph plane, Equations [22] and [23], that is, the plane in which the velocity components u, v are the Cartesian co-ordinates. Yet a great deal of difficulty still remains in solving compressible-flow problems arising in flight and industry.

It has been pointed out by Chaplygin that the differential equation satisfied in the hodograph plane by the stream function in two-dimensional compressible fluid flow can be reduced to the Laplace equation, provided that the equation of state in the (p, V)-plane ($V = 1/\rho$), Equation [1], be replaced by a straight line. Chaplygin chose this straight line as the tangent to the adiabatic curve at p_o, V_o corresponding to the stagnation (or impact) pressure of the gas. For an object immersed in a field of uniform flow (for instance, an airfoil in a uniform air stream) von Kármán proposed a straight-line tangent to the equation of state at the point (p_∞, V_∞) corresponding to the undisturbed uniform flow at infinity. This is known as the Kármán-Tsien method and is widely used in aeronautical engineering.

A natural extension of the above methods consists in approximating the equation of state by means of *not one but several* straight-line segments in the $(p, 1/\rho)$-plane. This method was discussed by the author in item (1)[2] of the bibliography at the end of the paper.[3] In the following this method is further extended and illustrated.

2 Fluid Flow Equations in the Physical and the Hodograph Planes

As an introduction to the polygonal approximation method which is explained in the next section, we review briefly the fundamental equations.

Elimination of the pressure from the force and continuity equations for the two-dimensional steady flow of a nonviscous compressible fluid satisfying a relation

$$p = p(\rho) \quad [1]$$

leads to the differential equation

$$u_x(1 - u^2/a^2) + v_y(1 - v^2/a^2) - (u_y + v_x)uv/a^2 = 0 \quad [2]$$

where subscripts denote partial derivatives, and a is the velocity of sound, given by

$$a^2 = dp/d\rho \quad [3]$$

If the flow is irrotational, then a velocity potential φ exists such that

$$\left.\begin{aligned} u &= \varphi_x \\ v &= \varphi_y \end{aligned}\right\} \quad [4]$$

Introducing φ in Equation [2] leads to the equation

$$\varphi_{xx}(1 - \varphi_x^2/a^2) + \varphi_{yy}(1 - \varphi_y^2/a^2) - 2\varphi_{xy}\varphi_x\varphi_y/a^2 = 0 \quad [5]$$

while in terms of the flow function ψ, where[4]

$$\left.\begin{aligned} \rho u &= \psi_y \\ \rho v &= \psi_x - \psi_x \end{aligned}\right\} \quad [6]$$

[2] becomes[5]

$$(\psi_y/\rho)_x(1 - \psi_y^2/\rho^2a^2) - (\psi_x/\rho)_y(1 - \psi_x^2/\rho^2a^2) + (\psi_x\psi_y/\rho^2a^2)[(\psi_y/\rho)_y - (\psi_x/\rho)_x] = 0 \quad [7]$$

Equations [2] and [7] are nonlinear equations, their nonlinearity arising not merely from the squares and products but also from the quantities a and ρ which are related with p and the velocity magnitude

$$w = (u^2 + v^2)^{1/2} \quad [8]$$

by means of the Bernoulli equation

$$w^2/2 + \int_{p_o}^{p} dp/\rho = 0 \quad [9]$$

where p_o is the stagnation pressure at which the gas velocity vanishes. When Equation [1] reduces to the adiabatic law

$$p = p_o\rho^\gamma/\rho_o^\gamma \quad [10]$$

Equations [3] and [9] become

$$a^2 = \gamma p/\rho \quad [11]$$

$$a^2 + (\gamma - 1)w^2/2 = a_o^2 \quad [12]$$

---

[1] Consulting Engineer, General Electric Company, Schenectady, N. Y. Mem. ASME.

[2] Numbers in parentheses refer to the Bibliography at the end of the paper.

[3] In (1) the constants c_i (see Equation [45]) were inadvertently replaced by their reciprocals. The author is indebted to his colleague, G. Horvay for aid in detecting this error and carrying out its correction.

Presented at the National Meeting of the Applied Mechanics Division, Chicago, Ill., June 17–19, 1948, of The American Society of Mechanical Engineers.

Discussion of this paper should be addressed to the Secretary, ASME, 29 West 39th Street, New York, N. Y., and will be accepted until July 11, 1949, for publication at a later date. Discussreceived after the closing date will be returned.

Note: Statements and opinions advanced in papers are to be understood as individual expressions of the author and not those of the Society. Paper No. 48—APM-23.

[4] Very often ψ is defined by

$$\psi_y = u\rho/\rho_o, \quad -\psi_x = v\rho/\rho_o$$

where ρ_o is the "stagnation" density.

[5] This equation, in contrast to Equation [5], does not assume that the flow is irrotational.

respectively, where a_o is the velocity of sound at the stagnation conditions p_o, ρ_o,

$$a_o^2 = \gamma p_o/\rho_o \quad [13]$$

Except for desultory attempts at integrating the Equations [5], [7] by successive approximation methods, by numerical and experimental methods, comparatively little progress has been made in the solution of these equations. Even for a flow around a circular cylinder it is not known up to what Mach number a solution of Equation [5] exists.

To translate the problem into the hodograph plane, in which u, v are rectangular co-ordinates, and w, $\theta = \tan^{-1}v/u$ polar co-ordinates, write Equations [4] and [6] in the form

$$\left.\begin{aligned} d\varphi &= u\,dx + v\,dy \\ d\psi &= -\rho v\,dx + \rho u\,dy \end{aligned}\right\} \quad [14]$$

Solving for dx, dy

$$\left.\begin{aligned} dx &= u\,d\varphi/(u^2+v^2) - v\,d\psi/\rho(u^2+v^2) \\ &= \cos\theta\,d\varphi/w - \sin\theta\,d\psi/\rho w \\ dy &= \sin\theta\,d\varphi/w + \cos\theta\,d\varphi/\rho w \end{aligned}\right\} \quad [15]$$

then substituting for $d\varphi$, $d\psi$

$$\left.\begin{aligned} d\varphi &= \varphi_w dw + \varphi_\theta d\theta \\ d\psi &= \psi_w dw + \psi_\theta d\theta \end{aligned}\right\} \quad [16]$$

there results

$$\left.\begin{aligned} dx &= x_w dw + x_\theta d\theta \\ &= (\cos\theta\,\varphi_w/w - \sin\theta\,\psi_w/\rho w)dw \\ &\qquad + (\cos\theta\,\varphi_\theta/w - \sin\theta\,\psi_\theta/\rho w)d\theta \\ dy &= y_w dw + y_\theta d\theta \\ &= (\sin\theta\,\varphi_w/w + \cos\theta\,\psi_w/\rho w)dw \\ &\qquad + (\sin\theta\,\varphi_\theta/w + \cos\theta\,\psi_\theta/\rho w)d\theta \end{aligned}\right\} \quad [17]$$

Applying the conditions

$$\left.\begin{aligned} (x_w)_\theta &= (x_\theta)_w \\ (y_w)_\theta &= (y_\theta)_w \end{aligned}\right\} \quad [18]$$

which render dx, dy perfect differentials, one obtains two equations, which upon multiplication by sin θ, cos θ, then by cos θ, $-\sin\theta$ and addition, yield

$$\left.\begin{aligned} \frac{\varphi_w}{w} &= \left(\frac{1}{\rho w}\right)' \psi_\theta, \\ \frac{\psi_w}{\rho_w} &= \frac{\varphi_\theta}{w^2} \end{aligned}\right\} \quad [19]$$

Here $'$ indicates differentiation with respect to w. Taking differentials of Equation [9] and eliminating dp by means of Equation [3] one obtains

$$\frac{d\rho}{dw} = -\frac{\rho w}{a^2} \quad [20]$$

and hence

$$\frac{d(1/\rho w)}{dw} = -\frac{1}{\rho w^2} - \frac{d\rho/dw}{\rho^2 w} = \frac{1}{\rho}\left(\frac{1}{a^2} - \frac{1}{w^2}\right) \quad [21]$$

Equations [19] may now be rewritten

$$\left.\begin{aligned} \frac{w}{\rho}\varphi_w &= \frac{1}{\rho^2}\left(\frac{w^2}{a^2} - 1\right)\psi_\theta = \frac{1}{\rho^2}(M^2-1)\psi_\theta \\ \frac{w}{\rho}\psi_w &= \varphi_\theta \end{aligned}\right\} \quad [22]$$

where M is the Mach number $= w/a$. Elimination of φ from the Equations [22] leads to

$$\frac{d}{dw}\left(\frac{w}{\rho}\psi_w\right) = \frac{w}{\rho}\left(\frac{1}{a^2} - \frac{1}{w^2}\right)\psi_{\theta\theta} \quad [23]$$

For the adiabatic law, Equation [10], elimination of ρ and a reduces Equation [23] to the form

$$w^2\psi_{ww} + w\,F(w)\,\psi_w + G(w)\,\psi_{\theta\theta} = 0 \quad [24]$$

where

$$\left.\begin{aligned} F(w) &= \frac{\left(1 - \frac{\gamma-3}{2}\frac{w^2}{a_o^2}\right)}{\left(1 - \frac{\gamma-1}{2}\frac{w^2}{a_o^2}\right)}, \\ G(w) &= \frac{\left(1 - \frac{\gamma+1}{2}\frac{w^2}{a_o^2}\right)}{\left(1 - \frac{\gamma-1}{2}\frac{w^2}{a_o^2}\right)} \end{aligned}\right\} \quad [25]$$

Product solutions of Equation [24] of the form

$$\psi = \cos k\theta\, w^k\, Y_k \quad [26]$$

where k is a constant were obtained by Chaplygin who pointed out that by introducing

$$\tau = (\gamma-1)w^2/2a_o^2 \quad [27]$$

and substituting Equation [26] in Equations [24] and [25], one is led to the hypergeometric differential equation for $Y_k(\tau)$ with coefficients which are functions of k and β.

If Equation [1] can be represented by a linear relation between p and $1/\rho$

$$p = A - B/\rho \quad [28]$$

where A and B are (positive) constants, then Equation [24] can be reduced to the Laplace equation in θ and a suitable function of w, $W(w)$, as follows. Equations [3] and [9] now yield

$$dp/d\rho = a^2 = B/\rho^2 \quad [29]$$

$$w^2 = a^2 - C = B/\rho^2 - C \quad [30]$$

where C is an appropriate constant, and one obtains

$$\frac{1}{\rho^2}\left(\frac{w^2}{a^2} - 1\right) = -\frac{C}{B} \quad [31]$$

so that Equation [22] reduces to

$$\left.\begin{aligned} \frac{w}{\rho}\varphi_w &= -\frac{C}{B}\psi_\theta \\ \frac{w}{\rho}\psi_w &= \varphi_\theta \end{aligned}\right\} \quad [32]$$

If now W is introduced by means of

$$dW = \sqrt{\frac{C}{B}}\,\frac{\rho}{w}\,dw \quad [33]$$

then Equation [32] become the Cauchy-Riemann equations in the functions ψ, $\sqrt{B/C}\,\varphi$ in the variables W, θ, so that $\psi + i\sqrt{B/C}\,\varphi$ becomes an analytic function of $W + i\theta$ (or of any analytic function of it) while at the same time Equation [23] reduces to the Laplace equation in W, θ.

Substitution from Equation [30] in Equation [33] leads to

$$W = \sqrt{\frac{C}{B}} \int \frac{\rho}{w}\, dw = \sqrt{C} \int \frac{dw}{w\sqrt{w^2 + C}}$$
$$= -\ln \frac{\sqrt{C} + \sqrt{w^2 + C}}{w} + K \quad \ldots\ldots [34]$$

where K is a constant.

It is also convenient to introduce the complex variable

$$\zeta = r\, e^{i\theta} = e^{W + i\theta} \quad \ldots\ldots [35]$$

where

$$r = e^{W} \quad \ldots\ldots [36]$$

The explicit relation between r and w is given by

$$r = K' \frac{w}{\sqrt{C} + \sqrt{w^2 + C}} = \frac{K'(\sqrt{w^2 + C} - \sqrt{C})}{w} \quad \ldots\ldots [37]$$

where K' is a constant. The lines θ = constant in the hodograph plane are transformed into the same lines in the ζ-plane. The radial distance $|\zeta| = r$ is a function of W, or w, only. Multiplying $\psi + i\sqrt{B/C}\,\varphi$ by i, we put

$$-\sqrt{\frac{B}{C}}\,\varphi + i\,\psi = f(\zeta) \quad \ldots\ldots [38]$$

thus identifying ψ with the imaginary part of $f(\zeta)$ in Equation [38].

It is of interest to note from Equation [38] that φ, ψ are *not* conjugate harmonics.

After φ, ψ have been determined in the hodograph plane, one must solve for the flow in the physical plane. Equations [15] yield

$$dz = dx + i\, dy = \frac{e^{i\theta}}{w}(d\varphi + i\, d\psi/\rho) \quad \ldots\ldots [39]$$

In case Equation [28] holds, utilizing Equations [30], [37], and [38], one reduces the above to

$$dz = \frac{e^{i\theta}}{w}\left[-\sqrt{\frac{C}{B}}\, Re(df) + i\sqrt{\frac{w^2 + C}{B}}\, Im(df)\right]$$
$$= \frac{1}{2\sqrt{B}}\left[\zeta df/K' - K'\, d\bar{f}/\bar{\zeta}\right] \quad \ldots\ldots [40]$$

where bars denote conjugates.

3 Polygonal Approximation to the Adiabatic in the $(p,\ 1/\rho)$-Plane

If the adiabatic relation, Equation [10] is approximated by means of *several* straight lines in the $(p,\ 1/\rho)$-plane

$$\left.\begin{aligned} p &= A_i - B_i/\rho \\ \rho_{i-1} &< \rho < \rho_i \end{aligned}\right\} \quad \ldots\ldots [41]$$

then relations, Equation [30], with proper values of B_i, C_i hold in each interval. At the transition points ρ_i, w takes on values w_i, yielding circles in the hodograph plane. There the sound velocity a is *discontinuous*, and one obtains from Equation [9], noting that $w = 0$ for $\rho = \rho_o$,

$$\left.\begin{aligned} C_1 &= B_1 \\ C_{i+1} - C_i &= (B_{i+1} - B_i)/\rho_i^2 = -\Delta(a^2) \end{aligned}\right\} \quad \ldots\ldots [42]$$

It is convenient to choose the constants K_i in Equation [34] so that the values of W join on continuously, and similarly for the r-values in Equation [37], so that one may consider a single $(W,\ \theta)$-plane and a single ζ-plane in which the vertices p_i, ρ_i correspond to the straight lines W_i, and to circles r_i, respectively.

The Equations [19] and [22] were obtained by making dx, dy perfect differentials, so that the integrals $\int dx$, $\int dy$ derived from Equation [17] are independent of the path of integration and yield x, y as true point functions of w, θ. At $w = w_i$ the independence of these integrals of the path of integration must be examined separately. Here we must make x_θ, y_θ continuous. Now from Equation [17] one obtains

$$\left.\begin{aligned} x_\theta &= \frac{\cos\theta}{w}\varphi_\theta - \frac{\sin\theta}{\rho w}\psi_\theta \\ y_\theta &= \frac{\sin\theta}{w}\varphi_\theta + \frac{\cos\theta}{\rho w}\psi_\theta \end{aligned}\right\} \quad \ldots\ldots [43]$$

The determinant of φ_θ, φ_θ in Equations [43] is equal to $1/\rho w^2$, and it, along with the coefficients of φ_θ, ψ_θ, is continuous at w_i. Hence φ_θ, ψ_θ themselves are continuous across $w = w_i$, and so are φ, ψ. It follows now from Equations [32] for each w-interval that ψ_w, $B_i/C_i\ \varphi_w$ are continuous at $w = w_i$. From the continuity of $\psi_w = \partial\psi/\partial w$ and from Equation [33], follows that $\psi_w = \partial\psi/\delta W$ is discontinuous at $W = W_i$ and that

$$\sqrt{\frac{C_i}{B_i}}\left.\frac{\partial\psi}{\partial W}\right|_{W_i^-} = \sqrt{\frac{C_{i+1}}{B_{i+1}}}\left.\frac{\partial\psi}{\partial W}\right|_{W_i^+} \quad \ldots\ldots [44]$$

the subscripts W_i^-, W_i^+ in Equation [44] referring to left-hand and right-hand derivatives at $W = W_i$ respectively. We shall put Equation [44] in the form

$$\left.\begin{aligned} \left.\frac{\partial\psi}{\partial W}\right|_{W_i^+} &= c_i \left.\frac{\partial\psi}{\partial W}\right|_{W_i^-} \\ c_i &= \sqrt{\frac{B_{i+1}\, C_i}{C_{i+1}\, B_i}} \end{aligned}\right\} \quad \ldots\ldots [45]$$

In terms of r this condition becomes

$$\left.\frac{\partial\psi}{\partial r}\right|_{r_i^+} = c_i \left.\frac{\partial\psi}{\partial r}\right|_{r_i^-} \quad \ldots\ldots [46]$$

Similarly, one obtains from the continuity of ψ, ψ_θ,

$$\left.\frac{\partial\varphi}{\partial W}\right|_{W_i^+} = \frac{1}{c_i}\left.\frac{\partial\varphi}{\partial W}\right|_{W_i^-} \quad \ldots\ldots [47]$$

$$\left.\frac{\partial\varphi}{\partial r}\right|_{r_i^+} = \frac{1}{c_i}\left.\frac{\partial\varphi}{\partial r}\right|_{r_i^-} \quad \ldots\ldots [48]$$

The ratio of the slopes $\partial\psi/\partial r$ at r_i is the reciprocal of dr/dw at the same r_i-values. Thus on the hodograph plane $\partial\psi/\partial w$ is continuous, while on the ζ-plane, $\partial\psi/\partial r$ is discontinuous at r_i.

The polygonal approximations, Equations [41], to the adiabatic Equation [10] may be viewed in two different ways. One way is to suppose that just enough heat is supplied to or taken away from the gas as it expands so that it obeys Equation [41]; or else one may imagine the existence of a fictitious gas for which the adiabatic reduces to Equation [41]. In either case the velocity of sound is discontinuous at ρ_i.

As an example, Fig. 1 shows in the $(p,\ 1/\rho)$-plane the adiabatic relation, Equation [10], over the range $1 < \rho_o/\rho < 1.6$, a three-interval approximation to it, with $\rho_1/\rho_o = 1.2$, $\rho_2/\rho_o = 1.4$, as well as the Chaplygin approximation. The functions are replotted on Fig. 2 in the $(p,\ \rho)$-plane. It will be noted in Fig. 2 that the slope $a^2 = dp/d\rho$ *increases* with p and ρ along the adiabatic, but *decreases* as ρ increases along the approximating hyperbolic segments; however, at each vertex ρ_i the change of slope a^2 makes up for accumulated divergence between the a^2 values throughout the interval. Fig. 3 shows w^2, a^2, M^2 plotted versus $1/\rho^2$; the dotted curves give the same quantities for the adiabatic

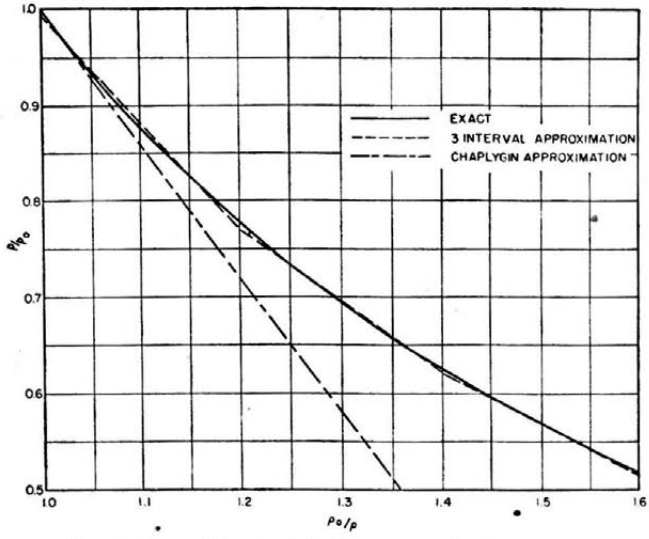

FIG. 1 THE p VERSUS $1/\rho$ CURVE AND ITS APPROXIMATIONS

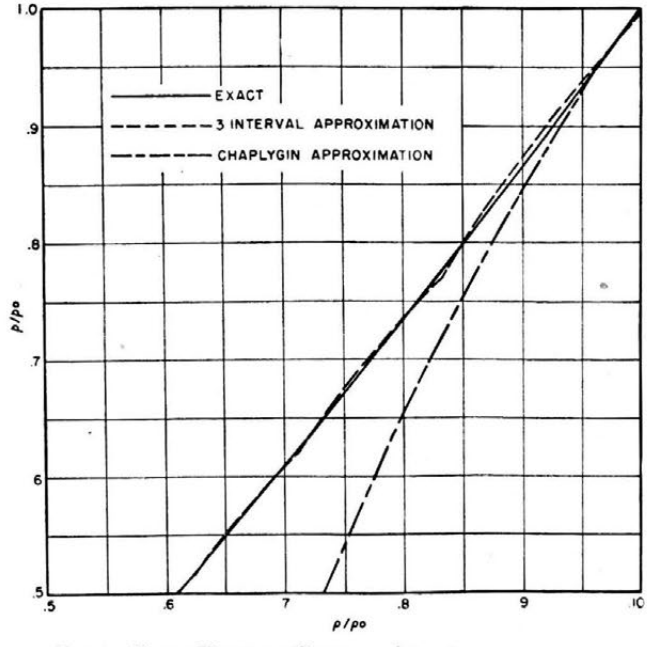

FIG. 2 THE p VERSUS ρ CURVE AND ITS APPROXIMATIONS

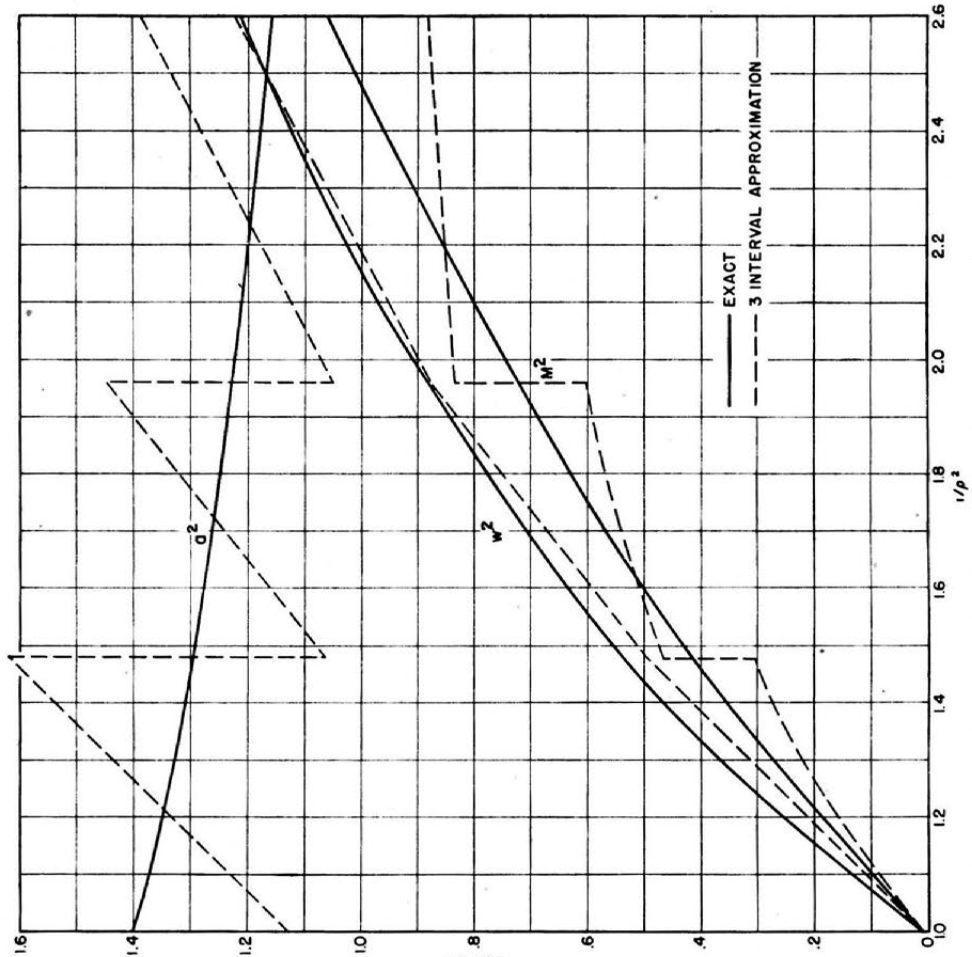

FIG. 3 THE CURVES q^2, w^2, M^2, AND THEIR THREE-INTERVAL APPROXIMATIONS

Equation [10] (for $\gamma = 1.4$). In the calculations leading to the curves of Figs. 1 and 2 and the figures that follow, it is assumed that $p_o = 1$, $\rho_o = 1$. This is not a serious restriction since by a choice of units any values of p_o, ρ_o can be reduced to this case. The reader who is irked by this procedure, however, will prefer to replace w^2 by $w^2\rho_o/p_o = \gamma w^2/a_o^2$, and a^2 by $a^2\rho_o/p_o = \gamma a^2/a_o^2$.

On account of its discontinuities and the gaps in its values, the Mach number M is obviously not a suitable variable to use in the polygonal approximation method.

Elimination of ρ, a from Equation [23] under the assumption of Equation [41] leads to Equation [24] but with F, G given not by Equation [25] but by

$$\left.\begin{aligned} F(w) &= 1 + \frac{w^2}{w^2 + c_i} \\ G(w) &= \frac{c_i}{w^2 + c_i}, \\ w_{i-1} &< w < w_i \end{aligned}\right\} \quad \ldots\ldots\ldots\ldots [49]$$

The values of F, G from Equations [25] and [49] are plotted on Fig. 4 for the example of Fig. 1 and 2. Also shown on Fig. 4 are the values of F, G based on Chaplygin's approximation.

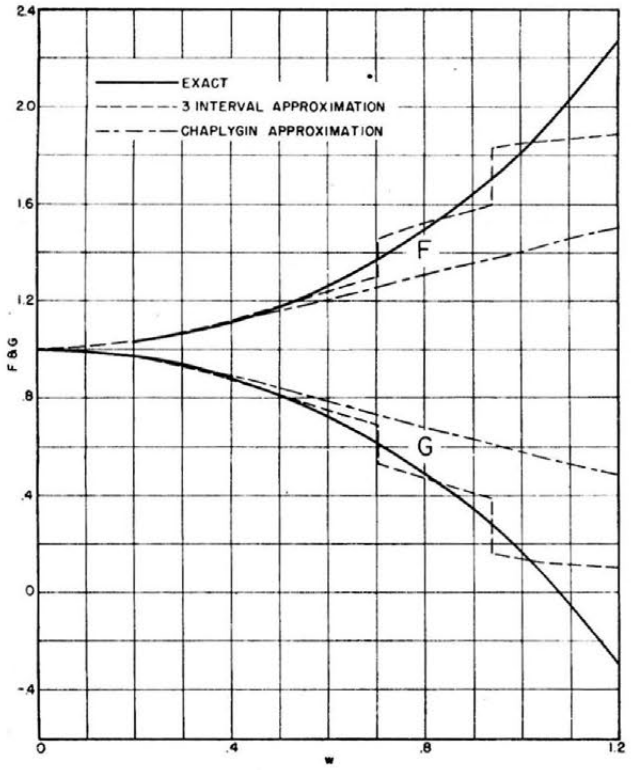

FIG. 4 THE COEFFICIENT F AND G OF CHAPLYGIN'S DIFFERENTIAL EQUATION AND THEIR APPROXIMATIONS

The present method may thus be viewed as consisting in approximating to the coefficients F, G, Equation [25] in Equation [24], by means of Equation [49], this choice of the approximations having the advantage that Equation [24] becomes Laplace equation in W, θ. At w_i the solutions ψ of Equation [24] are continuous and so are $\partial\psi/\partial w$.

The discrepancies in F, G on Fig. 4, deriving from the slopes on Fig. 2, are quite appreciable. To study the discrepancies of the solutions, a product type of solution

$$\psi = wY_1(\tau)\cos\theta \quad \ldots\ldots\ldots\ldots [50]$$

of the exact Equations [24] and [25] was compared with a corresponding solution

$$\left.\begin{aligned} \psi &= R\cos\theta \\ R &= \text{function of } w = R(r) \end{aligned}\right\} \quad \ldots\ldots\ldots\ldots [51]$$

of Equations [24] and [49] choosing $R = 0$, $dR/dr = 1$ at $r = 0$ so that R agrees with wY in value and slope at $r = 0$. Since $R\cos\theta$ is harmonic in the ζ-plane, it follows that the factor R in Equation [51] is a linear combination of r and $1/r$ in each interval (r_i, r_{i+1}). In the first interval the coefficient of $1/r$ is chosen as 0, and in passing from one interval to the next one the new coefficients are determined so as to render R continuous and so that Equation [51] satisfies the condition, Equation [46].

Table I gives the values of wY_1, of R_3, the function R for the three-interval approximation of Fig. 1, and of R_C, the function R for the Chaplygin approximation. Also shown are the differences $R_3 - wY_1$, $R_C - wY_1$. The values Y_1 were taken from Garrick and Kaplan (2). The Mach number refers to the exact solution. It will be noticed that the discrepancies are far smaller than one would expect on the basis of the differences in F and G. The table was continued into the supersonic interval where the third line segment on Fig. 1 gives a rather poor approximation to the adiabatic; the agreement there, while not as good as for $w < w_3$, is surprisingly good. Since the Chaplygin straight line is tangent to the adiabatic at p_o, $1/\rho_o$, the discrepancy close to $w = 0$ (and as far as $w = 0.6$) is smaller for the one-interval solution; but for larger w-values the Chaplygin solution becomes much worse.

TABLE 1

M	w	$Q_1 = wY_1$	R_3	R_C	$R_3 - Q_1$	$R_C - Q$
0	0.0000	0.0000	0	0	0	0
0.1	0.11832	0.1180	0.1177	0.1180	—0.0003	0
0.2	0.23575	0.2334	0.2328	0.2335	—0.0006	0.0001
0.3	0.35180	0.3441	0.3428	0.3444	—0.0013	0.0003
0.4	0.46591	0.4481	0.4452	0.4491	—0.0029	0.0010
0.5	0.57736	0.5438	0.5398	0.5466	—0.0040	0.0028
0.55	0.63194	0.5882	0.5840	0.5923	—0.0042	0.0041
0.60	0.68565	0.6300	0.6262	0.6361	—0.0038	0.0061
0.65	0.73854	0.6694	0.6658	0.6779	—0.0036	0.0085
0.70	0.79041	0.7061	0.7019	0.7177	—0.0042	0.0116
0.75	0.84133	0.7403	0.7358	0.7639	—0.0045	0.0236
0.80	0.89127	0.7719	0.7673	0.7916	—0.0046	0.0197
0.85	0.94012	0.8010	0.7963	0.8257	—0.0047	0.0247
0.90	0.98786	0.8275	0.8230	0.8580	—0.0045	0.0305
0.95	1.03456	0.8516	0.8471	0.8887	—0.0045	0.0371
1.00	1.08013	0.8735	0.8692	0.9177	—0.0043	0.0442
1.10	1.16788	0.9105	0.9069	0.9712	—0.0036	0.0607
1.20	1.25108	0.9394	0.9385	1.0200	—0.0009	0.0806
1.30	1.32979	0.9612	0.9656	1.0620	+0.0044	0.1008
1.40	1.40402	0.9769	0.9886	1.1004	0.0117	0.1235

4 SOLUTIONS BY THE METHOD OF REFLECTIONS

The product solution method for the determination of ψ was explained in (1) and utilized in Table 1. Another method, the method of reflections or images, is based on the following proposition.

Let $h(W, \theta)$ be an arbitrary harmonic function. Then either

$$\left.\begin{aligned} u &= h(W, \theta) + \frac{1 - c_i}{1 + c_i} h(2W_i - W, \theta) \text{ in } W > W_i, \\ u &= \frac{2}{1 + c_i} = h(W, \theta) \text{ in } W < W_i, \end{aligned}\right\} \quad \ldots [52]$$

or

$$\left.\begin{aligned} u &= h(W, \theta) + \frac{c_i - 1}{c_i + 1} h(2W_i - W, \theta) \text{ in } W < W_i, \\ u &= \frac{2c_i}{1 + c_i} h(W, \theta) \text{ in } W > W_i, \end{aligned}\right\} \quad \ldots [53]$$

furnishes a function u satisfying the boundary condition Equation [45] at $W = W_i$. Equation [52] is useful in finding a func-

tion u having the same singularity as h (for instance, that of a point source or vortex) in $W > W_i$ and satisfying Equation [45], while Equation [53] furnishes a function u satisfying Equation [45] and possessing the same singularities as h in $W < W_i$.

In applying the above to cases with several discontinuities, one runs into the difficulty of obtaining images of images. Thus consider the case of three-interval approximations with two lines of discontinuity at W_1, W_2, and assume that h has a singularity at the point $W = B$ lying between W_1, W_2. There is no loss in generality in assuming $W_1 = 0$. This may be accomplished by proper choice of K_1 in Equation [37]. We also put $W_2 = C$.[6]

Application of Equation [52] at $W_1 = 0$ shows that Equation [45] will be satisfied by the addition to h of

$$h_{-1} = \frac{1 - c_1}{1 + c_1} h(-W, \theta) \quad [54]$$

This term possesses a singularity at $W = B_{-1} = -B_1$, the image of B in $W = 0$, of "strength"

$$R_1 = \frac{1 - c_1}{1 + c_1} \quad [55]$$

Similarly, application of Equation [53] with W_2 replaced by C shows that to satisfy Equation [45] one may add to h

$$h_1 = \frac{c_2 - 1}{c_2 + 1} h(2C - W, \theta) \quad [56]$$

thus placing a singularity at $W = B_1 = 2C - B$, the image of B in $W = C$, of "strength"

$$R_2 = \frac{c_2 - 1}{c_2 + 1} \quad [57]$$

It will be found that the addition of Equation [56] now spoils the condition Equation [45] over $W = 0$, and it is necessary to add another term, namely

$$h_{-2} = R_1 h_1(-W, \theta) = R_1 R_2 h(W - 2C, \theta) \quad [58]$$

to restore this condition; this term is singular at $W = B_{-2} = B - 2C$, the image of B_1 in $W = 0$. Likewise, the addition of h_{-1} as well as of h_{-2} in no way helps the boundary condition Equation 45 at $W = C$, and additional terms are required to restore this condition. This process can clearly be continued leading to further singularities over a periodic array of points B_n which are the successive images of B in the two rectilinear boundaries, $W = 0$, $W = C$ (see Fig. 5). The position of these points is analogous to what one observes in a room with two parallel mirrors on opposite walls. Upon looking into either one, one sees one's own successive reflections extending into infinity and obtained by reflections back and forth across each mirror. Moreover, the intensity of each reflection is obtained from the image which is being reflected by multiplication by a proper "coefficient of reflection," which in the present case is equal to R_1 for reflection over the left-hand mirror $W = 0$, and R_2 for reflection across the right-hand mirror. There results the following infinite series

$$\psi = \sum_{n=-\infty}^{+\infty} h_n(W, \theta) \text{ for } 0 < W < C \quad [59]$$

where

$$\left.\begin{aligned} h_0(W, \theta) &= h(W, \theta) \\ h_{-n}(W, \theta) &= R_1 h_{n-1}(-W, \theta) \text{ for } n > 0 \\ h_n(W, \theta) &= R_2 h_{1-n}(2C - W, \theta) \text{ for } n > 0 \end{aligned}\right\} \quad [60]$$

The above infinite series converges provides that both R_1 and R_2 are numerically less than 1 and h does not become infinite "too rapidly" at infinity. The convergence is then as rapid as that of a geometric series.

It must be clearly understood that the series indicated by Equations [59] apply *only* in the strip $0 < W < C$ in Fig. 5 within which the singularity B lies. While the series indicated by Equations [59] converge outside of that strip too, it represents the *analytic continuation* of the function ψ within the strip between 0 and C across these boundaries, and *not* the values of ψ in these regions. Going back to the mirror analogy, Equation [59] for $W < 0$ or $W > C$ corresponds to the fictitious world of images observed in the mirror, and not at all to what is behind the looking glass. The true values of ψ in $W < 0$ or $W > C$ are not the analytic continuations of ψ which are continuous along with all of their derivatives across the boundaries $W = 0$, $W = C$, but functions which join on to these in the manner described by the boundary condition Equation [45] and the continuity of ψ itself. Within the region $W < 0$ application of the second Equation [52] shows that function ψ can be obtained by multiplying all the terms $n \geq 0$ in Equation [59] with singularities in $W > 0$, that is, at B, B_1, $B_2 \ldots$, by the factor $1 + R_1$. In this way there results the infinite series

$$\psi = \frac{2}{1 + c_1} \sum_{n=0}^{\infty} h_n(W, \theta) \quad [61]$$

for $W < 0$. Similarly, one obtains from Equations [53] and [59]

$$\psi = \frac{2c_2}{1 + c_2} \sum_{n=0}^{-\infty} h_n(W, \theta) \quad [62]$$

for $W > C$. Thus ψ is actually free from singularities except at B.

Introducing ζ as in Equation [38], one replaces the lines $W = 0$, $W = C$ by the circles $r = r_1 = 1$, $r = r_2 = e^C$, while the singular points B_n are transformed into

$$b_n = e^{B_n} \quad [63]$$

so that

$$\ldots, b_{-1} = 1/b_0, b_0 = b = e^B, b_1 = e^{2C}/b_0, b_2 = be^{2C}, \ldots \quad [64]$$

The reflections across $W = 0$, $W = C$ now correspond to inversions across the circles $r = 1$, $r = r_2 = e^C$. An additional singularity at $\zeta = 0$ corresponding to $W = -\infty$ may now appear, unless special provisions are made to eliminate it.

In practice it may be convenient to use the series, Equation [61] or Equation [62] for computing ψ in the range $0 < W < C$. This is done for Equation [62] by identifying ψ in Equation [62] with u in the second Equation [53], solving for h and substituting in the first Equation [53].

The nature of Equations [59] through [63] can be clarified by means of Fig. 6 which is based on the optical analogy mentioned

[6] Not to be confused with C in Equations [30] to [34].

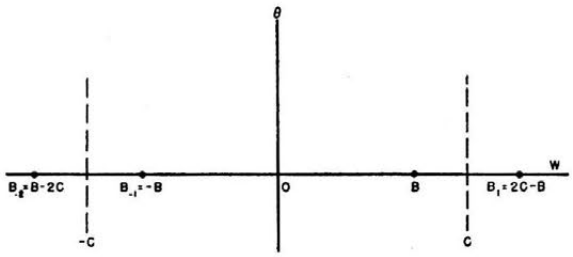

FIG. 5 REFLECTION OF SINGULARITY, W, θ-PLANE

above, but with the mirrors made "semitransparent." The terms in the series Equations [59] through [63] are represented by rays which start from the point B of Fig. 6 at a fixed angle with the horizontal and are reflected and transmitted at the boundaries W_1 and W_2 with reflection coefficients R_1, R_2 given by Equations [55] and [56] and transmission coefficients

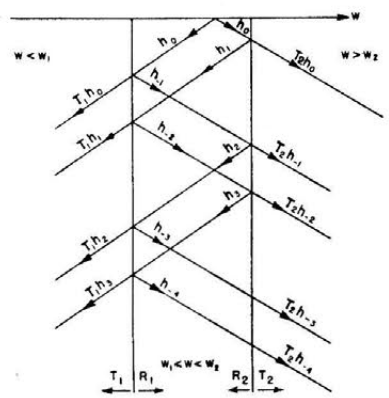

FIG. 6 REFLECTION RAY ANALOGY FOR FINDING IMAGES OF SINGULARITIES FOR THE CASE OF THREE RECTILINEAR INTERVALS

$$\left.\begin{aligned} T_1 &= 1 + R_1 \\ T_2 &= 1 + R_2 \end{aligned}\right\} \quad \ldots\ldots\ldots\ldots\ldots\ldots [65]$$

The transmitted rays T_1h_1, T_1h_2, . . . can be visualized as originating from the source points B_1, B_2, . . . on the W-axis, the transmitted rays T_2h_{-1}, T_2h_{-2}, . . . as originating from the source points B_{-1}, B_{-2}, ...

The optical analogy method is equally applicable to the case of more than three intervals. The case of five intervals is represented in Fig. 7. One now introduces reflection and transmission coefficients R_i, T_i for rays striking W_i from the left, R_i', T_i' for rays striking W_1 from the right, where

$$\left.\begin{aligned} R_i' &= \frac{1 - c_i}{1 + c_i} \\ T_i' &= \frac{2}{1 + c_i} = 1 + R_i' \\ R_i &= \frac{c_i - 1}{c_i + 1} = -R_i' \\ T_i &= \frac{2c_i}{c_i + 1} = 1 + R_i \end{aligned}\right\} \quad \ldots\ldots\ldots\ldots [66]$$

c_i being defined by Equation [45]. Corresponding to each ray segment there is a term obtained by multiplying the function

$$h(\ldots, \theta) \ldots\ldots\ldots\ldots\ldots\ldots\ldots [67]$$

by the coefficient placed on the ray, where the first argument is obtained by replacing W by $2W_i - W$ corresponding to *each* reflection the ray suffered on its way from B. (Transmissions do not affect the first argument in Equation [67].

The increased complexity due to the multiple boundaries as the number of intervals increases is partly compensated for by the decreased magnitudes of R_i, R_i'.

It is to be kept in mind that even in relatively simple flows in the physical plane, the function ψ may be mutliple-valued in the hodograph plane. Since in the solutions indicated above h is not restricted to single-valued functions, these solutions are applicable even to the multiple-valued cases.

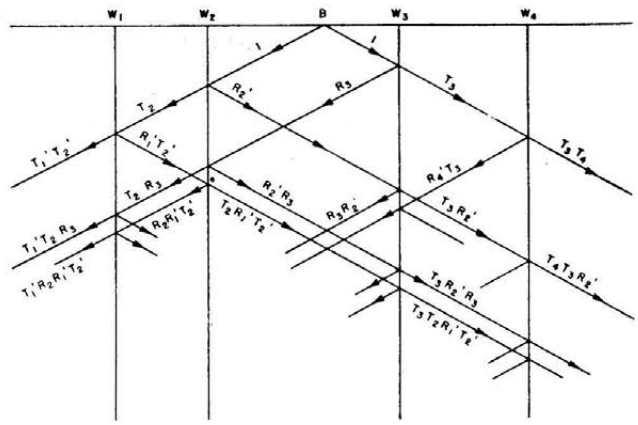

FIG. 7 REFLECTION RAY ANALOGY FOR FINDING IMAGES OF SINGULARITIES FOR THE CASE OF FIVE RECTILINEAR INTERVALS

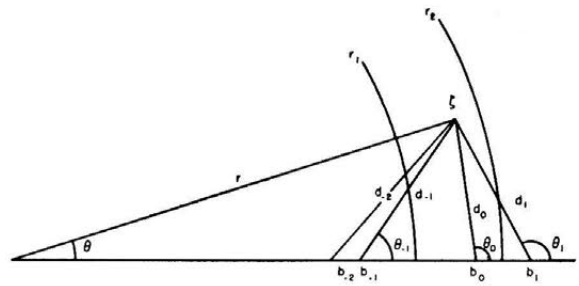

FIG. 8 REFLECTION OF SINGULARITY, r, θ-PLANE

5 EXAMPLE

We apply the method of the preceding paragraph to the flow function ψ which corresponds to a point source at $\zeta = b$, and put

$$h = Im\{\log(\zeta - b_o)\}B = \theta_0 \ldots\ldots\ldots\ldots [68]$$

where θ_0 is the argument of $\zeta - b_o = \zeta - b$, that is, the angle between this complex vector and the real ζ-axis. Inversion of $f(\zeta)$ in the circle $r = R$ is accomplished by replacing ζ by $R^2/\bar{\zeta}$ leading to $f(R^2/\bar{\zeta})$, bars denoting conjugates. For the case $f(\zeta) = \log(\zeta - b)$, this leads to

$$\log(R^2/\bar{\zeta} - b) = \log(\bar{\zeta} - R^2/b) - \log\bar{\zeta} + \log(-b) \ldots [69]$$

With $R = 1$, $R^2/b = 1/b = b_{-1}$, the imaginary part of Equation [69] yields (see Fig. 8)

$$\left.\begin{aligned} &-\theta_{-1} + \theta = \pi \\ &\theta_{-1} = \arg(\zeta - b_{-1}) \\ &\theta = \arg\zeta \end{aligned}\right\} \quad \ldots\ldots\ldots\ldots [70]$$

This leads to

$$h_{-1} = R_1(-\theta_{-1} + \theta) + \text{constant} \ldots\ldots\ldots [71]$$

Similar calculations of h_n for other n yield

$$\psi = \sum_{n=-\infty}^{+\infty} e_n\theta_n - \theta \sum_{n=-1}^{-\infty} e_n - \pi \sum_{n=1}^{+\infty} e_n \ldots\ldots [72]$$

for $r_1 < r < r_2$ where

$$\left.\begin{aligned} \theta_n &= \arg(\zeta - b_n) = Im \log(\zeta - b_n) \\ e_{-1} &= -R_1 \\ e_1 &= -R_2 \\ e_{\pm 2} &= R_1R_2 \\ e_{\pm 3} &= e_{\mp 2}\, e_{\pm 1} = -R_1R_2R_2, \ldots \end{aligned}\right\} \quad \ldots\ldots [73]$$

Inside the (unit) circle $r = r_1$ and outside the circle $r = r_2$ one obtains similarly from Equations [61] and [62]

$$\psi = \pi + \frac{2}{1 + c_1} \sum_{n=0}^{\infty} e_n(\theta_n - \pi) \ldots\ldots\ldots [74]$$

for $r < r_1$

$$\psi = \frac{2c_2}{1 + c_2} \left(\sum_{n=0}^{-\infty} e_n \theta_n - \theta \sum_{n=0}^{-\infty} e_n \right) + \theta \ldots\ldots [75]$$

for $r > r_2$

In choosing the θ-terms and the constant terms in Equations [72], [74], and [75] a slight departure from direct inversion in accordance with Equations [59] and [69] has been made so that without violating Equation [46] the function ψ is made free from singularities at $r = 0$ and vanishes for real $\zeta > b$.

As an example, the flow function ψ was calculated for the case of a point source at $b = b_o = 1.15$ for the (p, ρ)-approximations described in Section 3 of the paper and shown in Figs. 1 and 2. The images of the point source occur at

$b_1 = 1.2861$	$b_{-1} = .8696$
$b_2 = 1.7008$	$b_{-2} = .7776$
$b_3 = 1.9021$	$b_{-3} = .5880$
$b_4 = 2.5155, \ldots$	$b_{-4} = .5257, \ldots$

The coefficients c_1, c_2 are given by

$$c_1 = 1.1388$$
$$c_2 = 1.5633$$

leading to

$$e_{-1} = -R_1 = .06490$$
$$e_1 = -R_2 = -.21975$$

and to

$$e_{-2} = e_2 = -.01426$$
$$e_{-3} = -.00093$$
$$e_3 = .00313,$$
$$e_{-4} = e_4 = .00020, \ldots$$

The Equations [72], [74], and [75] become, with θ_1, ψ expressed in degrees ($\Delta\psi = 360$ deg for unit point source)

$$\psi = 180 \text{ deg} + .9351(\theta_o - 180 \text{ deg}) - .2055(\theta_1 - 180 \text{ deg}) - .0133(\theta_2 - 180 \text{ deg}) + .0029(\theta_3 - 180 \text{ deg}) + .0002(\theta_4 - 180 \text{ deg}) + \ldots,$$

for $0 \leqq r \leqq r_1$,

$$\psi = 41.522 \text{ deg} - .04999 + \theta_o - .2198\theta_1 - .0143\theta_2 + .0031\theta_3 + .0002\theta_4 + \ldots + .0649\theta_{-1} - .0143\theta_{-2} - .0009\theta_{-3} + .0002\theta_4 + \ldots,$$

$r_1 \leqq r \leqq r_2$,

$$\psi = -.2806\theta + 1.2198\theta_o + .0792\theta_{-1} - .0174\theta_{-2} - .0011\theta_{-3} + .0002\theta_{-4} + \ldots,$$

$r \geqq r_2$.

The plot of the curves $\psi =$ constant in the $\zeta = re^{i\theta}$ plane is shown in Fig. 9 for $\psi = 0$ deg, 20 deg, 40 deg, . . . Fig. 10 shows the same flow lines but in the hodograph plane.

As a further example, the field of a point vortex was considered. It will be recalled from Equation [38] that the conjugate harmonic of ψ is not a possible flux function (since $-\sqrt{B/C}\,\varphi + i\psi$ is analytic in ζ and not $\varphi + i\psi$). Hence, unlike the incompressible case, the conjugate harmonic of the point source solution will not do for a point vortex. Going back to Equations [59 through [62] we put

$$\left.\begin{aligned} h_o &= Re\,[\log(\zeta - b)] = \log d_o \\ d_o &= |\zeta - b| \end{aligned}\right\} \ldots\ldots\ldots [76]$$

[this identifies $f(\zeta)$ in Equation [38] with $i \log (\zeta - b)$]. Inversion in $r = R$ yields (see Fig. 8)

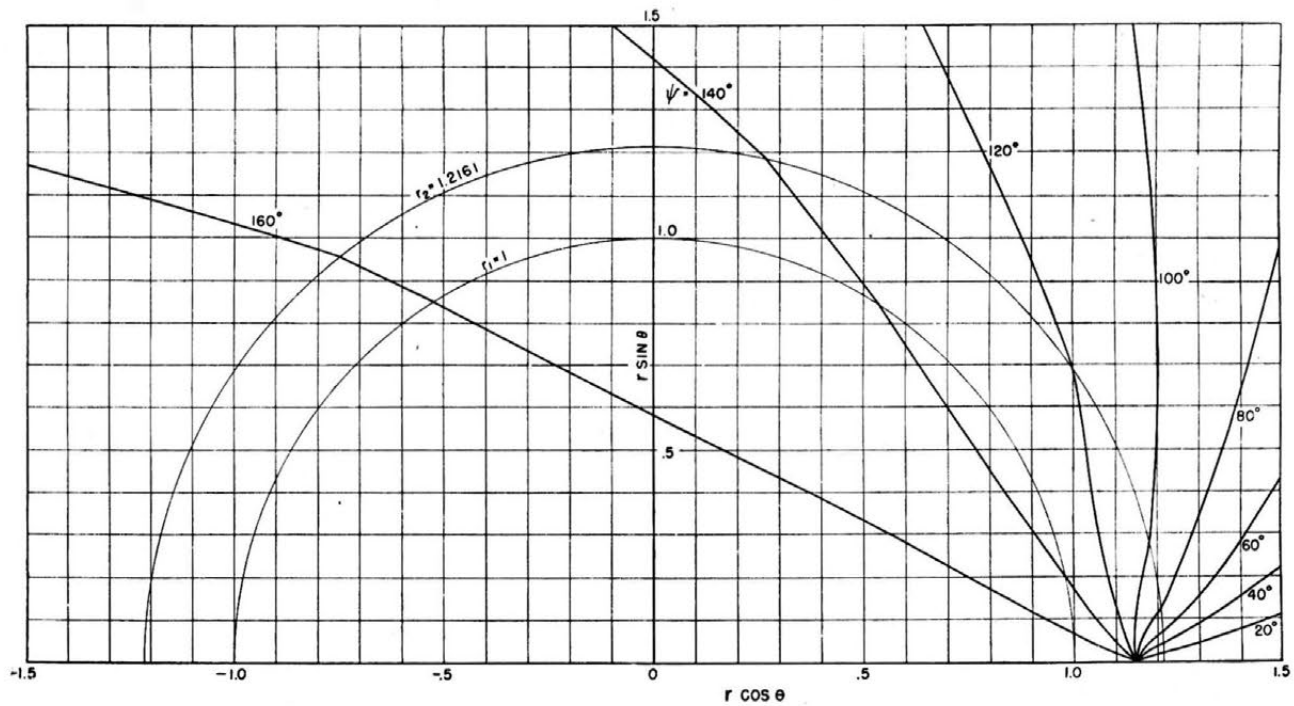

FIG. 9 STREAMLINES $\psi =$ CONSTANT IN THE ζ-PLANE FOR POINT SOURCE AT $r = 1.95$, $\theta = 0$

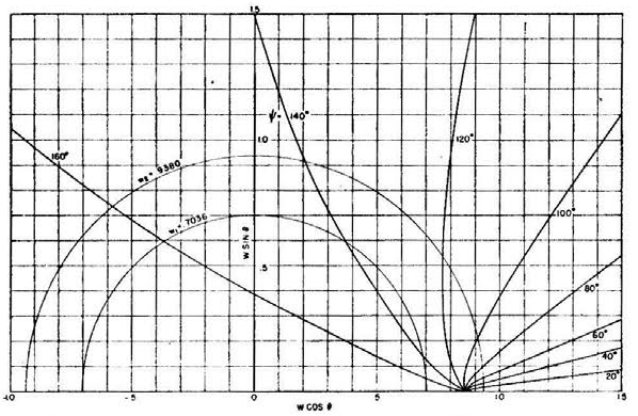

FIG. 10 STREAMLINES ψ = CONSTANT IN THE HODOGRAPH PLANE FOR POINT SOURCE AT $w = .8599$, $\theta = 0$

$$\left.\begin{aligned} &\log(\zeta - b) \longrightarrow \log(R^2/\bar{\zeta} - b) \\ &= \log\left(\bar{\zeta} - \frac{R^2}{b}\right) - \log\bar{\zeta} + \log(-b) \end{aligned}\right\} \quad [77]$$

On applying to $R = 1$ and taking real parts, one obtains

$$\left.\begin{aligned} &\log d_{-1} - \log r + \log b \\ &d_{-1} = \zeta - b_1 \end{aligned}\right\} \quad [78]$$

Comparison with Equations [70] and [71] shows that

$$h_{-1} = R_1(\log d_{-1} - \log r) + \text{constant} \quad [79]$$

Application to Equations [60] through [62] with $h_o = \log r_o$ leads to

$$\psi = \frac{2}{1 + c_1}\sum_{n=0}^{+\infty}(-1)^n e_n \log d_n, \quad [80]$$

for $r \leqq r_1 = 1$

$$\psi = \sum_{n=-\infty}^{+\infty}(-1)^n e_n \log d_n - \log r \sum_{n=-1}^{-\infty} e_n(-1)^n + K_1. \quad [81]$$

for $r_1 \leqq r \leqq r_2$,

$$\psi = \frac{2c_2}{1 + c_2}\left[\sum_{n=0}^{\infty}(-1)^n e_n \log d_n\right] + K_2 \log r + K_3 \quad [82]$$

for $r \geqq r_2$.

where the constants K_1, K_2, K_3 are so determined that ψ is continuous at r_1 and r_2, and Equation [46] holds. The latter condition is best applied by means of

$$\int \left.\frac{\partial\psi}{\partial r}\right|_{r_i}^{+} ds = c_i \int \left.\frac{\partial\psi}{\partial r}\right|_{r_i}^{-} ds \quad [83]$$

leading to an equation involving the sum of the coefficients of the logarithms whose argument vanishes inside the circle of integration.

Substitution of the previous values of r_1, r_2, b, e_n, b_n, c_1, c_2 into Equations [80] through [82] leads to the following three series

$$\psi = .9351 \log d_o + .2055 \log d_1 - .0133 \log d_2 - .0029 d_3 + .0002 \log d_4 + \ldots,$$

for $r \leqq r_1$,

$$\psi = -.0120 + .0890 \log r + \log d_o + .2198 \log d_1 - .1043 \log d_2 - .0031 \log d_3 + .0002 \log d_4 + \ldots - .0649 \log d_{-1} - .0143 \log d_{-2} + .0009 \log d_{-3} + .0002 \log d_{-4} + \ldots,$$

for $r_1 \leqq r \leqq r_2$,

$$\psi = -.0764 + .4387 \log r + 1.2198 \log d_o - .0792 \log d_{-1} - .0174 \log d_{-2} + .0011 \log d_{-3} + .0002 \log d_{-4} + \ldots,$$

for $r \geqq r_2$.

The flow lines for the above ψ are plotted on Fig. 11 for $\psi = 0, \pm .2, \pm .4, \ldots$. On Fig. 12 the aspect of the same flow lines in the hodograph plane is given.

It must be kept in mind that the examples just discussed, while they possess the required point-source singularity, are *not unique* solutions. It is clear that any solution which is free from singularities in the regions under consideration may be added to the above.

It is believed that the method outlined above is far more convenient from computational point of view than other methods that have been developed for handling these flows, for instance, the one given in (3).

6 DETERMINATION OF THE FLOW IN THE PHYSICAL PLANE

The point-source and the point-vortex solutions are of interest in connection with the flow through a grid of similar blades, the entering flow at infinity corresponding to a point source and a point vortex; the exit flow at infinity corresponding to a point sink and vortex. It is clear, however, that further functions ψ would have to be added to the above solutions to obtain blade shapes of practical interest. Nevertheless, it is of interest to find the aspect of the physical flow arising from a pure point vortex-source and a point vortex-sink. This can be determined by superposition of the above solutions and carrying out the integrations Equation [40]. For the present, however, this calculation was carried out only for the incompressible case for which the above equations simplify considerably.

For the incompressible case, the variable ζ may be directly identified with the hodograph variable

$$\zeta = w e^{i\theta} = u + iv \quad [84]$$

From Equation [38] it follows that the complex potential

$$\omega = \varphi - i\psi/\rho_o \quad [85]$$

is an analytic function of ζ

$$\omega = f(\zeta) \quad [86]$$

Since

$$\frac{d\omega}{dz} = \frac{\partial\omega}{\partial x} = \frac{\partial\varphi}{\partial x} - \frac{i}{\rho_o}\frac{\partial\psi}{\partial x} = u + iv = \zeta \quad [87]$$

we have

$$z = \int dz = \int \frac{d\omega}{\zeta} \quad [88]$$

Placing the point source and the point vortex, each of unit strength, at the point $\zeta = 1 + i$ and the point sink and the point vortex of similar strength at the point $\zeta = 1 - i$, we have

$$\left.\begin{aligned} \omega &= A \log(\zeta - a) + B \log(\zeta - b) \\ A &= 1 + i \\ B &= -1 + i \\ a &= 1 + i \\ b &= 1 - i \end{aligned}\right\} \quad [89]$$

The integration of Equation [88] yields

$$z = A \int \frac{d\zeta}{\zeta(\zeta - a)} + B \int \frac{d\zeta}{\zeta(\zeta - b)}$$

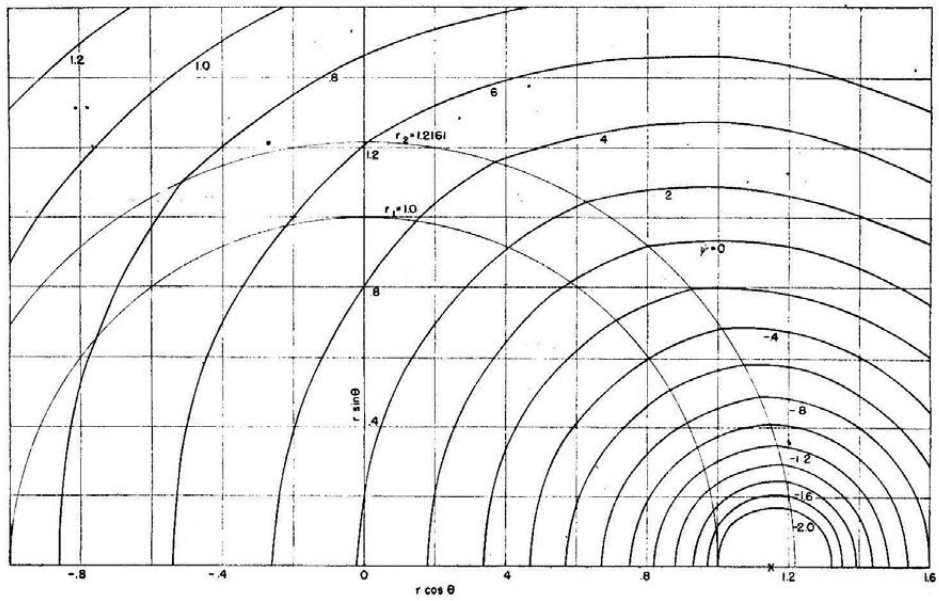

FIG. 11 STREAMLINES ψ = CONSTANT IN THE ζ-PLANE FOR POINT VORTEX AT $r = 1.15, \theta = 0$

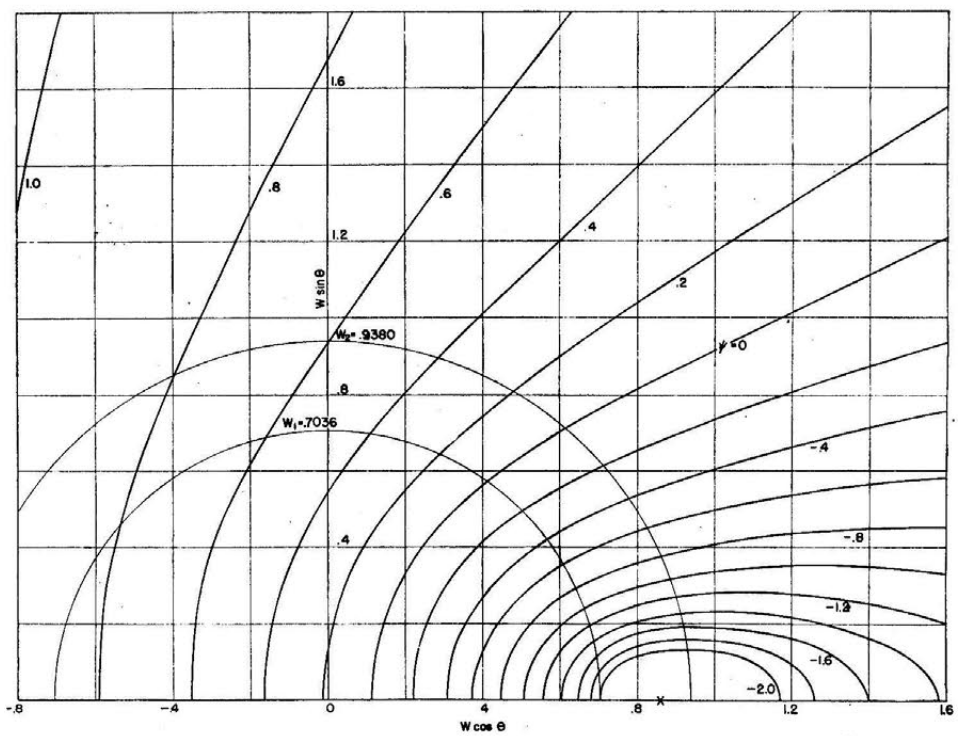

FIG. 12 STREAMLINES ψ = CONSTANT IN THE HODOGRAPH PLANE FOR POINT VORTEX AT $w = 0.8599, \theta = 0$

$$= \frac{A}{a}[-\log\zeta + \log(\zeta - a)] + \frac{B}{b}[-\log\zeta + \log(\zeta - b)] \quad \ldots\ldots [90]$$

For the values indicated in Equation [89] this reduces to

$$\omega = (1 + i)\log(\zeta - a) + (-1 + i)\log(\zeta - b) \ldots [91]$$

$$z = \log(\zeta - a) - \log(\zeta - b) \ldots\ldots [92]$$

The lines of flow in the hodograph were first obtained by superposition of the rectilinear flow lines corresponding to the point source and the circular flow lines corresponding to the point vortex leading to equiangular spirals passing through diagonally opposite corners of the resulting small squares formed by the above radial lines and circles. After the above logarithmic spirals have been constructed around the point $\zeta = 1 + i$, a similar set was obtained for the $\zeta = 1 - i$ as indicated in Fig. 13, and by superposition the streamlines of Fig. 14 were obtained. Finally, by substituting the values of ζ for these flow lines into Equation [92] the flow lines in the physical plane were found. These are shown on Fig. 15.

It will be noted from Equation [92] that the integration lead-

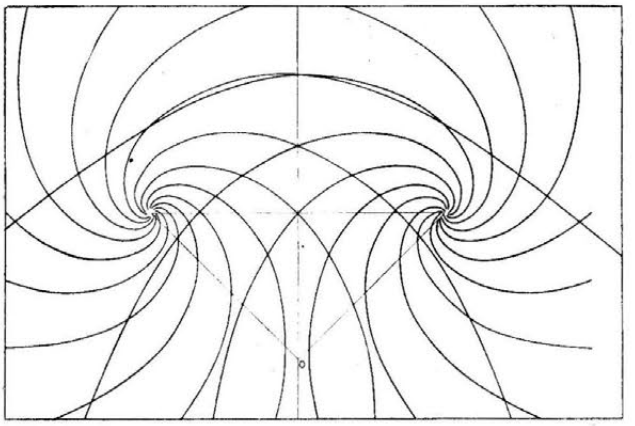

FIG. 13 STREAMLINES ψ = CONSTANT FOR A POINT VORTEX SOURCE AT $\zeta = 1 + i$; ALSO FOR A POINT VORTEX SINK AT $\zeta = 1 - i$. INCOMPRESSIBLE CASE.

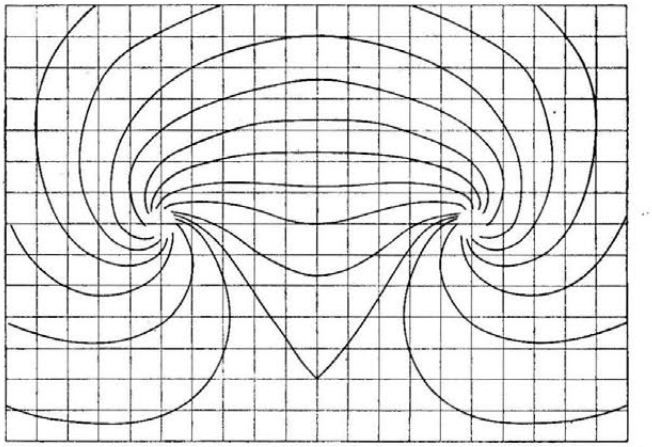

FIG. 14 STREAMLINES ψ = CONSTANT OBTAINED BY SUPERPOSITION OF THE STREAMLINES OF FIG. 13. INCOMPRESSIBLE CASE

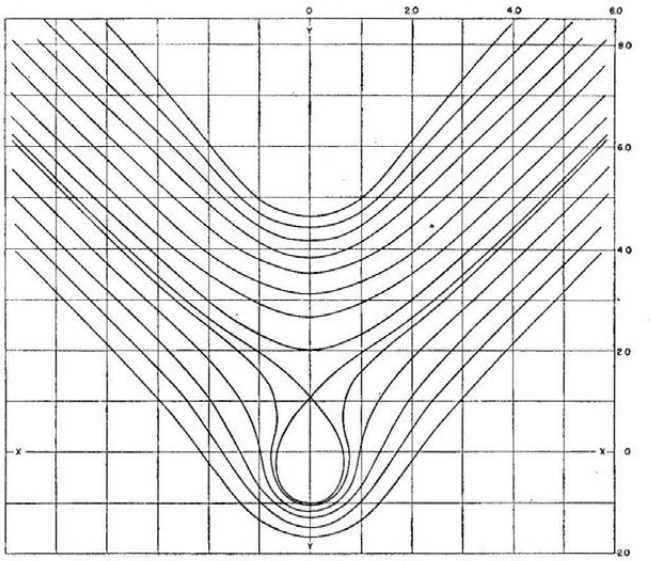

FIG. 15 STREAMLINES ψ = CONSTANT IN PHYSICAL PLANE CORRESPONDING TO FIG. 14

ing from the hodograph to the physical plane possesses no singularity at the origin $\zeta = 0$ as might ordinarily be expected from Equation [88]. The resulting flow is smooth and analytic in the whole physical plane, and corresponds to a 90-deg turn of the flow from its incident direction at infinity to its exit direction at infinity.

BIBLIOGRAPHY

1 "An Approximate Method of Integrating the Equations of Compressible Fluid Flow in the Hodograph Plane," by H. Poritsky. Proceedings Sixth International Congress of Applied Mechanics, Paris, France, Sept. 22–29, 1946.

2 "On the Flow of a Compressible Fluid by the Hodograph Method II—Fundamental Set of Particular Flow Solutions of the Chaplygin Differential Equation," by I. E. Garrick and Carl Kaplan, NACA ARR No. L4I29. War Time Report No. L147, November, 1944.

3 "Two-Dimensional Irrotational Mixed Subsonic and Supersonic Flow of a Compressible Fluid and the Upper Critical Mach Number," by H. S. Tsien and Y. H. Kuo, NACA Technical Note 995, May, 1946.

The Shape of a Piston Ring in Its Unrestrained State

By CHE-TYAN CHANG,[1] PHILADELPHIA, PA.

It is the purpose of this paper to develop, with mathematical means, a general equation between the free shape of a piston ring in its unrestrained state and the consequent radial-pressure pattern against the cylinder wall after its installation. It is up to the designer, first to decide upon the proper pressure distribution for his particular need, and then to use such an equation as a first guide to evaluate the proper free shape of the ring so that it will give him the required radial-pressure pattern after its installation in the cylinder.

Nomenclature

The following nomenclature and assumptions are used in this paper:

F = force
F_x = force component along direction of XX-axis
F_y = force component along direction of YY-axis
p = radial pressure; radial pressure tending to close ring is considered to be positive
M = bending moment; bending moment tending to close ring is considered to be positive
M_A = bending moment acting on neutral fiber of ring about an axis at point A and normal to plane of ring (see Fig. 1)
E = modulus of elasticity of piston-ring material
I = moment of inertia
w = face width of ring in its axial direction
R = radius of curvature referring to neutral fiber of ring in its unrestrained state; a variable
r = radius of curvature referring to neutral fiber of ring in its closed state; a constant
ρ = radius of vector
μ = radial deviation of a point on ring in its unrestrained state from its closed state
θ, α = polar angles
n = numerical constant
Z = arbitrary constant
s = shearing force
q = tensile or compressive force

Assumptions:

1 Material of piston ring follows ordinary laws of elasticity.
2 Thickness of ring in radial direction is comparatively small in relation to its diameter.

Introduction

In view of the great popularity of reciprocating-type internal-combustion engines employed today, the important role played by a piston ring either as a gas-sealing device or as an oil-controlling device, does not need to be overemphasized.

Because of the strict requirements imposed upon a ring for its proper functioning in the engine, the manufacturing of piston rings has been developed into a rather specialized business.

More emphasis has been placed on the development of high-strength materials as well as proper free shape of the ring in its unrestrained state than ever before, owing to the relatively high piston speeds adopted during recent years in the high-output aircraft and automotive engines.

It is quite natural to assume that a ring should exert a uniformly distributed radial pressure against the cylinder wall to obtain even wear, both of the ring and the wall. However, due to the presence of the end gap, it can be easily interpreted that the ring is quite similar to two curved cantilever beams joined at the back, opposite to the gap. At the relatively high running speeds of the engine, fluttering of the free ends of the ring frequently occurs if the ring is designed to exert uniform radial pressure against the cylinder wall after its installation. Such fluttering of the free ends of the ring often induces fatigue failure close to the ends.

To prevent such failures, the free ends must necessarily be stiffened. The general practice used today is to control the free shape of the ring in its unrestrained state, so that after being confined in a cylinder, the ring will exert additional radial pressure near the ends. A piston ring possessing such characteristics commonly is defined by the manufacturers as one having a plus "circularity" or an "ovality" value.

It is quite obvious that through the introduction of the additional pressure near the free ends of the ring, additional forces are introduced at the back or at the sides of the ring to balance the force statically. The readjustment of the radial-pressure distribution consequently causes the alteration of the free shape of the ring in its unrestrained state.

The choice of an ideal pressure-distribution pattern is governed by many other factors, such as wear and lubricating properties, engine type and service, piston speed, and so forth; consequently no attempt will be made in this paper to set forth any such ideal pattern.

It is the purpose of this paper to develop, with mathematical means, a general equation between the free shape of the ring in its unrestrained state and the consequent radial-pressure pattern against the cylinder wall after its installation. It is up to the designer, first to decide upon the proper pressure distribution for his particular need, and then to use such an equation as a first guide to evaluate the proper free shape of the ring so that it will give him the required radial-pressure pattern after its installation in the cylinder.

General Equation of Radial Pressure and Bending Moment Acting on a Ring in Its Closed State

In Fig. 1, suppose $ACBB'D$ is a thin piston ring in its closed state, and dF an infinitesimal radial thrust force acting on the ring periphery at point Q, then

$$dF = pwrd\theta \quad [1]$$

[1] Engineering Department, Wilkening Manufacturing Company.

Contributed by the Applied Mechanics Division and presented at the Annual Meeting, New York, N. Y., November 28–December 3, 1948, of The American Society of Mechanical Engineers.

Discussion of this paper should be addressed to the Secretary, ASME, 29 West 39th Street, New York, N. Y., and will be accepted until July 11, 1949, for publication at a later date. Discussion received after the closing date will be returned.

Note: Statements and opinions advanced in papers are to be understood as individual expressions of their authors and not those of the Society. Paper No. 48—A-21.

Resolving its components along the two axes

$$dF_x = dF \cos\theta = pwr \cos\theta \, d\theta \quad \ldots\ldots [2]$$

$$dF_y = dF \sin\theta = pwr \sin\theta \, d\theta \quad \ldots\ldots [3]$$

Applying conditions of static equilibrium in the plane of the ring, the following equations must be satisfied

$$\Sigma \, dM_A = 0 \quad \ldots\ldots [4]$$

$$\Sigma \, dF_y = 0 \quad \ldots\ldots [5]$$

$$\Sigma \, dF_x = 0 \quad \ldots\ldots [6]$$

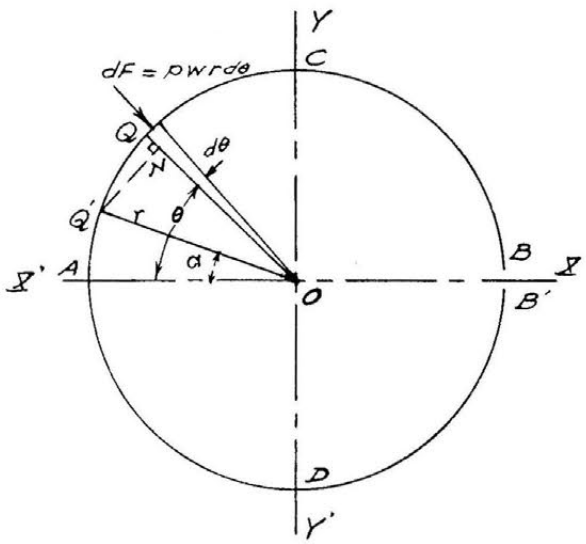

FIG. 1

Since the ring is symmetrical, referring to XX' axis, it is evident that the first two equations of equilibrium are fulfilled. This leaves the last equation to be satisfied, i.e., $\Sigma \, dF_x = 0$.

Since from Equation [2] $dF_x = pwr \cos\theta \, d\theta$, then Equation [6] becomes

$$\int_0^\pi pwr \cos\theta \, d\theta = 0 \quad \ldots\ldots [7]$$

Now Equation [7] will be satisfied, if the pressure intensity p at any point Q on the ring periphery can be expressed by an expression like the following

$$p = p_0 + p_2 \cos 2\theta + p_3 \cos 3\theta + \ldots + p_n \cos n\theta + \ldots [8]$$

Equation [8] obviously is an "even" function of the Fourier expression with the coefficient of the second term in this particular case being zero. (An even function is chosen here because the ring is symmetrical about the axis passing through the gap.)

Quoting Cohen (1):[2] "In treatise of analysis, it is proved that a function which is single-valued, of bounded variation, and has only a finite number of maxima and minima in an interval 2π in length, can be expressed uniquely as a Fourier series."

No matter what the pressure distribution is after the installation of the ring within the cylinder, the foregoing condition is always satisfied, and it can always be expressed in the form of a Fourier series of an even function such as the one expressed in Equation [8].

The mean pressure in such condition will always be p_0, i.e., the first term of Equation [8]; this is because

$$\frac{1}{\pi}\int_0^\pi p_n \cos n\theta d\theta = 0 \quad \ldots\ldots [9]$$

By referring to Fig. 1 again, suppose dM be the infinitesimal bending moment at point Q' due to the infinitesimal radial thrust force dF at point Q, then

$$\left.\begin{aligned} dM &= dF \, \overline{Q'N} \\ &= dF \, \overline{OQ'} \sin(\theta - \alpha) \\ &= dF \, r \sin(\theta - \alpha) \\ &= pwr^2 \sin(\theta - \alpha) \, d\theta \end{aligned}\right\} \quad \ldots\ldots [10]$$

where p is a function of the polar angle.

The resultant bending moment M at any point Q' evidently is produced through the combined effect of all the infinitesimal thrust force dF from point Q' all the way clockwise until reaching the free end B, therefore

$$\left.\begin{aligned} M &= \sum_{Q'}^{B} dM \\ &= \int_\alpha^\pi pwr^2 \sin(\theta - \alpha) \, d\theta \end{aligned}\right\} \quad \ldots\ldots [11]$$

If the ring has a uniform width, then

$$M = wr^2 \int_\alpha^\pi p \sin(\theta - \alpha) \, d\theta \quad \ldots\ldots [12]$$

By the foregoing reasoning, since the pressure intensity p at any point Q' can be expressed by an expression such as Equation [8], then by substituting Equation [8] into Equation [12]

$$\frac{M}{wr^2} = \int_\alpha^\pi p_0 \sin(\theta - \alpha) \, d\theta + \sum_{n=2}^{n=n} \int_\alpha^\pi p_n \cos n\theta \sin(\theta - \alpha) \, d\theta \quad \ldots\ldots [13]$$

The solution of the first term in Equation [13] is

$$p_0 (1 + \cos\alpha)$$

The solution (2) of the term

$$\int_\alpha^\pi p_n \cos n\theta \sin(\theta - \alpha) \, d\theta$$

in Equation [13] is

$$\frac{p_n}{2}\left\{\frac{\cos n\alpha - \cos[(n+1)\pi - \alpha]}{n+1} - \frac{\cos n\alpha - \cos[(n-1)\pi + \alpha]}{n-1}\right\}$$

Therefore Equation [13] finally will be resolved into the following general expression

$$\frac{M}{wr^2} = p_0 (1 + \cos\alpha) + 1/2 \sum_{n=2}^{n=n} p_n \left\{\frac{\cos n\alpha - \cos[(n+1)\pi - \alpha]}{n+1} - \frac{\cos n\alpha - \cos[(n-1)\pi + \alpha]}{n-1}\right\} \quad \ldots\ldots [14]$$

General Equation Between Shape of a Ring in Its Free State and Bending Moment Acting on Ring in Its Closed State

After the general expression of the bending moment M at any point Q is developed, the free shape of the piston ring in its unrestrained state can be determined easily if a definite relation can be found between the bending moment M and the free shape of the ring.

[2] Numbers in parentheses refer to the Bibliography at the end of the paper.

In Fig. 2, if $acbb'd$ be the shape assumed by a piston ring in its free state and $ACBB'D$ be the same ring in its restrained state after being confined in the cylinder, then, if R be the radius of curvature at any point q on the neutral fiber of the ring at its free state, and r be the radius of curvature of the point Q after the ring is installed in a cylinder; point Q in the restrained state is

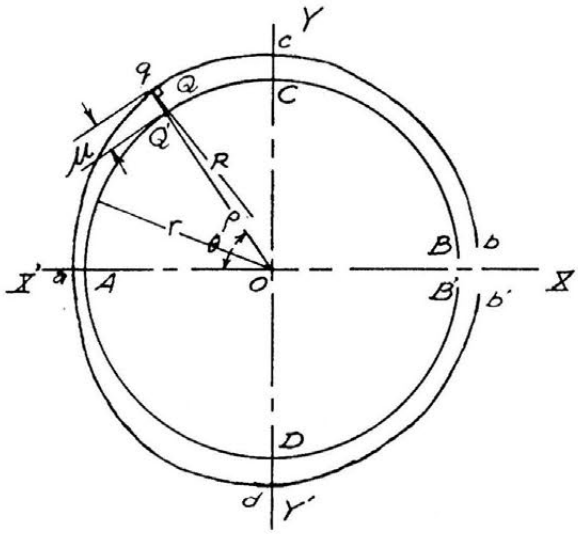

FIG. 2

assumed to take the position of point q on the free curve, since the closed state of the ring is a circle; therefore r is actually a constant along the circumference of the closed ring.

From Fig. 2 evidently

$$\rho = r + \mu \quad \ldots\ldots [15]$$

The relationship between the radius vector ρ at point q and the corresponding radius of curvature R at the same point can be found to be expressed by the following expression, thus (3)

$$\frac{1}{R} = \frac{\rho^2 + 2\left(\frac{d\rho}{d\theta}\right)^2 - \rho\frac{d^2\rho}{d\theta^2}}{\left[\rho^2 + \left(\frac{d\rho}{d\theta}\right)^2\right]^{3/2}} \quad \ldots\ldots [16]$$

Since $(d\rho)/(d\theta)$ in our case is of small magnitude, the second-power terms can be neglected, then

$$\frac{1}{R} = \frac{1}{\rho} - \frac{1}{\rho^2}\frac{d^2\rho}{d\theta^2} \quad \ldots\ldots [17]$$

Differentiating both sides of Equation [15] twice with regard to θ since r is a constant

$$\frac{d^2\rho}{d\theta^2} = \frac{d^2\mu}{d\theta^2} \quad \ldots\ldots [18]$$

We can also write Equation [15] in another way, thus

$$\rho = r\left(1 + \frac{\mu}{r}\right) \quad \ldots\ldots [19]$$

Substituting these expressions into Equation [17]

$$\frac{1}{R} = \frac{1}{r\left(1 + \frac{\mu}{r}\right)} - \frac{1}{r^2\left(1 + \frac{\mu}{r}\right)^2}\frac{d^2\mu}{d\theta^2} \quad \ldots\ldots [20]$$

Since $(\mu/r)^2 < 1$, we can apply the binominal theorem to expand the terms in the preceding equation, after multiplying out all the expanded terms and neglecting all high order of infinitesimals, Equation [20] finally can be reduced to

$$\frac{1}{r} - \frac{1}{R} = \frac{1}{r^2}\left(\mu + \frac{d^2\mu}{d\theta^2}\right) \quad \ldots\ldots [21]$$

From any treatise on elasticity or strength of materials (4), the change of curvature at point q due to the bending moment M acting on the same point is given by the expression

$$\frac{1}{r} - \frac{1}{R} = \frac{M}{EI} \quad \ldots\ldots [22]$$

Combining Equations [21] and [22], finally, we arrive at

$$\mu + \frac{d^2\mu}{d\theta^2} = \frac{Mr^2}{EI} \quad \ldots\ldots [23]$$

Now Equation [23] is a simple linear equation of second order, the complete solution of which is

$$\mu = A\cos\theta + B\sin\theta + \sin\theta\int\frac{Mr^2}{EI}\cos\theta d\theta - \cos\theta\int\frac{Mr^2}{EI}\sin\theta\, d\theta \quad \ldots\ldots [24]$$

where A and B are two constants of integration.

General Equation Between Free Shape of a Ring in Its Unrestrained State and Radial Pressure Acting on Ring in Its Closed State

It can also be shown that through the following treatment a direct relationship between the radial-pressure distribution and the free shape of the ring in its unrestrained state can be expressed mathematically. The evolution of the bending moment in this case is not required as an intermediate step.

Consider an elementary portion of the ring as a free body. After the ring is installed in the cylinder, the system of forces acting on this portion is shown in the accompanying free-body diagram, Fig. 3.

Referring to Fig. 3, applying general principles of static equilibrium of coplanar forces, we can easily arrive at the following three equations

$$pwr\, d\theta = ds + q\, d\theta \quad \ldots\ldots [25]$$

$$s\, d\theta = dq \quad \ldots\ldots [26]$$

$$d\, M = dq\, r \quad \ldots\ldots [27]$$

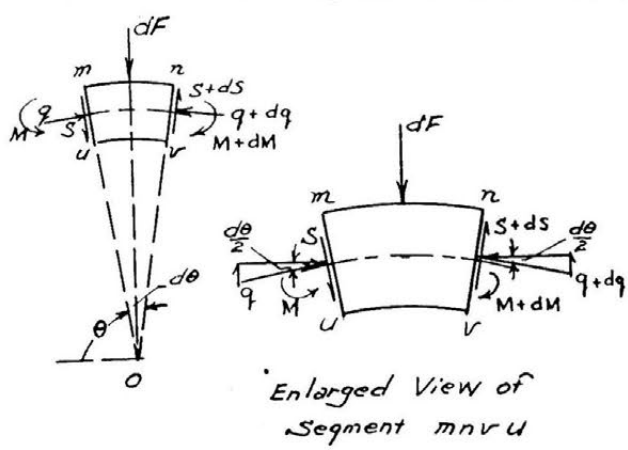

FIG. 3

By rearrangement, these three equations can also be written as

$$p = \frac{1}{wr}\frac{ds}{d\theta} + \frac{1}{wr}q \quad \ldots\ldots [28]$$

$$s = \frac{dq}{d\theta} \quad \ldots\ldots [29]$$

$$\frac{1}{r}\frac{dM}{d\theta} = \frac{dq}{d\theta} \quad \ldots\ldots [30]$$

Differentiate both sides of Equation [29] with regard to angle θ

$$\frac{ds}{d\theta} = \frac{d^2q}{d\theta^2} \quad \ldots\ldots [31]$$

Differentiating both sides of Equation [30] with regard to angle θ

$$\frac{1}{r}\frac{d^2M}{d\theta^2} = \frac{d^2q}{d\theta^2} \quad \ldots\ldots [32]$$

Combining Equations [31] and [32] we have

$$\frac{ds}{d\theta} = \frac{1}{r}\frac{d^2M}{d\theta^2} \quad \ldots\ldots [33]$$

By integrating both sides of Equation [27]

$$M = rq + C \quad \ldots\ldots [34]$$

where C is a constant of integration, at the free end of the ring

$$q = 0 \quad \text{and} \quad M = 0 \quad \text{and so,} \quad C = 0$$

or

$$M = rq \quad \ldots\ldots [35]$$

which is just the same as

$$q = \frac{M}{r} \quad \ldots\ldots [36]$$

Substituting Equations [33] and [36] into Equation [28], we get an equation of the following form

$$p = \frac{1}{wr^2}\left(M + \frac{d^2M}{d\theta^2}\right) \quad \ldots\ldots [37]$$

The solution of Equation [37] evidently will be the same as that given by Equation [14] provided the pressure distribution follows the same pattern.

From Equation [23] we already have a relationship between the free shape of the ring in its unrestrained state and the corresponding bending moment after its installations, which is

$$\mu + \frac{d^2\mu}{d\theta^2} = \frac{Mr^2}{EI}$$

which is the same as

$$M = \frac{EI}{r^2}\left(\mu + \frac{d^2\mu}{d\theta^2}\right) \quad \ldots\ldots [38]$$

By differentiating Equation [38] with regard to angle θ

$$\frac{dM}{d\theta} = \frac{EI}{r^2}\left(\frac{d\mu}{d\theta} + \frac{d^3\mu}{d\theta^3}\right) \quad \ldots\ldots [39]$$

By differentiating Equation [39] again with regard to angle θ

$$\frac{d^2M}{d\theta^2} = \frac{EI}{r^2}\left(\frac{d^2\mu}{d\theta^2} + \frac{d^4\mu}{d\theta^4}\right) \quad \ldots\ldots [40]$$

Substituting Equations [38] and [40] back into Equation [37], finally we arrive at an equation showing the general relationship between the free shape of the ring in its unrestrained state and the corresponding radial pressure expected after its installation in the cylinder; thus

$$p\frac{wr^4}{EI} = \mu + 2\frac{d^2\mu}{d\theta^2} + \frac{d^4\mu}{d\theta^4} \quad \ldots\ldots [41]$$

Equation [41] evidently is a linear equation of the 4th order; the solution of this equation is

$$\frac{EI}{wr^4}\mu = (C_1 + C_2\theta)\cos\theta + (C_3 + C_4\theta)\sin\theta$$
$$- {}^1/_2\,[\cos\theta \int p \sin\theta\, d\theta - \sin\theta \int p\cos\theta\, d\theta]$$
$$- {}^1/_2\,[\cos\theta \int\int p\cos\theta\,(d\theta)^2 + \sin\theta \int\int p\sin\theta\,(d\theta)^2]$$
$$\ldots\ldots [42]$$

where C_1, C_2, C_3, C_4 are four constants of integration. Since we usually select XX' axis in such a way so that it is the axis of symmetry with regard to the two halves of the ring, in that case the values of μ must be the same regardless of the sign of θ; therefore $C_2 = 0$, and $C_3 = 0$. Supposing again, we choose the YY' axis in such a way that the values of μ at $\theta = 0$, and at $\theta = \pi$ be the same, then $C_1 = 0$. Thereby Equation [42] can be reduced to

$$\frac{EI}{wr^4}\mu = C\theta\sin\theta - {}^1/_2\,[\cos\theta \int p\sin\theta\, d\theta - \sin\theta \int p\cos\theta\, d\theta]$$
$$- {}^1/_2\,[\cos\theta \int\int p\cos\theta\,(d\theta)^2 + \sin\theta \int\int p\sin\theta\,(d\theta)^2] \ldots [43]$$

where C evidently is the same as C_4 and can be determined by applying the condition at the free end, namely, at $\theta = \pi$, $M = 0$, or from Equation [38]

$$\left[\mu + \frac{d^2\mu}{d\theta^2}\right]_{\theta=\pi} = 0 \quad \ldots\ldots [44]$$

By its general appearance, Equation [43] does look complicated. On the other hand, we do arrive at the conclusion that if the pressure distribution is definite, i.e., if p is a definite function of θ, then the free shape of the ring in its unrestrained state also is definite and can be determined mathematically.

Illustrative Examples

At this point it seems desirable to introduce some examples to illustrate the general application of Equation [43].

For our purpose of illustrating, we might consider two special cases of pressure distribution: the first is the case of uniform pressure distribution; the other is the case of a pressure distribution of the form $p = p_0(1 + Z\cos 2\theta)$, which represents condition of a ring possessing high tip pressures.

These two cases evidently are special cases of the Fourier expression, Equation [8]; in the first case, we consider the first term only, and in the second case we consider two terms together.

Case 1. Uniform Pressure Distribution. In case the pressure distribution around the periphery of the ring is uniform, all the coefficients in Equation [8] starting from the second term are zero, or $p = p_0$.

Equation [43] then becomes

$$\frac{EI}{wr^4}\mu = C\theta\sin\theta - \frac{p_0}{2}\,[\cos\theta \int \sin\theta\, d\theta - \sin\theta \int \cos\theta\, d\theta]$$
$$- \frac{p_0}{2}\,[\cos\theta \int\int \cos\theta\,(d\theta)^2 + \sin\theta \int\int \sin\theta\,(d\theta)^2]$$

The solution of this equation is

$$\frac{EI}{wr^4}\mu = C\theta \sin\theta + p_0 \quad \ldots\ldots\ldots\ldots [45]$$

Differentiate both sides of Equation [45] twice with regard to angle θ

$$\frac{EI}{wr^4}\frac{d^2\mu}{d\theta^2} = -C\theta \sin\theta + 2C\cos\theta \quad \ldots\ldots\ldots [46]$$

Add Equations [45] and [46] together

$$\frac{EI}{wr^4}\left(\mu + \frac{d^2\mu}{d\theta^2}\right) = p_0 + 2C\cos\theta \quad \ldots\ldots\ldots [47]$$

Applying the condition given by Equation [44], i.e., Equation [47] should be zero at $\theta = \pi$, we find $C = p_0/2$.

Substituting the value of the constant back into Equation [45], finally, we have

$$\mu = \frac{p_0 wr^4}{EI}(1 + \theta/2 \sin\theta) \quad \ldots\ldots\ldots\ldots [48]$$

Case 2. Pressure Distribution of the Form. In case the pressure intensity p is a function of θ of the form

$$p = p_0(1 + Z\cos 2\theta) \quad \ldots\ldots\ldots\ldots [49]$$

Equation [49] evidently is also a special case of the Fourier series Equation [8] with the coefficient p_2 of the second term equal to Zp_0 and the coefficients of all the subsequent terms equal to zero.

Equation [43] in this case becomes

$$\frac{EI}{wr^4}\mu = C\theta\sin\theta$$

$$-\frac{p_0}{2}[\cos\theta\int(1 + Z\cos 2\theta)\sin\theta\, d\theta - \sin\theta\int(1 + Z\cos 2\theta)\cos\theta d\theta] - \frac{p_0}{2}[\cos\theta\int\int(1 + Z\cos 2\theta)\cos\theta\,(d\theta)^2 + \sin\theta\int\int(1 + Z\cos 2\theta)\sin\theta\,(d\theta)^2] \quad \ldots\ldots [50]$$

The solution of the second term of the right side of the equation is

$$-\frac{p_0}{2}\left[-\cos^2\theta + Z\frac{\cos\theta}{2}\left(-\frac{\cos 3\theta}{3} + \cos\theta\right) - \sin^2\theta - Z\frac{\sin\theta}{2}\left(\frac{\sin 3\theta}{3} + \sin\theta\right)\right]$$

By grouping the terms, and since $\cos^2\theta + \sin^2\theta = 1$, $\cos^2\theta - \sin^2\theta = \cos 2\theta$ and $\cos 2\theta = \cos 3\theta\cos\theta + \sin 3\theta\sin\theta$, the second term of the right side of the equation finally is reduced to

$$\frac{p_0}{2}(1 - Z/3\cos 2\theta)$$

In a similar way, the solution of the last term of the right side of Equation [50] is

$$\frac{p_0}{2}[1 + (5/9)Z\cos 2\theta]$$

Therefore the solution of Equation [50] is

$$\frac{EI}{wr^4}\mu = C\theta\sin\theta + p_0[1 + Z/9\cos 2\theta] \quad \ldots\ldots [51]$$

Differentiate both sides of Equation [51] twice with regard to angle θ

$$\frac{EI}{wr^4}\frac{d^2\mu}{d\theta^2} = 2C\cos\theta - C\theta\sin\theta - 4/9\, p_0 Z\cos 2\theta \quad \ldots [52]$$

Add Equations [51] and [52] together,

$$\frac{EI}{wr^4}\left(\mu + \frac{d^2\mu}{d\theta^2}\right) = 2C\cos\theta + p_0 - Z/3\, p_0\cos 2\theta \quad \ldots [53]$$

When $\theta = \pi$, the right side of Equation [53] becomes

$$-2C + p_0 - Z/3\, p_0$$

Applying the condition given by Equation [44], or

$$-2C + p_0 - Z/3\, p_0 = 0$$

we find

$$C = \frac{p_0}{2}(1 - Z/3)$$

Substituting the value of the constant C back into Equation [51], after multiplying out the terms and grouping them, finally we have

$$\mu = \frac{p_0 wr^4}{EI}\left[1 + \theta/2\sin\theta - Z/3\left(\theta/2\sin\theta - \frac{\cos 2\theta}{3}\right)\right] \quad \ldots [54]$$

ACKNOWLEDGMENT

The author wishes to express his appreciation to Mr. A. A. Dach for his kindness in checking the manuscript and to Mrs. Sylvia Woods for her assistance in preparing the paper.

BIBLIOGRAPHY

1 "Differential Equations," by Abraham Cohen, D. C. Heath & Company, New York, N. Y., 1933, chap. 14, p. 288.

2 "Mechanical Engineers' Handbook," by L. S. Marks, McGraw Hill Book Company, Inc., New York, N. Y., fourth edition. 1941. sec. 2, p. 167.

3 Reference (2), p. 164.

4 "Strength of Materials, Part 2," by S. Timoshenko, D. Van Nostrand Company, Inc., New York, N. Y., second edition, 1941. p. 68.

Numerical Solution of Elastoplastic Torsion of a Shaft of Rotational Symmetry[1]

By R. P. EDDY[2] and F. S. SHAW[3]

Using relaxation methods, an approximate numerical solution is found of the stress distribution in a shaft of rotational symmetry, which is subjected to a torque of sufficient magnitude to cause portions of the material to yield. It is assumed that the material of which the shaft is composed is isotropic and yields according to the condition of von Mises. The particular problem investigated is a shaft with a collar; results are presented showing the elastoplastic boundary, and the stress distribution, for two different amounts of plastic deformation.

Introduction

In this paper numerical relaxation methods are used to find, approximately, the stress distribution in a shaft of rotational symmetry and variable diameter, which is subjected to a torque sufficiently large to cause a portion of the material to yield.

It is assumed that the material is isotropic, and that below the yield point the behavior is perfectly elastic. It is also assumed that after yield the material exhibits perfect plasticity (i.e., there is no strain-hardening), while the yield condition requires that the maximum shearing stress has the constant value k equal to the yield stress in pure shear.

In essence, the method of solution is a development of the idea behind the Prandtl-Nadai soap-film sand-heap analogy for the Saint Venant torsion problem. A plastic stress function is introduced and, then, on the assumption that a portion of the material has yielded, it is possible, numerically, to construct the function. Using relaxation techniques, equilibrium requirements then enable the common boundary of the plastic and elastic domains to be located and the plastic and elastic stress functions to be found.

Elastic Behavior

Let Fig. 1 represent a shaft of circular cross section and variable diameter, with equal and opposite torques T, applied at the ends. Then, on making certain assumptions, it can be shown (1)[4] that the problem of finding the resulting stress distribution reduces to that of finding a stress function φ which satisfies the equation

$$\frac{\partial^2\varphi}{\partial r^2} - \frac{3}{r}\frac{\partial\varphi}{\partial r} + \frac{\partial^2\varphi}{\partial z^2} = 0 \quad \ldots\ldots\ldots\ldots [1]$$

on $AGJK$, Fig. 2, together with appropriate boundary conditions.

In obtaining this equation it is assumed that the only two nonzero stresses are $\tau_{r\theta}$, $\tau_{\theta z}$, and these in fact are sufficient to give a resultant which is equivalent to a pure torque only.

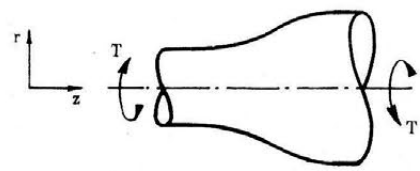

Fig. 1

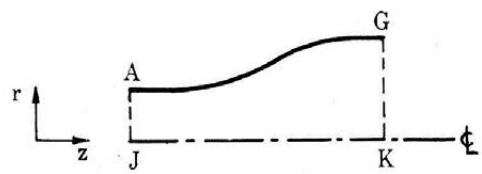

Fig. 2

Given the stress function φ, then from the equations of equilibrium the stresses are given by

$$\left.\begin{aligned} \tau_{r\theta} &= -\frac{1}{r^2}\frac{\partial\varphi}{\partial z} \\ \tau_{\theta z} &= \frac{1}{r^2}\frac{\partial\varphi}{\partial r} \end{aligned}\right\} \quad \ldots\ldots\ldots\ldots [2]$$

and the resultant stress q, by

$$\begin{aligned} q &= (\tau_{r\theta}^2 + \tau_{\theta z}^2)^{1/2} \\ &= \frac{1}{r^2}\left\{\left(\frac{\partial\varphi}{\partial r}\right)^2 + \left(\frac{\partial\varphi}{\partial z}\right)^2\right\}^{1/2} \quad \ldots\ldots\ldots [3] \end{aligned}$$

The requirement that the lateral surface of the shaft be free of external tractions leads to the condition that φ be constant on AG, i.e.

$$\varphi = \varphi_B \quad \ldots\ldots\ldots\ldots [4]$$

On the center line, symmetry demands that $\tau_{r\theta} = 0$, which requires that

$$\varphi_{JK} = \text{const} = 0 \quad \ldots\ldots\ldots\ldots [5]$$

without loss of generality.

With these values of φ, the applied torque is then given by

$$T = \int_0^{r_A} 2\pi r \cdot r\tau_{\theta z} \cdot dr = 2\pi\varphi_B \quad \ldots\ldots [6]$$

For this problem, the yield condition requires that

$$\tau_{r\theta}^2 + \tau_{\theta z}^2 = k^2 \quad \ldots\ldots\ldots\ldots [7]$$

---

[1] The conclusions presented in this paper were obtained in the course of research conducted under Contract N 7onr-358 sponsored jointly by the Office of Naval Research and the Bureau of Ships.

[2] Naval Ordnance Laboratory, Washington, D. C.; formerly of Brown University, Providence, R. I.

[3] Division of Aeronautics, Council for Scientific and Industrial Research, Melbourne, Australia; formerly of Brown University, Providence, R. I.

[4] Numbers in parentheses refer to the Bibliography at the end of the paper.

Contributed by the Applied Mechanics Division and presented at the Annual Meeting, New York, N. Y., November 28–December 3, 1948, of The American Society of Mechanical Engineers.

Discussion of this paper should be addressed to the Secretary ASME, 29 West 39th Street, New York, N. Y., and will be accepted until July 11, 1949, for publication at a later date. Discussion received after the closing date will be returned.

Note: Statements and opinions advanced in papers are to be understood as individual expressions of their authors and not those of the Society. Paper No. 48—A-20.

so that, for the behavior to be everywhere elastic, it is necessary that

$$q_{max} < k$$

that is

$$\left[\left(\frac{\partial\varphi}{\partial r}\right)^2 + \left(\frac{\partial\varphi}{\partial z}\right)^2\right]^{1/2}_{max} < kr^2 \quad \ldots\ldots [8]$$

Plastic Behavior

As for the plastic problem, assuming that at yield the only two nonzero stress components are $\bar{\tau}_{r\theta}$, $\bar{\tau}_{\theta z}$, the equations of equilibrium are satisfied by the introduction of a plastic stress function $\bar{\varphi}$ such that

$$\left.\begin{aligned} \bar{\tau}_{r\theta} &= -\frac{1}{r^2}\frac{\partial\bar{\varphi}}{\partial z} \\ \bar{\tau}_{\theta z} &= \frac{1}{r^2}\frac{\partial\bar{\varphi}}{\partial r} \end{aligned}\right\} \quad \ldots\ldots [9]$$

Using the yield condition, Equation [7], and Equations [9], the equation to be satisfied by the plastic stress function is

$$\left[\left(\frac{\partial\bar{\varphi}}{\partial r}\right)^2 + \left(\frac{\partial\bar{\varphi}}{\partial z}\right)^2\right]^{1/2} = kr^2 \quad \ldots\ldots [10]$$

Also, for the same reason as before, it is required that on the boundary

$$\bar{\varphi} = \text{const} = \bar{\varphi}_B \quad \ldots\ldots [11]$$

It is known that, for the elastic problem, the maximum resultant stress q_{max}, occurs on the surface of the shaft; consequently, the material will first commence to yield at some point on the boundary AG, and further increase in torque will be accompanied by the growth of a region of plastic material in the neighborhood of that point.

At the common boundary of the elastic and plastic domains, consideration of the equilibrium of an element of material demands that

$$\begin{aligned} \tau_{r\theta} &= \bar{\tau}_{r\theta} \\ \tau_{\theta z} &= \bar{\tau}_{\theta z} \end{aligned}$$

that is

$$\left.\begin{aligned} \frac{\partial\varphi}{\partial z} &= \frac{\partial\bar{\varphi}}{\partial z} \\ \frac{\partial\varphi}{\partial r} &= \frac{\partial\bar{\varphi}}{\partial r} \end{aligned}\right\} \quad \ldots\ldots [12]$$

From these, if C is the common boundary, we obtain

$$\left(\frac{\partial\varphi}{\partial t}\right)_C = \left(\frac{\partial\bar{\varphi}}{\partial t}\right)_C$$

where $(\partial\varphi/\partial t)_C$ means the tangential derivative of φ on C. Hence on C

$$\bar{\varphi}_C = \varphi_C + \text{const}$$

Without loss of generality we may put

$$\bar{\varphi}_B = \varphi_B \quad \ldots\ldots [13]$$

and consequently, require that

$$\bar{\varphi}_C = \varphi_C \quad \ldots\ldots [14]$$

together with Equations [12]. Note, however, that the actual position of C is unknown; in fact, its determination forms the core of the problem.

Complete Statement of Problem

To sum up, then, the complete elastoplastic problem reduces to the following:

(*a*) In the elastic region E, Fig. 3

$$\frac{\partial^2\varphi}{\partial r^2} - \frac{3}{r}\frac{\partial\varphi}{\partial r} + \frac{\partial^2\varphi}{\partial z^2} = 0 \quad \ldots\ldots [1]$$

together with the overriding condition

$$\left[\left(\frac{\partial\varphi}{\partial r}\right)^2 + \left(\frac{\partial\varphi}{\partial z}\right)^2\right]^{1/2} < kr^2 \quad \ldots\ldots [8]$$

(*b*) In the plastic region P

$$\left[\left(\frac{\partial\bar{\varphi}}{\partial r}\right)^2 + \left(\frac{\partial\bar{\varphi}}{\partial z}\right)^2\right]^{1/2} = kr^2 \quad \ldots\ldots [10]$$

The boundary conditions are

(*c*) On JK

$$\varphi = 0 \quad \ldots\ldots [5]$$

(*d*) On $ABDFG$

$$\varphi_B = \bar{\varphi}_B = \text{const} \quad \ldots\ldots [13]$$

(*e*) The position of the common boundary BHF is unknown, but on it

$$\varphi_C = \bar{\varphi}_C \quad \ldots\ldots [14]$$

together with

$$\frac{\partial\varphi}{\partial r} = \frac{\partial\bar{\varphi}}{\partial r}, \qquad \frac{\partial\varphi}{\partial z} = \frac{\partial\bar{\varphi}}{\partial z} \quad \ldots\ldots [12]$$

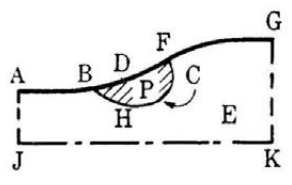

Fig. 3

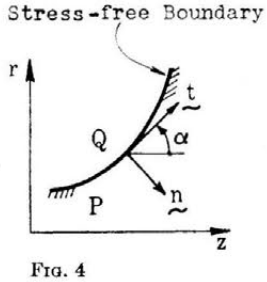

Fig. 4

The Plastic Stress Function

Let Fig. 4 represent a portion of the plastic region, together with the stress-free profile.

At some point Q on the shaft boundary

$$\frac{\partial\bar{\varphi}}{\partial r} = \frac{\partial\bar{\varphi}}{\partial n}\sin\alpha + \frac{\partial\bar{\varphi}}{\partial t}\cos\alpha$$

$$= \frac{\partial\bar{\varphi}}{\partial n}\sin\alpha$$

since $\bar{\varphi}$ is constant on the boundary.

Similarly

$$\frac{\partial\bar{\varphi}}{\partial z} = \frac{\partial\bar{\varphi}}{\partial n}\cos\alpha$$

so that from Equation [10]

$$\left[\left(\frac{\partial\bar{\varphi}}{\partial r}\right)^2 + \left(\frac{\partial\bar{\varphi}}{\partial z}\right)^2\right]^{1/2} = \frac{\partial\bar{\varphi}}{\partial n} = kr^2 \quad \ldots\ldots [15]$$

This relation is also true for any contour

$$\bar{\varphi} = \text{const} = C_i$$

where ($i = 1, 2, \ldots$) within the plastic region.

If now it is assumed that a certain region adjacent to the shaft boundary has yielded, it is possible, approximately,[5] to construct the plastic stress function $\bar{\varphi}$ within that region. For, let $-\Delta\bar{\varphi}$ be a constant decrement of the plastic stress function; then, from Equation [15], we have

$$\Delta n = -\frac{\Delta\bar{\varphi}}{k r_Q^2} \quad \ldots\ldots [16]$$

where $r_Q = r_Q(z)$ is the radius of the shaft at the point Q considered. Hence starting from the shaft boundary on which $\bar{\varphi} = \bar{\varphi}_B$, from Equation [16] increments Δn (of the inner normal) may be calculated at points along the boundary to give points like Q_1 which in turn constitute a contour

$$\bar{\varphi} = \text{const} = \bar{\varphi}_B - \Delta\bar{\varphi}$$

Using the now known position of Q_1, a better approximation $\bar{\varphi}_1$, may then be found from the relation

$$\Delta n_1 = -\frac{\Delta\bar{\varphi}}{k}\left(\frac{2}{r_Q + r_{Q1}}\right)^2 \quad \ldots\ldots [17]$$

In general, the length Δn_1 will vary with the boundary point chosen, so that the contour $\bar{\varphi}_1 = \text{const}$, will not be parallel to the contour $\bar{\varphi}_B$. Having obtained the $\bar{\varphi}_1$ contour, the procedure may be repeated to give other contours $\bar{\varphi}_2 = \text{const}$, $\bar{\varphi}_3 = \text{const}$, etc. The normals used in constructing $\bar{\varphi}_2$ are now measured at right angles to $\bar{\varphi}_1$. This is illustrated in Fig. 5.

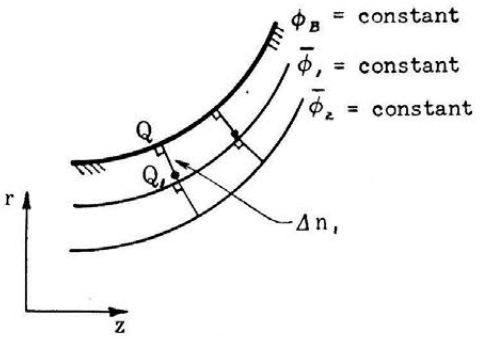

FIG. 5

Thus with $\bar{\varphi}_B(=\varphi_B)$ given, for any assumed plastic region, $\bar{\varphi}$, and consequently $\partial\bar{\varphi}/\partial z$, $\partial\bar{\varphi}/\partial r$ can be found uniquely everywhere within that region to within the limits of accuracy of the construction outlined.

NONDIMENSIONAL TREATMENT

In the numerical solution of problems, some generality can be obtained by making the quantities concerned nondimensional. To do this, let L be some suitable reference length pertinent to the problem, and put

$$r = \rho L \qquad z = \zeta L \qquad h = \alpha L$$
$$\varphi = D\Phi \qquad \bar{\varphi} = D_y\bar{\Phi}$$

where D, D_y are two constants having the dimensions of torque.

Using these, the differential Equation [1] becomes

$$\frac{\partial^2\Phi}{\partial\rho^2} - \frac{3}{\rho}\frac{\partial\Phi}{\partial\rho} + \frac{\partial^2\Phi}{\partial\zeta^2} = 0 \quad \ldots\ldots [3a]$$

the stresses are given by

$$\left.\begin{aligned} \tau_{r\theta} &= \frac{D}{L^3}\tau'_{\theta z} \\ \tau_{\theta z} &= \frac{D}{L^3}\tau'_{\theta z} \end{aligned}\right\} \quad \ldots\ldots [2b]$$

$$q = \frac{D}{L^3}q' \quad \ldots\ldots [3b]$$

where

$$\left.\begin{aligned} \tau_{r\theta}' &= -\frac{1}{\rho^2}\frac{\partial\Phi}{\partial\zeta} \\ \tau_{\theta z}' &= \frac{1}{\rho^2}\frac{\partial\Phi}{\partial\rho} \end{aligned}\right\} \quad \ldots\ldots [2a]$$

$$q' = \frac{1}{\rho^2}\left[\left(\frac{\partial\Phi}{\partial\rho}\right)^2 + \left(\frac{\partial\Phi}{\partial\zeta}\right)^2\right]^{1/2} \quad \ldots\ldots [3a]$$

and the torque T is given by

$$T = 2\pi D\Phi_B \quad \ldots\ldots [6a]$$

Here the nondimensional stresses $\tau'_{r\theta}$, etc., are mere numbers, and for a given shape of shaft can be computed once and for all when Φ_B has been prescribed. Thus if any actual stress component or resultant is known (or is desired to be attained) at a particular point a, say, the value of D can be computed. For example, from Equation [3b]

$$D = L^3 q_a/q_a' \quad \ldots\ldots [18]$$

and eliminating D between Equation [6a] and [18] yields a relation between the stress resultant at a particular point, and the torque which produces it, namely

$$T = 2\pi L^3\Phi_B\, q_a/q_a' \quad \ldots\ldots [19]$$

Let q_m' be the maximum nondimensional resultant stress,[6] and let D_y, T_y denote the values of D and T corresponding to the commencement of yield. Then, from Equations [6a] and [18]

$$\left.\begin{aligned} D_y &= L^3k/q_m' \\ &= T_y/2\pi\Phi_B \end{aligned}\right\} \quad \ldots\ldots [20]$$

and from Equation [21]

$$T_y = 2\pi L^3\Phi_B k/q_m' \quad \ldots\ldots [21]$$

Thus when k has been determined experimentally for the material of which the shaft is composed, and q_m' has been computed for the shape of the shaft in question, the torque at which the shaft first commences to yield is easily computed.

As the torque increases from T_y to T_1, say, the plastic region will commence to grow; in it, however, the stress resultant remains constant, i.e., $q_{\max} = k$. Hence since D_y remains constant, it is necessary to modify Equation [8a]. To do this let

$$T_1 = \beta T_y; \quad \beta > 1$$

then the required relation is

$$T_1 = 2\pi D_y\beta\bar{\Phi}_B \quad \ldots\ldots [22]$$

To construct the plastic stress function the nondimensional relation is

$$\Delta\nu = \frac{\Delta\bar{\Phi}}{q_m'\rho^2} \quad \ldots\ldots [23]$$

where $n = L\nu$. Finally, the conditions to be satisfied at the

[5] It is also possible to obtain an analytical solution for the plastic stress function $\bar{\varphi}$; however, its numerical evaluation would be rather tedious since it involves nontabulated elliptical functions.

[6] q_m' is of course still a number, and can be found from the nondimensional elastic solution.

elastoplastic boundary are

$$\bar{\Phi}_C = \Phi_C \quad \ldots\ldots [14a]$$

together with either

or

$$\left.\begin{aligned} \frac{\partial \bar{\Phi}}{\partial \rho} &= \frac{\partial \Phi}{\partial \rho} \\ \frac{\partial \bar{\Phi}}{\partial \zeta} &= \frac{\partial \Phi}{\partial \zeta} \end{aligned}\right\} \quad \ldots\ldots [12a]$$

It is easy to show that the satisfaction of Equation [14a] together with one of Equation [12a] insures the satisfaction of the other relation of Equation [12a].

Method of Solution

In finding an approximate numerical solution to a particular problem by relaxation methods, two main steps are involved: (a) The appropriate governing equation is replaced by its finite difference equation, so that, by inscribing a mesh of lines on the actual domain of the problem we obtain for each intersection point of the mesh a simple algebraic equation: (b) Using the relaxation techniques, the resulting set of simultaneous equations is then approximately solved numerically.

With respect to the latter step, familiarity with terminology and details of the modus operandi of relaxation methods is assumed here;[7] and accordingly no description will be given.

Let Fig. 6 represent a portion of the superimposed mesh. Then

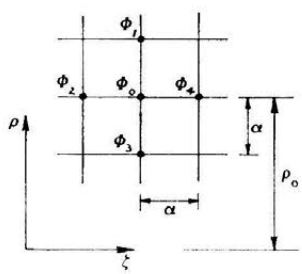

Fig. 6

the finite-difference approximation to Equation [1a] is given by

$$\left(1 - \frac{3\alpha}{2\rho_0}\right)\Phi_1 + \Phi_2 + \left(1 + \frac{3\alpha}{2\rho_0}\right)\Phi_3 + \Phi_4 - 4\Phi_0 = 0 \ldots [1b]$$

and for the stress components, Equations [2a], expressions like

$$\frac{\partial \Phi}{\partial \zeta} = \frac{\Phi_4 - \Phi_2}{2\alpha}$$

are available.[8]

For the purpose of discussion, let it be assumed that the elastic problem (i.e., no portion of *ABDFG*, Fig. 3, has as yet yielded) has been solved, so that the (nondimensional) numerical set of values of the stress function is available. Using this, the elastoplastic solution for some particular torque T_1, may be found in the following manner:

1 From the elastic solution, compute the shear stress components, Equations [2a], and so, from Equation [3a], obtain the values of the resultant shear stress at each mesh point, including those on the outer boundary. Although the maximum resultant stress q_m', will occur on the boundary, it is unlikely that it will occur at a mesh point; consequently, plotting the values of q' along the boundary in the neighborhood of the maximum enables both the value and position of q_m' to be determined.

Since the elastic solution is nondimensional, this maximum may be regarded as the stress at which yielding commences, Equation [7]. Thus a numerical value is available for k, and so the plastic stress function may be constructed within any desired region.

This is the situation represented in Fig. 7 where it is convenient to consider the elastic and plastic stress functions as being plotted with ordinates normal to the $\rho\zeta$-plane. The curves represent the trace of the elastic and plastic stress-function surfaces on a plane perpendicular to the $\rho\zeta$-plane at the point of maximum resultant stress.

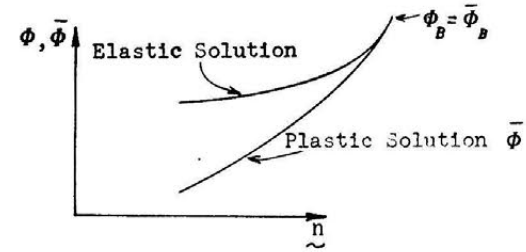

Fig. 7

2 Multiply the elastic solution by the chosen constant β ($T_1 = \beta T_y$, $\beta > 1$), so that on the boundary the stress function will have the value Φ_{B1}. Since $\Phi_{B1} = \bar{\Phi}_{B1}$, in so far as the plastic stress function is concerned, the alteration merely entails adding a constant everywhere, of value $\Phi_{B1} - \Phi_B$, to the solution already constructed. In the neighborhood of the point of initial yield the new elastic stress function Φ_1, will have values less than those of the new plastic stress-function surface, and it is a simple matter to determine (by interpolation formulas) the line of intersection of the two surfaces, represented by point 1 in Fig. 8. Obviously, the conditions of tangency, Equation [12a], at point 1, i.e., at the meet of the two surfaces, will not be satisfied.

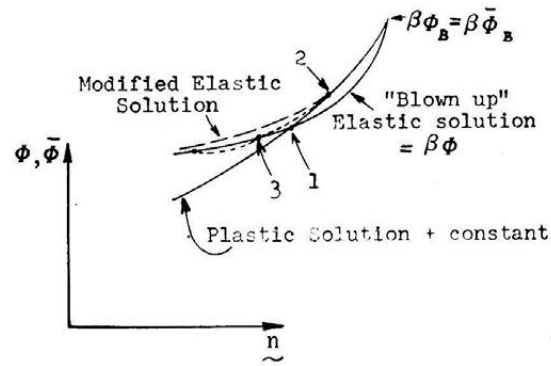

Fig. 8

3 Adjust the position of the common boundary, always keeping it on the $\bar{\Phi}_1$ surface, keeping all other values of Φ_1 held fixed, until the tangent condition is satisfied approximately. This is easily done using an appropriate finite-difference formula for the first derivative and will give a new position for Φ_{C1} represented by point 2 in Fig. 8.

4 Now, however, as both the position of the boundary C of the elastic portion of the problem, and also the values of the elastic stress function Φ_C on that boundary have been modified, at points like 3 the elastic differential equation [1a] will no longer be satisfied. Hence keeping the new position of C and the new values of

[7] Details are available in several papers; see, for example, reference (2).

[8] Further discussion on finite-difference approximations is given in Appendix 2.

Φ_C held fixed, compute the residuals at points like 3 and so, by relaxation, satisfy the differential equation in the elastic portion of the problem. This can be done, but at the expense of again violating the tangent condition, and leads to the modified elastic solution as shown in Fig. 8. Now, however, the lack of agreement in the tangent condition will not be as bad as that of the first step.

5 Readjust the position of the common boundary, and repeat the general procedure until all conditions are satisfied. In practice it will be found that three or four (shrewdly chosen) positions of the common boundary are all that are necessary.

Results

The problem solved was that of a shaft[9] with a collar, details of which are given in Fig. 9. Due to symmetry it was necessary to treat only one quarter of it, i.e., the portion *ABCDEF*.

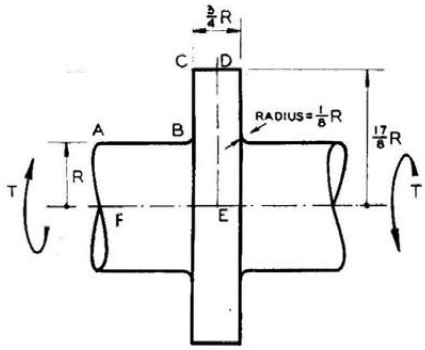

Fig. 9

For computation it was found convenient to take $L = R/8$, $\Phi_B = 4096$, R being the radius of the parallel portion of the shaft.

Fig. 10 gives the elastic solution.[10] It shows values of the stress function, and values and contours of the resultant stress q'. As can be seen, the magnitude of the maximum stress q_m', is 49, compared with 32 on the boundary of the parallel portion of the shaft where the stress is constant. There is thus a stress-concentration factor of 1.53.

From Equations [19] and [21] the relations between actual stresses and torques are

$$T = 16\pi R^3(q_a/q_a')$$

and

$$T_y = 16\pi\, R^3 k/49$$

In order to confine the region of yield to the neighborhood of the stress concentration, the elastoplastic problem was solved for an applied torque of $T_1 = 1.50T_y$. The result is given in Fig. 11. Fig. 12 shows the region adjacent to the yielded portion in rather more detail. As well as the final position of the common boundary, it shows the initial intersection of the two stress-function surfaces which forms the starting approximation.

Fig. 13 is the result of applying still more torque, of amount $T_2 = 1.55\ T_y$. As indicated, the torque is now sufficient to produce a narrow strip of plastic material all along the surface of the parallel portion of the shaft.

Discussion

At first sight the result shown in Fig. 11 is rather surprising. Although the applied torque is $1^1/_2$ times the torque at which yielding commences, the area that has yielded is quite small. This is due of course to the fact that in the neighborhood of the stress concentration the stress gradient is quite large; for more spectacular results it would be necessary to decrease the stress concentration by using a larger corner radius.

The result of Fig. 11 may, however, be misleading. Thus let T_B be the value of the applied torque at which the surface of the parallel portion of the shaft commences to yield. Then it can be shown[11] that the torque necessary to produce yielding over the entire cross section of the shaft is $1^1/_3\ T_B$.

Hence, although a torque of $1.53T_y$ merely produces the small region of yielded material shown in Fig. 11, a torque of $2.04\ T_y$ $(= 1.53 \times 1.\dot{3}\ T_y)$ is sufficient to insure complete yield, and so failure of the shaft.

In a paper by Weigand (5), there are given the results of experimentally determined stress-concentration factors for shafts of a somewhat similar nature[12] to that investigated here. In so far as it is possible to extrapolate from the experimental results given, the agreement with the value of 1.53 given here is excellent.

It is obvious that the procedure used here may be applied without much modification to the problem of a hollow shaft. If the inner surface should happen to contain a re-entrant corner having a small root radius, then it is quite possible that yielding may first start at the root. To solve such a problem merely entails the construction of a second plastic stress function "attached" to the inner boundary (on which $\Phi = 0$), the rest of the procedure being unchanged.

Appendix 1

Analytical Solution of Elastoplastic Problem in a Uniform Circular Shaft

For a shaft of uniform radius R, using the independent variable $\rho = r/R$, the elastic stress function Equation [3] reduces to the equation

$$\frac{\partial^2\varphi}{\partial\rho^2} - \frac{3}{\rho}\frac{\partial\varphi}{\partial\rho} = 0$$

the solution of which is

$$\varphi = c\rho^4 + d$$

The requirement $\varphi(0) = 0$

gives $d = 0$

leaving the constant c still to be determined.

The plastic stress function $\bar{\varphi}$ is required to satisfy the equation

$$\frac{\partial\bar{\varphi}}{\partial\rho} = k\ R^3\rho^2$$

which, using the boundary condition

$$\bar{\varphi}(1) = \bar{\varphi}_B = T/2\pi$$

has the solution

$$\bar{\varphi} = \bar{\varphi}_B - \frac{kR^3}{3}(1 - \rho^3)$$

It is now required to find the value ρ_0, of ρ, and the constant c, such that the conditions of the free boundary, Equations [12] and [14] are satisfied.

From Equations [14] is obtained

$$4c\rho_0^3 = kR^3\rho_0^2$$

[9] The elastic solution for this shaft has already been found by finite-difference methods some time ago (see references 3 and 4).

[10] The figure is actually a composite one. For the main portion of the shaft α was taken as 1; however, in the neighborhood of the stress concentration, $\alpha = 1/4$.

[11] See Appendix 1.

[12] Weigand's results are for stepped shafts. However, for the dimensions of the shaft with collar treated herein, the difference in the stress distribution at the stress concentration would be very small.

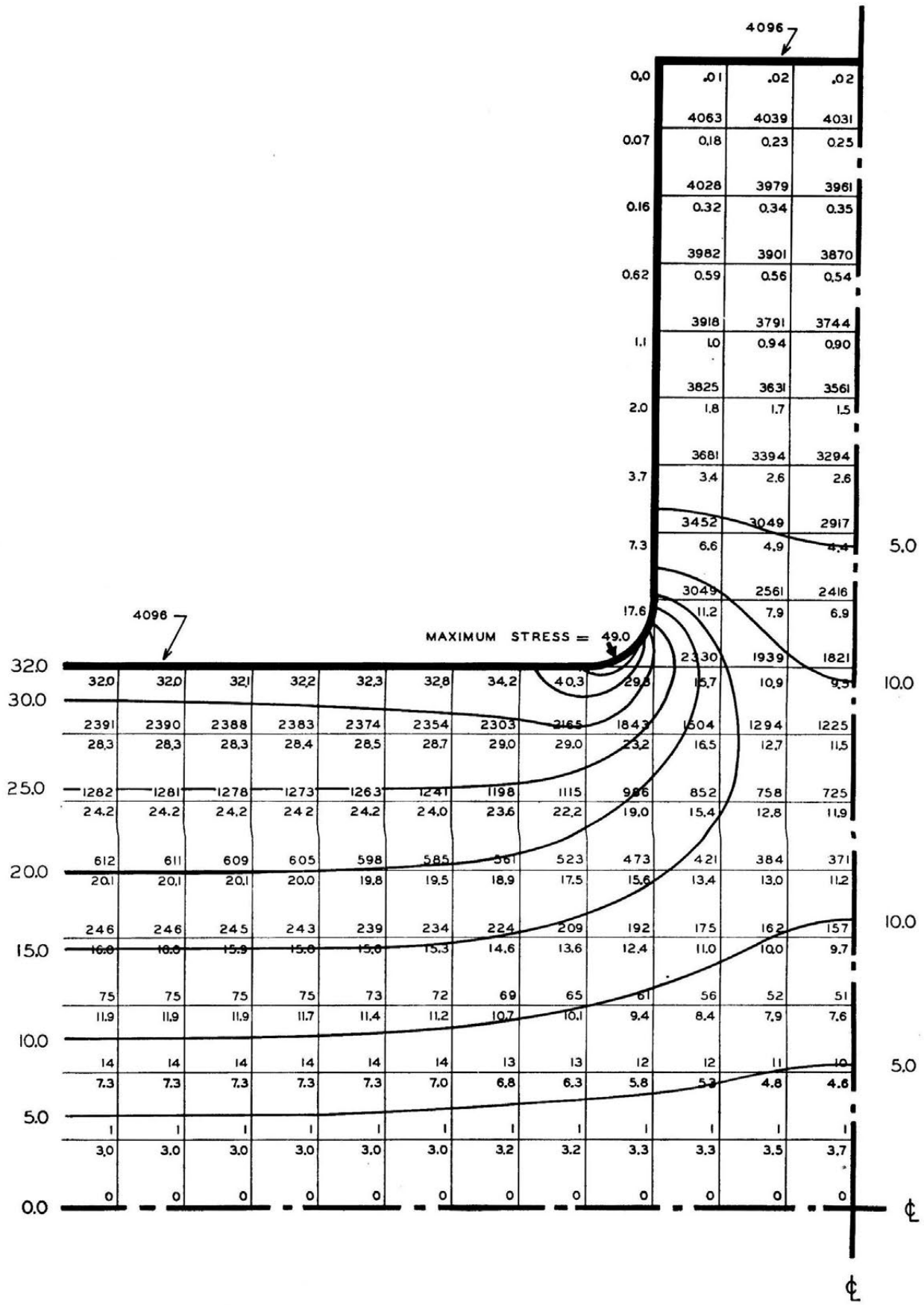

FIG. 10 ELASTIC CASE STRESS FUNCTION Φ AND STRESS RESULTANT q'

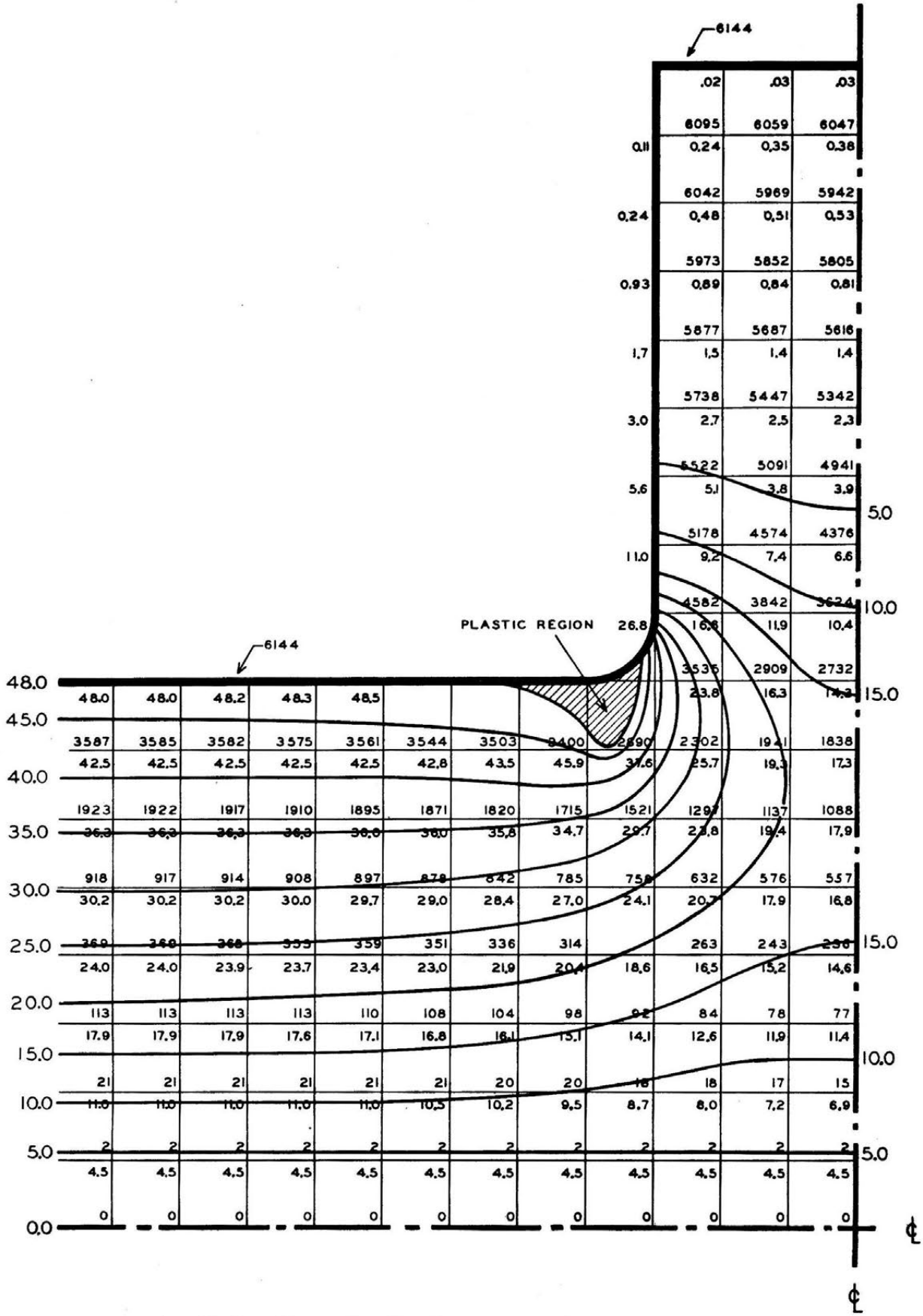

FIG. 11 FIRST PLASTIC CASE T_1; STRESS FUNCTION Φ AND STRESS RESULTANT q'

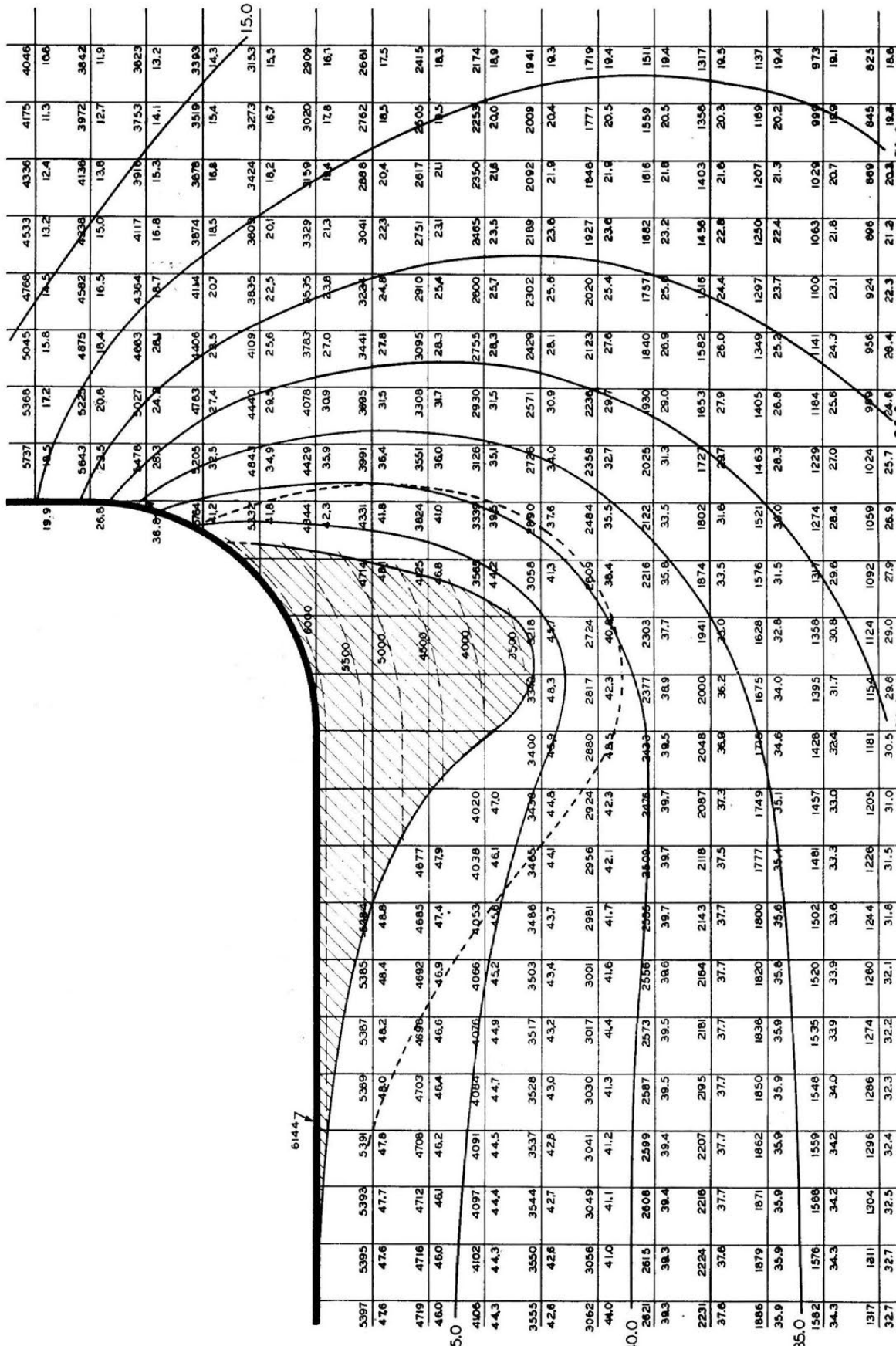

FIG. 12 ENLARGED VIEW OF PLASTIC REGION FOR FIRST PLASTIC CASE, T_1

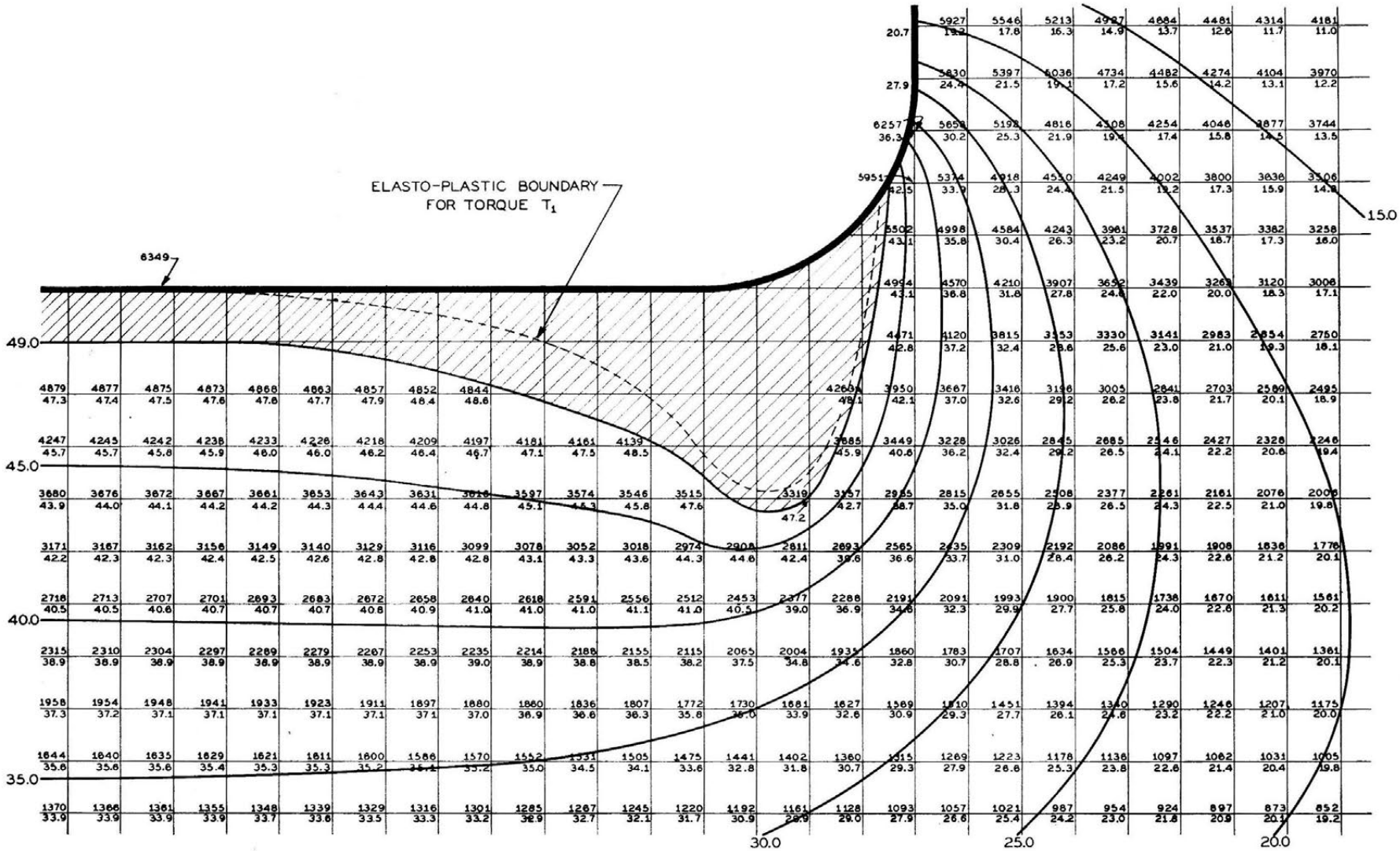

FIG. 13 ENLARGED VIEW OF PLASTIC REGION FOR SECOND PLASTIC CASE, T_2

whence

$$c = kR^3/4\rho_0 \quad [24]$$

while continuity of the stress functions, Equation [14], gives

$$c\rho_0^4 = \varphi_B - \frac{kR^3}{3}(1 - \rho_0^3) \quad [25]$$

Elimination of c between Equations [24] and [25] gives, finally

$$\bar{\varphi}_B = \frac{kR^3}{3}\left(1 - \frac{\rho_0^3}{4}\right) \quad [26]$$

Obviously, for

$$\bar{\varphi}_B = kR^3/4, \quad \rho_0 = 1 \quad [27]$$

and for

$$\bar{\varphi}_B = kR^3/3, \quad \rho_0 = 0 \quad [28]$$

Let $T_y = 2\pi\bar{\varphi}_{By} = 2\pi kR^3/4$ be the torque at which the surface of the shaft commences to yield. Then, for a greater torque $T_1 = \beta T_y = 2\pi\beta kR^3/4$, the value of ρ_0 is given by

$$\rho_0^3 = 4\left[1 - \frac{3}{kR^3}\left(\frac{\beta kR^3}{4}\right)\right]$$

$$= 4 - 3\beta$$

that is

$$\rho_0 = (4 - 3\beta)^{1/3} \quad [29]$$

Thus it is evident that a uniform shaft fails by complete yielding for an applied torque of amount 1.3̇ times that for which the surface of the shaft commences to yield.

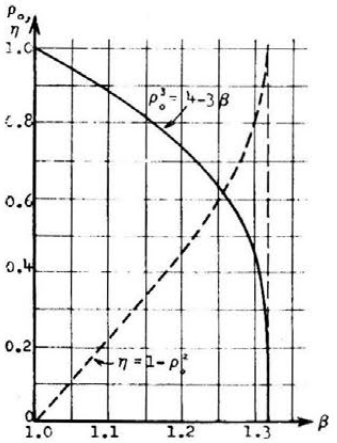

FIG. 14

The actual torque required to cause failure is, from Equation [27]

$$T_F = 2\pi R^3 k/3$$

The relation, Equation [29], is shown graphically in Fig. 14. The dotted curve, $\eta = 1 - \rho_0^2$, indicates the relative amount of the cross section of the shaft that has yielded for a given β. The runaway nature of the failure is evident.

The stress components in the two regions are given by the following:

(*a*) Elastic region

$$\tau_{r\theta} = 0$$

$$\tau_{\theta z} = \frac{1}{R^3\rho^2}\frac{\partial\varphi}{\partial\rho}$$

$$= \frac{k\rho}{(4 - 3\beta)^{1/3}}$$

(*b*) Plastic region

$$\bar{\tau}_{r\theta} = 0$$

$$\bar{\tau}_{\theta z} = \frac{1}{R^3\rho^2}\frac{\partial\bar{\varphi}}{\partial\rho}$$

$$= k$$

as is to be expected.

Appendix 2

FINITE DIFFERENCE APPROXIMATION ADJACENT TO CENTER LINE JK

Along the first mesh line above the axis, the expression $(1 - 3h/2r_0)$, Equation [1*b*] is negative, which means that an increase in Φ at any point on the second line above the axis will decrease the residual at the point below it. Such anomalous behavior leads to false results, and must be circumvented by use of a different expression for the residual on the line $r = h$ (i.e., $\rho = \alpha$).

To develop suitable formulas, use is made of the fact that due to axial symmetry Φ is an even function of ρ for ζ = const.

Use of the fourth-degree curve

$$\Phi = a + b\rho^2 + c\rho^4$$

leads to the equation (for the line $\rho = \alpha$)

$$\Phi_1 + \frac{1}{3}\Phi_2 + \Phi_3 + 5\Phi_4 - \frac{22}{3}\Phi_0 = 0$$

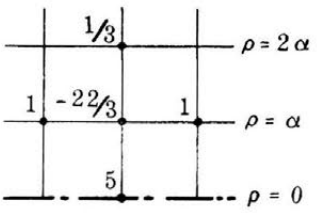

FIG. 15

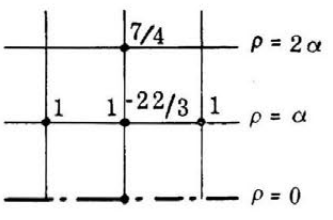

FIG. 16

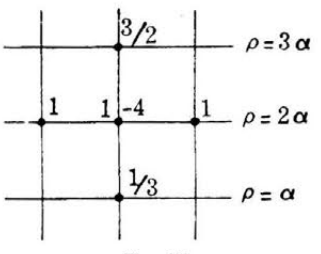

FIG. 17

From this, in the usual manner the residual operator, Fig. 15, and the relaxation operators, Figs. 16 and 17, are obtained.

BIBLIOGRAPHY

1 "Theory of Elasticity," by S. Timoshenko, McGraw-Hill Book Company, Inc., New York, N. Y., 1934, p. 276.

2 "An Introduction to Relaxation Methods," by F. S. Shaw, CSIR Division of Aeronautics, Report SM 78, September, 1946.

3 "Relaxation Methods in Theoretical Physics," by R. V. Southwell, Oxford University Press, London, England, 1946, p. 152.

4 "The Solution of the Torsion Problem for Circular Shafts of Varying Radius," by A. Thom and J. Orr, Proceedings of the Royal Society of London, England, series A, vol. 131, 1931, pp. 30–37.

5 "Determination of the Stress Concentration Factor of a Stepped Shaft Stressed in Torsion by Means of Precision Strain Gages," by A. Weigand, NACA TM no. 1179, September, 1947.

Stress Concentration Around a Triaxial Ellipsoidal Cavity[1]

By M. A. SADOWSKY[2] and E. STERNBERG,[3] CHICAGO, ILL.

Previous investigations[4] have been concerned with the stress concentrations around internal cavities in the shape of an ellipsoid of revolution. This paper contains an exact closed solution, in terms of Jacobian elliptic functions, for the stress distribution around a general triaxial ellipsoidal cavity in an infinite elastic body. The body at infinity is in a uniform state of stress whose principal directions are parallel to the axes of the cavity, the magnitudes of the principal stresses at infinity being arbitrary. The solution covers as limiting cases the known results for spherical and spheroidal cavities. The technically important aspects of the ensuing stress concentration are discussed in detail.

Nomenclature

The following nomenclature is used in the paper:

(x, y, z) = Cartesian co-ordinates

(u, v, w); $(\sigma_x, \cdots \tau_{xy}, \cdots)$ = Cartesian components of displacement and stress, respectively

e = dilatation

$(\alpha_1, \alpha_2, \alpha_3)$ = orthogonal curvilinear co-ordinates in general, and ellipsoidal co-ordinates in particular

(u_1, u_2, u_3); $(\tau_{11}, \cdots \tau_{23}, \cdots)$ = orthogonal curvilinear components of displacement and stress, respectively

X, Y, Z, F = harmonic stress functions

Δ = Laplacian operator

G, ν = shear modulus and Poisson's ratio, respectively

(a, b, c) = semiaxes of the ellipsoidal cavity

$\rho_1 = \frac{b}{a}, \rho_2 = \frac{c}{b}$ = shape ratios of cavity

$\xi = \frac{x}{a}, \eta = \frac{y}{b}, \zeta = \frac{z}{c}$ = dimensionless co-ordinates

Statement of Problem

We consider a homogeneous, isotropic, elastic body of infinite extent which possesses a cavity in the shape of a triaxial ellipsoid, and assume that the body at infinity is in a uniform state of stress whose principal directions are parallel[5] to the axes of the cavity. If the Cartesian co-ordinate axes are chosen coincident with the axes of the ellipsoid, Fig. 1, the stress field at infinity is characterized by

$$\left.\begin{aligned} \sigma_x = \sigma_1, \quad \sigma_y = \sigma_2, \quad \sigma_z = \sigma_3 \\ \tau_{xy} = \tau_{yz} = \tau_{zx} = 0 \end{aligned}\right\} \quad \cdots\cdots\cdots\cdots [1]$$

where $\sigma_1, \sigma_2, \sigma_3$ are arbitrarily prescribed principal stresses. The problem to be treated presently consists of the determination of

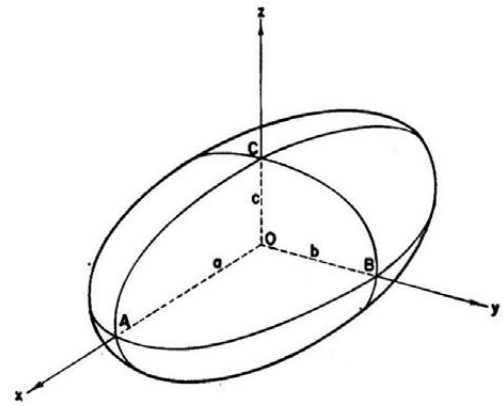

Fig. 1 Ellipsoidal Cavity and Cartesian Co-Ordinate System

the stress distribution induced by the given loading at infinity. The surface of the cavity is to be free from boundary stresses.

In the absence of body forces, the foregoing problem is equivalent to establishing a displacement field $[u, v, w]$ which satisfies the equations of equilibrium

$$\left.\begin{aligned} [\Delta u, \Delta v, \Delta w] - \frac{1}{2\nu - 1} \, grad\, e = 0 \\ e = div[u, v, w] \end{aligned}\right\} \quad \cdots\cdots [2]$$

and gives rise to an associated field of stress

$$\left.\begin{aligned} \sigma_x = \frac{2\nu G}{1 - 2\nu} e + 2G \frac{\partial u}{\partial x}, \ldots, \ldots \\ \tau_{yz} = G\left(\frac{\partial w}{\partial y} + \frac{\partial v}{\partial z}\right), \ldots, \ldots \end{aligned}\right\} \quad \cdots\cdots [3][6]$$

which conforms to conditions [1] at infinity, while leaving the internal boundary of the ellipsoidal cavity free from surface tractions.

---

[1] This investigation was carried on as part of a research program conducted by the Armour Research Foundation under Contract Nobs 28377 with the David Taylor Model Basin, Washington, D. C.

[2] Associate Professor of Mathematics, Illinois Institute of Technology. Mem. ASME.

[3] Associate Professor of Mechanics, Illinois Institute of Technology. Mem. ASME.

[4] See reference (3), p. 93, et seq., and reference (4). Numbers in parentheses refer to the Bibliography at the end of the paper.

Contributed by the Applied Mechanics Division and presented at the Annual Meeting, New York, N. Y., November 28–December 3, 1948, of The American Society of Mechanical Engineers.

Discussion of this paper should be addressed to the Secretary, ASME, 29 West 39th Street, New York, N. Y., and will be accepted until July 11, 1949, for publication at a later date. Discussion received after the closing date will be returned.

Note: Statements and opinions advanced in papers are to be understood as individual expressions of their authors and not those of the Society. Paper No. 48—A-29.

[5] The case of an arbitrary orientation of the principal stress directions relative to the axes of the cavity presents, essentially, no difficulties beyond those encountered in the current loading case.

[6] Formulas not given explicitly are obtained by cyclic permutations.

Basic Solutions in Orthogonal Curvilinear Co-Ordinates[7]

In order to render manageable the boundary conditions for the surface of the cavity, it is imperative to introduce curvilinear co-ordinates. For this purpose, we recall here that a curvilinear co-ordinate system is defined by a transformation

$$x = x(\alpha_1, \alpha_2, \alpha_3); \ \ldots; \ \ldots\ldots\ldots\ldots\ldots [4]$$

and that the corresponding co-ordinate surfaces, $\alpha_i = \text{const}$, are mutually orthogonal provided that

$$\left.\begin{aligned} &\frac{\partial x}{\partial \alpha_i}\frac{\partial x}{\partial \alpha_j} + \frac{\partial y}{\partial \alpha_i}\frac{\partial y}{\partial \alpha_j} + \frac{\partial z}{\partial \alpha_i}\frac{\partial z}{\partial \alpha_j} = 0 \\ &(i \neq j) \end{aligned}\right\} \ldots\ldots\ldots [5]$$

The differential of arc length is given by

$$ds^2 = \sum_{i=1}^{3}\left(\frac{d\alpha_i}{h_i}\right)^2 \ldots\ldots\ldots\ldots\ldots\ldots [6]$$

where

$$\frac{1}{h_i^2} = \left(\frac{\partial x}{\partial \alpha_i}\right)^2 + \left(\frac{\partial y}{\partial \alpha_i}\right)^2 + \left(\frac{\partial z}{\partial \alpha_i}\right)^2 \ldots\ldots\ldots [7]$$

and the direction cosines of the co-ordinate lines with respect to the Cartesian co-ordinate axes obey

$$\cos(\alpha_i, x) = h_i \frac{\partial x}{\partial \alpha_i}, \ \ldots, \ \ldots\ldots\ldots\ldots\ldots [8]$$

Finally, we note that

$$\frac{\partial \alpha_i}{\partial x} = h_i^2 \frac{\partial x}{\partial \alpha_i}, \ \ldots, \ \ldots\ldots\ldots\ldots\ldots [9]$$

and record the curvilinear transforms of the gradient and the Laplacian operator

$$\text{grad} \equiv \left[h_1\frac{\partial}{\partial \alpha_1}, \ h_2\frac{\partial}{\partial \alpha_2}, \ h_3\frac{\partial}{\partial \alpha_3}\right] \ldots\ldots\ldots [10]$$

$$\Delta \equiv h_1h_2h_3\left[\frac{\partial}{\partial \alpha_1}\left(\frac{h_1}{h_2h_3}\frac{\partial}{\partial \alpha_1}\right) + \frac{\partial}{\partial \alpha_2}\left(\frac{h_2}{h_3h_1}\frac{\partial}{\partial \alpha_2}\right) + \frac{\partial}{\partial \alpha_3}\left(\frac{h_3}{h_1h_2}\frac{\partial}{\partial \alpha_3}\right)\right] \ldots\ldots [11]$$

The problem formulated previously will be approached on the basis of the following general solutions of Equations [2], which are due to J. Boussinesq[8] and admit the vectorial representation

$$\left.\begin{aligned} &(a)\ 2G[u, v, w] = x\ \text{grad}\ X - [(3-4\nu)X, 0, 0] \\ &(b)\ 2G[u, v, w] = y\ \text{grad}\ Y - [0, (3-4\nu)Y, 0] \\ &(c)\ 2G[u, v, w] = z\ \text{grad}\ Z - [0, 0, (3-4\nu)Z] \\ &(d)\ 2G[u, v, w] = \text{grad}\ F \end{aligned}\right\} \ldots [12][9]$$

where

$$\Delta X = \Delta Y = \Delta Z = \Delta F = 0 \ldots\ldots\ldots\ldots [13]$$

The displacement fields given by Equations [12] and generated by the arbitrary harmonic functions X, Y, Z, and F, will be referred to as basic solutions (a), (b), (c), and (d), respectively.

By aid of Equations [10], [8] we obtain for the curvilinear scalar components u_i $(i = 1, 2, 3)$ of the displacement fields associated with the basic solutions, Equations [12], the intrinsic forms

$$\left.\begin{aligned} &(a)\ 2Gu_i = h_i\left[x\frac{\partial X}{\partial \alpha_i} - (3-4\nu)\frac{\partial x}{\partial \alpha_i}X\right] \\ &(b)\ \ldots. \\ &(c)\ \ldots. \\ &(d)\ 2Gu_i = h_i\frac{\partial F}{\partial \alpha_i} \end{aligned}\right\} \ldots\ldots [14]$$

The corresponding stress fields are most conveniently established by applying to Equations [14] the displacement-stress relations[10] referred to orthogonal curvilinear co-ordinates. This computation yields

$$(a)\left\{\begin{aligned} &\tau_{11} = h_1^2 x\frac{\partial^2 X}{\partial \alpha_1^2} + \left(h_1\frac{\partial h_1}{\partial \alpha_1}x - 2h_1^2\frac{\partial x}{\partial \alpha_1}\right)\frac{\partial X}{\partial \alpha_1} \\ &\quad - \frac{h_2^2}{h_1}\frac{\partial h_1}{\partial \alpha_2}x\frac{\partial X}{\partial \alpha_2} - \frac{h_3^2}{h_1}\frac{\partial h_1}{\partial \alpha_3}x\frac{\partial X}{\partial \alpha_3} \\ &\quad + 2\nu\left(h_1^2\frac{\partial x}{\partial \alpha_1}\frac{\partial X}{\partial \alpha_1} - h_2^2\frac{\partial x}{\partial \alpha_2}\frac{\partial X}{\partial \alpha_2} - h_3^2\frac{\partial x}{\partial \alpha_3}\frac{\partial X}{\partial \alpha_3}\right) \\ &\ldots. \\ &\ldots. \\ &\tau_{23} = h_2h_3 x\frac{\partial^2 X}{\partial \alpha_2 \partial \alpha_3} \\ &\quad + \left(h_2\frac{\partial h_3}{\partial \alpha_2}\frac{\partial X}{\partial \alpha_3} + h_3\frac{\partial h_2}{\partial \alpha_3}\frac{\partial X}{\partial \alpha_2}\right)x \\ &\quad - (1-2\nu)\,h_2h_3\left(\frac{\partial x}{\partial \alpha_2}\frac{\partial X}{\partial \alpha_2} + \frac{\partial x}{\partial \alpha_2}\frac{\partial X}{\partial \alpha_3}\right) \\ &\ldots. \\ &\ldots. \end{aligned}\right.$$

$$(d)\left\{\begin{aligned} &\tau_{11} = h_1^2\frac{\partial^2 F}{\partial \alpha_1^2} + h_1\frac{\partial h_1}{\partial \alpha_1}\frac{\partial F}{\partial \alpha_1} - \frac{h_2^2}{h_1}\frac{\partial h_1}{\partial \alpha_2}\frac{\partial F}{\partial \alpha_2} \\ &\quad - \frac{h_3^2}{h_1}\frac{\partial h_1}{\partial \alpha_3}\frac{\partial F}{\partial \alpha_3} \\ &\ldots. \\ &\ldots. \\ &\tau_{23} = h_2h_3\frac{\partial^2 F}{\partial \alpha_2 \partial \alpha_3} + h_3\frac{\partial h_2}{\partial \alpha_3}\frac{\partial F}{\partial \alpha_2} + h_2\frac{\partial h_3}{\partial \alpha_2}\frac{\partial F}{\partial \alpha_3} \\ &\ldots. \\ &\ldots. \end{aligned}\right. \ldots [15][11]$$

Ellipsoidal Co-Ordinates and Ellipsoidal Harmonics[12]

In the particular problem under consideration, the shape of the internal boundary suggests the use of ellipsoidal co-ordinates. The corresponding co-ordinate transformation, which relates the Cartesian co-ordinates x, y, z to the ellipsoidal co-ordinates $\alpha_i (i = 1, 2, 3)$, is most conveniently introduced by aid of the Jacobian elliptic functions[13] $sn\ \alpha_i$, $cn\ \alpha_i$, and $dn\ \alpha_i$. For reasons of symme-

[7] For a treatment of general, orthogonal curvilinear co-ordinates and their applications in the theory of elasticity, see, for example, reference (1), arts. 19–22C, 58, 96.

[8] Reference (2). In this connection see also references (3) and (4).

[9] The unessential coefficient $2G$ is introduced for computational convenience.

[10] See reference (1), p. 54, equations [36], and p. 102, equations [18].

[11] Equations [15b, c] are obtained from Equations [15a] by replacing x, X successively with y, Y and z, Z.

[12] See reference (5), chap. XXIII, and reference (6), chap. XI.

[13] An exposition of the theory of Jacobian elliptic functions is given in reference (5), chap. XXII.

try it is expedient to define auxiliary complex arguments $\beta_i (i = 1, 2, 3)$ as follows

$$\left.\begin{aligned} \beta_1 &= \alpha_1 + iK' \\ \beta_2 &= K + i\alpha_2 \\ \beta_3 &= \alpha_3 \end{aligned}\right\} \quad \ldots\ldots\ldots\ldots\ldots\ldots [16]$$

where $4K$ and $2iK'$ are the real and imaginary periods of $sn\beta j (j = 1, 2, 3)$ corresponding to the modulus k. For the complementary modulus k' we have

$$k' = \sqrt{1 - k^2} \ldots\ldots\ldots\ldots\ldots\ldots [17]$$

Furthermore, let

$$s_i = sn\ \beta_i, \quad c_i = cn\ \beta_i, \quad d_i = dn\ \beta_i \ldots\ldots [18]^{14}$$

By Equations [16], [18], and well-known identities for elliptic functions, we obtain

$$\left.\begin{aligned} s_1 &= \frac{1}{ksn\alpha_1}, & s_2 &= \frac{1}{dn(\alpha_2, k')}, & s_3 &= sn\alpha_3 \\ c_1 &= \frac{dn\alpha_1}{iksn\alpha_1}, & c_2 &= \frac{-ik'sn(\alpha_2, k')}{dn(\alpha_2, k')}, & c_3 &= cn\alpha_3 \\ d_1 &= \frac{cn\alpha_1}{isn\alpha_1}, & d_2 &= \frac{k'cn(\alpha_2, k')}{dn(\alpha_2, k')}, & d_3 &= dn\alpha_3 \end{aligned}\right\} \ldots [19]$$

With the notation of Equations [18] the co-ordinate transformation in question may now be written as

$$\left.\begin{aligned} x &= kms_1s_2s_3 \\ y &= -\frac{km}{k'}\, c_1c_2c_3 \\ z &= \frac{im}{kk'}\, d_1d_2d_3 \end{aligned}\right\} \quad \ldots\ldots\ldots\ldots [20]^{15}$$

The moduli k and k' as well as the parameter m are related to the semiaxes a, b, c of the ellipsoidal cavity, Fig. 1, in accordance with

$$k = \sqrt{\frac{a^2 - b^2}{a^2 - c^2}}, \quad m = \sqrt{a^2 - b^2} \ldots\ldots [21]^{16}$$

and a, b, c are assumed to be ordered by

$$0 < c < b < a \ldots\ldots\ldots\ldots\ldots\ldots [22]$$

Equations [20] imply

$$\frac{x^2}{m^2s_i^2} - \frac{y^2}{m^2c_i^2} - \frac{k^2z^2}{m^2d_i^2} = 1 \ldots\ldots\ldots\ldots [23]$$

and by inspection of Equations [23], [19], we note that the co-ordinate surfaces $\alpha_1 = \text{const.}$, $\alpha_2 = \text{const}$, and $\alpha_3 = \text{const}$ form a triply orthogonal[17] family of ellipsoids, hyperboloids of one sheet and hyperboloids of two sheets, respectively, Fig. 2. As the ellipsoidal co-ordinates α_i traverse the ranges

$$0 < \alpha_1 \leqslant K, \quad K' \geqslant \alpha_2 \geqslant 0, \quad K \geqslant \alpha_3 \geqslant 0 \ldots\ldots [24]$$

the foregoing quadrics cover the first octant of the Cartesian space.[18] If $\alpha_1{}^\circ$ is chosen such that

$$s_1{}^\circ \equiv sn(\alpha_1{}^\circ + iK') = \frac{1}{ksn\alpha_1{}^\circ} = \frac{a}{m} \ldots\ldots [25]$$

we confirm by Equations [23], [21], and the identities

$$c_i^2 = 1 - s_i^2, \quad d_i^2 = 1 - k^2s_i^2 \ldots\ldots [26]$$

that the ellipsoid $\alpha_1 = \alpha_1{}^\circ$ has semiaxes a, b, c and thus coincides

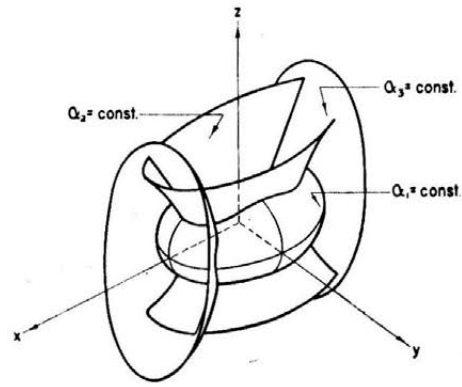

FIG. 2 CO-ORDINATE SURFACES OF ELLIPSOIDAL CO-ORDINATE SYSTEM

with the surface of the cavity, which accounts for the form of Equations [21].

The local scale coefficients h_i, according to Equations [7], [20], here become

$$h_1 = \frac{i}{kmq_2q_3}, \quad h_2 = \frac{1}{kmq_3q_1}, \quad h_3 = \frac{i}{kmq_1q_2} \ldots\ldots [27]$$

with

$$q_1 = \sqrt{s_2^2 - s_3^2}, \quad q_2 = i\sqrt{s_1^2 - s_3^2}, \quad q_3 = \sqrt{s_1^2 - s_2^2} \ldots [28]$$

The remaining differential-geometric elements appropriate to ellipsoidal co-ordinates are readily computed. In particular, if $U(\beta_1, \beta_2, \beta_3)$ is harmonic, Laplace's equation by Equations [11], [16], [27], [28] appears as

$$\frac{\Delta U}{kmh_1h_2h_3} = q_1^2\frac{\partial^2 U}{\partial\beta_1^2} + q_2^2\frac{\partial^2 U}{\partial\beta_2^2} + q_3^2\frac{\partial^2 U}{\partial\beta_3^2} = 0 \ldots\ldots [29]$$

Equation [29] is separable, and is satisfied by the Lamé products

$$U = A_1(\beta_1)A_2(\beta_2)A_3(\beta_3) \ldots\ldots\ldots\ldots [30]$$

provided that $A_i(\beta_i) (i = 1, 2, 3)$ are solutions of the Lamé equation

$$\frac{d^2A_i}{d\beta_i^2} - [n(n+1)k^2s_i^2 - p(1+k^2)]A_i = 0 \ldots\ldots [31]$$

The arbitrary separation constants n, p determine the degree and the species, respectively, of the foregoing ellipsoidal harmonics. Corresponding to each nonnegative integral value of n, there are $2n + 1$ distinct values of p for which Equation [31] has periodic solutions. These solutions, which are known as Lamé functions of the first kind and degree n, will be denoted by $\lambda_n^{(p)}(\beta_i)$. The associated second solution of Lamé's equation, i.e., the Lamé functions of the second kind here denoted by $\Lambda_n^{(p)}(\beta_i)$, are obtainable from $\lambda_n^{(p)}$ by a quadrature which we refer to the real arguments α_i instead of the former complex arguments β_i

$$\Lambda_n^{(p)}(\alpha_i) = \lambda_n^{(p)}(\alpha_i)\int_0^{\alpha_i} \frac{dt}{[\lambda_n^{(p)}(t)]^2} \ldots\ldots [32]$$

[14] The modulus of any elliptic function is understood to be k unless otherwise specified; see, for example, s_2, c_2, d_2 in Equations [19].

[15] Although the subsequent computations involve complex-valued functions, any result which possesses geometric or physical significance is real, as is readily verified by aid of Equations [19].

[16] This particular choice of k and m is explained subsequently.

[17] The orthogonality may be verified at once by Equations [5].

[18] It should be noted that the infinity of the Cartesian space corresponds to $\alpha_1 = 0$.

It will be essential to keep in mind that the functions $\Lambda_n^{(p)}(\alpha_i)$ are not periodic. Furthermore, from Equations [32]

$$\Lambda_n^{(p)}(0) = 0 \quad \text{[33]}$$

According to Equation [30], and using the foregoing notation for the Lamé functions of the first and second kind, the product solutions of Laplace's Equation [29] take the form

$$U_n^{(p)}(\alpha_1, \alpha_2, \alpha_3) = \prod_{i=1}^{3} [\lambda_n^{(p)}(\alpha_i) \text{ or } \Lambda_n^{(p)}(\alpha_i)]$$
$$p = 1,2, \ldots . 2n + 1$$
$$n = 0, 1, 2, 3, \ldots . \quad \text{[34]}$$

CONSTRUCTION OF SOLUTION TO CAVITY PROBLEM

The initial step in the solution of the problem stated previously consists of extending the uniform stress field, Equations [1], throughout the entire space. As this will violate the boundary conditions for the surface of the cavity

$$\tau_{11} = \tau_{12} = \tau_{13} = 0 \text{ at } \alpha_1 = \alpha_1^{\circ} \quad \text{[35]}$$

we shall have to determine next a solution which, when superimposed on the uniform stress field, removes the stress residuals at $\alpha_1 = \alpha_1^{\circ}$, while leaving undisturbed the stresses at infinity, Equations [1]. The solution sought, consequently, must vanish at infinity. With a view toward this procedure, we first transform the uniform stress field, given by Equations [1], into ellipsoidal co-ordinates. By means of Equations [1], [8], [27] and the law of transformation[19] for the components of stress, we obtain

$$\tau_{11} = \frac{-1}{(k')^2 q_2^2 q_3^2} [(k')^2 \sigma_1 c_1^2 d_1^2 s_2^2 s_3^2 + \sigma_2 s_1^2 d_1^2 c_2^2 c_3^2 - \sigma_3 s_1^2 c_1^2 d_2^2 d_3^2]$$

$$\tau_{22} = \frac{-1}{(k')^2 q_3^2 q_1^2} [(k')^2 \sigma_1 s_1^2 c_2^2 d_2^2 s_3^2 + \sigma_2 c_1^2 s_2^2 d_2^2 c_3^2 - \sigma_3 d_1^2 s_2^2 c_2^2 d_3^2]$$

$$\tau_{33} = \frac{-1}{(k')^2 q_1^2 q_2^2} [(k')^2 \sigma_1 s_1^2 s_2^2 c_3^2 d_3^2 + \sigma_2 c_1^2 c_2^2 s_3^2 d_3^2 - \sigma_3 d_1^2 d_2^2 s_3^2 c_3^2] \quad \text{[36]}$$

$$\tau_{23} = \frac{-s_2 c_2 d_2 s_3 c_3 d_3}{(k')^2 q_1^2 q_2 q_3} [(k')^2 \sigma_1 s_1^2 + \sigma_2 c_1^2 - \sigma_3 d_1^2]$$

$$\tau_{31} = \frac{-s_3 c_3 d_3 s_1 c_1 d_1}{(k')^2 q_2^2 q_3 q_1} [(k')^2 \sigma_1 s_2^2 + \sigma_2 c_2^2 - \sigma_3 d_2^2]$$

$$\tau_{12} = \frac{-s_1 c_1 d_1 s_2 c_2 d_2}{(k')^2 q_3^2 q_1 q_2} [(k')^2 \sigma_1 s_3^2 + \sigma_2 c_3^2 - \sigma_3 d_3^2]$$

We now have to construct the aggregate of solutions needed to eliminate the residual stresses $\tau_{11}, \tau_{12}, \tau_{13}$ at $\alpha_1 = \alpha_1^{\circ}$ of the stress distribution, Equations [36]. This is achieved by appropriate choice of the stress functions (displacement potentials) X, Y, Z, F appearing in Equations [15]. In selecting these harmonic functions, we are guided by the requirements that the stress fields so generated are to be regular in the region exterior to the cavity and must vanish at infinity; they furthermore must possess the periodic structure and symmetry with respect to α_2, α_3 which is inherent in the uniform field, Equations [36]. It follows, in particular, that Lamé functions of the first kind in α_1 and those of the second kind in α_2 or α_3 are not admissible in Equations [34].

[19] Reference (1), Equations [9], p. 80.

A survey of all available Lamé products reveals that the only stress functions with the required properties are as follows

$$\begin{aligned} &(1) \quad X = mS_1 s_2 s_3 \\ &(2) \quad Y = \frac{-m}{k'} C_1 c_2 c_3 \\ &(3) \quad Z = \frac{im}{k^2 k'} D_1 d_2 d_3 \\ &(4) \quad F_1 = km^2 \alpha_1 \\ &(5) \quad F_2 = km^2 L_1 l_2 l_3 \end{aligned} \quad \text{[37]}^{20}$$

The preceding ellipsoidal harmonics involve the Lamé functions of the first kind $s_i = sn\beta_i$, $c_i = cn\beta_i$, $d_i = dn\beta_i$, 1, and l_i, where

$$l_i = l(\beta_i) = s_i^2 - \frac{2}{p(1 + k^2)} \quad \text{[38]}$$

and p will be given subsequently.

The Lamé functions of the second kind S_1, C_1, D_1, α_1, and L_1, whose argument is α_1, correspond, respectively, to the functions of the first kind s_1, c_1, d_1, 1, l_1, and may be obtained by a direct application of the quadrature Formula [32]. Carrying out the necessary integrations, and thereafter dropping inconvenient constant multipliers, we arrive at

$$\begin{aligned} S_1 &= [\alpha_1 - E(\alpha_1)] s_1 \\ C_1 &= [(k')^2 \alpha_1 - E(\alpha_1)] c_1 + \frac{d_1}{s_1} \\ D_1 &= \frac{c_1}{s_1} - d_1 E(\alpha_1) \\ L_1 &= \left\{ 2k^2 \alpha_1 + p(1 + k^2) [E(\alpha_1) - \alpha_1] \right\} l_1 + \frac{2c_1 d_1}{s_1} \end{aligned} \quad \text{[39]}$$

where

$$E(\alpha_1) = \int_0^{a_1} dn^2 t dt \quad \text{[40]}$$

is the incomplete elliptic integral of the second kind.

The three separate factors in each of the five Lamé products appearing in Equations [37] belong to the same pair of values of n and p in Lamé's Equations [31]. The values of n and p corresponding to these five products in Equations [37] are listed here

$$\begin{aligned} &(1) \quad n = 1, \quad p = 1 \\ &(2) \quad n = 1, \quad p = \frac{1}{1 + k^2} \\ &(3) \quad n = 1, \quad p = \frac{k^2}{1 + k^2} \\ &(4) \quad n = 0, \quad p = 0 \\ &(5) \quad n = 2, \quad p = 2 \frac{+}{(-)} 2 \frac{\sqrt{1 - k^2 + k^4}}{1 + k^2} \end{aligned} \quad \text{[41]}$$

We note that a single ellipsoidal harmonic of the first degree is to be used in connection with each of the basic solutions (*a*), (*b*), and (*c*), whereas two distinct harmonic functions of degree two in addition to one of zero degree are admissible in conjunction with basic solution (*d*). Thus it appears that we have at our disposal six solutions for the purpose at hand. However, the six solutions which so arise are found to be linearly dependent.

[20] The unessential constant coefficients are introduced for future computational convenience.

This linear dependence is eliminated by deleting the ambiguity of sign of the fifth of Equations [41], and retaining merely the positive sign. Equations [37] then lead to five linearly independent solutions which will be designated as Solutions 1, 2, 3, 4, and 5, respectively. The corresponding stress fields are established by means of Equations [15], [27], [28], [37], [38], [93], [40]. We now record the results of this lengthy computation

Solution 1

$$\left.\begin{aligned}
\tau_{11} &= \frac{S_1}{ks_1}\left[(2-4\nu)\frac{c_1^2d_1^2s_2^2s_3^2}{q_2^2q_3^2}-2\nu\right] + \frac{s_1c_1d_1s_2^2s_3^2}{kq_2^2q_3^2}\left[\frac{1}{q_3^2}-\frac{1}{q_2^2}+\frac{2-2\nu}{s_1^2}\right]\\
\tau_{22} &= \frac{s_1S_1}{k}\left[(2-4\nu)\frac{c_2^2d_2^2s_3^2}{q_1^2q_3^2}-\frac{2\nu}{s_1^2}\right] + \frac{s_1c_1d_1s_2^2s_3^2}{kq_2^2q_3^2}\left[\frac{2\nu}{s_1^2}-\frac{1}{q_3^2}\right]\\
\tau_{33} &= \frac{s_1S_1}{k}\left[(2-4\nu)\frac{s_2^2c_3^2d_3^2}{q_1^2q_2^2}-\frac{2\nu}{s_1^2}\right] + \frac{s_1c_1d_1s_2^2s_3^2}{kq_2^2q_3^2}\left[\frac{2\nu}{s_1^2}+\frac{1}{q_2^2}\right]\\
\tau_{23} &= \frac{(2-4\nu)s_1s_2c_2d_2s_3c_3d_3S_1}{kq_1^2q_2q_3}\\
\tau_{31} &= \frac{s_2^2s_3c_3d_3}{kq_1q_2^2q_3}\left[(2-4\nu)c_1d_1S_1+\frac{s_2^2}{q_2^2}-2\nu\right]\\
\tau_{12} &= \frac{s_2c_2d_2s_3^2}{kq_1q_2q_3^2}\left[(2-4\nu)c_1d_1S_1-\frac{s_2^2}{q_3^2}-2\nu\right]
\end{aligned}\right\}\ldots[42]$$

Solution 2

$$\left.\begin{aligned}
\tau_{11} &= \frac{C_1}{kc_1}\left[(2-4\nu)\frac{s_1^2d_1^2c_2^2c_3^2}{(k')^2q_2^2q_3^2}-2\nu\right] + \frac{s_1c_1d_1c_2^2c_3^2}{kq_2^2q_3^2}\left[\frac{1}{q_3^2}-\frac{1}{q_2^2}-\frac{2-2\nu}{c_1^2}\right]\\
\tau_{22} &= \frac{c_1C_1}{k}\left[(2-4\nu)\frac{s_2^2d_2^2c_3^2}{(k')^2q_1^2q_3^2}-\frac{2\nu}{c_1^2}\right] - \frac{s_1c_1d_1c_2^2c_3^2}{kq_2^2q_3^2}\left[\frac{2\nu}{c_1^2}+\frac{1}{q_3^2}\right]\\
\tau_{33} &= \frac{c_1C_1}{k}\left[(2-4\nu)\frac{c_2^2s_3^2d_3^2}{(k')^2q_1^2q_2^2}-\frac{2\nu}{c_1^2}\right] + \frac{s_1c_1d_1c_2^2c_3^2}{kq_2^2q_3^2}\left[-\frac{2\nu}{c_1^2}+\frac{1}{q_2^2}\right]\\
\tau_{23} &= (2-4\nu)\frac{c_1s_2c_2d_2s_3c_3d_3C_1}{k(k')^2q_1^2q_2q_3}\\
\tau_{31} &= \frac{c_2^2s_3c_3d_3}{kq_1q_2^2q_3}\left[(2-4\nu)\frac{s_1d_1C_1}{(k')^2}+\frac{c_3^2}{q_2^2}+2\nu\right]\\
\tau_{12} &= \frac{s_2c_2d_2c_3^2}{kq_1q_2q_3^2}\left[(2-4\nu)\frac{s_1d_1C_1}{(k')^2}-\frac{c_2^2}{q_3^2}+2\nu\right]
\end{aligned}\right\}\ldots[43]$$

Solution 3

$$\left.\begin{aligned}
\tau_{11} &= \frac{-D_1}{kd_1}\left[(2-4\nu)\frac{s_1^2c_1^2d_2^2d_3^2}{(k')^2q_2^2q_3^2}+2\nu\right] + \frac{s_1c_1d_1d_2^2d_3^2}{k^5q_2^2q_3^2}\left[\frac{1}{q_3^2}-\frac{1}{q_2^2}+\frac{k^2(2\nu-2)}{d_1^2}\right]\\
\tau_{22} &= \frac{-d_1D_1}{k}\left[(2-4\nu)\frac{s_2^2c_2^2d_3^2}{(k')^2q_1^2q_3^2}+\frac{2\nu}{d_1^2}\right] - \frac{s_1c_1d_1d_2^2d_3^2}{k^3q_2^2q_3^2}\left[\frac{1}{k^2q_3^2}+\frac{2\nu}{d_1^2}\right]\\
\tau_{33} &= \frac{-d_1D_1}{k}\left[(2-4\nu)\frac{d_2^2s_3^2c_3^2}{(k')^2q_1^2q_2^2}+\frac{2\nu}{d_1^2}\right] + \frac{s_1c_1d_1d_2^2d_3^2}{k^3q_2^2q_3^2}\left[\frac{1}{k^2q_2^2}-\frac{2\nu}{d_1^2}\right]\\
\tau_{23} &= -(2-4\nu)\frac{d_1s_2c_2d_2s_3c_3d_3D_1}{k(k')^2q_1^2q_2q_3}\\
\tau_{31} &= \frac{d_2^2s_3c_3d_3}{kq_1q_2^2q_3}\left[(-2+4\nu)\frac{s_1c_1D_1}{(k')^2}+\frac{d_3^2}{k^4q_2^2}+\frac{2\nu}{k^2}\right]\\
\tau_{12} &= \frac{s_2c_2d_2d_3^2}{kq_1q_2q_3^2}\left[(-2+4\nu)\frac{s_1c_1D_1}{(k')^2}-\frac{d_2^2}{k^4q_3^2}+\frac{2\nu}{k^2}\right]
\end{aligned}\right\}\ldots[44]$$

Solution 4

$$\left.\begin{aligned}
\tau_{11} &= \frac{s_1c_1d_1}{kq_2^2q_3^2}\left[\frac{1}{q_3^2}-\frac{1}{q_2^2}\right]\\
\tau_{22} &= -\frac{s_1c_1d_1}{kq_2^2q_3^4}\\
\tau_{33} &= \frac{s_1c_1d_1}{kq_2^4q_3^2}\\
\tau_{23} &= 0\\
\tau_{31} &= \frac{s_3c_3d_3}{kq_1q_2^4q_3}\\
\tau_{12} &= -\frac{s_2c_2d_2}{kq_1q_2q_3^4}
\end{aligned}\right\}\ldots[45]$$

Solution 5

$$\left.\begin{aligned}
\tau_{11} &= \frac{-1}{kq_2^2q_3^2}[6k^2s_1^2-p(1+k^2)]L_1l_2l_3 + \frac{(q_2^2-q_3^2)}{kq_2^4q_3^4}s_1c_1d_1L_1'l_2l_3 + \frac{2s_2^2c_2^2d_2^2}{kq_3^4q_1^2}L_1l_3 - \frac{2s_3^2c_3^2d_3^2}{kq_1^2q_2^4}L_1l_2\\
\tau_{22} &= \frac{-1}{kq_1^2q_3^2}[6k^2s_2^2-p(1+k^2)]L_1l_2l_3 + \frac{2(q_3^2-q_1^2)}{kq_1^4q_3^4}s_2^2c_2^2d_2^2L_1l_3 + \frac{2s_3^2c_3^2d_3^2}{kq_1^4q_2^2}L_1l_2 - \frac{s_1c_1d_1}{kq_2^2q_3^4}L_1'l_2l_3\\
\tau_{33} &= \frac{-1}{kq_1^2q_2^2}[6k^2s_3^2-p(1+k^2)]L_1l_2l_3 + \frac{2(q_1^2-q_2^2)}{kq_1^4q_2^4}s_3^2c_3^2d_3^2L_1l_2 + \frac{s_1c_1d_1}{kq_2^4q_3^2}L_1'l_2l_3 - \frac{2s_2^2c_2^2d_2^2}{kq_1^4q_3^2}L_1l_3
\end{aligned}\right\}\ldots[46]$$

$$\left.\begin{aligned} \tau_{23} &= -\frac{2s_2c_2d_2s_3c_3d_3L_1}{kq_1{}^2q_2q_3} \\ \tau_{31} &= -\frac{s_3c_3d_3l_2}{kq_1q_2{}^4q_3}\left[q_2{}^2L_1{}' - \frac{8(1-p)}{3p}\right] \\ \tau_{12} &= -\frac{s_2c_2d_2l_3}{kq_1q_2q_3{}^4}\left[q_3{}^2L_1{}' + \frac{8(1-p)}{3p}\right] \end{aligned}\right\} \quad \begin{matrix}..[46]\\(\text{cont.})\end{matrix}$$

With regard to solution [5], it should be observed that according to Equations [41]

$$p = 2 + 2\frac{\sqrt{1-k^2+k^4}}{1+k^2} \quad \ldots\ldots\ldots\ldots [47]$$

and by Equations [39], [40], and [16]

$$L_1{}' = \frac{dL_1}{d\alpha_1} = \frac{dL_1}{d\beta_1} = \frac{2L_1s_1c_1d_1}{l_1} + \frac{8(1-p)}{3pl_1} \quad \ldots\ldots [48]$$

The complete solution to our problem is given by a linear combination of the uniform stress field, Equations [36], and the five component solutions, Equations [42, 43, 44, 45, 46]. We may write symbolically

$$[\text{Sol}] = [\text{uniform field}] + \sum_{N=1}^{5} A_N[\text{Sol } N] \quad \ldots. [49]$$

where the coefficients A_N are to be determined consistent with the boundary conditions for the surface of the cavity, Equations [35]. These boundary conditions demand that for $\alpha_1 = \alpha_1{}^\circ$ the stress components τ_{11}, τ_{12}, τ_{13} vanish identically in the arguments α_2, α_3 (or equivalently, in β_2, β_3). By imposing the foregoing requirement upon the linear combination, Equations [49], we are led to sixteen linear equations in the coefficients of superposition, $A_N(N = 1, 2 \ldots 5)$. The system of equations so obtained is compatible, and can be reduced to the following five linearly independent equations which we now record in matrix form:

$$\left.\begin{bmatrix} P_1 & P_2 & P_3 & 0 & J \\ T_1 & T_2 & T_3 & 0 & -L_1{}' \\ s_1{}^2 & -c_1{}^2 & \dfrac{-d_1{}^2}{k^2} & 0 & \bar{p} \\ s_1{}^2T_1 & -c_1{}^2T_2 & \dfrac{-d_1{}^2T_3}{k^2} & 0 & -l_1L_1{}' \\ s_1{}^4 & c_1{}^4 & \dfrac{d_1{}^4}{k^4} & 1 & l_1\bar{p} \end{bmatrix}\begin{bmatrix} A_1 \\ A_2 \\ A_3 \\ A_4 \\ A_5 \end{bmatrix} = \begin{bmatrix} \dfrac{-kc_1d_1}{s_1} & \dfrac{-ks_1d_1}{(k')^2c_1} & \dfrac{k^5s_1c_1}{(k')^2d_1} \\ ks_1c_1d_1 & \dfrac{-ks_1c_1d_1}{(k')^2} & \dfrac{k^3s_1c_1d_1}{(k')^2} \\ 0 & 0 & 0 \\ ks_1{}^3c_1d_1 & \dfrac{ks_1c_1{}^3d_1}{(k')^2} & \dfrac{-ks_1c_1d_1{}^3}{(k')^2} \\ 0 & 0 & 0 \end{bmatrix}\begin{bmatrix} \sigma_1 \\ \sigma_2 \\ \sigma_3 \end{bmatrix} \right\} \quad \ldots\ldots [50]$$

Equations [50] involve the auxiliary notations

$$\left.\begin{aligned} \bar{p} &= \frac{8(1-p)}{3p} \\ T_1 &= (1-2\nu)\,[1 + 2S_1c_1d_1] \\ T_2 &= (1-2\nu)\left[1 - \frac{2}{(k')^2}s_1C_1d_1\right] \\ T_3 &= (1-2\nu)\left[1 + \frac{2k^2}{(k')^2}s_1c_1D_1\right] \\ P_1 &= -\frac{1}{s_1{}^2}\left[\frac{2\nu S_1}{c_1d_1} + T_1 + 1\right] \\ P_2 &= -\frac{1}{c_1{}^2}\left[\frac{2\nu C_1}{s_1d_1} - T_2 - 1\right] \\ P_3 &= -\frac{1}{d_1{}^2}\left[\frac{2\nu D_1}{s_1c_1} - k^2(T_3+1)\right] \\ J &= \frac{L_1}{s_1c_1d_1}\,[2k^2l_1 + (2-p)\,(1+k^2)] \end{aligned}\right\} \quad \begin{matrix}.....[51]\\(\text{cont.})\end{matrix}$$

It should be emphasized that all functions of α_1 appearing in Equations [50], [51] are to be evaluated[21] at $\alpha_1{}^\circ$. An explicit presentation of the solution for the unknown A_N is quite lengthy and will be omitted here. Indeed, it is more advantageous to solve Equations [50] subsequent to the substitution of the numerical values appropriate to a cavity of a particular shape. In any case, Equations [49, 36, 42, 43, 44, 45, 46], together with the solution of Equations [50] constitute the complete solution of the problem under consideration.

Numerical Evaluation and Discussion of Technically Significant Stress Concentrations

The solution for the stress distribution around a triaxial ellipsoidal cavity, established in the preceding section, depends upon the values of the principal stresses σ_1, σ_2, σ_3 at infinity, the position parameters (ellipsoidal co-ordinates) α_1, α_2, α_3, and the shape ratios $\rho_1 = b/a$, $\rho_2 = c/b$ where a, b, c are the semiaxes of the cavity as indicated in Fig. 1. The solution, furthermore, involves Poisson's ratio ν. For fixed values of σ_1, σ_2, σ_3, ρ_1, ρ_2, and ν, the stress components are found to depend solely upon the dimensionless co-ordinates $\xi = x/a$, $\eta = y/b$, $\zeta = z/c$. It follows that the maximum stress concentrations are functions of the loads, the shape of the cavity, as well as the elastic properties of the medium, but are not influenced by the absolute size of the cavity. Analogous conclusions are, clearly, characteristic of all problems of the type under discussion.

[21] The superscript zero which these functions ought to bear was suppressed for the sake of convenience.

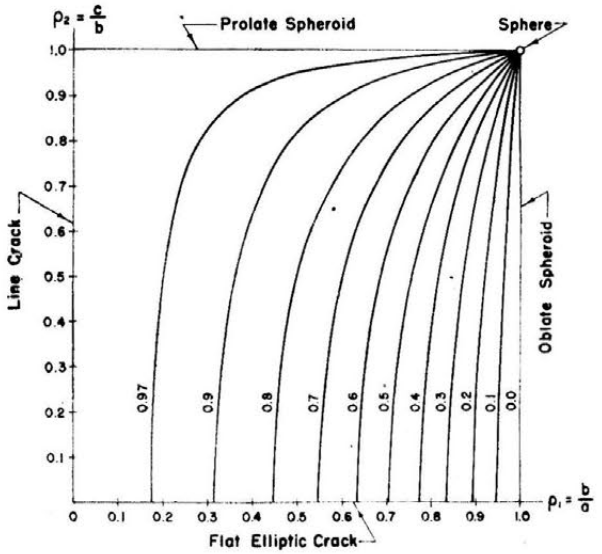

Fig. 3 Iso-Modular Curves: k^2 = Const

The shape ratios ρ_1, ρ_2 enter the stress distribution implicitly through the modulus k and the cavity parameter $\alpha_1{}^\circ$. In view of Equations [21], [25], we have the relations

$$k = \sqrt{\frac{1-\rho_1{}^2}{1-\rho_1{}^2\rho_2{}^2}}, \quad sn\ \alpha_1{}^\circ = \sqrt{1-\rho_1{}^2\rho_2{}^2} \ldots\ldots [52]$$

and from Equation [22]

$$0 < \rho_1 = \frac{b}{a} < 1, \quad 0 < \rho_2 = \frac{c}{b} < 1 \ldots\ldots [53]$$

Fig. 3, which is based on the first of Equations [52], shows "isomodular" curves, that is, the lines k^2 = constant in the ρ_1, ρ_2-plane (shape plane). As the square $0 \leqslant \rho_1 \leqslant 1, 0 \leqslant \rho_2 \leqslant 1$ is traversed, the ellipsoidal cavity assumes all possible shapes. This diagram, in particular, also indicates the various degenerate cases which correspond to the limiting shape ratios $\rho_1 = 0, 1$ and $\rho_2 = 0, 1$. The dependence upon ρ_1 and ρ_2 of any displacement or stress component for fixed values of ξ, η, ζ may be represented by a surface erected over the unit square in the shape plane. Once k and $sn\ \alpha_1{}^\circ$, corresponding to a given pair of shape ratios are determined, all remaining shape-dependent elements of the solution are readily computed by aid of available tables[22] of Jacobian elliptic functions or theta functions, Jacobi's zeta function, and complete elliptic integrals. In particular, for any specific choice of σ_1, σ_2, σ_3, and ν, the solution of Equations [50] for the coefficients of superposition $A_N (N = 1, 2, \ldots 5)$ is now numerically obtainable.

Since the significant stress concentrations occur along the Cartesian co-ordinate axes $Oxyz$, the following relations are pertinent to the evaluation of the component solutions, Equations [42, 43, 44, 45, 46], at interior and surface points of the body
for

$$\left.\begin{aligned} &y = \eta = 0, \quad z = \zeta = 0, \quad x \geqslant a \\ &\xi = \frac{x}{a} = \frac{sn\alpha_1{}^\circ}{sn\alpha_1}, \quad \alpha_2 = K', \quad \alpha_3 = K \\ &\sigma_x = \tau_{11}, \quad \sigma_y = \tau_{33}, \quad \sigma_z = \tau_{22} \end{aligned}\right\} \ldots\ldots [54]$$

for

$$\left.\begin{aligned} &x = \xi = 0, \quad z = \zeta = 0, \quad y \geqslant b \\ &\eta = \frac{y}{b} = \frac{sn\alpha_1{}^\circ dn\alpha_1}{sn\alpha_1 dn\alpha_1{}^\circ}, \quad \alpha_2 = K', \ \alpha_3 = 0 \\ &\sigma_x = \tau_{33}, \quad \sigma_y = \tau_{11}, \quad \sigma_z = \tau_{22} \end{aligned}\right\} \ldots\ldots [55]$$

for

$$\left.\begin{aligned} &x = \xi = 0, \quad y = \eta = 0, \quad z \geqslant c \\ &\zeta = \frac{z}{c} = \frac{sn\alpha_1{}^\circ\, cn\alpha_1}{sn\alpha_1\, cn\alpha_1{}^\circ}, \quad \alpha_2 = \alpha_3 = 0 \\ &\sigma_x = \tau_{33}, \quad \sigma_y = \tau_{22}, \quad \sigma_z = \tau_{11} \end{aligned}\right\} \ldots\ldots [56]$$

The normal stresses σ_x, σ_y, σ_z are principal stresses along $Oxyz$, as is apparent at once from considerations of symmetry. The foregoing formulas permit the determination of α_1, corresponding to a given value of ξ, η, or ζ, belonging to a point chosen on either the x, y, or z-axis for a cavity of prescribed shape. With α_1, α_2, α_3 known, the remaining position-dependent elements of the solution, for points on the Cartesian co-ordinate axes, are again readily found by means of the numerical tables previously referred to.

In connection with the numerical evaluation of the incomplete elliptic integral of the second kind, Equation [40], it should be recalled that

$$E(\alpha_1) = Z(\alpha_1) + \frac{\alpha_1 E}{K} \ldots\ldots [57][23]$$

where $Z(\alpha_1)$ is the zeta function of Jacobi. Here K and $E = E(K)$

[22] See references (7, 8, 9, 10).

[23] Equation [57] is needed in the use of reference (10), which contains extensive tabulations of the zeta function of Jacobi.

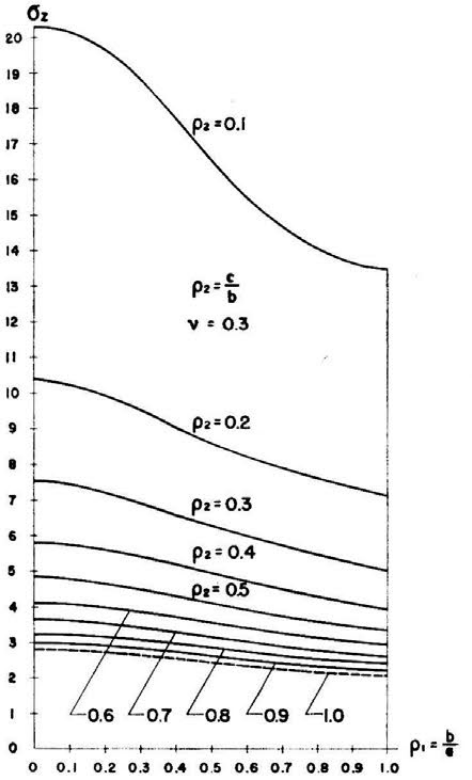

FIG. 4 UNIAXIAL TENSION $\sigma_z = 1$ AT ∞ σ_z AT POINT A FOR VARIOUS SHAPE RATIOS

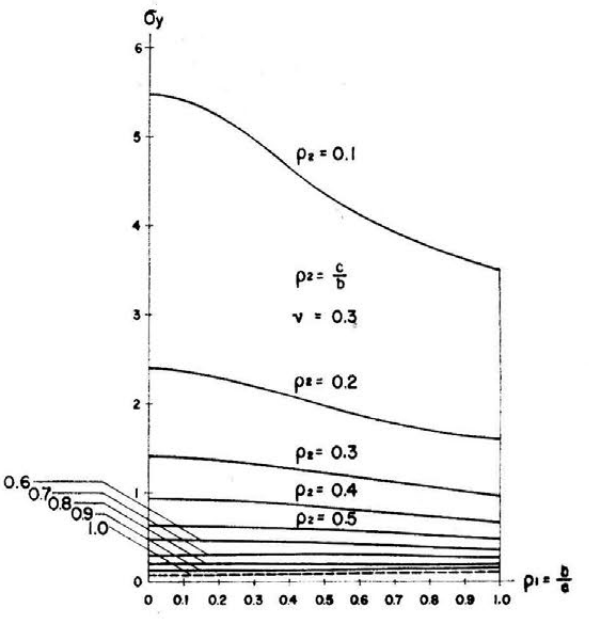

FIG. 5 UNIAXIAL TENSION $\sigma_z = 1$ AT ∞ σ_y AT POINT A FOR VARIOUS SHAPE RATIOS

are at the same time the complete elliptic integrals of the first and second kind associated with the modulus k

$$\left.\begin{aligned} K &= \int_0^{\pi/2} \frac{dt}{\sqrt{1 - k^2 \sin^2 t}} \\ E &= \int_0^{\pi/2} \sqrt{1 - k^2 \sin^2 t}\, dt \end{aligned}\right\} \quad \ldots\ldots\ldots [58]$$

We now turn to a discussion of the numerical results obtained, and confine our attention to the technically most interesting case in which the uniform state of stress at infinity is one of unit uniaxial tension parallel to the smallest semiaxis c of the cavity. We thus put

$$\sigma_1 = 0, \sigma_2 = 0, \sigma_3 = 1 \ldots\ldots\ldots\ldots\ldots [59]$$

in Equations [50].

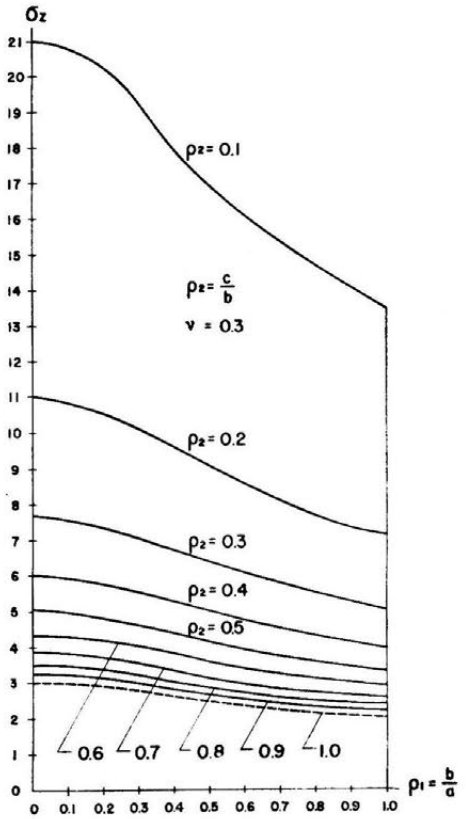

FIG. 6 UNIAXIAL TENSION $\sigma_z = 1$ AT ∞ σ_z AT POINT B FOR VARIOUS SHAPE RATIOS

The important stress concentrations in this instance take place at the extremities of the semiaxes a and b, i.e., at points A and B, Fig. 1. Figs. 4 and 5 show σ_z and σ_y at point A as a function of the shape ratio ρ_1, for various values of the shape ratio ρ_2. The analogous diagrams for σ_z and σ_x at point B are given in Figs. 6 and 7. All of these curves are based upon Poisson's ratio $\nu = 0.3$, and may be interpreted as profiles of the respective stress surfaces erected over the basic unit square in the shape plane, Fig. 3.

The curves for $\rho_2 = 1$ apply to a cavity in the shape of a prolate ellipsoid of revolution, and coincide with the results obtained by the authors in a previous investigation.[24] The stress values for $\rho_1 = 1$, i.e., the right end points of the curves under consideration, are in agreement with the corresponding results given by H. Neuber[25] for the case where the boundary of the cavity is an oblate ellipsoid of revolution. In particular, the stress-concentration factors reduce to those appropriate to a spherical cavity for $\rho_1 = \rho_2 = 1$. The limiting stress values as ρ_1 approaches zero, i.e., the left end points of the foregoing curves, are of special in-

[24] See reference (4), Figs. 7, 8, 10, 11.

[25] Reference (3), equation 133 on p. 98 and equation 136 on p. 99. See also Fig. 58.

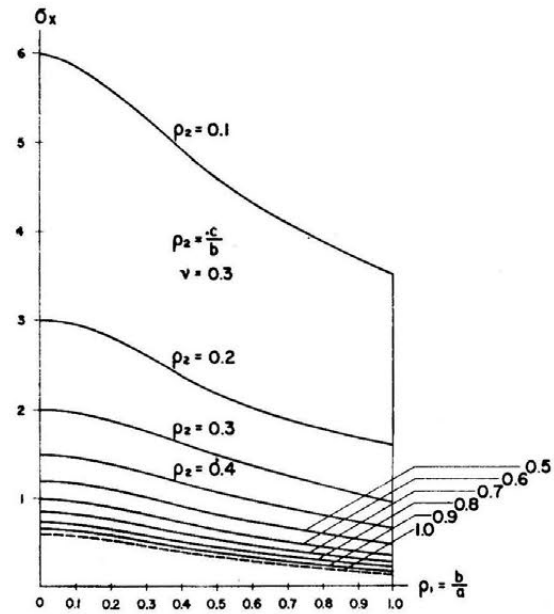

FIG. 7 UNIAXIAL TENSION $\sigma_z = 1$ AT ∞ σ_x AT POINT B FOR VARIOUS SHAPE RATIOS

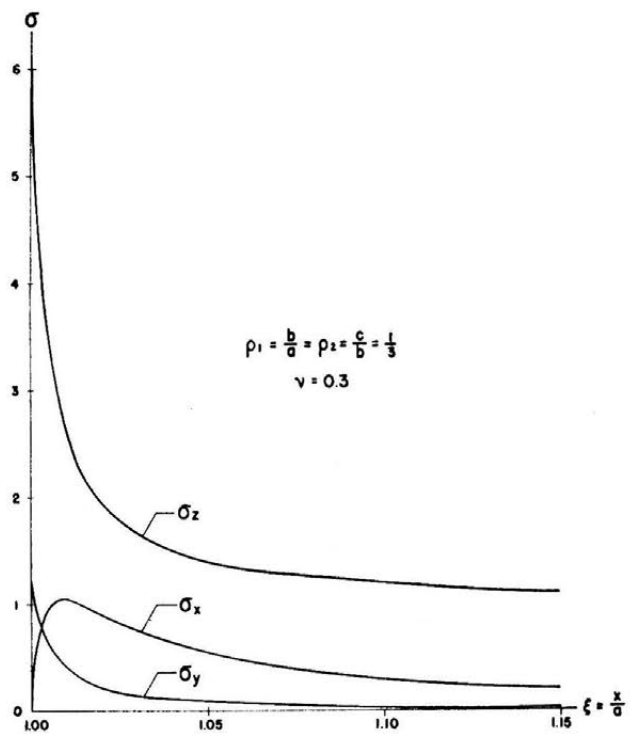

FIG. 8 UNIAXIAL TENSION $\sigma_z = 1$ AT ∞ σ_x, σ_y, AND σ_z ALONG THE x-AXIS

terest since they are representative of an internal line crack along the x-axis. It should be recognized that the ellipsoids in the neighborhood of the line crack possess an elliptic cross section in the plane Oyz, which ranges from a circle to a straight-line segment parallel to the y-axis as ρ_2 traverses the range from unity to zero. We note that the line crack induces finite stress concentrations as long as $\rho_2 > 0$. As was to be anticipated, the line-crack values of σ_z at point B, Fig. 6, coincide with the hoop stresses which arise in the presence of an infinitely long, elliptic cylindrical hole at the end points of the major axis of its cross section. The plane solution of the problem to which we are referring is due to C. E. Inglis.[26]

Regardless of the value of ρ_1, all of the stress-concentration factors under discussion rise rapidly and tend to infinity as the shape ratio ρ_2 decreases and approaches the limiting value zero which corresponds to a flat, elliptic crack[27] in the plane Oxy. With the exception of σ_y at point A, the stress-concentration factors for fixed values of ρ_2 are found to be monotone decreasing functions of ρ_1, and thus steadily decline as the cavity is inflated from the line crack to an oblate ellipsoid of revolution. σ_y at point A, Fig. 5, rises with increasing ρ_1 in the neighborhood of the prolate spheroidal cavity, given by $\rho_2 = 1$. However, the values of this stress component throughout the range of ρ_2, for which the reversal of its monotone character occurs, are seen to be insignificantly small. It is interesting to observe that for all shapes other than the oblate spheroid, σ_z and σ_x at the point B are larger, respectively, than σ_z and σ_y at the point A. The maximum stress concentration is found in σ_z at the point B.

Fig. 8 illustrates the variation along the x-axis of the principal stresses σ_x, σ_y, and σ_z. The curves shown are based upon the sample shape ratios $\rho_1 = \rho_2 = 1/3$ and again on the Poisson ratio $\nu = 0.3$. This diagram indicates the rate of decay of the stress concentration. The stresses σ_y and σ_z are steadily decreasing functions of ξ whereas σ_x attains its interior maximum approximately at $\xi = 1.009$. We observe that the state of stress in the vicinity of point A is one of triaxial tension, and that the uniform, uniaxial state of stress $\sigma_z = 1$ is practically restored at $\xi = 1.2$.

Finally, we consider the influence of Poisson's ratio ν upon the stresses at point A, illustrated by the curves in Fig. 9, which again refer to the sample shape ratios $\rho_1 = \rho_2 = 1/3$. It is seen that while the stress σ_z, which acts parallel to the uniform stress field at infinity, is essentially unaffected by changes in ν, the transverse stress σ_y depends sensitively upon Poisson's ratio.

ACKNOWLEDGMENT

The assistance of Miss D. M. Kell and Mr. R. F. Sell in voluminous numerical computations is gratefully acknowledged. The authors are greatly indebted to the Administration of the David Taylor Model Basin, Washington, D. C., for permission to publish the material contained in this paper.

[26] See, for example, reference (3), p. 48, et seq.

[27] The term "flat, elliptic crack" is used to describe a separation of the material throughout the interior of a plane region bounded by an ellipse.

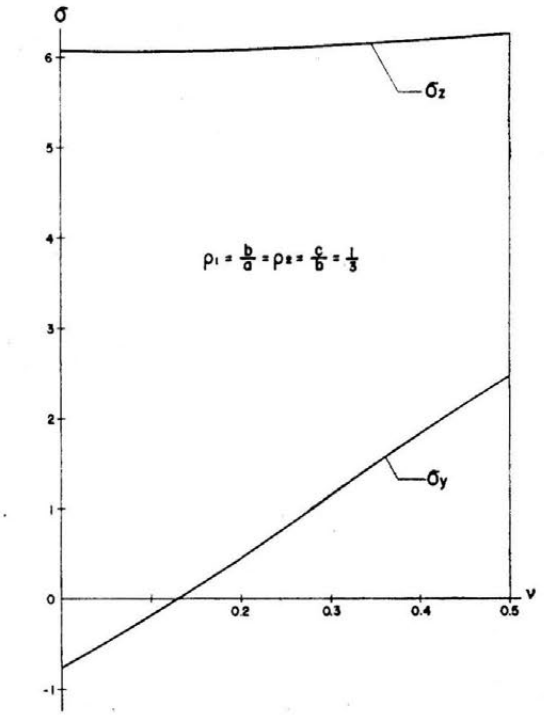

FIG. 9 UNIAXIAL TENSION $\sigma_z = 1$ AT ∞ ν-DEPENDENCE OF σ_y AND σ_z AT POINT A

BIBLIOGRAPHY

1 "A Treatise on the Mathematical Theory of Elasticity," by A. E. H. Love, fourth edition, Dover Publications, New York, N. Y., 1944.

2 "Applications des Potentiels," by J. Boussinesq, Gauthier-Villars, Paris, France, 1885.

3 "Kerbspannungslehre," by H. Neuber, J. W. Edwards, Ann Arbor, Mich., 1944.

4 "Stress Concentration Around an Ellipsoidal Cavity in an Infinite Body Under Arbitrary Plane Stress Perpendicular to the Axis of Revolution of the Cavity," by M. A. Sadowsky and E. Sternberg, JOURNAL OF APPLIED MECHANICS, Trans. ASME, vol. 69, 1947, p. A-191.

5 "A Course of Modern Analysis," by E. T. Whittaker and G. N. Watson, fourth edition, University Press, Cambridge, England, 1935.

6 "The Theory of Spherical and Ellipsoidal Harmonics," by E. W. Hobson, University Press, Cambridge, England, 1931.

7 "Smithsonian Mathematical Formulae and Tables of Elliptic Functions," by Sir George Greenhill and R. L. Hippisley, first reprint, The Smithsonian Institution, Washington, D. C., 1939.

8 "Smithsonian Elliptic Functions Tables," by G. W. and R. M. Spenceley, The Smithsonian Institution, Washington, D. C., 1947.

9 "Die Elliptischen Funktionen von Jacobi," by L. M. Milne-Thompson, Julius Springer, Berlin, Germany, 1931.

10 "The Zeta Function of Jacobi," by L. M. Milne-Thompson, Proceedings of the Royal Society of Edinburgh, Scotland, vol. 52, 1931–1932, pp. 236–250.

Stability of Linear Oscillating Systems With Constant Time Lag

By H. I. ANSOFF,[1] PROVIDENCE, R. I.

This paper discusses the influence of constant time delay in transmission of the control signal upon the output system of a closed-cycle control device. The use of Nyquist's stability criterion permits investigation of the control signal proportional to any derivative of the displacement. The stability criteria are given in closed form.

Introduction

IT is well known that closed-cycle control systems exhibit a time lag between the input and the output signal. This time lag is due partly to the inertia and damping present in the system and partly to the inherent delay in transmission of the control signal. This paper discusses the effect of a time delay due to the transmission of the signal upon the stability of the output system of a closed-cycle control device.

The feedback is assumed to be proportional to the nth derivative of the displacement and to be delayed by a constant time τ. The system is further assumed to be linear and to possess viscous damping.

Under these conditions, it is shown that steady-state modes[2] will exist only with a very critical combination of the parameters of the system. The problem of stability is then investigated by means of the Nyquist stability criterion. For $n \leqq 2$, it is shown that under appropriate conditions there exists a band spectrum of values of τ for which the system will be stable. For $n > 2$ the system is shown to be unconditionally unstable. The case of $n = 1$ corresponds to a combination of the viscous and the "error-rate damping" used in servomechanism design.

The following nomenclature is used:

t = independent variable, time
τ = constant time lag
θ = dependent variable
I, R, K = constant parameters of system
S = magnitude of feedback signal

Statement of the Problem

The differential equation of the freely oscillating output system of a closed-cycle control device with viscous damping is given by (1)[3]

$$I\ddot{\theta}(t) + R\dot{\theta}(t) + K\theta(t) = 0 \quad \ldots\ldots [1]$$

where dots indicate differentiation, and I, R, and K are taken as real and positive.

We introduce a feedback term proportional to $\dot{\theta}(t)$, of constant magnitude S, and lagging behind $\dot{\theta}(t)$ by a constant τ. Equation [1] becomes

$$I\ddot{\theta}(t) + R\dot{\theta}(t) + K\theta(t) = -S\dot{\theta}(t-\tau) \quad \ldots\ldots [2]$$

A solution of this is given by

$$\theta = \sum_{n=0}^{N} \theta_n e^{z_n t} \quad \ldots\ldots [3]$$

Substituting this into Equation [2] and equating the coefficients for each n, we obtain the characteristic equation

$$z_n^2 I + z_n R + S z_n e^{-z_n \tau} + K = 0 \quad \ldots\ldots [4]$$

If $e^{-z_n\tau}$ is expanded into its series, it is easily seen that, in general, Equation [4] possesses an infinity of roots. Therefore, rather than attempt a solution in closed form given by Equation [3], we are forced to seek the stability conditions for the system Equation [2] in terms of the parameters of the system.

This problem has been attacked by numerous writers. The present treatment differs from the others in its application of the Nyquist stability criterion to the operational form of Equation [2] and in presenting the final results in an easily computed closed form. This paper is of wider scope than the majority of the preceding ones, since it formulates stability conditions for feedback proportional to any derivative of θ.

Steady-State Solutions

If Equation [2] has steady-state solutions, some values of z_n in Equation [3] will be purely imaginary. Setting $z_n = i\omega$, ω real, and substituting this into Equation [4], we obtain

$$-\omega^2 I + i\omega R + iS\omega e^{-i\omega\tau} + K = 0 \quad \ldots\ldots [5]$$

Separating the real and the imaginary parts, we obtain

$$S \cos \omega\tau = -R \quad \ldots\ldots [6a]$$

$$S\,\omega \sin \omega\tau = \omega^2 I - K \quad \ldots\ldots [6b]$$

Since S and R are real and positive it follows from Equation [6a] that for integer n

$$\pi\left(\frac{1}{2} + 2n\right) \leqq \omega\tau \leqq \pi\left(\frac{3}{2} + 2n\right) \quad \ldots\ldots [7]$$

With this in mind, Equations [6] can be written

$$\sin \omega\tau = \pm\sqrt{1 - \left(\frac{R}{S}\right)^2} \quad \ldots\ldots [8a]$$

$$\sin \omega\tau = \frac{I\omega^2 - K}{S\omega} \quad \ldots\ldots [8b]$$

Now, if the system of Equations [8] has solutions for real values of ω, then the system described by Equation [2] will possess steady-state modes of oscillation.

---

[1] Formerly Research Assistant, Brown University. Now Mathematician, The Rand Corporation, Santa Monica, Calif. Jun. ASME.

[2] Here and in the following the term "steady-state" will be used, as in electrical engineering, to designate continuous oscillations of constant amplitude.

[3] Numbers in parentheses refer to Bibliography at end of paper.

Contributed by the Applied Mechanics Division and presented at the Annual Meeting, New York, N. Y., November 28–December 3, 1948, of The American Society of Mechanical Engineers.

Discussion of this paper should be addressed to the Secretary, ASME, 29 West 39th Street, New York, N. Y., and will be accepted until July 11, 1949, for publication at a later date. Discussion received after the closing date will be returned.

Note: Statements and opinions advanced in papers are to be understood as individual expressions of their authors and not those of the Society. Paper No. 48—A-22.

Given the positive real parameters of the system I, R, K, and S, and the time lag τ, we can determine the existence of solutions of Equations [8] by the following procedure: Plot the graphs of $\sin \omega\tau$ and $(I\omega^2 - K)/(S\omega)$ versus ω. Because of condition given by Equation [7], $\omega\tau$ has a limited periodic range which is indicated by a solid line in Fig. 1. On the same graph we draw two lines $\pm\sqrt{1 - (R/S)^2}$ parallel to the ω-axis. Now if the three graphs have a common point of intersection (such as A in Fig. 1), system, Equations [8], has a steady-state mode, and the value of ω

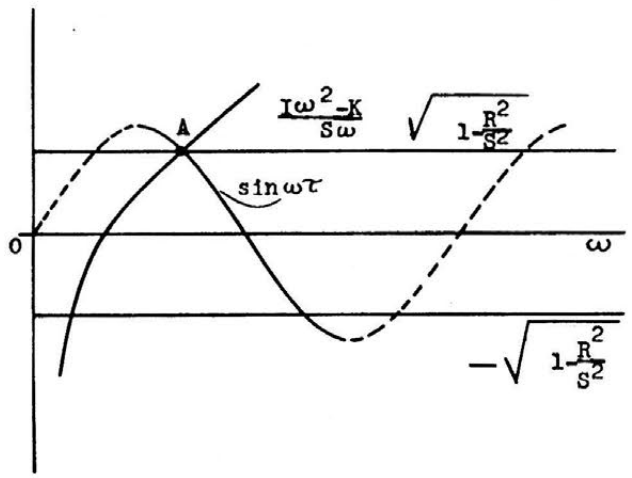

FIG. 1 SOLUTION OF EQUATION [8]

at the common point of intersection is the steady-state frequency. Since I, K, and S are positive and real, the graph of $(I\omega^2 - K)/(S\omega)$ will be monotonically increasing in ω. It will have only two points in common with the lines $\pm\sqrt{1 - (R/S)^2}$, and the system of Equations [8] can, consequently, have at most two steady-state modes for a given combination of parameters $I, R, K, S,$ and τ.

On the other hand, given the parameters of the system I, R, K, and S, we can determine whether a steady-state solution exists and also what value of τ is required for its existence. As before, we plot $(I\omega^2 - K)/(S\omega)$ and $\pm\sqrt{1 - (R/S)^2}$ versus ω. Denote the co-ordinates of the two points of intersection by (ω_n, a_n), where $n = 1, 2$. Then a time lag

$$\tau_n = \frac{\sin^{-1} a_n}{\omega_n}, \quad (n = 1, 2) \ldots\ldots\ldots\ldots\ldots [9]$$

will produce a steady-state mode, provided Equation [7] is satisfied.

It should be clear from the foregoing that only a very critical combination of constants of the system will produce steady-state solutions. Therefore, in the derivation of the stability criterion for almost all systems, we will be safe in assuming that Equation [4] has no pure imaginary roots.

A MECHANICAL MODEL

Some of the foregoing results are easily interpreted in terms of a mechanical model used by Minorsky.[4]

This model consists of an oscillating pendulum of moment of inertia I and equivalent spring constant K (for small deflections). The lower end is immersed in a viscous bath which produces a viscous resistance R. A small gyroscope mounted on the pendulum transmits a signal to an electric motor. The motor in turn moves a weight which produces a feedback torque on the pendulum. The coupling between the gyro and the motor can be adjusted to produce a feedback torque proportional to $\dot{\theta}(t)$, which is the time derivative of the angular displacement.

Applied to this system, Equation [2] becomes the equation of motion; the term $I\ddot{\theta}(t)$ represents the torque due to inertia, $R\dot{\theta}(t)$ the torque due to viscous resistance, $K\theta(t)$ the torque due to gravity, and $S\dot{\theta}(t - \tau)$ the feedback torque due to the counterweight.

If again we assume existence of steady-state solutions and substitute $\theta = \theta_0 e^{i\omega t}$ into Equation [2], we get

$$-\theta_0\omega^2 I e^{i\omega t} + i\theta_0\omega R e^{i\omega t} + i\theta_0\omega S e^{i\omega(t-\tau)} + \theta_0 K e^{i\omega t} = 0 \ldots [10]$$

which leads directly to Equation [4].

Equation [10] can be represented by means of a vector diagram, Fig. 2, similar to the impedance diagrams used in alternating-current circuit analysis. Using polar co-ordinates we plot $\theta_0 K$ along the initial ray and $-\theta_0\omega^2 I$, 180 deg ahead of it (the common term $e^{i\omega t}$ is left out). The term $i\theta_0\omega R$ is plotted along the 90-deg ray, and the term $i\theta_0\omega S e^{-i\omega\tau}$ along the ray which forms an angle $-\omega\tau$ with the 90-deg ray.

It is now clear that in order for the equation of motion, Equation [10], to be satisfied, the vectors in Fig. 2 must be in equilib-

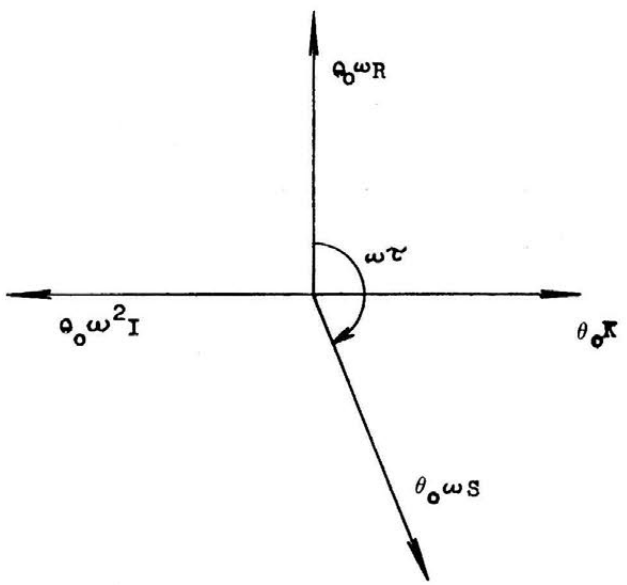

FIG. 2 EQUILIBRIUM VECTOR DIAGRAM

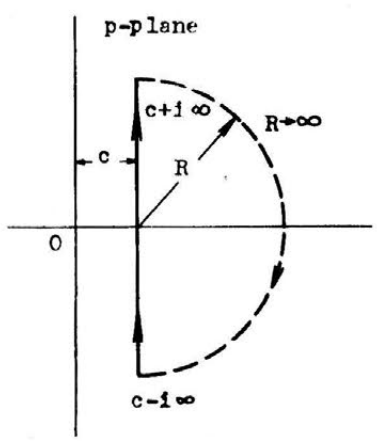

FIG. 3 THE BROMWICH CONTOUR

[4] Although the general method of approach in this section follows closely that of Minorsky, the present results disagree with his findings: see reference (4).

rium. This requires that the vector $i\omega Se^{-i\omega\tau}$ be in either the third or the fourth quadrant (which is just a different form of stating Equation [7]). It is further necessary that $S \geqq R$. Interpreted physically, this means that in order to maintain oscillations, the power supplied by the feedback torque (given by $\omega^2 S$) should be at least as great as the power dissipated by the pendulum (given by $\omega^2 R$). (It should be noted that because of phase considerations the condition $\omega^2 S > \omega^2 R$ does not necessarily imply instability.)

The Stability Criterion for Feedback Proportional to $\dot{\theta}(t - \tau)$

Denoting the Laplace transform[5] of $\theta(t)$ by $F(p)$, we have

$$F(p) \equiv \mathcal{L}[\theta(t)]$$

Taking the transform of Equation [2], we get (6)

$$(p^2 I + pR + K + Spe^{-\tau p})F(p) = pI\theta_0 + I\dot{\theta}_0 + R\theta_0 \ldots [11]$$

where θ_0 and $\dot{\theta}_0$ are used to denote the values at $t = 0$.

Letting

$$\left.\begin{aligned} L(p) &= pI\theta_0 + I\dot{\theta}_0 + R\theta_0 \\ \text{and} \\ Y(p) &= p^2 I + pR + K \end{aligned}\right\} \ldots\ldots [12]$$

we get[6]

$$F(p) = \frac{L(p)}{Y(p) + Spe^{-p\tau}} = \frac{L(p)}{Y(p)} \frac{1}{1 + S\dfrac{pe^{-p\tau}}{p^2 I + pR + K}} \ldots [13]$$

Whence by Mellin's inversion theorem (6, 7)

$$\theta(t) = \frac{1}{2\pi i}\int_\Gamma \frac{L(p)}{Y(p)} \frac{1}{1 + S\dfrac{pe^{-p\tau}}{p^2 I + pR + K}} e^{pt}\, dp \text{ for } t > 0 \ldots\ldots [14]$$

where Γ is a contour enclosing all of the roots of the denominator in the p-plane.

Evaluating this integral by the method of residues we would obtain

$$\theta(t) = \sum_0^n A_n e^{p_n t} \ldots\ldots [15]$$

where p_n are the values of the roots of the denominator. In the "Statement of the Problem," we have shown, however, that there is an infinity of roots. Therefore a closed form of solution is not obtainable by this method.

Turning to the question of stability, we note that if Equation [15] contains p_n with positive real parts, the solution represents an unstable system, and $\theta(t)$ will increase without limit. The existence of p_n with positive real parts thus becomes a criterion of stability. This means that we must determine the existence of any poles of the integrand of Equation [14] in the right half of the p-plane or, which is the same thing, the existence of zeros of the denominator of the integrand in the right half of the p-plane.

Now consider $Y(p)$ which is the first factor of the denominator in Equation [14]. Consulting Equations [12], we see that $Y(p)$ is the transform of a system described by the differential Equation [1]. The solution of this equation is known to be stable. Therefore $Y(p)$ will have no zeros in the right half of the p-plane.

It remains to examine the solutions of

$$1 + S\frac{pe^{-p\tau}}{p^2 I + pR + K} = 0 \ldots\ldots [16]$$

In order to do this, we make use of the Cauchy index theorem,[7] which may be stated as follows:

Hypothesis: 1 $w = f(p)$ is an analytic function in a simply connected domain D bounded by a contour β
2 $f(p) \neq 0$ for p on β

Conclusion: If p traverses β in a counterclockwise direction, then w will traverse a closed curve in the w-plane. Further, the number of zeros of $f(p)$ in D is equal to the number of times the contour in the w-plane encircles the origin.

For β we choose a Bromwich contour shown in Fig. 3. Since we assume that there are no roots on the imaginary axis, we are assured of enclosing all of the roots in the right half of the p-plane by setting $c = 0$.

Examining the behavior of Equation [16] along the contour, we note that for $p = \pm i\infty$

$$\frac{pe^{-p\tau}}{p^2 I + pR + K} = 0$$

Consequently, we may limit our study of Equation [16] to the straight-line contour along the imaginary axes in the range $-i\infty \leqq p \leqq i\infty$.[8]

Before proceeding with the application of the theorem, we divide the second factor of Equation [16] by K and set the result equal to $f(p)$. We get

$$f(p) = A\frac{pe^{-p\tau}}{ap^2 + bp + 1} \ldots\ldots [17a]$$

where

$$A = \frac{S}{K}, \quad a = \frac{I}{K}, \quad b = \frac{R}{K} \ldots\ldots [17b]$$

Letting $p = i\alpha$ in Equations [17] and simplifying the result, we get

$$f(i\alpha) = \frac{\alpha A e^{-i(\alpha\tau - \varphi)}}{[(1 - \alpha^2 a)^2 + (b\alpha)^2]^{1/2}} \ldots\ldots [18a]$$

where

$$\tan\varphi = \frac{-a\alpha^2 + 1}{b\alpha} \ldots\ldots [18b]$$

A graph of Equation [18a] is shown in Fig. 4, for $-\infty < \alpha \leqq 0$. It is a sensed spiral starting at the origin when $\alpha = -\infty$ and returning to the origin when $\alpha = 0$. As α increases from 0 to $+\infty$, the graph follows the second branch of the spiral which is symmetrical to the first branch with respect to the real axis.

We are now ready to apply the Cauchy index theorem. Equation [16] can be rewritten in the form

$$f(p) + 1 = 0 \ldots\ldots [19]$$

Now as p varies along the imaginary axis between $-i\infty$ and $+i\infty$, the contour Γ encloses all of the roots in the right half of the p-plane and the number of times $f(p)$ encloses point $(-1, 0)$ in Fig. 4 will be equal to the number of these roots. Because of

[5] Taking of the Laplace transform of an unknown function naturally raises the question of its existence. Since we are seeking a combination of parameters leading to a solution which is stable in t (we exclude even the steady-state modes), $\theta(t)$ will satisfy the convergence requirements of the Laplace integral.

[6] For other examples of this procedure see reference (2).

[7] See, for example, A. Hurwitz, reference (8).

[8] See Appendix of this paper for a proof showing that Equation [17a] remains zero along the closing semicircular path of the contour.

the symmetry of the two branches, unstable roots will occur in pairs. Therefore we need only to investigate the behavior of one of the branches of $f(p)$.

It is now possible to give the first formulation of the stability criterion for the system represented by Equation [2]. The system will be stable if and only if the graph of $f(p)$ does not enclose the point (—1, 0). By direct examination it follows that if $b > A$ in Equation [18a], then $|f(i\alpha)| < 1$ and the system cannot possibly become unstable. Reference to Equation [17a] shows that this implies that the system will always be stable if

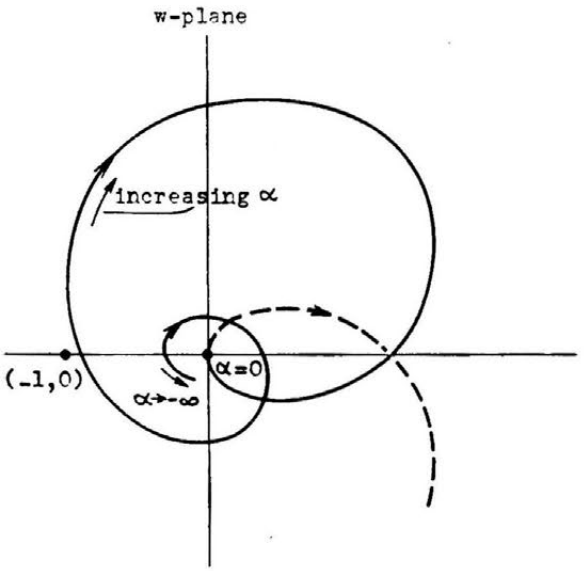

FIG. 4 GRAPH OF EQUATIONS [18a] FOR $-\infty < \alpha \leqq 0$

$$R > S$$

This coincides with the conclusions at the end of the section, "A Mechanical Model," and means that in this case the power dissipated is greater than the feedback power.

Assuming that $S > R$($S = R$ is trivial for all practical purposes) set

$$\frac{A\alpha}{[(1 - \alpha^2 a)^2 + (b\alpha)^2]^{1/2}} = \pm 1 \quad \ldots\ldots [20]$$

and solving for α we get

$$\alpha^2 = \frac{-(b^2 - 2a - A^2) \pm \sqrt{(b^2 - 2a - A^2)^2 - 4a^2}}{2a^2} \quad [21]$$

Thus there are, in general, four real values of α (two for each branch of the curve) for which $|f(i\alpha)| = 1$. The conditions for existence of these values are

$$b^2 - 2a - A^2 < 0$$

and

$$(b^2 - 2a - A^2)^2 - 4a^2 > 0$$

If these are combined with the aid of Equation [17b] we get $S > R$. Therefore a danger of instability exists whenever $S > R$.

Since the magnitude of the radius vector of the spiral, as given by the left side of Equation [20], is a continuous function of α, we may differentiate it in order to determine its extremum values. It turns out to have only one maximum for each branch which occurs at $\alpha = \pm 1/a^{1/2}$.

Thus on each branch the magnitude of the radius vector of the spiral attains the value of 1 twice, say, at α_1 and α_2, and a maximum once. It follows that the magnitude of the radius will be greater than 1 between α_1 and α_2 and will be less than 1 everywhere else. Along the positive branch ($\alpha \geqq 0$) let

$$\left.\begin{aligned} \beta_1 &= -\alpha_1\tau + \varphi_1 \\ \text{and} \\ \beta_2 &= -\alpha_2\tau + \varphi_2 \end{aligned}\right\} \quad \ldots\ldots [22a]$$

and along the negative branch ($\alpha \leqq 0$)

$$\beta_1 = -\alpha_1\tau + \varphi_1 - \pi$$

and

$$\beta_2 = -\alpha_2\tau + \varphi_2 - \pi \quad \ldots\ldots [22b]$$

(the subtraction of π is made necessary by the factor α in front of Equation [18a]. This form of Equations [22] makes the radius vector always positive.)

Note from Equation [18b] that as α increases along each branch the phase angle in Equations [22] decreases monotonically along each branch from $\pi/2$ to $-\pi/2$. Hence if $\alpha_1 > \alpha_2$ (on either branch) we have $-\alpha_2 > -\alpha_1$ and $\varphi_2 < \varphi_1$. Consequently, if $\alpha_1 > \alpha_2$, $\beta_2 > \beta_1$ or, in other words, the angle β, shown on Fig. 5, is a monotone decreasing in α.

Now we know from the foregoing that as α_1 increases to α_2 the magnitude of the radius remains greater than 1. Then $\beta_1 > \beta_2$ and the shaded sector in Fig. 5, obtained by a positive (counterclockwise) rotation from the smaller to the larger value of β, will enclose all of the values of the radius vector which are greater than 1.

Thus the stability criterion is reduced to the requirement that

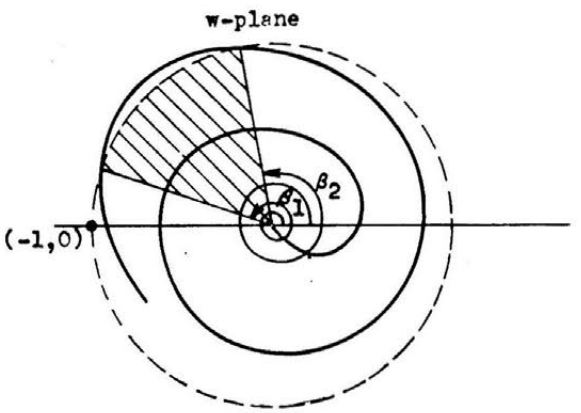

FIG. 5 A STABLE CONFIGURATION

the shaded sector on Fig. 5 does not include the negative real axis. This can be stated as follows:

The system will be stable if no integer n can be found such that

$$\beta_1 \gtrless (2n + 1)\pi \gtrless \beta_2 \quad \ldots\ldots [23]$$

Clearly, if $|\beta_1 - \beta_2| > 2\pi$, the system becomes unstable since then there is a complete turn of the spiral with the magnitude of the radius vector greater than 1. If $|\beta_1 - \beta_2| < 2\pi$, Condition [23] can be satisfied within a certain range of values of the time lag τ which will now be determined. The extreme case is shown in Fig. 6. As seen from Fig. 6, if $\beta_2 > \beta_1$ we must have for stability

$$\left.\begin{aligned} \beta_2 &< (2n + 1)\pi \\ \beta_1 &> (2n + 1)\pi - 2\pi = (2n - 1)\pi \end{aligned}\right\} \quad \ldots\ldots [24]$$

Using Equation [22a] and keeping in mind that $\tau \geqq 0$, we ob-

tain after simple transformations the following range in τ within which the system will be stable

$$\frac{\varphi_2 + (2n-1)\pi}{\alpha_2} < \tau < \frac{\varphi_1 + (2n+1)\pi}{\alpha_1} \quad \ldots\ldots [25]$$

where $\alpha_1 > \alpha_2$ and n is allowed integer positive values.

If Equation [22b] is used, it can be shown that Formula [25] remains valid if magnitudes of α_2 and α_1 are used in the denominator.

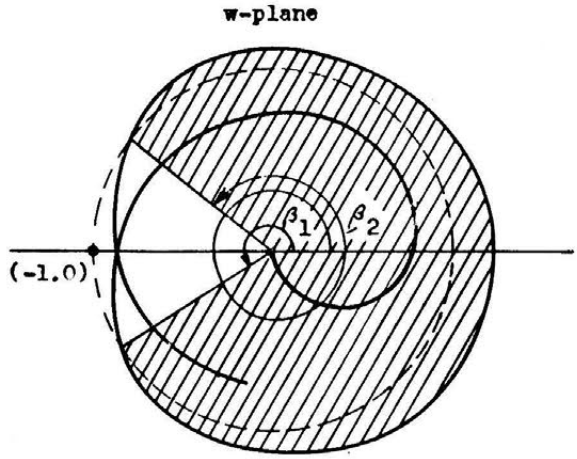

FIG. 6 A CRITICAL CONFIGURATION

Examination of Formula [25] shows that, in general, for any given system (fixed α_1, α_2 and φ_1, φ_2) τ is allowed a band spectrum of values for increasing n with the band width given by Formula [25]. It should be noted, however, that the spectrum will terminate at some value of n after which

$$\frac{\varphi_2 + (2n-1)\pi}{\alpha_2} > \frac{\varphi_1 + (2n+1)\pi}{\alpha_1} \quad \ldots\ldots [26]$$

This is due to the fact that $\beta_2 - \beta_1$ increases with increasing τ and Condition [26] corresponds to $\beta_2 - \beta_1$ exceeding 2π (see sentence after Formula [23].

STABILITY CRITERION FOR FEEDBACK PROPORTIONAL TO $\theta(t-\tau)$

For this case Equation [2] becomes

$$I\ddot{\theta}(t) + R\dot{\theta}(t) + K\theta(t) = -S\theta(t-\tau) \quad \ldots\ldots [27]$$

The discussion of the steady-state behavior is similar to the sections, "Steady-State Solutions," and "A Mechanical Model," with one important difference. Since the feedback power is now given by $S\omega$ and the power dissipated is still $\omega^2 R$, the system will have no steady-state frequencies at $\omega > S/R$.

Equation [14] now becomes

$$\theta(t) = \frac{1}{2\pi i}\int_\Gamma \frac{L(p)}{Y(p)} \frac{1}{1 + S\dfrac{e^{-p\tau}}{p^2 I + pR + K}} e^{pt}\, dp \ldots. [28]$$

Equations [15] and [16] still apply and Equation [17a] becomes

$$f(p) = A\frac{e^{-p\tau}}{ap^2 + bp + 1} \quad \ldots\ldots [29]$$

with A, a, b still given by Equation [17b].

As before, $f(\pm i\infty) = 0$, and we use a contour consisting of the imaginary axis.

Equations [18] become

$$f(i\alpha) = \frac{Ae^{-i(\alpha\tau - \varphi)}}{[(1-\alpha^2 a)^2 + (b\alpha)^2]^{1/2}} \quad \ldots\ldots [30a]$$

and

$$\tan\varphi = \frac{-b\alpha}{-a\alpha^2 + 1} \quad \ldots\ldots [30b]$$

A graph of Equation [30a] is shown in Fig. 7 for $-\infty < \alpha < 0$. It is a sensed spiral with the intercept S/K on the positive real axis when $\alpha = 0$. The graph is symmetrical with respect to the real axis. The radius vector has a minimum at $\alpha = 0$ and maxima at

$$\alpha = \pm\left(\frac{2a - b^2}{2a^2}\right)^{1/2}$$

Now if $(2a - b^2)/(2a^2) < 0$ and $S/K \leqq 1$, the spiral cannot possibly enclose the point $(-1, 0)$. Using Equation [17b], we get

$$S < K;\ R^2 > 2IK \quad \ldots\ldots [31]$$

which are the conditions under which the system is always stable.

Setting the amplitude of Equation [30a] equal to 1 and solving we obtain

$$\alpha^2 = \frac{-(b^2 - 2a) \pm \sqrt{(b^2-2a)^2 - 4(1-A^2)a^2}}{2a^2} \quad \ldots [32]$$

If Equation [32] has no positive α^2, $S < K$ is automatically implied, and the system is stable (note that the converse is not true; $S < K$ does not guarantee stability).

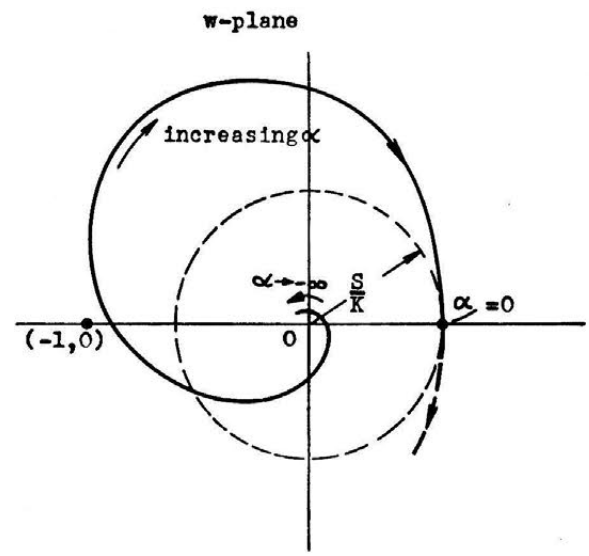

FIG. 7 GRAPH OF EQUATION [30a] FOR $-\infty < \alpha \leqq 0$

If Equation [32] has positive α^2, the system is in danger of instability. The following cases are possible:

(a) Equation [32] has two $\alpha^2 > 0$ (in this case $2IK > R^2$ and $S < K$). This case is identical to the last case of the preceding section. Criteria [23] and [25] apply.

(b) Equation [32] has one distinct $\alpha^2 > 0$. Then if $S < K$, using Equation [30a] and $\alpha > 0$, we get the following stability criterion (this is the case of equal roots)

$$\tau \neq \frac{n\pi + \varphi}{\alpha} \quad \ldots\ldots [33]$$

with n, any odd integer.

Thus the system will be stable for all values of the time lag τ save for those specified by Equation [33].

(c) Equation [32] has one $\alpha^2 > 0$. Then if $S \geqq K$, we get the most stringent stability criterion. Using $\alpha > 0$ and Equation [30a], we obtain the following stability criterion

$$0 < \tau < \frac{\pi + \varphi}{\alpha} \quad \ldots\ldots\ldots\ldots\ldots\ldots [34]$$

STABILITY CRITERION FOR FEEDBACK PROPORTIONAL TO $\ddot{\theta}(t - \tau)$

For this case Equation [2] becomes

$$I\ddot{\theta}(t) + R\dot{\theta}(t) + K\theta(t) = -S\ddot{\theta}(t - \tau) \quad \ldots\ldots\ldots [35]$$

Equation [14] now becomes

$$\theta(t) = \frac{1}{2\pi i} \int_\Gamma \frac{1}{1 + S \dfrac{p^2 e^{-p\tau}}{p^2 I + pR + K}} \frac{L(p)}{Y(p)} e^{pt}\, dp \ldots [36]$$

Equations [15] and [16] still apply and Equation [17a] becomes

$$f(p) = \frac{Ap^2 e^{-p\tau}}{ap^2 + bp + 1} \quad \ldots\ldots\ldots\ldots\ldots [37]$$

with A, a, b still given by Equation [17b].

Now as $p \to \pm i\infty$, $|f(\pm i\infty)| \to (A/a) = (S/I)$. The graph of Equation [37] for the range $-\infty < \alpha \leqq 0$ is shown in Fig. 8.

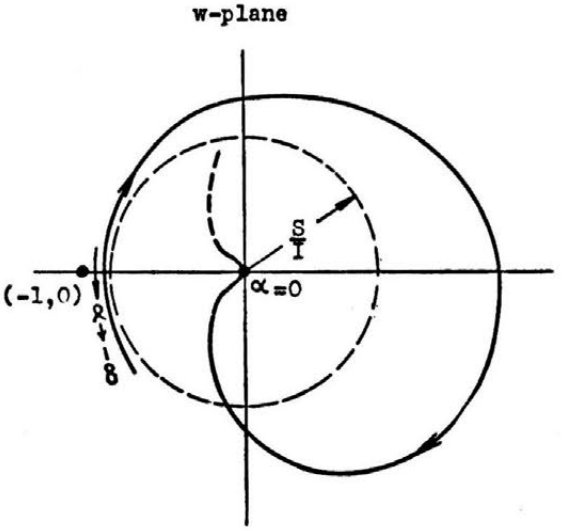

FIG. 8 GRAPH OF EQUATION [39a] FOR $-\infty < \alpha \leqq 0$

The branch of the graph for $0 \leqq \alpha < \infty$ is symmetrical to the branch shown with respect to the real axis.

It is clear from the preceding that if $S/I > 1$ the system cannot possibly be stable, since the spiral will eventually enclose the point (—1, 0) as α tends to ∞; consequently the system will be unstable if $S > I$.

The radius vector of Equation [37] has a minimum at $\alpha = 0$ and at

$$\alpha = \pm \left(\frac{2}{2a - b^2}\right)^{1/2}$$

as shown by elementary differentiation, consequently the system will always be stable if

$$S < I \text{ and } R^2 > 2IK \quad \ldots\ldots\ldots\ldots [38]$$

Now setting $p = i\alpha$ in Equation [37], and reducing it to our usual form we get

$$f(i\alpha) = \frac{A\alpha^2 e^{-i(\alpha\tau - \varphi)}}{[(1 - \alpha^2 a)^2 + (b\alpha)^2]^{1/2}} \quad \ldots\ldots\ldots [39a]$$

and

$$\tan \varphi = \frac{b\alpha}{a\,\alpha^2 - 1} \quad \ldots\ldots\ldots\ldots\ldots [39b]$$

Setting the amplitude equal to ± 1 and solving, we get

$$\alpha^2 = \frac{2a - b^2 \pm \sqrt{(2a - b^2)^2 - 4(a - A)}}{2(a - A)} \quad \ldots\ldots [40]$$

According to Equation [17b], $(a - A) > 0$ implies $I > S$ which we have already shown to be a necessary condition for stability. Therefore we need consider only $I > S$ in Equation [40]. But this makes Equation [40] identical in behavior to Equation [21]. Similarly, the total angle of Equations [39] can be shown to be monotone decreasing in α. Consequently, the conclusions following Equations [22] apply to this case, and the stability criterion will be given by Equation [23], and the allowable range in τ by Equation [25].

STABILITY FOR FEEDBACK PROPORTIONAL TO HIGHER DERIVATIVES

Consider a general case of feedback proportional to the nth derivative of $\theta(t)$.

Equation [2] is generalized to

$$I\ddot{\theta} + R\dot{\theta}(t) + K\theta(t) = -S\theta^{(n)}(t - \tau) \quad \ldots\ldots [41]$$

Then by a now familiar procedure we obtain

$$f(p) = \frac{Ap^n e^{-p\tau}}{ap^2 + bp + 1} \quad \ldots\ldots\ldots\ldots\ldots [42]$$

Now, referring to Fig. 4, let $p = 0$. Then $|f(p)| = 0$ except when $n = 0$ in Equation [42].

If $p \to \pm i\infty$

$$|f(p)| \to \frac{A}{a} |p|^{n-2}$$

Thus $|f(p)| \to \infty$ except for $n = 0, 1, 2$. The stability of the system has been discussed for these three values of n in the three preceding sections of the paper. For all other values of n, the graph of (7.2) will necessarily enclose the point (—1, 0). We conclude:

If the feedback signal is proportional to $\theta^n(t - \tau)$ the system will be unconditionally unstable whenever $n > 2$.

SUMMARY

For purposes of comparison, Fig. 9(a, b, c), show the general behavior of the magnitude of the radius vector ρ versus α for the three cases in which stability is possible. Fig. 9(d) shows the general behavior for $n > 2$.

The results of the three sections on "Stability Criteria for Feedback," and Fig. 9, show that for $n \leq 2$, the system will be unconditionally stable, if certain relations between the parameters of the system are satisfied in each case. The greatest latitude in the choice of the parameters is found for $n = 1$, where the condition $R > S$ is sufficient to insure stability. The narrowest restriction occurs for $n = 2$, where $S > I$ is sufficient to produce instability.

If the foregoing requirements for unconditional stability are not satisfied, the system may still be stable for a specified range in the time lag τ. In the most general case it is possible to ob-

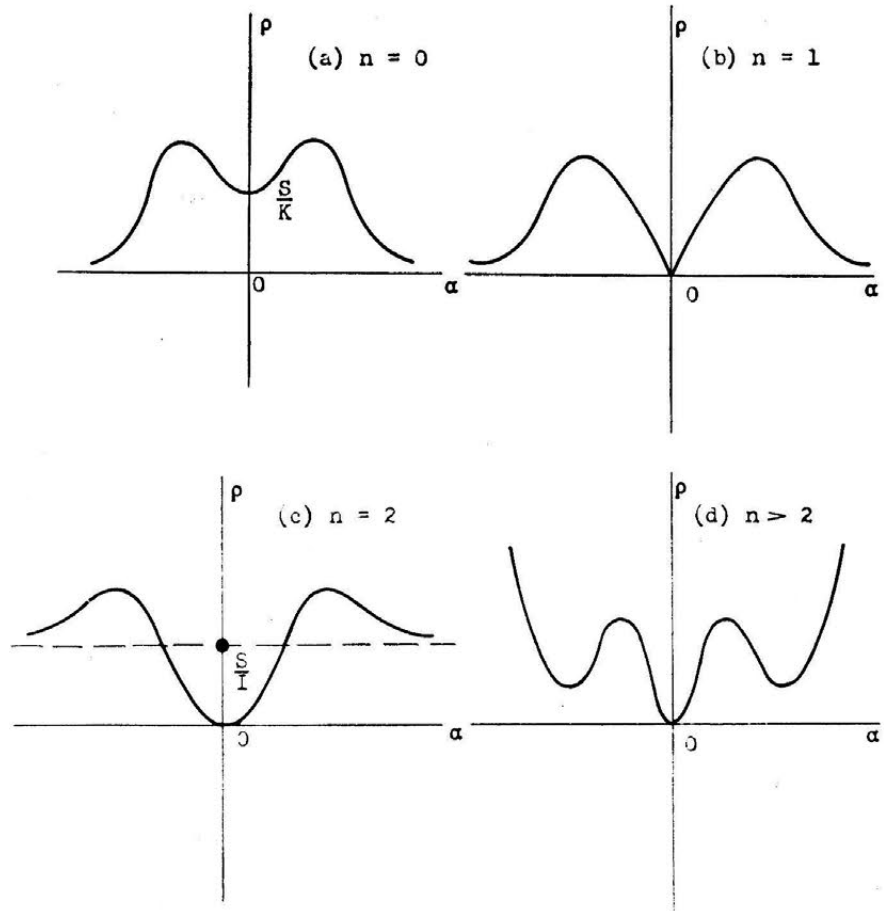

FIG. 9 MAGNITUDE OF THE RADIUS VECTOR ρ VERSUS α

tain a band spectrum of values of τ for which a given system will be stable. The band width tends to zero as the value of τ is increased. This indicates that in systems of this type large time lags will produce instability.

It should be kept in mind that the systems treated in this paper were assumed to be linear. Any comparison of experimental results to our conclusions should involve allowance for the existing nonlinearity. Thus, for example, the band spectrum described would produce hunting in an actual system rather than a physical breakdown due to excessive vibrations, as predicted by our results.

ACKNOWLEDGMENT

The general method of solution used in this paper was suggested by J. A. Krumhansl, Assistant Professor of Physics, Brown University. He also independently obtained the results for the section of this paper on "Stability Criterion for Feedback Proportional to $\dot{\theta}\,(t-\tau)$."

BIBLIOGRAPHY

1 "Servomechanism Fundamentals," by H. Lauer, et al, McGraw-Hill Book Company, Inc., New York, N. Y., 1947.

2 "Servomechanisms," by L. A. McColl, D. Van Nostrand Company, Inc., New York, N. Y., 1945.

3 "A Note on Stability Calculations and Time Lag," by Seymour Sherman, *Quarterly of Applied Mathematics*, vol. 5, 1947, p. 92.

4 "Self-Excited Oscillations in Dynamical Systems," by N. Minorsky, JOURNAL OF APPLIED MECHANICS, Trans. ASME, vol. 64, 1942, p. A-65.

5 "Time-Lag in a Control System," by A. Callender, D. Hartree, and A. Porter, Philosphical Trans., Royal Society of London, series A, vol. 235, 1936, pp. 415–444.

6 "Transients in Linear Systems," by M. F. Gardner and J. L. Barnes, John Wiley & Sons, Inc., New York, N. Y., 1942.

7 "Complex Variable and Operational Calculus," by N. W. McLachlan, The Macmillan Company, New York, N. Y., 1942.

8 "Funktionentheorie," by A. Hurwitz, J. Springer, Berlin, Germany, 1929, p. 106.

Appendix

BEHAVIOR ON SEMICIRCLE OF BROMWICH CONTOUR

We still have to justify the assumption made in the three sections, "Stability Criteria for Feedback," that $f(p) \to 0$ along the semicircle of the contour as $r \to \infty$.

Let

$$p = re^{i\theta} = r(\cos\theta + i\sin\theta)$$

and substitute into Equation [42]

$$f(re^{i\theta}) = \frac{Ar^n e^{in\theta} e^{-r(\cos\theta + \sin\theta)}}{ar^2 e^{i2\theta} + bre^{i\theta} + 1} \quad \ldots\ldots\ldots [43]$$

and note that for any fixed θ in the range $\pi/2 > \theta > -\pi/2$

$$|f(re^{i\theta})| \to \frac{A}{a} r^{n-2} e^{-r\cos\theta} \to 0 \text{ as } r \to \infty \quad \ldots\ldots\ldots [44]$$

for all n.

Dynamic Capacity of Rolling Bearings

By GUSTAF LUNDBERG[1] and ARVID PALMGREN[2]

This paper is a condensation of a comprehensive theory for fatigue failure in rolling bearings.[3] The character of bearing fatigue failures is analyzed, and the effect of the volume of stressed material is assessed by means of modification of Weibull's statistical theory of failure. The variables affecting bearing capacity are examined, and general formulas are set up relating the variables to the bearing capacity. Unknown exponents in the formulas are evaluated by means of extensive tests, and the final formulas are compared to experimental results.

CALCULATION of the dynamic capacity of rolling bearings has previously been based on empirical formulas which have been used with considerable success for bearing types of conventional design. In this paper the foundation is laid for a unified theory of the dynamic capacity for rolling bearings, in which regard is taken of the dispersion in material fatigue strength from one volume element to another. Hertz's theory for contact fatigue strength has been developed and extended for calculation of the stress variation which can be taken to be the most dangerous when bodies roll with respect to each other. Although the new theory still does not take account of all factors which affect the life, it does give a satisfactory agreement with experimental tests.

Magnitude of Shear-Stress Amplitude

An understanding of the character of fatigue failure can be obtained from a study of the change in the material which takes place in bearing rings under rolling loads. The fatigue cracks start from certain weak points, for example, slag inclusions within the material. These weak points give rise to strong local stress concentrations in the surrounding material. Before the fatigue crack develops, slip takes place in the material. Therefore the causes of fatigue can be sought in the slip, which changes the characteristics of the material in the immediate neighborhood of the weak point.

Fig. 1 shows a cross section cut through the raceway in the middle of a fatigued bearing ring.

Slag inclusions are usually elongated in the process of rolling, and therefore the fatigue cracks start in directions parallel to the direction of rolling. At times slag inclusions have more of a sharp-cornered shape, whereupon fatigue cracks occasionally extend in a 45-deg direction.

Fig. 2 shows how the shear stresses occurring in the direction of rolling vary with the depth z_0, where this shear stress has its greatest value. The distances a and b are contact ellipse half-axes, q the maximum pressure in the contact area.

Introduce an auxiliary quantity t, from which the shape of the pressure area is determined so that

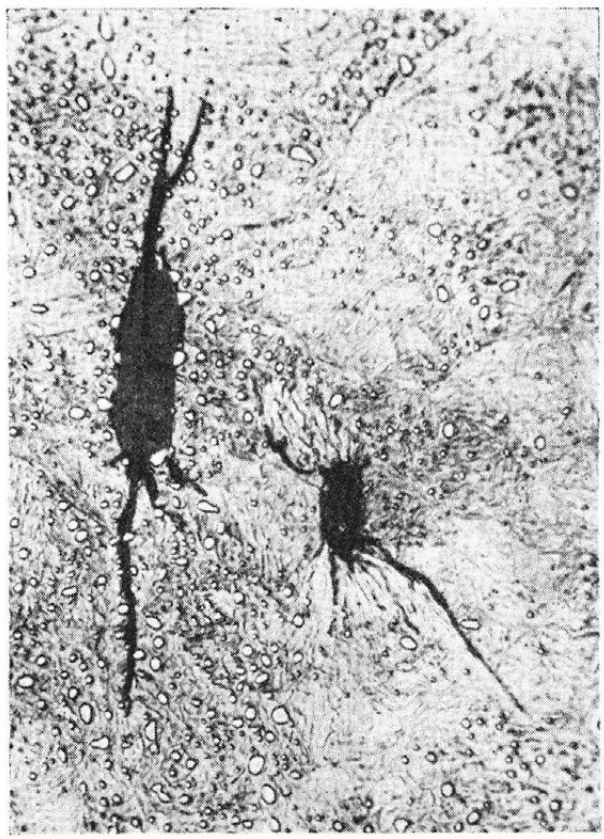

Fig. 1 Radial Cross Section Through Bearing Race in Fatigued Bearing; 1000×

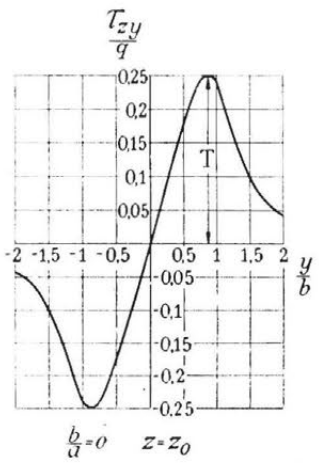

Fig. 2

[1] Professor, Chalmers University of Technology, Gothenburg, Sweden.

[2] In Charge of Engineering and Mechanical Research, SKF, Gothenburg, Sweden.

[3] "Dynamic Capacity of Rolling Bearings," by G. Lundberg and A. Palmgren, *Acta Polytechnica*, Mechanical Engineering Series, vol. 1, no. 3, Stockholm, Sweden, 1947.

Contributed by the Applied Mechanics Division and presented at the Annual Meeting, New York, N. Y., November 28–December 3, 1948, of The American Society of Mechanical Engineers.

Discussion of this paper should be addressed to the Secretary, ASME, 29 West 39th Street, New York, N. Y., and will be accepted until July 11, 1949, for publication at a later date. Discussion received after the closing date will be returned.

Note: Statements and opinions advanced in papers are to be understood as individual expressions of their authors and not those of the Society. Paper No. 48—A-19.

$$\frac{b}{a} = \sqrt{(t^2 - 1)\,(2t - 1)} \quad \ldots\ldots [1]$$

The depth of the point of maximum stress is obtained from

$$z = z_0 = \zeta b$$

$$\zeta = \frac{1}{(t + 1)\sqrt{2t - 1}} \quad \ldots\ldots [2]$$

Research shows that the largest number of fatigue cracks start at this depth.

Table 1 presents corresponding values of t, b, T, and ζ.

TABLE 1 DEPENDENCE ON t OF BEARING CONFORMITY FACTORS

t	1	1.02	1.05	1.1	1.2	1.2808
b/a	0	0.2050	0.3358	0.5020	0.7849	1
T	0.2500	0.2475	0.2436	0.2371	0.2241	0.2139
ζ	0.5000	0.4854	0.4651	0.4347	0.3842	0.3509

The magnitude of the shear-stress amplitude is

$$\tau_0 = Tq, \quad T = \frac{\sqrt{2t - 1}}{2t(t + 1)} \quad \ldots\ldots [3]$$

During the passage of one roll body the shear stress varies between $\pm Tq$. The determining factor for material fatigue is twice the amplitude of the relative shear stress (i.e., $2T$). Fig. 3 shows how $2T$ varies with the shape of the contact area. As a comparison, the relative shear stress decisive at static loading T_{st}, is drawn in. The comparison shows that this static stress cannot be taken as a basis for the estimation of fatigue failure.

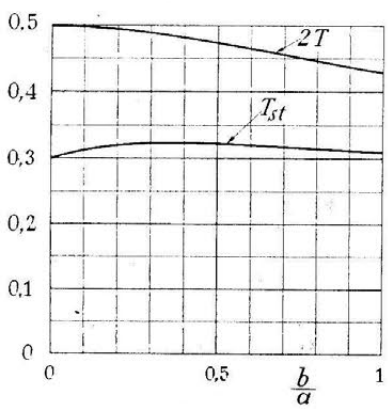

FIG. 3

STATISTICAL METHOD FOR TREATING FATIGUE PROBLEMS

For a statistical treatment of fatigue problems, consideration must be given to the fact that the material changes little by little through the action of repeated loads. Plastic flow appears in the neighborhood of the weak points of the material and continually increases in size until finally a microscopic crack forms which grows slowly to macroscopic magnitude. At this point the macroscopic stress distribution is disturbed and the fatigue no longer follows the expected course since the assumptions for calculating the macroscopic stresses are no longer valid. However, that is only in an advanced stage of fatigue, a stage where the continuance of the destructive process swiftly leads to rupture.

Changes in the material condition can, as long as the fatigue crack has a microscopic extent, be taken as dependent chiefly on the extent of the macroscopic stress in the element of volume considered, that is, on the stress amplitude in the plane which is most dangerous from a fatigue viewpoint, and on the amount of material in the element of volume. It is also possible that changes in the amount of material are dependent on the depth of the volume element below the surface. That assumption has been shown to be necessary for the presentation of fatigue failure in rolling bearings.

A useful resultant formula for statistical presentation of different fatigue problems is thus

$$\log \frac{1}{S(N)} \sim \int_V \left[\int_N \mathfrak{F}[\tau(n);\ z]dn\right]^e dV \quad \ldots\ldots [4]$$

where $S(N)$ is the probability that the material will endure N million stresses, $\tau(n)$ the stress amplitude at the depth z with the nth loading, dV the infinitesimal element of volume, and V the whole volume.

For highly concentrated loads, as, for example, in rolling bearings, considerable simplifications can be introduced in the calculation if it is observed that only the conditions in the neighborhood of the point where the maximum fatigue-stress amplitude occurs are decisive for the probability of fatigue.

LIFE FORMULA FOR ROLLING BEARINGS

When setting up the life formula, the known fact that the more concentrated the load, the greater the endurance, must be considered.

This fact has been proved by Neuber, among others, in a study of concentrated stress conditions in fillets and by Föppl-Huber with a study of the first flow lines occurring for contact between a cylindrical and a plane body. Neuber and Föppl-Huber sought the explanation of the dependence on volume in the crystalline nature of the material.

Comprehensive investigations by Weibull of the static breaking strength of brittle bodies have resulted in a statistical theory of strength based on the theory of probability, where the dependence of strength on volume is explained by the dispersion in material strength.

Weibull's theory, however, is based on the assumption that the first crack results in a break. The frequent examples of cracks which do not reach the surface seem to show that this assumption is not valid for fatigue failure in rolling bearings. Therefore, in setting up the life formula, consideration should be given to the fact that the probability of a fatigue break occurring must be taken to be dependent on the depth z_0 at which the most dangerous stress occurs.

The life formula therefore should be written

$$\log \frac{1}{S} = \mathfrak{F}(\tau_0,\ N,\ z_0)V \quad \ldots\ldots [5]$$

For practical reasons it is desirable to give the functional relationship as a power function

$$\mathfrak{F}(\tau_0,\ N,\ z_0) \sim \frac{\tau_0^c N^e}{z_0^h} \quad \ldots\ldots [6]$$

Here S is the probability that the material will endure for N million stress cycles, τ_0 is the decisive stress amplitude, and V is the volume representative of the stress concentration.

If $h = 0$, a life formula corresponding to Weibull's theory is obtained.

As an expression for the magnitude of the stressed volume, one can choose

$$V \sim az_0l \quad \ldots\ldots [7]$$

where

a = major half-axis of pressure ellipse
l = circular length of raceway

The three lengths, a, l, and z_0, give an expression for the stress extension within the raceway in the directions of width, length, and depth.

As a result of the expressions given for z_0 and τ_0 in Equations [2] and [3] and with the help of Equations [5], [6], and [7] is found

$$\log \frac{1}{S} \sim \frac{T^c a l}{(zb)^{h-1}} \left(\frac{Q}{ab}\right)^e N^e \quad \ldots\ldots [8]$$

where Q is the roll-body load.

For point contact according to Hertz's theory of elastic contact

$$a \sim b \sim \sqrt[3]{QD_a} \quad \ldots\ldots [9]$$

For line contact

$$a \sim l_a, \; b \sim \sqrt{\frac{Q D_a}{l_a}} \quad \ldots\ldots [10]$$

where l_a is the roll body's length of contact, D_a the roll-body diameter.

If u is the number of stress cycles per revolution and L is the life in millions of revolutions, then from Equations [8] to [10]

$$\log \frac{1}{S} \sim \left[\frac{Q}{{D_a}^2}\right]^{\frac{c-h+2}{3}} {D_a}^{2-h} u^e L^e l \quad \ldots\ldots [11]$$

with point contact, and

$$\log \frac{1}{S} \sim \left[\frac{Q}{{D_a}^2}\right]^{\frac{c-h+1}{2}} \left[\frac{D_a}{l_a}\right]^{\frac{c-h-1}{2}} {D_a}^{2-h} u^e L^e l \quad \ldots [12]$$

with line contact, where the proportionality factor depends upon the conformity between rolling body and bearing race.

The life Formulas [11] and [12] give the life L which with the probability S occurs for the roll-body load Q. Specifically, for $L = 1$ and $S = 0.9$, the dynamic-capacity value is found corresponding to the load Q_c.

Since $l \sim D_a$, from Equations [11] and [12]

$$Q_c \sim {D_a}^{\frac{2c+h-5}{c-h+2}} \quad \ldots\ldots [13]$$

with point contact and

$$Q_c \sim {D_a}^{\frac{c+h-3}{c-h+1}} {l_a}^{\frac{c-h-1}{c-h+1}} \quad \ldots\ldots [14]$$

with line contact.

Since the roll-body load is proportional to the bearing load, Q_c and Q are proportional to the basic dynamic capacity C, and the actual bearing load F, respectively.

From Equations [11] and [12]

$$L = \left(\frac{C}{F}\right)^p \quad \ldots\ldots [15]$$

where

$$p = \frac{c - h + 2}{3e} \quad \ldots\ldots [16]$$

with point contact, and

$$p = \frac{c - h + 1}{2e} \quad \ldots\ldots [17]$$

with line contact.

For radial bearings, the load on the rolling element depends upon the position of the rolling element. In that case, Q_e and Q, respectively, represent mean values of the rolling-element loads, that is, equivalent rolling-element loads.

With rotation, each point of the rotating inner ring passes through the loaded zone. All points on the inner ring are thus equally stressed, but the loads on the rolling elements, and hence the stress amplitudes, vary cyclically with the rotation. For a load which varies periodically with time, introduce the cubic mean value as the approximate mean load

$$Q_{ci} = \sqrt[3]{\frac{1}{2\pi} \int Q^3(\psi) d\psi} \quad \ldots\ldots [18]$$

where the angle ψ gives the position of the roll body.

Each point of the stationary outer ring supports, under rotation, a constant rolling-element load and therefore a constant stress amplitude. The rolling-element load and consequently the stress amplitude are dependent upon the position of the point in the outer ring. The probability that the whole outer ring, $l = \pi D_e$, will endure is the product of probabilities that the different sections of the ring will endure. Therefore it is found from Equation [11] or [12] that

$$\log \frac{1}{S_e} \sim \int Q^w(\psi) L^e \frac{D_e}{2} d\psi = Q_{ce}{}^w L^e \pi D_e \quad \ldots\ldots [19]$$

where the equivalent roll-body load

$$Q_{ce} \sim \left[\frac{1}{2\pi} \int Q^w(\psi) d\psi\right]^{\frac{1}{w}} \quad \ldots\ldots [20]$$

Here

$$w = pe \quad \ldots\ldots [21]$$

Determination of Exponents in Life Formula

The exponents c, h, and e occurring in the formulas for life dispersion, Equations [11] and [12], can be regarded as material characteristics and determined experimentally. The exponents can be found by determining the exponent p in the life formula, Equation [15], the dependence of the basic dynamic capacity upon the bearing size (the exponent of D_a, Formula [13] for point contact), and the dispersion of bearing life under uniform conditions of operation.

The logarithms of Equations [11] and [12] for constant service conditions are

$$\log \log \frac{1}{S} = e \log L + \quad \ldots\ldots [22]$$

Therefore the probability S, for a sufficiently large test series, gives the relative number of bearings which will endure L million revolutions. In a graph with co-ordinates log $1/S$ and L, set up on logarithmic scales, the life formula is represented by a straight line, whose slope gives the magnitude of the exponent e.

Fig. 4 shows test series with self-aligning ball bearings,[4] and deep-groove ball bearings.[5] The step diagram obtained with a finite number of bearings agrees very well in both cases with a straight line having the slope $e = 10/9$.

Fig. 5 shows a test series for spherical roller bearings.[6] The exponent e for this test series is 1.5.

The dispersion in material strength characteristics can vary quite appreciably for different test series. Therefore it is quite natural that the exponent e may have appreciably different values

[4] SKF, 1309.
[5] SKF, 6309.
[6] SKF, I-37906.

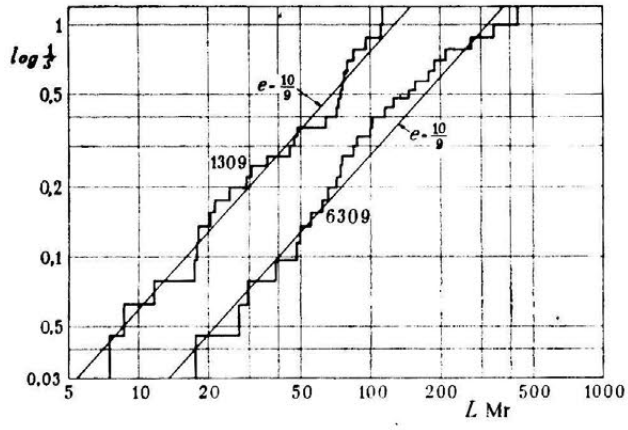

FIG. 4

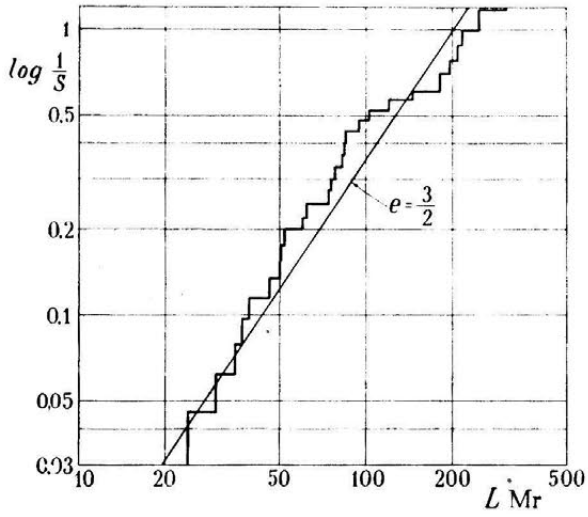

FIG. 5

for different test series of the same bearing. To determine with certainty whether the exponent e is dependent on the bearing type or not, an investigation should be carried out with test series of different bearing types in such a manner that the material in the different bearing types can be considered statistically similar. No such research series is as yet available. The available statistical material indicates that the exponent e has a lower value for ball bearings than for roller bearings, as shown by the research results in Figs. 4 and 5.

For the purpose of determining the exponent p for ball bearings, there are at present available extensive results from tests with self-aligning ball bearings,[4] and deep-groove ball bearings.[5] In these test series, great care has been taken to see that the material and the manufacture in the different series are statistically similar. The test results are given in Fig. 6 where each point represents the median life of a group of 30 bearings. In this series the exponent, $p = 3$, corresponds to the solid line. For determination of the exponent p for roller bearings, no similar reliable test series is now available. The indications are, however, that the exponent p may be somewhat higher for roller bearings than for ball bearings.

However, there would be very great practical difficulties if the exponent p were taken as different for point and line contact. Hence it seems justifiable from a practical viewpoint to calculate for all bearings with a common value, $p = 3$, without regard to whether point or line contact is present.

For determination of the dependence of the basic dynamic capacity on the size of the bearings, the results from tests on approximately 1500 bearings are given in Fig. 7. This shows that within the test range from $D_a = 1.5$ mm up to 25 mm, the basic dynamic capacity $C = FL^{1/3}$ can be taken as proportional to $D_a^{1.8}$ corresponding to the solid line.

In Table 2 respective values of the exponents corresponding to $e = 10/9$ and $3/2$ are given for $p = 3$ and an exponent of 1.8 for D_a with point contact. For the assumed values of the exponents in the life formulas by study of the dependence of capacity upon the conformity between roll body and bearing rings, according to Equations [13] or [14]

$$Q_c = A\left[\frac{2R}{D_a}\cdot\frac{r}{r-R}\right]^{0.41}\frac{\left[1 \mp \frac{D_a\cos\alpha}{d_m}\right]^{1.39}}{\left[1 \pm \frac{D_a\cos\alpha}{d_m}\right]^{1/3}}\left(\frac{D_a}{d_m}\right)^{0.3} D_a^{1.8}\, Z^{-\frac{1}{3}} \quad \ldots\ldots [23]$$

for point contact, and

$$Q_c = B\,\frac{\left[1 \mp \frac{D_a\cos\alpha}{d_m}\right]^{29/27}}{\left[1 \pm \frac{D_a\cos\alpha}{d_m}\right]^{1/3}}\left(\frac{D_a}{d_m}\right)^{2/9} D_a^{29/27}\, l_a^{1/9}\, Z^{-\frac{1}{3}} \quad \ldots [24]$$

for line contact where

$$B = 10.82\, A^{20/27} \quad \ldots\ldots [25]$$

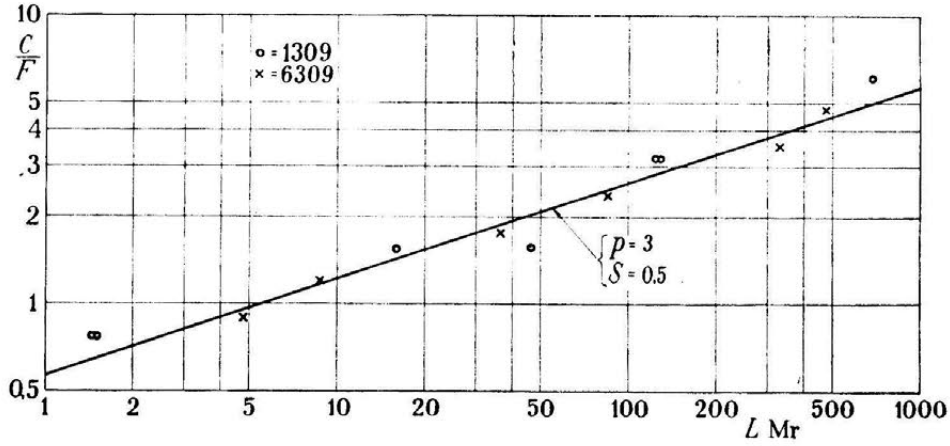

FIG. 6

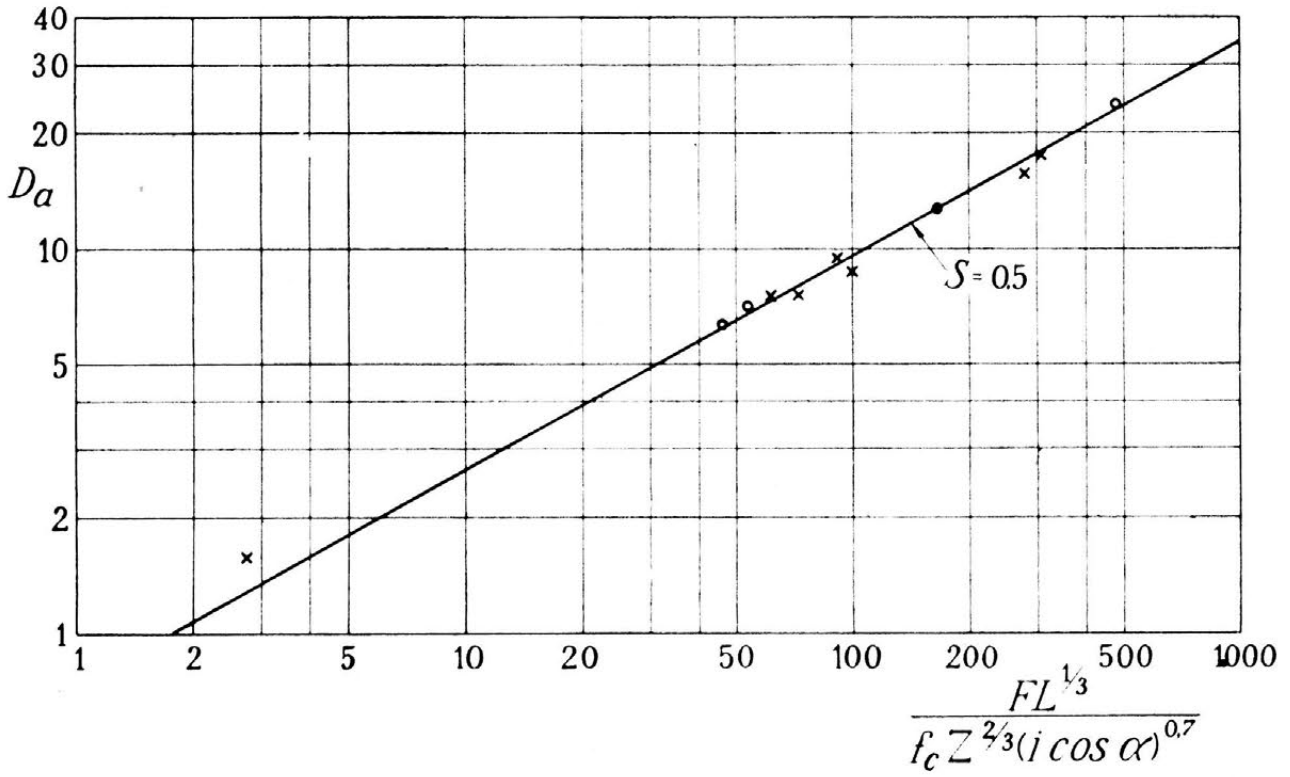

FIG. 7

TABLE 2 RELATIONS BETWEEN EXPONENTS IN CAPACITY FORMULAS

			Point contact		Line contact		
e	c	h	p	exp D_a	p	exp D_a	exp l_a
10/9	10 1/3	2 1/3	3	1.8	..	...	...
3/2	10 1/3	2 1/3	..	1.8	3	1.07	0.78

where r is the raceway, and R the roll-body profile radius, D_a and l_a the roll-body diameter and contact length, respectively, d_m the pitch diameter of the roll-body set, α the contact angle, and Z the number of rolling elements per row; A is a material constant. The upper signs are valid for the inner ring, the lower signs for the outer ring.

From the test series in Figs. 6 and 7 it is found that $A = 10$.

For SKF steel with a hardness of 61.7 to 64.5 Rockwell C (750 . . . . . 825 Vickers), and with units in kilograms and millimeters, on the average

$$A = 10, \quad B = 60$$

Figs. 6 and 7 show the comparison between theory and tests for self-aligning ball bearings (mark o) and deep-groove ball bearings (mark x) where f_c enters into the theoretical value. The solid line corresponds to the theory. The comparison shows good agreement between theory and experience.

Basic Dynamic Capacity

In the calculation of the basic dynamic capacity of the bearing, consideration should be given to the probability of fatigue in the different parts of the bearing. The basic dynamic capacity of the bearings is thus dependent on the capacity C_i of the inner-ring contact, and the capacity C_e of the outer-ring contact.

The basic dynamic capacity C of the bearing is obtained from C_i and C_e by the observation that the probability that a bearing will endure is the product of the probabilities that the various parts will endure. If S_i is the probability that the inner ring of the bearing will endure and S_e is the probability that the outer ring will endure, then according to Equations [11] and [12] for a bearing load

$$\left.\begin{aligned} \log \frac{1}{S_i} &= k_i F^w L^e \\ \log \frac{1}{S_e} &= k_e F^w L^e \end{aligned}\right\} \quad \ldots\ldots\ldots\ldots [26]$$

where k_i and k_e are proportionality factors. The probability that the bearing will endure is found from the product law

$$\log \frac{1}{S} = (k_i + k_e) F^w L^e \quad \ldots\ldots\ldots\ldots [27]$$

If $L = 1$ and S_i, S_e, and $S = 0.9$, then $F = C_i$, C_e, and C. From Equations [26] and [27], it is found that

$$C = g_e C_i$$

$$g_e = \left[1 + \left(\frac{C_i}{C_e}\right)^w\right]^{-\frac{1}{w}} \quad \ldots\ldots\ldots\ldots [28]$$

For Swedish SKF steel, $w = 10/3$ and $9/2$ for point and line contact, respectively.

Thrust Bearings. A centric thrust-bearing load is distributed uniformly among the rolling elements for satisfactory operating conditions. Thus for single-row bearings

$$\left.\begin{aligned} C_i &= Q_{ci} Z \sin \alpha \\ C_e &= Q_{ce} Z \sin \alpha \end{aligned}\right\} \quad \ldots\ldots\ldots\ldots [29]$$

where Q_{ci} and Q_{ce} are obtained from Equations [23] and [24] for point and line contact, respectively.

One obtains for the following conventional bearing types:

Thrust ball bearings, $\alpha \neq 90$ deg

$$C = f_c (i \cos \alpha)^{0.7} tg\, \alpha\, Z^{2/3} D_a^{1.8} \quad \ldots\ldots\ldots [30]$$

Thrust roller bearings, $\alpha \neq 90$ deg

$$C = f_c (i \cos \alpha)^{0.78} tg\, \alpha\, Z^{2/3} D_a^{1.07} l_a^{0.78} \quad \ldots\ldots\ldots [31]$$

Thrust ball bearings, $\alpha = 90$ deg

$$C = f_c i^{0.7} Z^{2/3} D_a^{1.8} \quad \ldots\ldots\ldots\ldots [32]$$

Thrust roller bearings, $\alpha = 90$ deg

$$C = f_c i^{0.78} Z^{3/4} D_a^{1.07} l_a^{0.78} \quad \ldots\ldots\ldots\ldots [33]$$

where i is the number of active rows of rolling elements.

For thrust bearings the higher values of f_1, given in Table 3, are valid for centric load and uniform load distribution on the rolling elements. For a non-self-aligning thrust bearing, an eccentric

TABLE 3 CONVENTIONAL BEARING TYPES

Type	Point Contact of Ball Bearings			Line Contact of Roller Bearings		
C	$f_c f_a i^{0.7} Z^{2/3} D_a^{1.8}$			$f_c f_a i^{7/9} Z^{2/3} D_a^{29/27} l_{ai}^{7/9}$		
f_c	$g_c f_1 f_2 \left[\frac{2r_i}{2r_i - D_a}\right]^{0.41}$			$g_c f_1 f_2$		
g_c	$\left[1 + \left(\frac{C_i}{C_e}\right)^{10/3}\right]^{-0.3}$			$\left[1 + \left(\frac{C_i}{C_e}\right)^{9/2}\right]^{-2/9}$		
$\frac{C_i}{C_e}$	$f_2 \left[\frac{r_i}{r_e}\frac{2r_e - D_a}{2r_i - D_a}\right]^{0.41}$			$f_2 \left[\frac{l_{ai}}{l_{ae}}\right]^{7/9}$		
Type	Radial Bearing	Thrust Bearing		Radial Bearing	Thrust Bearing	
		$\alpha \neq 90$	$\alpha = 90$		$\alpha \neq 90$	$\alpha = 90$
γ	$\frac{D_a \cos\alpha}{d_m}$		$\frac{D_a}{d_m}$	$\frac{D_a \cos\alpha}{d_m}$		$\frac{D_a}{d_m}$
f_a	$(\cos\alpha)^{0.7}$	$(\cos\alpha)^{0.7} \cdot \operatorname{tg}\alpha$	1	$(\cos\alpha)^{7/9}$	$(\cos\alpha)^{7/9} \cdot \operatorname{tg}\alpha$	1
f_1 *	3.7—4.1	6 — 10		18 — 25	36 — 60	
f_2	$\frac{\gamma^{0.3}(1-\gamma)^{1.39}}{(1+\gamma)^{1/3}}$		$\gamma^{0.3}$	$\frac{\gamma^{2/9}(1-\gamma)^{29/27}}{(1+\gamma)^{1/3}}$		$\gamma^{2/9}$
f_3	$1.04 f_4$	f_4	1	$1.14 f_4$	f_4	1
f_4	$\left[\frac{1-\gamma}{1+\gamma}\right]^{1.72}$			$\left[\frac{1-\gamma}{1+\gamma}\right]^{38/27}$		

* Units in kg and mm

bearing load is caused by a slight variation in the thickness of the bearing rings at the bottom of the groove, and, when the bearing is equipped with self-aligning support washers, by the frictional resistance to the alignment of the washer. An unequal load distribution on the rolling elements can also be caused by eccentricity or out-of-roundness of the raceways. For most thrust bearings the theoretical value of the basic capacity must be reduced, often to about 60 per cent, on the basis of unequal distribution of load among the rolling bodies. The lower values of f_1, given in the tables, correspond to that reduction.

Radial Bearings. With radial bearings the load distribution must be found among the rolling elements. For a single-row bearing with radial relative displacement of the rings

$$\left.\begin{aligned} C_i &= (0.407 \ldots\ldots 0.419) Q_{ci} Z \cos\alpha \\ C_e &= (0.389 \ldots\ldots 0.367) Q_{ce} Z \cos\alpha \end{aligned}\right\} \ldots\ldots [34]$$

The former values are valid for point contact and the latter values for line contact.

One obtains for the following conventional bearing types:

Radial ball bearings

$$C = f_e (i \cos\alpha)^{0.7} Z^{2/3} D_a^{1.8} \ldots\ldots\ldots\ldots\ldots [35]$$

Radial roller bearings

$$C = f_e (i \cos\alpha)^{0.78} Z^{2/3} D_a^{1.07} l_a^{0.78} \ldots\ldots\ldots\ldots [36]$$

Also with radial bearings must be considered the faults in the bearings resulting from the manufacturing process. For rigid-bearing types, in particular multirow bearings, it is best to calculate with the lower value of f_1, although the higher value can be used for completely self-aligning bearings. For roller bearings the highest values may be used only if the rollers or races are so shaped as to avoid edge pressure. This can be achieved, for instance, by crowning the rollers and making the bearings sufficiently self-aligning.

Of course for all kinds of bearings which are not completely self-aligning, consideration must be given, in the calculation of the bearing equivalent load P, to the moment loads arising due to deflections in shafts and bearing housings or due to imperfect mounting conditions.

In order for the basic dynamic capacity C to be valid with $S = 0.9$, that is, for 90 per cent of the bearings, deep-groove ball bearings should be calculated with the maximum value of the groove radius. Thus $r_{i\,\max}$, $r_{e\,\max}$, and $D_{a\,\min}$ should be substituted in the formulas.

If it is assumed that the material quality is constant, the choice of the value of coefficient f_1 depends on the bearing design and degree of precision. Since these factors differ greatly in different bearings and influence each other in a complicated manner, the value of f_1 must be determined for each bearing entirely on the basis of tests.

After consideration of what is known concerning the average capacity of different bearing types and variations, the values given in Table 4 can be suggested.

For some conventional conformity values, f_c may be found from Table 5.

Within the ordinary range of dimensions, the contact length l_a of the rolling element can be estimated for conventional roller bearings by

$$l_a = l_r - 1.2\, l_r^{0.4} \text{ mm} \quad [37]$$

for bearings with grinding relief grooves and by

$$l_a = 0.9\, l_r \text{ mm} \quad [38]$$

for bearings without relief but allowing for end radii. Here l_r is the length of the rolling element. In certain bearing designs, for example, double-row spherical roller bearings with loose guide rings, a special calculation of l_a is required.

Equivalent Loads of Bearings

The bearing life for arbitrary conditions of load and rotation can be determined from the equation

$$L = \left(\frac{C}{P}\right)^3 \quad [39]$$

where C is the basic capacity of the bearing, and P is the so-called equivalent load. Since the definition of basic capacity differs for thrust and radial bearings, one should distinguish between the equivalent radial load P_r and the equivalent thrust load P_a. In this paper $P = P_r$ for radial bearings, and $P = P_a$ for thrust bearings.

A functional relationship exists between the equivalent loads P_a, P_r, and the bearing thrust and radial-load components F_a, F_r, which gives a relation between the effects of F_a and F_r on the equivalent life of the bearing. These functional relationships are clear from the solid-line curves in Figs. 9 and 10.

Fig. 9 is valid for deep-groove ball bearings with nominal contact angle $\alpha = 0$. The contact angle α assumed with load is found from Table 6, where D and d are the bearing outer diameter and bore, respectively.

The points marked with x are taken from four test series totaling 210 bearings, carried out by SKF, Gothenburg, with deep-groove ball bearings.[6] In these tests special care was taken to make the four series statistically similar in regard to both material and manufacture. The points marked with o come from test series carried out by SKF Philadelphia.[7] The agreement is satisfactory.

In Fig. 10 the dotted line represents a single-row bearing, the solid line a double-row bearing with point contact. For angular-contact bearings the contact angle varies with the load so that cot α is found from Table 6.

Both rows are loaded if

$$F_a < (1.67 \ldots\ldots 2.00)\, F_r\, tg\, \alpha \quad [40]$$

for point and line contact, respectively.

Only one row is loaded if F_a is greater than that value. In that case the life for the double-row bearings can be calculated as well from the theory of single-row bearings as from the theory of double-row bearings; P_{r1} and P_r are the equivalent loads if the bearing is considered as single-row or double-row, respectively.

[7] With bearings of SKF type 6308.

TABLE 4 VALUES OF FACTOR f_1 FOR DIFFERENT BEARINGS

Bearing Type		f_1
Self-aligning ball bearings		4.1
Single row deep groove ball bearings without filling slots		3.9
Double row deep groove ball bearings without filling slots		3.7
Angular contact boll bearings		3.9
Thrust ball bearings, $\alpha = 90°$		6
Single row cylindrical roller bearings:	Raceways and rollers cylindrical	19
	One race convex	20
	Rollers crowned	24
Double row cylindrical roller bearings:	Cylindrical rollers	18
	Rollers crowned	21
Tapered roller bearings:	Raceways and rollers tapered	19
	Rollers or raceways some chamfer	20
	One race convex	20
Self-aligning radial roller bearings		21
Self-aligning thrust roller bearings		50

TABLE 5 VALUES OF f_c FOR VARIOUS BEARING TYPES

Bearing Type	f_1	$\frac{r_i}{D_a}$	$\frac{r_a}{D_a}$	γ	0	0.02	0.05	0.1	0.2	0.3	0.4
Self-aligning Ball Brg.	4.1	0.54	—		0	1.26	1.76	2.36	3.34	3.88	3.77
Deep-groove Ball Brg.	3.9	0.52	0.52		0	3.65	4.77	5.67	6.12	5.71	4.94
Angular Contact Ball Brg.	3.9	0.52	0.53		0	3.35	4.43	5.39	6.00	5.68	4.93
Thrust Ball Brg.	6	0.545	0.545		0	4.19	5.52	6.79	8.36	9.44	10.29
Spherical Roller Brg.	21	—	—	f_c	0	7.05	8.66	9.94	10.57	9.96	8.83
Cylindrical Roller Brg.	20	—	—		0	6.71	8.24	9.47	10.06	9.49	8.41
Tapered Roller Brg.	20	—	—		0	6.71	8.24	9.47	10.06	9.49	8.41
Spherical Thrust Roller Brg.	50	—	—.		0	17.9	21.8	24.5	25.5	23.8	21.0

TABLE 6 VALUES OF X, V, AND Y. VALUES FOR CONVENTIONAL BEARING TYPES

$P_r = X\,V\,F_r + Y\,F_a$	$\frac{C_i}{C_e}$	V		Single Row Bearings $P_r \geqq V\,F_r$		Double Row Bearings			
		For Fixed Outer Ring Load	For Fixed Inner Ring Load			$P_r \geqq 2\,V\,F_r$		$P_r \leqq 2\,V\,F_r$	
				X	$\frac{Y}{\cot\alpha}$	X	$\frac{Y}{\cot\alpha}$	X	$\frac{Y}{\cot\alpha}$
Self-Aligning Ball Bearings..	1 . . . 2	1	1	—	—	0.6	0.7	1	0.5
Deep Groove Ball Brgs. $\alpha_0 = 0°$	0.4 . . . 0.8	1	1.2	0.5	0.4	—	—	—	—
Angular Contact Ball Brgs. $\alpha_0 = 30° \ldots 40°$	0.5 . . . 1	1	1.2	0.2	0.5	0.4	0.8	1	0.5
Spherical Roller Brgs.	0.5 . . . 1	1	1.3	0.4	0.4	0.6	0.7	1	0.5
Tapered Roller Brgs. $\alpha_0 = 10° \ldots 30°$	0.5 . . . 1	1	1.3	0.3	0.5	0.5	0.8	1	0.5
Cylindrical Roller Bearings...	0.5 . . . 1	1	1.3	1	—	—	—	1	—

Variation of Contact Angle with Load

	α_0	0°			30°			40°		
Deep Groove and Angular Contact Ball Bearings	$\frac{F_a^*}{D^2 - d^2}$	0.01	0.03	0.09	0	0.2	0.4	0	0.2	0.7
	$\cot\alpha$	5	4	3	1.7	1.5	1.4	1.2	1.1	1.0

*) Units in kg and mm.

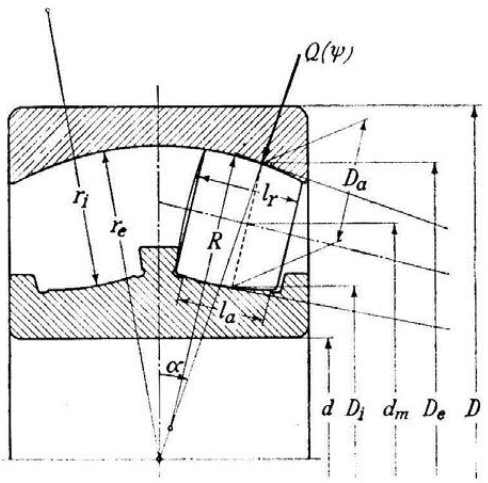

FIG. 8

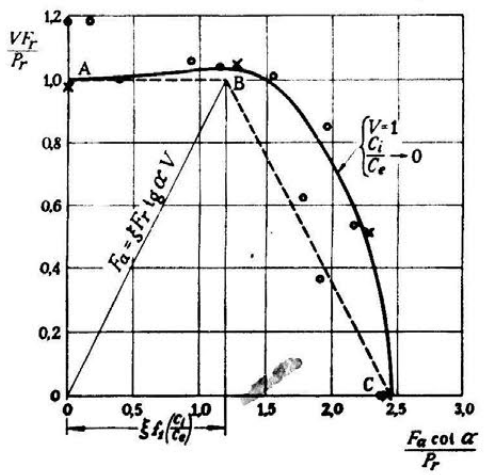

FIG. 9

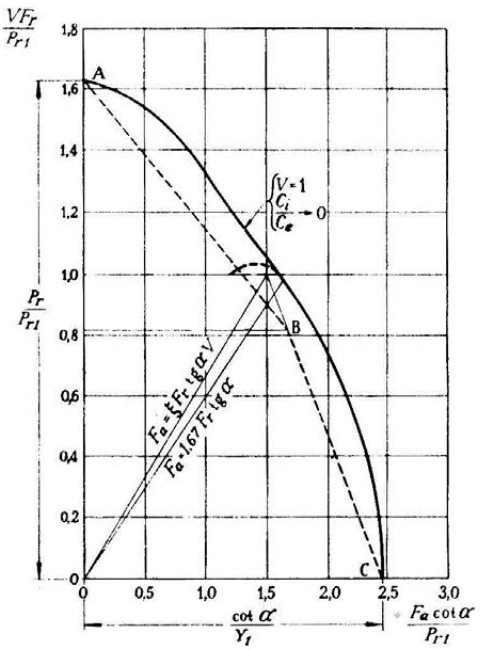

FIG. 10

For practical reasons it is better to calculate on the basis of the broken lines ABC in Figs. 9 and 10, in place of the solid curves. The calculation is done then according to the formula and values in Table 6, where V is a factor which takes regard of the rotation relations of the bearing; that is, a "rotation factor," X is a "radial factor," and Y is a "thrust factor."

The values have been corrected with regard to combined loads.

The equivalent thrust load P_a of a bearing is found from the equation

$$Y\,P_a = P_r \quad \ldots\ldots\ldots\ldots\ldots\ldots [41]$$

where P_r is obtained from Table 6: Y is the thrust factor for pure thrust load, that is, for $F = 0$

Slow-Motion Pictures of Impact Tests by Means of Photoelasticity

By LUDWIG FOEPPL,[1] MUNICH, GERMANY

The experiments described in this paper were carried out in investigating the distribution of stresses and their variation with time in a test bar subject to bending stresses resulting from an impact. While a series of tests has been made, only two of them will be dealt with in detail. In the first test the impact is of moderate intensity, so that the response is entirely elastic. The test results will be compared with a theoretical treatise by St. Venant and Flamant published in 1889. In the second test the impact is strong enough to break the test bar.

Test Apparatus

THE test setup for carrying out the investigation on the distribution of bending stresses resulting from an impact is shown in Figs. 1 and 2. A bar consisting of plastic

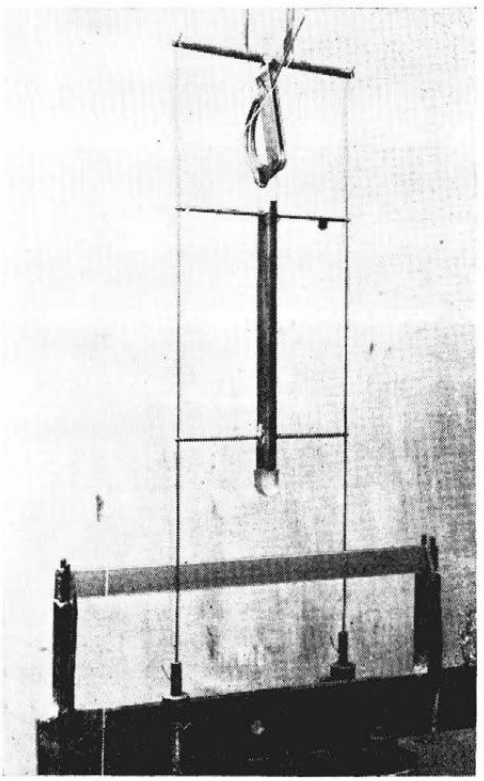

Fig. 1 Test Setup

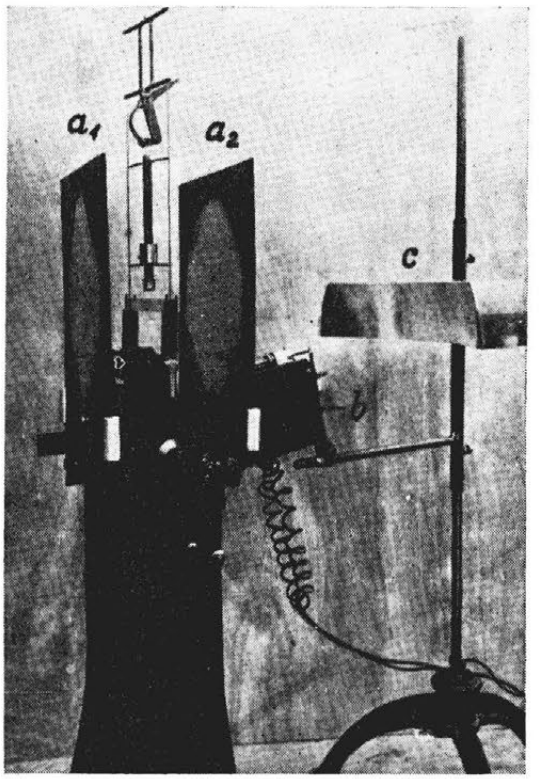

Fig. 2 Bar With Impact Mechanism in Place Between Polaroids

"Dekorit" as used in these photoelastic tests is supported at the ends (see Fig. 1). Each support consists of a fork, in which the bar is placed to avoid lateral shifting, and a rubber band is drawn over it to press the ends of the bar firmly against the support. This setup corresponds to a mild clamping of the bar ends. On the center of the bar supported in this way, a hammer falls from a height of 2 meters (6 ft). To the lower end of the hammer is attached a cylindrical cap of Dekorit, the axis of which is normal to the axis of the test bar, so that a uniform transmission of impact over the entire width is ensured. Thus a state of plane stress is produced in the test bar. This effect is made visible by placing the test setup between the two polaroids of the photoelastic apparatus and sending light rays through it. In the figure two vertical guide wires for the hammer and the releasing mechanism can be seen. The dimensions of the test bar are length l = 28.5 cm (11.2 in.), rectangular cross section of b = 1 cm (0.39 in.) breadth, and h = 2 cm (0.79 in.) height. From the specific weight, γ = 1.3 grams per cu cm, the weight of the test bar results as

$$P = l \cdot b \cdot h \cdot \gamma = 28.5 \cdot 1 \cdot 2 \cdot 1.3 = 74 \text{ grams } (0.163 \text{ lb})$$

As shown in Fig. 2, the bar with the impact mechanism is placed between the polaroids a_1 and a_2 of the photoelastic apparatus. The concave mirror c is an elliptical mirror produced in the author's laboratory. The curvature of the mirror could not be

---

[1] Professor of Applied Mechanics, Munich Institute of Technology.

Contributed by the Applied Mechanics Division and presented at the Annual Meeting, New York, N. Y., November 28–December 3, 1948, of The American Society of Mechanical Engineers.

Discussion of this paper should be addressed to the Secretary, ASME, 29 West 39th Street, New York, N. Y., and will be accepted until July 11, 1949, for publication at a later date. Discussion received after the closing date will be returned.

Note: Statements and opinions advanced in papers are to be understood as individual expressions of their authors and not those of the Society. Paper No. 48—A-24.

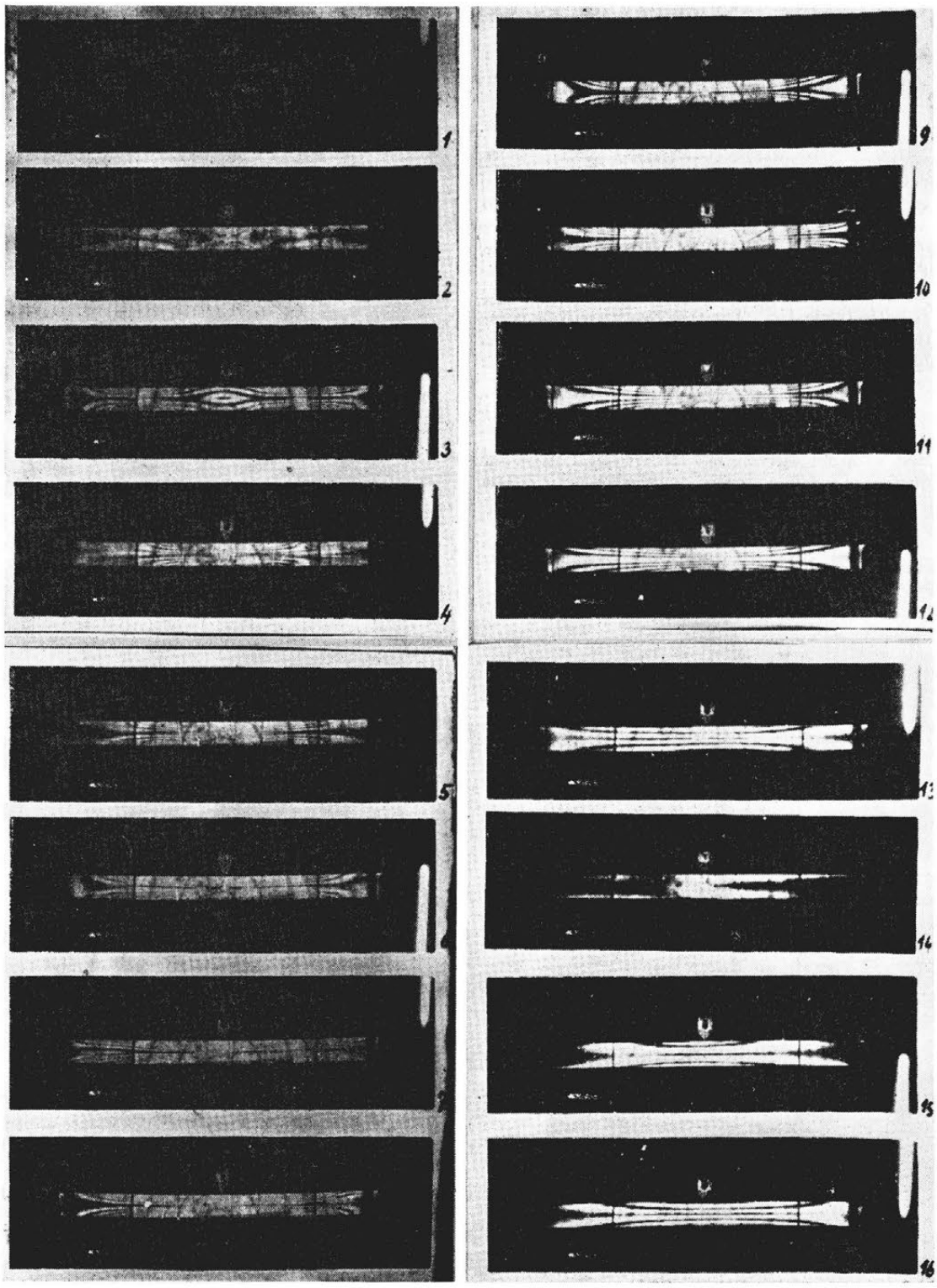

FIG. 3 FRAMES TAKEN FROM FIRST TEST

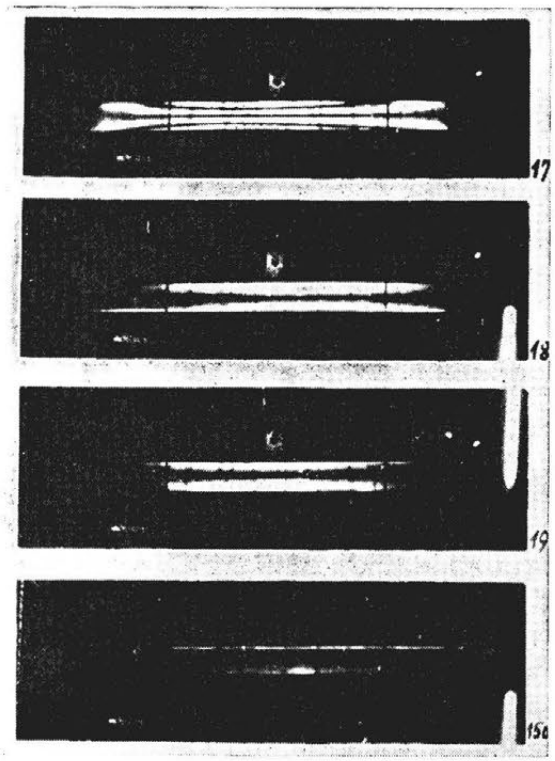

FIG. 3 (*Continued*)

varied continuously. Therefore the curves visible in the mirror separate regions with different radii of curvature. These curves appear in the pictures of isochromatics, which will be discussed later, as circular arcs and should not be confused with the isochromatics themselves.

At one focus of the concave mirror the electric arc of an arc lamp b is centered, while at the other focus, which is on the other side of the polaroids, the objective of the slow-motion camera is located (not visible in Fig. 2).

First Test

Illustrations from the first test are shown in Fig. 3.

Impact weight Q = 60 grams (0.132 lb)
Impact height H = 200 cm (6 ft 7 in.)
Frame speed, 3020 frames per sec

Frame 1 shows the test bar in its initial state immediately before the impact. Between this view and the second one, the impact weight has begun to touch the test bar. The increasing transparency of the entire bar shows that meanwhile stresses due to the impact have appeared over the entire length of the bar. The distribution of isochromatics, characteristic for bending stresses (see frame 2) shows that the bending stresses are noticeable only in the vicinity of the field of impact, while on both sides of the axis of symmetry the stresses rapidly decrease as indicated by the isochromatics turning toward the boundaries of the bar. At both sides of the axis of symmetry and at a distance approximately equal to the double height of the bar, the bending stress approaches zero (frame 2). At a somewhat greater distance, i.e., where the wires guiding the impact weight appear as sharp dark lines in the picture, again a low stress is indicated by the isochromatics at the lower and upper edges of the bar. This stress must show a sign opposite to that of the stress arising in the central part of the bar, i.e., the line of curvature, while reaching its lowest point in the center of the bar, reverses its concavity downward at points farther away from the center. This experimental result agrees well with the theory to be developed later. Probably a great number of bending-stress waves run along the bar, are reflected at the ends, and are superimposed on the initial waves.

Frame 3 is especially interesting. A comparison with frame 2 shows a relieving of the center cross section. The maximum bending stress here appears on cross sections of the bar located about one quarter of the entire length away from the center cross section, as indicated by the crowding of isochromatics in these cross sections.

Frame 4 again shows an increase of bending stresses in the center cross section. This increase continues in frames 5 to 8. In frames 7 and 8 the number of isochromatics in the center cross section is approximately equal, as can be ascertained by enlarging the pictures. In frame 9 the number of isochromatics is on the decrease, so that the maximum is probably reached between frames 7 and 8. At the same time, frames 4 to 7 show that zero points of moments, which in frame 4 are still about halfway between the point of impact and the supports, shift farther toward the supports in frames 5 to 7. This phenomenon also agrees with the theoretical deductions, as will be seen later. The relieving of the bar, i.e., its swinging back from its maximum deflection, can be observed in the decreasing number of isochromatics in frames 9 to 13. Frame 14 shows the last phase of contact between impact weight and bar. Frames 15 to 19 correspond to free oscillations of the bar, free of external loads at different instants of this oscillation process.

In order to prove that the stressing of the bar is elastic during the entire impact, frame 150 of this series is also shown, where the free oscillations have vanished. A comparison with frame 1 demonstrates that the impact did not leave any residual stresses, and therefore there are no permanent deformations.

We have conducted several tests similar to the one described here, in which the impact weight, the impact height, and the bar height were varied. The corresponding series of pictures does not offer any new information, as compared with the first test.

Second Test

Frames taken from the second test are shown in Fig. 4.

Bar length l = 28.5 cm (11.2 in.)
Bar height h = 2 cm (0.79 in.)
Impact weight, 240 gm (0.529 lb)
Impact height H = 600 cm (19 ft, 8 in.)
Frame speed, 1980 frames per sec

In this test the impact weight is not shown in the illustrations since it does not consist of transparent Dekorit. Frame 1 shows the bar before the impact. In frame 2 there is already a great number of isochromatics in the central part of the bar. Since the number of isochromatics is increasing rapidly, the separate isochromatics can be discerned only with difficulty. During this test, as well as during the first one, the slow-motion camera was adjusted to a time of exposure that amounted to $^1/_6$ of the time interval between the separate frames. In frame 3 the number of isochromatics has further increased. In frame 4 the first signs of tearing at the tension side of the bar appear. The progress of rupture can be observed clearly in the remaining views.

Theoretical Considerations

St. Venant and Flamant[2] dealt with the theory of a bar elastically stressed by an impact at its center, as in test 1 of this paper. The solution as offered in this treatise will be given here. If y stands for the deflection and x for the cross-sectional co-ordinate,

[2] St. Venant and Flamant, *Journal de l'école polytechnique*, Paris, France, vol. 59, 1889.

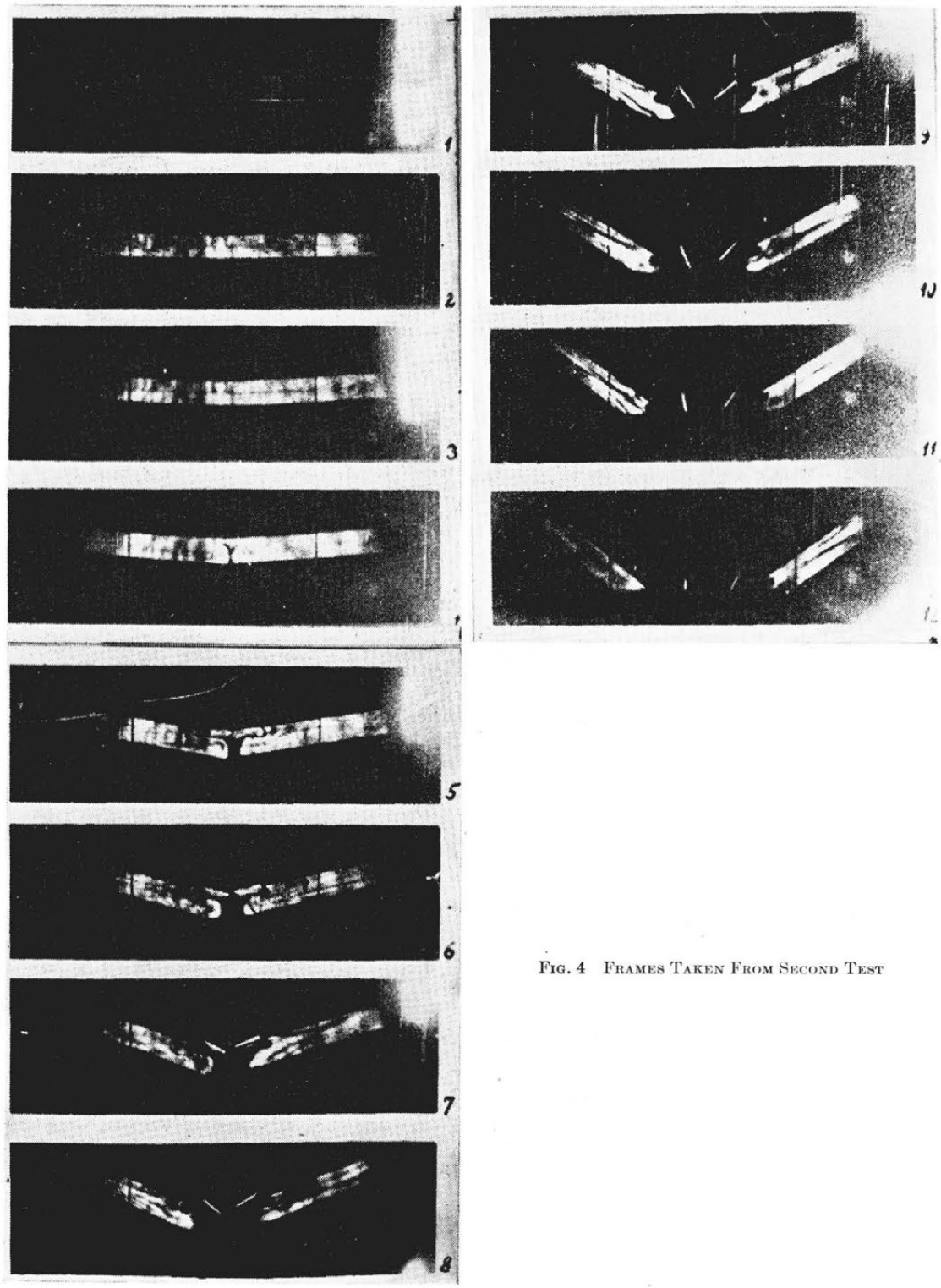

FIG. 4 FRAMES TAKEN FROM SECOND TEST

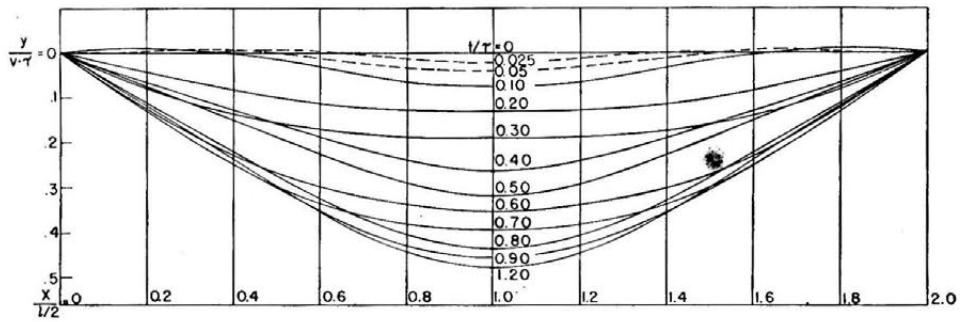

FIG. 5 SUMMATION OF VALUES OF EQUATION [1] BY ST. VENANT AND FLAMANT

$x = 0$ corresponding to the left support, the solution of the differential equation is

$$y = v\tau \sum_m \frac{4}{m^3} \frac{\dfrac{\sin 2m\dfrac{x}{l}}{\cos m} - \dfrac{\sinh 2m\dfrac{x}{l}}{\cosh m}}{\dfrac{1}{\cos^2 m} - \dfrac{1}{\cosh^2 m} + \dfrac{2}{m}\dfrac{P}{Q}} \sin m^2 \frac{t}{\tau} \quad \ldots [1]$$

where v is the velocity of the impact weight at the moment of impact, τ is an abbreviation for

$$\tau = \frac{l^2}{4}\sqrt{\frac{P}{lgEI}} \quad \ldots [2]$$

where P is the weight of the bar, EI its stiffness against bending, and g the acceleration due to gravity. The summation in Equation [1] extends to all values m that satisfy the "period equation"

$$\frac{2P}{Q} = m\,(\tan m - \tanh m) \quad \ldots [3]$$

where Q is the impact weight.

For the values of $P/Q = {}^1/_2$, 1, and 2, St. Venant and Flamant calculated the seven lowest values of m that satisfy the period Equation [3]. For $P/Q = 1$ they found the following values:

$m_0 = 1.19161$	$m_4 = 13.42093$
$m_1 = 4.11972$	$m_5 = 16.55021$
$m_2 = 7.18994$	$m_6 = 19.68824$
$m_3 = 10.29839$	

In the present tests the weight of the bar is $P = 74$ grams (0.16 lb). τ, according to Equation [2], which represents time, results in the example as

$$\tau = \frac{28.5^2}{4}\sqrt{\frac{0.074 \times 3}{28.5 \times 27{,}000 \times 2 \times 981}} \approx \frac{1}{400} \text{ sec}$$

E is the modulus of elasticity of the Dekorit bar. Its value $E =$ 27,000 kg per sq cm (390,000 psi) has been introduced from an elastic tensile test.

In our first test $P/Q = 74/60 = 1.23$.

St. Venant and Flamant calculated the functions of curvature $y(x)$ at different times t after the impact of the weight Q, by using Equation [1] and the first seven values of the period Equation [3]. The results of their long calculations are represented in curves. For $P/Q = 1$ these curves are given in Fig. 5. They represent the summation values of Equation [1] without the factor $v\tau$, i.e., they are pure numbers. The ratio $x/(l/2)$ is used as abscissa.

A comparison of these curves with the results of test 1 of this paper shows a good degree of conformity. Since in test 1 about 3000 pictures have been taken each second, the time interval between pictures is ${}^1/_{3000}$ sec $= {}^1/_{75}\ \tau$, if the value of τ, as previously given, is used. In the discussion of test series 1 we have found that the maximum bending occurred between frames 7 and 8, i.e., approximately 7.5 frames after the impact. This would correspond to a $t/\tau = 1$ in good agreement with the bending curves in Fig. 4, as the St. Venant curves are based upon $P/Q = 1$. There the maximum deflection occurs at $t/\tau = 1.2$. The curves further show that at $t/\tau = 0.3$ the initial curvature in the center cross section has almost vanished, and then again begins to increase. Also, this effect is clearly shown in the present photoelastic tests. The reversal of curvature shortly after the impact can be found in the curves until $t/\tau = 0.15$. The gradual shifting of the zero point of moments toward the supports appears in these graphs as well.

In concluding our evaluation, it may be stated that the results constitute an excellent verification of the mathematical deductions of St. Venant and Flamant.

RESULTS AND RECOMMENDATIONS

The verification of the classical theory by photoelastic tests is an important result of this report. Theory and experiments indicate that shortly after the beginning of impact, an initial bending stress in the center cross section vanishes almost completely. It is only at a later time that the bending stresses again increase. Just this effect should be more closely investigated by varying conditions of support of the bar. In this connection it also would be interesting to investigate test bars with variable height subject to impact tests.

ACKNOWLEDGMENT

The author wishes to acknowledge the valuable assistance of his former assistant, Dr. E. Moench, during these experiments

Fracture of Gray-Cast-Iron Tubes Under Biaxial Stresses

By R. C. GRASSI[1] and I. CORNET,[2] BERKELEY, CALIF.

The fracture of gray-cast-iron thin-wall tubes was investigated, for various ratios of axial to tangential stress ranging from pure tension to pure compression, yielding data for some stress ratios not previously reported. Analysis of the results reveals that the present theories of fracture do not account completely for the data obtained, thus indicating the need for further investigations of similar materials.

Introduction

THERE have been numerous investigations of materials under combined stresses. These investigations have been concerned with state of stress, deformation to fracture, and theories of metal flow in general. Most of these studies have been limited to mild steel, and alloys of aluminum and magnesium. Justifiably the emphasis has been on these materials because of the applicability of the results to problems of working and forming these metals. However, data for the fracture of brittle materials subjected to biaxial stress are meager and inconclusive as to acting fracture law. Investigators have developed mathematical expressions for the laws of behavior of metals under combined stress. These laws have clarified the dependence of fracture stress on stress state. The validity and applicability of these fracture laws to brittle materials, such as cast iron, have not been determined.

Studies of the fracture of cast-iron tubes under biaxial stress date back to the work of Cook and Robertson (1)[3] in 1911, and Ros and Eichinger (2) in 1926. The work of Siebel and Maier (3) in 1933, constitutes the latest data reported for the study of cast iron under combined stresses.

Purpose and Scope

The purpose of this investigation was to extend the work of previous investigators on gray cast iron in the tension-compression quadrant, and to obtain for material from the same foundry heat data in the tension-tension quadrant. In addition, the data obtained were to be analyzed to determine the applicability and validity of existing laws of fracture for the brittle material studied. The gray cast iron used was of the following composition: C 3.48 per cent, Mn 0.52 per cent, Si 2.41 per cent, P 0.31 per cent, and S 0.14 per cent. The data obtained represent the result of testing 41 tube specimens and 7 solid cylindrical specimens.

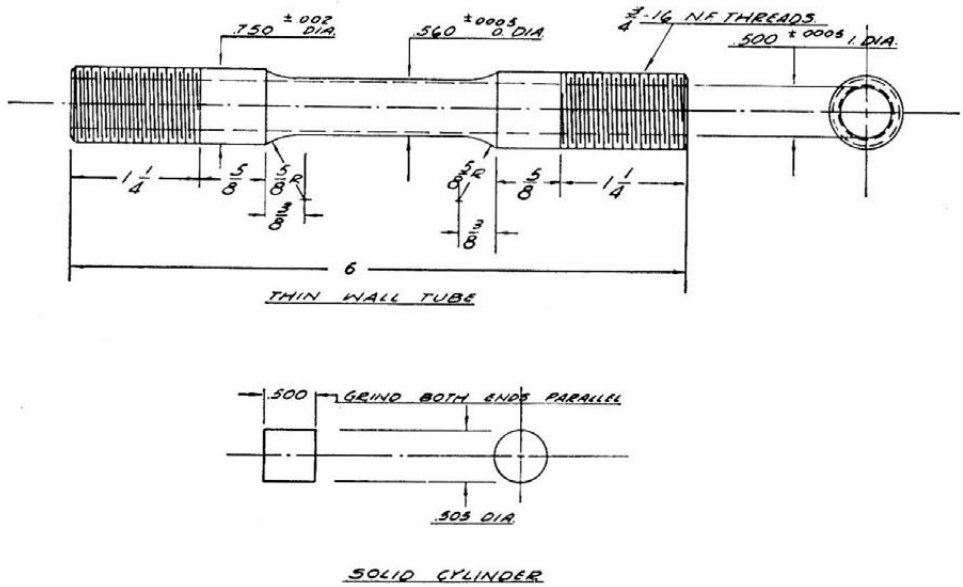

Fig. 1 Gray-Cast-Iron Fracture Specimens

Procedure

The specimens used are shown in Fig. 1. The tube specimen was mounted in the grips as shown in Fig. 2, and stressed according to the desired ratio of axial to tangential stress (referred to as "stress ratio") by the proper combination of internal pressure

[1] Assistant Professor of Mechanical Engineering, University of California. Mem. ASME.

[2] Assistant Professor of Mechanical Engineering, University of California.

Contributed by the Applied Mechanics Division and presented at the Annual Meeting, New York, N. Y., November 28–December 3, 1948, of The American Society of Mechanical Engineers.

Discussion of this paper should be addressed to the Secretary, ASME, 29 West 39th Street, New York, N. Y., and will be accepted until July 11, 1949, for publication at a later date. Discussion received after the closing date will be returned.

Note: Statements and opinions advanced in papers are to be understood as individual expressions of their authors and not those of the Society. Paper No. 48—A-15.

[3] Numbers in parentheses refer to the Bibliography at the end of the paper.

and axial tension or compression. The solid cylindrical specimens were tested in compression.

A modified two-cylinder Diesel injection pump was used to produce the internal pressure. The pressure was measured by a calibrated Bourdon-type gage which was accurate to $\pm 1/2$ per

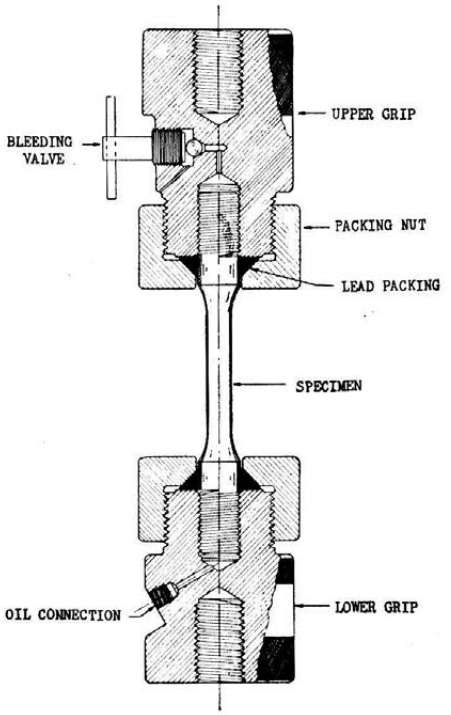

FIG. 2 GRIP SECTIONS FOR STUDY OF FRACTURE OF GRAY CAST IRON UNDER BIAXIAL STRESS

cent. The axial loading of the specimen was accomplished on a 200,000-lb Southwark-Emery testing machine, using the 10,000-lb scale with a least division of 10 lb.

The tube specimens were machined from cast bars 1.2 in. diam and 22 in. long, all cast bars being from the same heat. Three specimens were machined from each cast bar which had been previously given a 1-hr anneal at 1000 F (4). The specimens were drilled and reamed to produce the internal diameter, and then rough-turned. The blank was then mounted on a mandrel and finish-turned and threaded. A circular-radius tool was used for the finished cut, which produced a smooth surface with no discontinuity at the radii.

The loading of the specimen, for both axial tension and compression, followed a schedule (refer to Appendix) in which predetermined increments of axial load and internal pressure were used to maintain the desired ratio of axial stress to tangential stress. The specimen holder shown in Fig. 2 was used for axial tension and compression of the tube specimens. However, for axial compression, alignment of the tube specimen was controlled by means of a surface gage and dial indicator. For both axial tension and compression, the technique used was such as to provide tests upon which there would be no effect of eccentricity. The solid cylindrical specimens were tested in a die set with polished anvils, designed to obtain axial loading; the ends of the specimens were lubricated, and the anvils polished to reduce friction effects.

For some of the tube specimens tested, strain measurements were taken at various stages during loading. The relatively small amount of ductility obtained, as revealed by these measurements, will be referred to in the discusion.

RESULTS

Values of true stress at fracture are plotted on Fig. 3. All data plotted in this figure are for the tube specimens shown in Fig. 1. Stress values are based on cross-section area at fracture. Pertinent formulas are given in the Appendix.

Except for stress ratios between —2.7 and —∞ the cast-iron tubes possess so little ductility that the cross-section areas at fracture are equal to the original cross-section areas, within limits of experimental error. Between stress ratios of —2.7 and —∞, there is increased ductility, and the true stresses differ from nominal stresses as much as 3 per cent.

Shown in Fig. 4 are the fractures obtained under various stress ratios. Under pure tension loads and for stress ratios to approximately +1.2, fractures occurred across the tube perpendicular to the axis of the specimen. From stress ratios of +1.2 to —2.7, the

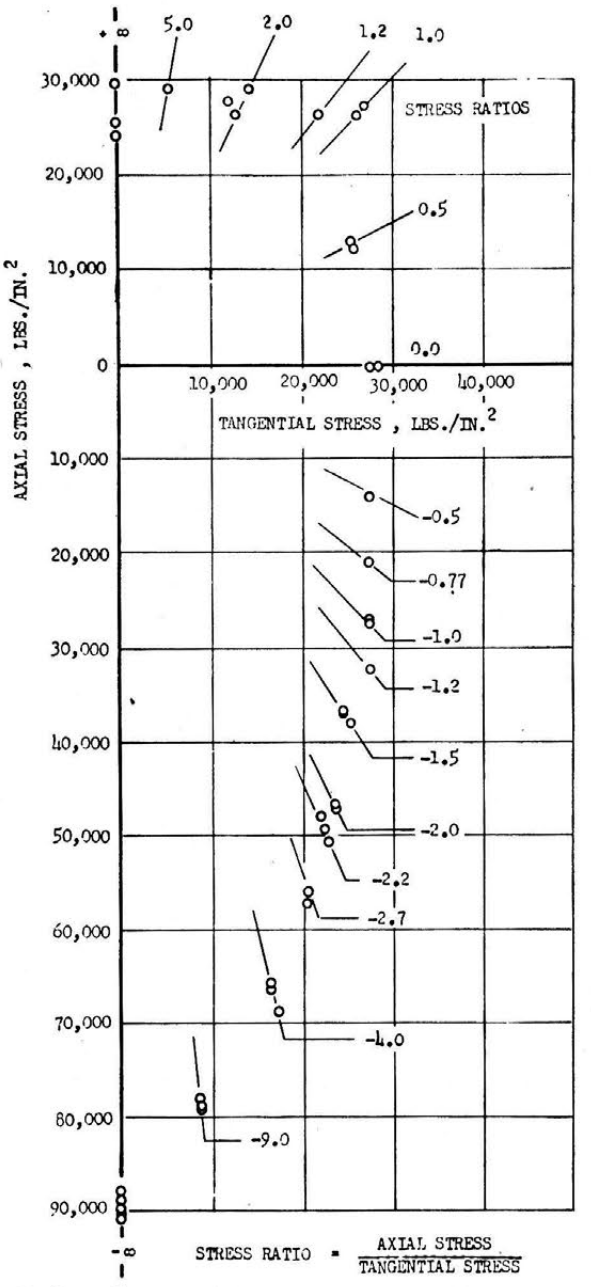

FIG. 3 TRUE STRESS AT FRACTURE FOR VARIOUS STRESS RATIOS, GRAY CAST IRON

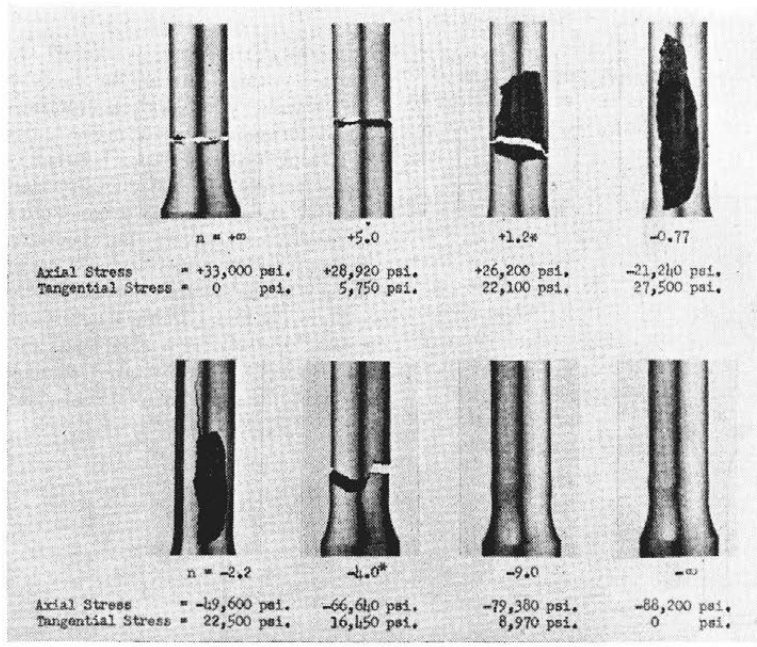

FIG. 4 FRACTURES OBTAINED IN GRAY CAST IRON UNDER VARIOUS TRUE STRESS RATIOS
[n = true stress ratio = (axial stress)/(tangential stress).]
*Note that these bars were broken apart on removing from grips.

fracture pattern consisted of blowouts of sections generally 2 to 4 times longer than their width, irregular in outline, and oriented with the length of the blowout fragment parallel to the length of the tube. At the stress ratio —4, fractures obtained were either longitudinal blowouts or an irregular diagonal crack in the tube which is shown in Fig. 4. All fractures discussed to this point were characterized by negligible ductility. The fractures at stress ratios of —9 and —∞ were preceded by uniform circumferential bulging at one end or at both ends of the tube, a short distance from the fillet. Failure actually occurred through the formation on the bulge of fine diagonal cracks, at approximately 45 deg with the axis of the tube. Fig. 5 shows the fracture condition on these bulges clearly.

For pure compression, the average true stress for seven solid cylinders was 96,200 psi, as compared to a value of 89,700 psi for five tube specimens. The difference in averages was reasonable, considering the dissimilarity of the specimens.

In general, data within the tension-compression field are much more reproducible than within the tension-tension field, as may be noted in Fig. 3.

DISCUSSION

In the studies of the fracture of cast-iron tubes under biaxial stress, Cook and Robertson (1) subjected thick-walled cast-iron tubes to the combined effect of internal pressure and compression. Ros and Eichinger (2) later obtained data for thin-walled cast-iron tubes subjected to internal pressure plus tension, which was followed by the work of Siebel and Maier (3), who also used thin-walled cylinders of gray cast iron. Research of previous investigators has been plotted in Fig. 6, based upon a manuscript of J. E. Dorn (5). These data are for different cast irons of unspecified compositions. In general, these results have been interpreted to conform to the maximum normal stress theory for fracture, with some reservation by Gensamer (6) and Dorn (5). Furthermore, there are no experimental data given between stress ratios —1 and —∞.

The ideal theories most generally applied for fracture of metals under biaxial stress may be represented graphically as in Fig. 7.

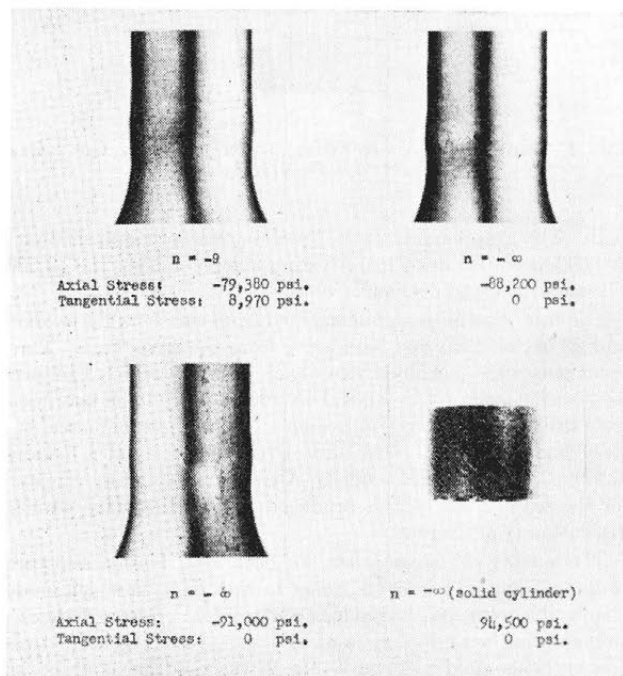

FIG. 5 DUCTILE FRACTURES OF GRAY CAST IRON
[n = true stress ratio = (axial stress)/(tangential stress).]

The theories are expressed quantitatively in the Appendix of this paper and are discussed at length (5, 7, 8).

Reference to Figs. 3 and 7 reveals the inapplicability of the hydrostatic tension theory to cast iron. In the tension-tension quadrant the shear-stress and normal-stress theories cannot be differentiated. In the tension-compression quadrant, the maximum-normal-stress theory is clearly distinguishable from the maximum-shear-stress theory. The effective-stress theory is rep-

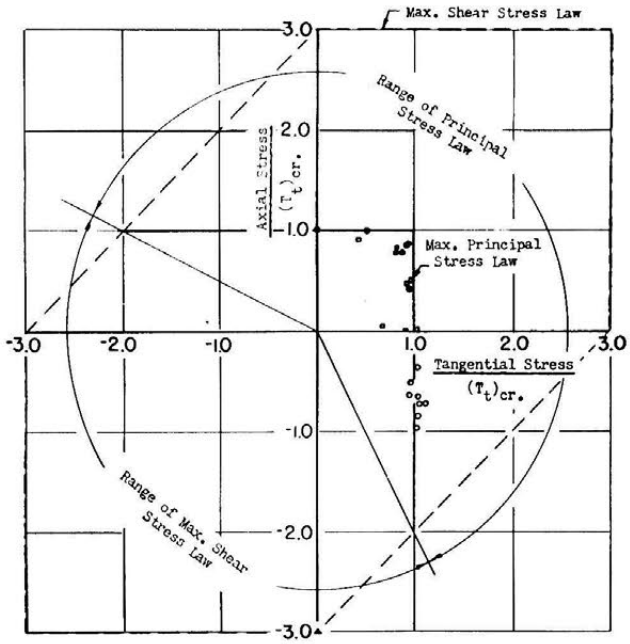

FIG. 6 FRACTURE OF CAST IRON UNDER BIAXIAL STRESS
[Modified after J. E. Dorn, reference (5).]

Symbols: ○ = data of Cook and Robertson
● = data of Ros and Eichinger
□ = data of Maier
Δ = assumed fracture in compression
$(Tt)_{cr}$ = critical fracture stress in simple tension

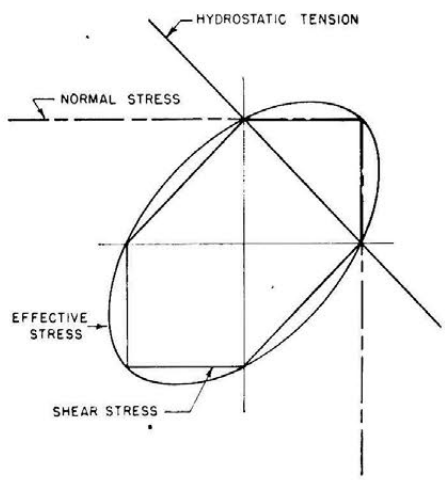

FIG. 7 IDEALIZED STRESS THEORIES FOR FRACTURE OF METALS UNDER BIAXIAL STRESS

resented by an ellipse circumscribed about the figure of the maximum-shear-stress theory.

The normal-stress theory is not operative in the entire tension-compression quadrant because it does not provide for failure in compression. The compressive strength of cast iron, which is 2.5 to 4.5 times its tensile strength, precludes the applicability of the shear-stress theory for fracture unless the theory is modified. J. E. Dorn (5) and others have postulated that the maximum-shear-stress theory holds for the stress ratios between pure compression and the region where the normal-stress theory prevails, as illustrated in Fig. 6.

The results obtained from this investigation, as shown in Fig. 3, indicate that the fracture of thin-walled cast-iron tubes under biaxial stress cannot be accounted for completely by the conventional fracture theories. A modified maximum-shear-stress theory for fracture, with a limiting condition represented by a line drawn from the stress value at pure compression at an angle of 45 deg with the axial stress ordinate, would not be in accord with the data obtained. The lack of agreement with a modified maximum-shear-stress theory for fracture may not be attributed to experimental error and therefore would point to the fact that the fracture of cast iron under biaxial stress departs from conventional fracture theories. Cast iron could be considered as a material composed of a matrix of carbon steel with interspersed graphite. It is possible that under comparatively low tensile stresses the graphite flakes would give rise to sharp notches which grow to cause brittle failure. Under high compressive stresses cast iron sustains loads approximately equal to those of a carbon steel. Cast iron is set apart from materials which have generally been studied under biaxial stress because of factors such as ductility, work hardening, ratio of compressive to tensile strength, and the like.

There is sufficient ductility present, particularly at the stress ratios of —4, —9, and —∞, to permit measurable deformation. The deformation present, which results in less than 2 per cent change in cross-section area, has little effect on the calculation of stresses. It is recognized that for the ratio of —9 and —∞ the circumferential bulges result in tension stresses at the outer fibers and give rise to tension failure. For a representative bar at —∞ stress ratio, the bulge diameter was 0.583 in., with a radius of curvature at the bulge of 0.61 in., and the diameter at the center of the gage length of 0.569 in. at failure.

The local circumferential bulging of the tube specimen was not gradual in nature but appeared at stresses very close to fracture, and, for the stress ratio of —∞, occurred at a stress which was within 2 per cent of the value obtained at fracture. Strain history of bars at representative stress ratios was obtained by measuring the diameter change of the specimen at various stages during loading. These were interrupted tests, but the data obtained therefrom were consistent with those from continuous tests.

At the present time, some investigators (9) interested in the fracture of metals are beginning to approach the problem from a micromechanical viewpoint. It is believed that this trend of thought ultimately will yield theory more in accord with the data. Development of such theory will take time and necessitate further investigations.

There is a need of data and theory, by the design engineer, for brittle materials under combined stresses. This is particularly evident when one considers the application of cast iron as pressure castings, cylinders, valves, fittings, and pipe. Such applications subject cast iron to combined stresses and may result in failures unaccounted for by published design data. Thus the fracture of cast irons for various stress ratios, particularly for those ratios not previously obtained, should be of great interest to the design engineer.

CONCLUSIONS

1 Fracture data are given for gray-cast-iron thin-wall tubes under tension-tension and tension-compression stresses, including stress ratios not previously reported.

2 The type of fracture and ductility at various ratios of axial to tangential stress is reported.

3 The fracture data may be explained in part by the maximum-normal-stress theory, but cannot be entirely accounted for by present theories of fracture.

4 The need for further investigations of similar material is evident if a comprehensive fracture law is to be established and necessary design information provided.

BIBLIOGRAPHY

1 "The Strength of Thick Hollow Cylinders Under Internal Pressure," by G. Cook and A. Robertson, *Engineering*, vol. 92, 1911, pp. 786–789.

2 "Versuche zur Klärung der Frage der Bruchgefahr," by M. Ros and A. Eichinger, Proceedings of the Second International Congress for Applied Mechanics, 1926, pp. 315–327.

3 "Der Einfluss Mehrachsiger Spannungszustände auf das Formanderungsvermögen metallischer Werkstoffe," by E. Siebel and A. Maier, *Zeit. VDI*, vol. 77, 1933, pp. 1345–1349.

4 "Cast Iron," by H. Bornstein and J. W. Bolton, ASM Metals Handbook, section on "Heat Treatment of Cast Iron," 1939, p. 638.

5 "Effect of Stress State on the Fracture Strength of Metals," by J. E. Dorn, in "Fracturing of Metals," ASM, 1948, pp. 32-50.

6 "Strength of Metals Under Combined Stresses," by M. Gensamer, ASM, 1940, pp. 58–60.

7 Reference (6), pp. 1–106.

8 "Plastic Flow in Metals," by J. J. Jelinek, A. J. Latter, E. Thomsen, and J. E. Dorn, OPRD, Report of Research Project NRC—548, May, 1945.

9 "Mechanism of Fracture of Glass and Similar Brittle Solids," by N. W. Taylor, *Journal of Applied Physics*, vol. 18, 1947, pp. 943–955.

Appendix

Stresses, stress ratios, and loading schedules for the tube tests may be calculated by use of the following formulas:

Let

Q = load, lb
p = pressure, psi
σ_a = normal stress in axial direction
σ_t = normal stress in tangential direction (circumferential or hoop stress)
d_i = inner diameter (initially 0.500 in.)
d_o = outer diameter (initially 0.560 in.)
h = tube-wall thickness (initially 0.030 in.)

Then

$$\sigma_a = \frac{Q + \pi/4(d_i^2 p)}{(d_o^2 - d_i^2)\pi/4} \quad [1]$$

$$\sigma_t = \frac{pd_i}{2h} \quad [2]$$

If we let

$$n = \frac{\sigma_a}{\sigma_t} \quad [3]$$

where n is referred to as "the stress ratio" then

$$\sigma_a = \frac{npd_i}{2h} = \frac{Q + \pi/4(d_i^2 p)}{(d_o^2 - d_i^2)\pi/4} \quad [4]$$

For conditions of negligible ductility, d_i, d_o, and h are known, and the relationship between Q, p, and n is obtained

$$Q = 0.785\ p\ (0.53n - 0.25) \quad [5]$$

The last relationship permits the preparation of a schedule of axial loads and internal pressures for any predetermined stress ratio.

Fracture stress theories: Let

σ_1 = algebraically greatest principal stress
σ_2 = intermediate principal stress
σ_3 = algebraically least principal stress

Then the fracture stress theories discussed may be stated as follows:

Maximum normal stress, $\sigma_N = \sigma_1$

Maximum shear stress, $\tau = \dfrac{\sigma_1 - \sigma_3}{2}$

Effective stress (quadratic invariant), $\sigma_E =$

$$\frac{\sqrt{(\sigma_1 - \sigma_2)^2 + (\sigma_2 - \sigma_3)^2 + (\sigma_3 - \sigma_1)^2}}{2}$$

Hydrostatic tension (linear invariant), $\sigma = \dfrac{\sigma_1 + \sigma_2 + \sigma_3}{3}$

These theories are generally called "fracture laws."

A Strain-Energy Expression for Thin Elastic Shells

By H. L. LANGHAAR,[1] URBANA, ILL.

A derivation is given for the strain energy of an isotropic elastic shell whose radii of curvature are sufficiently large that strains may be assumed to vary linearly throughout the thickness. The work of Love (1)[2] has been the only previous general investigation which expresses the strain energy in terms of the displacements of the middle surface. The effects of the tangential displacements upon the energy due to bending are found to differ appreciably from Love's results in the first-order terms. As in the classical large-deflection theory of flat plates, quadratic terms in the derivatives of the normal deflection are retained in the strain tensor, but quadratic terms which involve the tangential displacements are neglected. Special forms of the general energy expression derived in this paper are given for shells in the shapes of flat plates, circular cylinders, elliptical cylinders, ellipsoids of revolution, and spheres. These applications, as well as certain intuitive observations, provide checks on the theory.

Introduction

THE undeformed middle surface of a shell is defined parametrically, with respect to a given system of rectangular Cartesian co-ordinates X, Y, Z, by equations of the type

$$X = X(x, y),\ Y = Y(x, y),\ Z = Z(x, y) \quad [1]$$

The variables x, y are surface co-ordinates, since any pair of values of x and y define a point on the middle surface. The loci y = const, and x = const are curves on the undeformed middle surface, respectively, called the x-co-ordinate lines and the y-co-ordinate lines. The surface co-ordinates x, y, are selected in such a way that the co-ordinate lines coincide with the lines of principal curvature on the undeformed middle surface. The distance ds between two points on the undeformed middle surface, which have co-ordinates x, y, and $(x + dx, y + dy)$, is then given by a differential quadratic form of the type

$$ds^2 = E\,dx^2 + G\,dy^2 \quad [2]$$

Here, E and G are each functions of x and y.

The positive sense on a co-ordinate line is defined to be the sense in which its co-ordinate increases. Through any point P, on the undeformed middle surface, there pass three mutually perpendicular fixed straight axes, such that one axis is normal to the surface, and the other two axes are, respectively, tangent to the x and y co-ordinate lines. The tangential axes are given the same senses as the corresponding co-ordinate lines, and a positive sense is arbitrarily assigned to the normal axis. The displacement vector of the point P is defined by its rectangular components (u, v, w), upon these axes. Then u and v are, respectively, the displacements in the directions of the x and y-co-ordinate lines, and w is the normal displacement.

For the application of the principle of virtual work or the principle of least action to problems of elastic shells, it is desirable that the strain energy be expressed as a function of the displacement vector of the middle surface, since there is no simple way to express the virtual work of the external forces, if a displacement vector is not explicitly employed. Also, the use of the displacement vector obviates the need for compatibility conditions. A general formula for the strain energy of an elastic shell, in terms of the displacement vector of the middle surface, was derived by Love (1). Love's theory shows that the strain energy of a shell is a power series function of the thickness, in which only odd exponents occur. The linear term represents the energy due to stretching of the middle surface, and the third-power term represents energy due to bending. Higher-power terms are ordinarily negligible. Love has remarked[3] that his formula for the third-power term is not entirely satisfactory.

Some intuitive considerations will disclose certain properties which should be anticipated in an expression for the energy of bending of an elastic shell. It is evident that displacements out of the original middle surface, due to the tangential displacements u and v, are infinitesimals of higher order than u and v. Consequently, except for second-order effects, a displacement vector, for which w is zero, defines a deformation of the middle surface into itself. Bending of the shell, under this condition, can be attributed to two first-order effects. Any small element of the middle surface, with center at a point P, has its center displaced to a neighboring point Q on the original middle surface, and since the principal curvatures of the middle surface are slightly different at P than at Q, the element experiences changes of curvature, i.e., the element is bent. Obviously, the bending depends, in a finite manner, upon the tangential displacements u and v. It is less apparent that the bending also depends upon derivatives of u and v. This is most easily seen if we consider a particular point P on the middle surface, which remains fixed when the middle surface is deformed into itself. A small element of the middle surface, with center at P, then experiences bending, only as a result of rotations of normal sections of the element about the normal line through P. For example, a surface element of a cylinder is bent, if the element is rotated about its normal line and is simultaneously deformed, so that it remains in the original cylindrical surface. Rotations of normal sections of the middle surface about their normal line are determined solely by the derivatives u_y and v_x, and therefore these derivatives, but not the derivatives u_x and v_y, should occur in the expression for the energy due to bending. This reasoning leads to the further conclusion that the derivatives u_y and v_x should vanish from the bending term if P is a spherical point (i.e., a point where the two principal curvatures have the same sign and magnitude), since, at a spherical point,

---

[1] University of Illinois. Mem. ASME.

[2] Numbers in parentheses refer to the Bibliography at the end of the paper.

Contributed by the Applied Mechanics Division and presented at the Annual Meeting, New York, N. Y., November 28–December 3, 1948, of The American Society of Mechanical Engineers.

Discussion of this paper should be addressed to the Secretary, ASME, 29 West 39th Street, New York, N. Y., and will be accepted until July 11, 1949, for publication at a later date. Discussion received after the closing date will be returned.

Note: Statements and opinions advanced in papers are to be understood as individual expressions of their authors and not those of the Society. Paper No. 48—A-9.

[3] Reference (1), art. 329.

rotations within the middle surface cause no changes of curvature.

The foregoing discussion shows that Love's theory (1) does not correctly express the effects of the tangential displacements upon the energy due to bending. Love's formula for the energy of bending, per unit of area of the middle surface[4] is

$$W_2 = 1/2\ D\ [(\kappa_1 + \kappa_2)^2 - 2(1 - \nu)(\kappa_1\kappa_2 - \tau^2)] \ldots\ldots [A]$$

in which D is the flexural rigidity of the shell, ν is Poisson's ratio, and κ_1, κ_2, and τ are quantities defined by the following equations:[5]

$$\left.\begin{aligned}
\kappa_1 &= \frac{1}{\sqrt{E}}\frac{\partial}{\partial x}\left(\frac{1}{\sqrt{E}}\frac{\partial w}{\partial x} + \frac{u}{r_1}\right) \\
&\quad + \frac{1}{\sqrt{EG}}\frac{\partial \sqrt{E}}{\partial y}\left(\frac{1}{\sqrt{G}}\frac{\partial w}{\partial y} + \frac{v}{r_2}\right) \\
\kappa_2 &= \frac{1}{\sqrt{G}}\frac{\partial}{\partial y}\left(\frac{1}{\sqrt{G}}\frac{\partial w}{\partial y} + \frac{v}{r_2}\right) \\
&\quad + \frac{1}{\sqrt{EG}}\frac{\partial \sqrt{G}}{\partial x}\left(\frac{1}{\sqrt{E}}\frac{\partial w}{\partial x} + \frac{u}{r_1}\right) \\
\tau &= \frac{1}{\sqrt{E}}\frac{\partial}{\partial x}\left(\frac{1}{\sqrt{G}}\frac{\partial w}{\partial y} + \frac{v}{r_2}\right) \\
&\quad - \frac{1}{E\sqrt{G}}\frac{\partial \sqrt{E}}{\partial y}\frac{\partial w}{\partial x} - \frac{1}{\sqrt{E}\,r_1}\frac{\partial v}{\partial x}
\end{aligned}\right\} \ldots [B]$$

Here r_1 and r_2 are the radii of curvature of normal sections of the undeformed middle surface in the directions of the x and y co-ordinate lines. The quantities E and G have been defined by Equation [2].

It is seen that Equation $[B]$ contains the derivatives u_x and v_y, and that these terms consequently enter into the expression, Equation $[A]$, for the energy due to bending. This is seemingly erroneous, since it has been shown, by intuitive reasoning, that the derivatives u_x and v_y do not contribute to the energy of bending. Furthermore, Equation $[B]$ contains the derivative v_x, but not the derivative u_y. Clearly, the derivatives u_y and v_x have similar effects, and an energy formula which contains the one derivative, but not the other, is of doubtful accuracy. Various special cases also discredit Equations $[A]$ and $[B]$. For example, the deformation of a spherical surface into itself cannot entail bending, and therefore W_2 should vanish if Equations $[A]$ and $[B]$ are applied to a spherical shell, and w is set equal to zero. However, this is not the case.

Aside from Love's work, there have been numerous investigations of the general theory of shells. E. Trefftz (2) and E. Reissner (3) have presented new derivations of the general differential equations of shells. W. Chien (4) has made an elaborate and critical study of the subject, which may serve as a gage for appraising special theories. However, recent investigators, unlike earlier writers, have not applied the variational principles of Bernoulli and Hamilton to the general shell problem. The work of Marguerre (5) is an exception to this statement, but his theory is restricted to the case of shells that are almost flat, so that the energy due to bending is approximated, with sufficient accuracy, by the flat-plate formula.

This paper provides an analytical derivation of the strain energy of a thin isotropic elastic shell, in a form suitable for the application of the principle of virtual work and the principle of least action. The theory which is developed is approximate; in fact, the essence of shell theory is a set of approximations which reduces a three-dimensional problem to a two-dimensional problem. The degree of approximation in the theory is of the order that is usual in the theories of beams and plates; accuracy greater than this seemingly leads to severe complications.

[4] Reference (1), Equation [38].

[5] Ibid., art. 326, Equation [26].

Results of the Theory

Since a detailed study of the theory is not essential for an understanding of the results, the mathematical developments are deferred to the Appendix. For the presentation of the results of the theory, some further geometrical considerations are required.

The direction of the normal to the undeformed middle surface is defined by a unit normal vector which is directed toward the side of the surface for which the normal deflection w is defined to be positive. The components of this vector upon the X, Y, Z-axes are respectively denoted by α, β, γ. These components are functions of the parameters x and y which have been defined by Equation [1]. The unit vector (α, β, γ) may be determined readily by the fact that it has the same direction (though not necessarily the same sense or magnitude) as the vector whose components on the X, Y, Z-axes are

$$Y_xZ_y - Z_xY_y,\ Z_xX_y - X_xZ_y,\ X_xY_y - Y_xX_y \ldots\ldots [3]$$

Here, and elsewhere in this paper, the subscripts x and y denote partial derivatives.

The Gaussian theory of surfaces rests upon the following fundamental differential expressions

$$\left.\begin{aligned}
E &= X_x^2 + Y_x^2 + Z_x^2 \\
G &= X_y^2 + Y_y^2 + Z_y^2 \\
e &= \alpha X_{xx} + \beta Y_{xx} + \gamma Z_{xx} \\
g &= \alpha X_{yy} + \beta Y_{yy} + \gamma Z_{yy} \\
\mathcal{E} &= \alpha_x^2 + \beta_x^2 + \gamma_x^2 \\
\mathcal{G} &= \alpha_y^2 + \beta_y^2 + \gamma_y^2
\end{aligned}\right\} \ldots\ldots [4]$$

The general theory of surfaces supplements Equation [4] by three other differential expressions (usually denoted by F, f, and $\mathcal{F}$), but these are zero, due to the fact that the lines of principal curvature have been selected as co-ordinate lines.

Equation [4] defines the quantities E and G, which determine the distance between two neighboring points of the undeformed middle surface (see Equation [2]). The angle $d\theta$ between surface normals erected at the points x, y, and $(x + dx, y + dy)$ is given by the equation

$$d\theta^2 = \mathcal{E}dx^2 + \mathcal{G}dy^2 \ldots\ldots [5]$$

Equations [2] and [5] show the physical significance of the quantities E, G, $\mathcal{E}$, and $\mathcal{G}$. In the present case, the quantities e and g may be interpreted by the fact that the curvatures of normal sections of the undeformed middle surface, in the directions of the x and y co-ordinate lines, are respectively

$$1/r_1 = e/E,\ \ 1/r_2 = g/G \ldots\ldots [6]$$

The normal distance from the undeformed middle surface, measured positively in the direction of the vector (α, β, γ), and negatively in the other direction, is denoted by z. Any point in the undeformed shell may be located by its distance z from the middle surface, and by the co-ordinates x, y, of the foot of the normal dropped from the point to the middle surface. Consequently, the variables (x, y, z) constitute a system of curvilinear space co-ordinates. These co-ordinates are employed exclusively in the subsequent development. It may be shown that the co-ordinates (x, y, z) are orthogonal, i.e., the three co-ordinate lines through any point in space are mutually perpendicular. This is a consequence of the fact that the co-ordinate lines on the undeformed middle surface are lines of principal curvature.

Seven functions A_1, B_1, C_1, A_2, B_2, C_2, C_2' occupy a central position in the theory. These functions are defined as follows

$$\left.\begin{aligned}
A_1 &= \sqrt{E}\,u_x + \frac{E_y v}{2\sqrt{G}} - ew + \frac{1}{2}w_x^2 \\
B_1 &= \sqrt{G}\,v_y + \frac{G_x u}{2\sqrt{E}} - gw + \frac{1}{2}w_y^2 \\
C_1 &= \frac{1}{2}\Big[\sqrt{E}\,u_y + \sqrt{G}\,v_x - \frac{E_y u}{2\sqrt{E}} - \frac{G_x v}{2\sqrt{G}} + w_x w_y\Big]
\end{aligned}\right\} \ldots [7]$$

$$\left.\begin{aligned}
A_2 &= \left(\frac{eE_x}{E} - e_x\right)\frac{u}{\sqrt{E}} + \left(\frac{eE_y}{E} - e_y\right)\frac{v}{\sqrt{G}} \\
&\quad + (\mathcal{E} - 2e^2/E)w + \frac{E_x w_x}{2E} - \frac{E_y w_y}{2G} - w_{xx} + \frac{ew_x^2}{E} \\
B_2 &= \left(\frac{gG_x}{G} - g_x\right)\frac{u}{\sqrt{E}} + \left(\frac{gG_y}{G} - g_y\right)\frac{v}{\sqrt{G}} \\
&\quad + (\mathcal{G} - 2g^2/G)w - \frac{G_x w_x}{2E} + \frac{G_y w_y}{2G} - w_{yy} + \frac{gw_y^2}{G} \\
C_2 &= \left(\frac{e}{E} - \frac{g}{G}\right)\sqrt{G}\,v_x - \left(\frac{e}{E} - \frac{g}{G}\right)\frac{G_x v}{2\sqrt{G}} \\
&\quad + \frac{E_y w_x}{2E} + \frac{G_x w_y}{2G} - w_{xy} + \frac{ew_x w_y}{E} \\
C_2' &= -\left(\frac{e}{E} - \frac{g}{G}\right)\sqrt{E}\,u_y + \left(\frac{e}{E} - \frac{g}{G}\right)\frac{E_y u}{2\sqrt{E}} \\
&\quad + \frac{E_y w_x}{2E} + \frac{G_x w_y}{2G} - w_{xy} + \frac{gw_x w_y}{G}
\end{aligned}\right\} \ldots [8]$$

The following additional notations are employed:

μ = shear modulus of material
ν = Poisson's ratio
h = thickness of shell (not necessarily a constant)

With the preceding notations, the strain energy due to stretching of the middle surface of the shell is

$$U_1 = \frac{\mu}{1-\nu}\int\int\left\{\frac{A_1^2}{E^2} + \frac{B_1^2}{G^2} + 2\nu\frac{A_1 B_1}{EG} + 2(1-\nu)\frac{C_1^2}{EG}\right\}h\sqrt{EG}\,dx\,dy \ldots\ldots [9]$$

The strain energy due to bending of the shell is

$$U_2 = \frac{\mu}{12(1-\nu)}\int\int\left\{\frac{A_2^2}{E^2} + \frac{B_2^2}{G^2} + 2\nu\frac{A_2 B_2}{EG} + 2(1-\nu)\frac{C_2 C_2'}{EG}\right\}h^3\sqrt{EG}\,dx\,dy \ldots\ldots [10]$$

Equation [9] agrees completely with Love's expression for the strain energy due to stretching of the middle surface, with the exception that quadratic terms of Equation [7] were not retained in Love's theory. However, Equation [10] is different from Love's expression for the energy due to bending.

The quadratic terms in Equations [7] and [8] are significant for some problems of flat plates. Flat plates are somewhat exceptional in their behavior, since membrane strains of the middle plane are quadratic functions of the normal deflections. On the other hand, it is intuitively obvious that the membrane strains due to the normal deflections of the middle surface of a nondevelopable curved shell are ordinarily first-order quantities. Consequently, the quadratic terms in Equations [7] and [8] are less important for curved shells than for flat plates, and it is frequently advisable to drop these terms.

Also, in the interest of simplicity, it is usually advisable to discard the terms $(\mathcal{E} - 2e^2/E)\,w$ and $(\mathcal{G} - 2g^2/G)\,w$ in Equation [8]. These terms are of the order of the square of the curvature. Their significance will be shown in the discussion of cylindrical shells.

It is seen that the derivatives u_x and v_y do not enter into the expression Equation [10] for the energy due to bending. In the introduction it was indicated that this is a necessary condition for a correct energy formula. Also, in accord with introductory remarks, the derivatives u_y and v_x vanish from the bending term at any spherical point, since, by Equation [6], the factor $(e/E - g/G)$ is zero at a spherical point.

The strains at any point in a shell consist primarily of the extensions, per unit length, in the x, y, and z-directions, and the reduction of the angle between line elements initially in the x and y-directions. These quantities are represented, in the conventional manner, by ϵ_x, ϵ_y, ϵ_z, and γ_{xy}. In terms of the functions defined by Equations [7] and [8], these strains are given by

$$\left.\begin{aligned}
\epsilon_x &= E^{-1}(A_1 + A_2 z) \\
\epsilon_y &= G^{-1}(B_1 + B_2 z) \\
\epsilon_z &= \frac{-\nu(\epsilon_x + \epsilon_y)}{1-\nu} \\
\gamma_{xy} &= 2(EG)^{-1/2}\sqrt{(C_1 + C_2 z)(C_1 + C_2' z)}
\end{aligned}\right\} \ldots [11]$$

The expressions for ϵ_x, ϵ_y, and γ_{xy} in Equation [11] are purely geometrical, and therefore they are valid even if inelastic action occurs.

Flat Plates

A flat plate is a special type of shell which is characterized by the conditions

$$e = g = \mathcal{E} = \mathcal{G} = 0$$

The quantities E and G depend upon the type of co-ordinate system that is established on the middle plane. No restriction is placed upon the co-ordinates other than that they be orthogonal. If rectangular Cartesian co-ordinates are used, $E = G = 1$. Then Equations [7], [8], [9], and [10] yield the classical equations for the strain energy of a flat plate with large deflections (6a).

In the case of large axially symmetrical deflections of a circular plate, polar co-ordinates (r, θ) are convenient, i.e., $x = r$ and $y = \theta$. Then $E = 1$ and $G = r^2$. Due to symmetry of the deflection pattern

$$u = u(r), \quad v = 0, \quad w = w(r)$$

Hence Equations [7], [8], [9], and [10] yield

$$U_1 = \frac{2\pi\mu}{1-\nu}\int\Big[(u_r + {}^1/_2\,w_r^2)^2 + u^2/r^2 + 2\nu(u/r)(u_r + {}^1/_2 w_r^2)\Big]h\,r\,dr \ldots\ldots [12]$$

$$U_2 = \frac{\pi\mu}{6(1-\nu)}\int\Big[r\,w_{rr}^2 + r^{-1}w_r^2 + 2\nu w_r w_{rr}\Big]h^3\,dr \ldots [13]$$

The Euler differential equations for the integral $U_1 + U_2$ are the same as the classical differential equations for large deflections of a circular plate that is loaded by a constant bending-

moment distribution and a constant radial tension on its periphery (6*b*).

Circular Cylindrical Shells

For this problem, cylindrical co-ordinates (x, θ) are employed, i.e.

$$X = x, \quad Y = a\cos\theta, \quad Z = a\sin\theta$$

Then, by Equation [4]

$$E = 1, G = a^2, e = 0, g = -a, \mathcal{E} = 0, \mathcal{G} = 1$$

in which a is the radius of the middle surface of the shell. Consequently, when third and fourth-power terms are neglected, Equations [7], [8], [9], and [10] yield

$$U_1 = \frac{\mu a}{1-\nu}\int\int\Big[u_x^2 + a^{-2}(v_\theta + w)^2 + 2\nu a^{-1}u_x(v_\theta + w) + {}^1/_2(1-\nu)(v_x + a^{-1}u_\theta)^2\Big]h\,dx\,d\theta \quad \ldots\ldots [14]$$

$$U_2 = \frac{\mu a}{12(1-\nu)}\int\int\Big[w_{xx}^2 + a^{-4}(w_{\theta\theta} + w)^2 + 2\nu a^{-2}w_{xx}(w_{\theta\theta} + w) + 2(1-\nu)\,a^{-2}(w_{x\theta} - v_x)(w_{x\theta} + a^{-1}u_\theta)\Big]h^3\,dx\,d\theta \quad [15]$$

Equations [14] and [15] are general energy expressions for a thin circular cylindrical shell with small deflections. If u and v are set equal to zero, and w is considered to be a function of θ alone, Equation [15] reduces to

$$U_2 = \frac{\mu L}{12(1-\nu)a^3}\int_0^{2\pi}(w_{\theta\theta} + w)^2h^3\,d\theta \quad \ldots\ldots [16]$$

in which L is the length of the cylinder. This is equivalent to the known formula for the energy of bending of a thin ring. In contrast to straight-beam theory, in which the curvature is the second derivative of the deflection with respect to the axial co-ordinate, the change of curvature of a circular ring (7) due to radial deflections is $a^{-2}(w_{\theta\theta} + w)$. However, if the radius of the ring is very large compared to the deflection w, the term w in this expression may be discarded, with small error, and the resulting formula is equivalent to that for a straight beam. An approximation of this type results when the terms $(\mathcal{E} - 2e^2/E)\,w$ and $(\mathcal{G} - 2g^2/G)\,w$ are discarded from Equation [8], for then the finite w term disappears from Equation [15].

In the case of axially symmetrical deformation of a circular cylindrical shell, $u = u(x)$, $v = 0$, and $w = w(x)$. If these simplifications are introduced into Equations [14] and [15], and if the finite w term is neglected in Equation [15], the following differential equation for w may be derived by the principle of virtual work

$$w_{xxxx} + 12h^{-2}a^{-2}(1-\nu^2)\,w = 6(1-\nu)\mu^{-1}h^{-3}P \quad \ldots [17]$$

Here P denotes the external radial load per unit area of the middle surface. Equation [17] is a known equation (6*c*) for symmetrically loaded circular cylindrical shells. It is noteworthy that the present derivation of this equation neglects the terms $(\mathcal{E} - 2e^2/E)\,w$ and $(\mathcal{G} - 2g^2/G)\,w$ of Equation [8]. If this approximation had not been made, the coefficient of w in Equation [17] would have been increased by the term a^{-4}, and the left side of the equation would have been augmented by the term $2\nu a^{-2}w_{xx}$.

Elliptic Cylindrical Shells

In the case of a shell whose middle surface is an elliptical cylinder with major radius a and minor radius b, parameters (x, θ) may be chosen in such a way that

$$X = x, \quad Y = a\cos\theta, \quad Z = b\sin\theta$$

Here, θ is written instead of y. It follows from these equations and Equation [4]

$$E = 1, \quad G = a^2\sin^2\theta + b^2\cos^2\theta$$
$$\alpha = 0, \quad \beta = b\,G^{-1/2}\cos\theta, \quad \gamma = a\,G^{-1/2}\sin\theta$$
$$e = 0, \quad g = -a\,b\,G^{-1/2}$$

Then, if quadratic terms, and the terms $(\mathcal{E} - 2e^2/E)\,w$ and $(\mathcal{G} - 2g^2/G)\,w$ are neglected in Equations [7] and [8], there results

$$\left.\begin{aligned} A_1 &= u_x \\ B_1 &= \sqrt{G}\,v_\theta + \frac{abw}{\sqrt{G}} \\ C_1 &= {}^1/_2(u_\theta + \sqrt{G}\,v_x) \\ A_2 &= -w_{xx} \\ B_2 &= \frac{-3a\,b\,(a^2-b^2)v}{2\,G^2}\sin 2\theta + \frac{(a^2-b^2)\,w_\theta}{2\,G}\sin 2\theta - w_{\theta\theta} \\ C_2 &= a\,b\,v_x/G - w_{x\theta} \\ C_2' &= \frac{-a\,b\,u_\theta}{G\sqrt{G}} - w_{x\theta} \end{aligned}\right\} \quad [18]$$

The general strain-energy expression for a thin elliptic cylindrical shell with small deformations is obtained by substituting Equations [18] in Equations [9] and [10].

If $u = 0$, $w = 0$, $v = v(x)$, and if the thickness h is constant, Equations [9] and [18] yield

$$U_1 = {}^1/_2\mu h\int\int\sqrt{G}\,v_x^2\,dx\,d\theta$$

Since the circumference c of the cylinder is given by the equation

$$c = \int\sqrt{G}\,d\theta$$

it follows

$$U_1 = {}^1/_2\mu h\,c\int v_x^2\,dx$$

This is the elementary expression for the energy of torsion of a cylindrical shell.

In this case there is also some energy of bending, since Equations [10] and [18] yield

$$U_2 = \frac{\mu h^3}{12(1-\nu)}\int\int G^{-2}B_2^2\sqrt{E\,G}\,dx\,d\theta$$

The existence of energy of bending is explained by the fact that an element of an elliptic cylindrical shell experiences changes of curvature when it is displaced circumferentially. It may be verified by Equations [6] and [18] that, if P and Q are two points on a cross section of the undeformed middle surface, which are separated by a distance v, then the difference of maximum normal curvatures at P and at Q is B_2/G. Since $\sqrt{E\,G}\,dx\,d\theta$ represents an element of area of the middle surface, the preceding equation for U_2 is consequently correlated with the elementary formula for the energy of bending of a beam.

Shell in Form of an Ellipsoid of Revolution

If the middle surface of a shell is an ellipsoid of revolution, with axial length $2a$ and equatorial diameter $2b$, it is possible to choose parameters $x = \theta$ and $y = \phi$, such that

$$X = b\sin\theta\cos\phi, \quad Y = b\sin\theta\sin\phi, \quad Z = a\cos\theta$$

Then, by Equation [4]

$$E = a^2 \sin^2\theta + b^2\cos^2\theta,\ G = b^2\sin^2\theta$$

$$\alpha = a\,E^{-1/2}\sin\theta\cos\phi,\ \beta = a\,E^{-1/2}\sin\theta\sin\phi,\ \gamma = b\,E^{-1/2}\cos\theta$$

$$e = -a\,b\,E^{-1/2},\ g = -a\,b\,E^{-1/2}\sin^2\theta$$

Then, neglecting quadratic terms, and the terms $(\mathfrak{E} - 2e^2/E)w$ and $(\mathfrak{G} - 2g^2/G)w$, in Equations [7] and [8]

$$\left.\begin{aligned} A_1 &= \sqrt{E}\,u_\theta + a\,b\,E^{-1/2}w \\ B_1 &= b[v_\phi + b\,E^{-1/2}u\cos\theta + a\,E^{-1/2}w\sin\theta]\sin\theta \\ C_1 &= {}^1/_2[\sqrt{E}\,u_\phi + bv_\theta\sin\theta - b\,v\cos\theta] \end{aligned}\right\} \quad [19]$$

$$\left.\begin{aligned} A_2 &= {}^1/_2\,E^{-1}(a^2 - b^2)[w_\theta - 3\,a\,b\,E^{-1}u]\sin 2\theta - w_{\theta\theta} \\ B_2 &= -{}^1/_2\,E^{-1}b^2[w_\theta + {}^1/_2(a/b)(a^2 - b^2)E^{-1}(1 - \cos 2\theta)\,u]\sin 2\theta - w_{\phi\phi} \\ C_2 &= a\,E^{-1/2}(1 - a\,b\,E^{-1})(v_\theta\sin\theta - v\cos\theta) + w_\phi\cot\theta - w_{\theta\phi} \\ C_2' &= -(a/b)(1 - a\,b\,E^{-1})u_\phi + w_\phi\cot\theta - w_{\theta\phi} \end{aligned}\right\} \quad [20]$$

Substitution of Equations [19] and [20] in Equations [9] and [10] yields the expressions for the energy of stretching and the energy of bending of a thin axially symmetrical ellipsoidal shell with small deflections.

Spherical shells are included in the class of shells whose middle surfaces are ellipsoids of revolution. For a spherical shell, $a = b$, and consequently, $E = a^2$. Equations [19] and [20] then reduce to

$$\left.\begin{aligned} A_1 &= a(u_\theta + w) \\ B_1 &= a[v_\phi + u\cos\theta + w\sin\theta]\sin\theta \\ C_1 &= {}^1/_2\,a[u_\phi + v_\theta\sin\theta - v\cos\theta] \end{aligned}\right\} \quad [21]$$

$$\left.\begin{aligned} A_2 &= -w_{\theta\theta} \\ B_2 &= -w_\theta\sin\theta\cos\theta - w_{\phi\phi} \\ C_2 &= C_2' = w_\phi\cot\theta - w_{\theta\phi} \end{aligned}\right\} \quad [22]$$

Since u and v do not occur in Equation [22], the energy due to bending depends only upon the radial deflection w. This is in agreement with the intuitive observation that small tangential displacements cannot contribute to the bending of a spherical shell.

Acknowledgment

The author is deeply indebted to Dr. C. Lanczos, from whom he received ideas and viewpoints that led to this investigation.

BIBLIOGRAPHY

1 "The Mathematical Theory of Elasticity," by A. E. H. Love, fourth edition, Cambridge University Press, London, England, 1934. (*a*) Equation [4], art. 24, p. 60. (*b*) Equation [17], art. 69, p. 102. See also Equation [24], art. 70, p. 104.

2 "Ableitung der Schalenbiegungsgleichungen mit dem Castiglianoschen Prinzip," by E. Trefftz, *Zeit. für Angewandte Mathematik und Mechanik*, vol. 15, February, 1935, pp. 101–108.

3 "A New Derivation of the Equations for the Deflections of Elastic Shells," by E. Reissner, *American Journal of Mathematics*, vol. 63, 1941, pp. 177–184.

4 "The Intrinsic Theory of Thin Shells and Plates," by W. Z. Chien, *Quarterly of Applied Mathematics*, vol. 1, January, 1944, pp. 297–327; vol. 2, April, 1944, pp. 43–59, and vol. 2, July, 1944, pp. 120–135.

5 "Zur Theorie der gekrümmten Platte grosser Formänderung," by K. Marguerre, Proceedings of the Fifth International Congress of Applied Mechanics, Cambridge, Mass., 1938.

6 "Theory of Plates and Shells," by S. Timoshenko, McGraw-Hill Book Company, Inc., New York, N. Y., 1940. (*a*) Equation [48], p. 50, and Equation [203], p. 345. (*b*) Equation [195], p. 331. (*c*) Equation [227], p. 391.

7 "Theory of Elastic Stability," by S. Timoshenko, McGraw-Hill Book Company, Inc., New York, N. Y., art. 38, 1936, p. 204.

8 "An Introduction to Differential Geometry," by L. P. Eisenhart, Princeton University Press, 1940.

Appendix

Derivation of Equations (8)

Derivations of the general Equations [7], [8], [9], [10], and [11] are given in this Appendix.

Displacement Vector

As a consequence of the orthogonality of the co-ordinates (x, y, z), the metric tensor for these co-ordinates takes the following form

$$g_{ij} = \begin{pmatrix} g_{11} & 0 & 0 \\ 0 & g_{22} & 0 \\ 0 & 0 & 1 \end{pmatrix},\ g^{ij} = \begin{pmatrix} 1/g_{11} & 0 & 0 \\ 0 & 1/g_{22} & 0 \\ 0 & 0 & 1 \end{pmatrix} \quad [23]$$

It may be readily shown, by the methods of differential geometry, that the components of the tensor g_{ij} are expressed in terms of $E, G, e, g, \mathfrak{E}, \mathfrak{G}$ by the equations

$$\left.\begin{aligned} g_{11} &= E - 2\,e\,z + \mathfrak{E}\,z^2 \\ g_{22} &= G - 2\,g\,z + \mathfrak{G}\,z^2 \end{aligned}\right\} \quad [24]$$

Power-series expansions for the reciprocals of g_{11} and g_{22} yield

$$\left.\begin{aligned} g^{11} &= E^{-1} + 2\,e\,E^{-2}z + \ldots. \\ g^{22} &= G^{-1} + 2\,g\,G^{-2}z + \ldots. \end{aligned}\right\} \quad [25]$$

where here, and in the following, power series are cut off after the linear terms.

With Equations [24] and [25], the following expressions for the Christoffel symbols are derived directly

$$\left.\begin{aligned} \left\{\begin{matrix}1\\1\,1\end{matrix}\right\} &= \frac{E_x}{2E} + \left(\frac{eE_x}{E^2} - \frac{e_x}{E}\right)z + \ldots. \\ \left\{\begin{matrix}1\\1\,2\end{matrix}\right\} &= \left\{\begin{matrix}1\\2\,1\end{matrix}\right\} = \frac{E_y}{2E} + \left(\frac{e\,E_y}{E^2} - \frac{e_y}{E}\right)z + \ldots. \\ \left\{\begin{matrix}2\\2\,1\end{matrix}\right\} &= \left\{\begin{matrix}2\\1\,2\end{matrix}\right\} = \frac{G_x}{2G} + \left(\frac{g\,G_x}{G^2} - \frac{g_x}{G}\right)z + \ldots. \\ \left\{\begin{matrix}2\\2\,2\end{matrix}\right\} &= \frac{G_y}{2G} + \left(\frac{g\,G_y}{G^2} - \frac{g_y}{G}\right)z + \ldots. \\ \left\{\begin{matrix}2\\1\,1\end{matrix}\right\} &= -\frac{E_y}{2G} - \left(\frac{g\,E_y}{G^2} - \frac{e_y}{G}\right)z + \ldots. \\ \left\{\begin{matrix}1\\2\,2\end{matrix}\right\} &= -\frac{G_x}{2E} - \left(\frac{e\,G_x}{E^2} - \frac{g_x}{E}\right)z + \ldots. \\ \left\{\begin{matrix}1\\1\,3\end{matrix}\right\} &= \left\{\begin{matrix}1\\3\,1\end{matrix}\right\} = -\frac{e}{E} + \left(\frac{\mathfrak{E}}{E} - \frac{2e^2}{E^2}\right)z + \ldots. \\ \left\{\begin{matrix}2\\2\,3\end{matrix}\right\} &= \left\{\begin{matrix}2\\3\,2\end{matrix}\right\} = -\frac{g}{G} + \left(\frac{\mathfrak{G}}{G} - \frac{2g^2}{G^2}\right)z + \ldots. \\ \left\{\begin{matrix}3\\1\,1\end{matrix}\right\} &= e - \mathfrak{E}\,z \\ \left\{\begin{matrix}3\\2\,2\end{matrix}\right\} &= g - \mathfrak{G}\,z \end{aligned}\right\} \quad [26]$$

All other Christoffel symbols of the second kind are zero.

The covariant displacement vector is denoted by u_i. The

components of this vector are functions of (x, y, z). The significance of the vector u_i is that the scalar component of displacement in the direction of any unit vector ξ^i is $u_i\,\xi^i$.

The general strain tensor is

$$\epsilon_{ij} = {}^1/_2(u_{i,j} + u_{j,i} + g^{mn}\,u_{m,i}\,u_{n,j}) \ldots\ldots\ldots [27]$$

Here, commas signify covariant derivatives. Equation [27] is taken from the general theory of elasticity. This equation has been derived, for the case of rectangular Cartesian co-ordinates, by Love (1*a*). Since Equation [27] is a tensor equation which reduces to the proper form for rectangular Cartesian co-ordinates, it is valid for arbitrary co-ordinates. When the quadratic terms are retained in Equation [27], the magnitudes of the displacements and the rotations are unrestricted, provided that the strains are small. The significance of the strain tensor is that the extension, per unit length, of a line element with the initial direction of any unit vector ξ^i is $\epsilon_{ij}\,\xi^i\,\xi^j$. Also, it may be shown that the angular decrement (shearing strain) between two line elements with initial directions of two perpendicular unit vectors ξ^i and η^i is $2\,\epsilon_{ij}\,\xi^i\,\eta^j$.

It is assumed, as in the theories of beams and plates, that the shearing stress upon any plane element parallel to the middle surface of the shell is negligible. Since the shearing stress is proportional to the shearing strain, this condition is expressed by the equations

$$\epsilon_{13} = \epsilon_{23} = 0 \ldots\ldots\ldots\ldots\ldots [28]$$

Equations [27] and [28] yield

$$\left.\begin{aligned} u_{1,3}\,(1 + g^{11}\,u_{1,1}) + u_{3,1}\,(1 + u_{3,3}) + g^{22}\,u_{2,1}\,u_{2,3} &= 0 \\ u_{2,3}\,(1 + g^{22}\,u_{2,2}) + u_{3,2}\,(1 + u_{3,3}) + g^{11}\,u_{1,2}\,u_{1,3} &= 0 \end{aligned}\right\} \ldots [29]$$

The quadratic terms in Equation [29] are of the type which are neglected in plate theory, and it is assumed that they are negligible in the present case. Then Equation [29] become

$$\left.\begin{aligned} u_{1,3} + u_{3,1} &= 0 \\ u_{2,3} + u_{3,2} &= 0 \end{aligned}\right\} \ldots\ldots\ldots\ldots\ldots [30]$$

Equations [26] and [30] yield

$$\left.\begin{aligned} \partial u_1/\partial z + \partial u_3/\partial x + 2u_1\left[\frac{e}{E} - \left(\frac{\mathcal{E}}{E} - \frac{2\,e^2}{E^2}\right)z\right] &= 0 \\ \partial u_2/\partial z + \partial u_3/\partial y + 2u_2\left[\frac{g}{G} - \left(\frac{\mathcal{G}}{G} - \frac{2\,g^2}{G^2}\right)z\right] &= 0 \end{aligned}\right\} \ldots [31]$$

Equation [31] may be solved by power series in z. To this end, it is convenient to set

$$\left.\begin{aligned} u_1\big|_{z=0} &= u\sqrt{E} \\ u_2\big|_{z=0} &= v\sqrt{G} \\ u_3\big|_{z=0} &= w \end{aligned}\right\} \ldots\ldots\ldots\ldots\ldots [32]$$

Then, in view of the physical significance of the vector u_i, the variables (u, v, w) are the rectangular components of the displacement of a point of the middle surface upon the orthogonal triad of straight axes which are respectively tangent to the x, y, and z co-ordinate lines at the given point. In view of Equations [32], the vector u_i is represented by the following power series

$$\left.\begin{aligned} u_1 &= u\sqrt{E} + pz + \ldots. \\ u_2 &= v\sqrt{G} + qz + \ldots. \\ u_3 &= w + rz + \ldots. \end{aligned}\right\} \ldots\ldots\ldots\ldots [33]$$

Substitution of Equations [33] in Equations [31] gives directly

$$\left.\begin{aligned} u_1 &= u\sqrt{E} - (2eE^{-1/2}u + w_x)z + \ldots. \\ u_2 &= v\sqrt{G} - (2gG^{-1/2}v + w_y)z + \ldots. \end{aligned}\right\} \ldots\ldots [34]$$

Covariant differentiation now yields, with the aid of Equations [26]

$$\left.\begin{aligned} u_{1,1} &= \sqrt{E}\,u_x + \frac{E_y v}{2\sqrt{G}} - ew - \left\{\frac{2eu_x}{\sqrt{E}} + \left(e_x - \frac{eE_x}{E}\right)\frac{u}{\sqrt{E}} + \frac{e_y v}{\sqrt{G}} - \mathcal{E}\,w - \frac{E_x w_x}{2E} + \frac{E_y w_y}{2G} + w_{xx}\right\} z + \ldots. \\ u_{1,2} &= \sqrt{E}\,u_y - \frac{G_x v}{2\sqrt{G}} - \left\{\frac{2eu_y}{\sqrt{E}} + \left(e_y - \frac{eE_y}{E}\right)\frac{u}{\sqrt{E}} - \frac{g_x v}{\sqrt{G}} - \frac{E_y w_x}{2E} - \frac{G_x w_y}{2G} + w_{xy}\right\} z + \ldots. \\ u_{2,1} &= \sqrt{G}\,v_x - \frac{E_y u}{2\sqrt{E}} - \left\{\frac{2gv_x}{\sqrt{G}} + \left(g_x - \frac{gG_x}{G}\right)\frac{v}{\sqrt{G}} - \frac{e_y u}{\sqrt{E}} - \frac{E_y w_x}{2E} - \frac{G_x w_y}{2G} + w_{xy}\right\} z + \ldots \\ u_{2,2} &= \sqrt{G}\,v_y + \frac{G_x u}{2\sqrt{E}} - gw - \left\{\frac{2gv_y}{\sqrt{G}} + \left(g_y - \frac{gG_y}{G}\right)\frac{v}{\sqrt{G}} + \frac{g_x u}{\sqrt{E}} - \mathcal{G}\,w + \frac{G_x w_x}{2E} - \frac{G_y w_y}{2G} + w_{yy}\right\} z + \ldots. \end{aligned}\right\} \ldots [35]$$

Strain Tensor

It is assumed that quadratic terms involving the derivatives of the tangential displacements u and v may be discarded from the strain tensor. This approximation has been previously used to obtain Equations [30]. Accordingly, Equation [27] is approximated by

$$\left.\begin{aligned} \epsilon_{11} &= u_{1,1} + \frac{1}{2}\,w_x{}^2 \\ \epsilon_{22} &= u_{2,2} + \frac{1}{2}\,w_y{}^2 \\ \epsilon_{12} = \epsilon_{21} &= \frac{1}{2}\,(u_{1,2} + u_{2,1}) + \frac{1}{2}\,w_x w_y \end{aligned}\right\} \ldots\ldots [36]$$

These components will be represented by the following power series

$$\left.\begin{aligned} \epsilon_{11} &= A_1 + Pz + \ldots. \\ \epsilon_{22} &= B_1 + Qz + \ldots. \\ \epsilon_{12} = \epsilon_{21} &= C_1 + Rz + \ldots. \end{aligned}\right\} \ldots\ldots\ldots [37]$$

When Equations [35] are substituted in Equations [36], and the result is compared with Equation [37], it is seen that A_1, B_1, and C_1 are given by Equations [7], and that the coefficients P, Q, and R are given by

$$P = -\frac{2eu_x}{\sqrt{E}} + \left(\frac{eE_x}{E} - e_x\right)\frac{u}{\sqrt{E}} - \frac{e_y v}{\sqrt{G}} + \mathcal{E}w + \frac{E_x w_x}{2E} - \frac{E_y w_y}{2G} - w_{xx}$$

$$Q = -\frac{2gv_y}{\sqrt{G}} - \frac{g_x u}{\sqrt{E}} + \left(\frac{gG_y}{G} - g_y\right)\frac{v}{\sqrt{G}} + \mathfrak{G}w - \frac{G_x w_x}{2E} + \frac{G_y w_y}{2G} - w_{yy}$$

$$R = -\frac{eu_y}{\sqrt{E}} - \frac{gv_x}{\sqrt{G}} + \frac{eE_y u}{2E\sqrt{E}} + \frac{gG_x v}{2G\sqrt{G}} + \frac{E_y w_x}{2E} + \frac{G_x w_y}{2G} - w_{xy} \quad \ldots\ldots\ldots [38]$$

Equations [25] and [37] yield the following mixed form for the strain tensor

$$\left.\begin{aligned} \epsilon_1{}^1 &= E^{-1}A_1 + E^{-1}(2eE^{-1}A_1 + P)z + \ldots. \\ \epsilon_2{}^2 &= G^{-1}B_1 + G^{-1}(2gG^{-1}B_1 + Q)z + \ldots. \\ \epsilon_2{}^1 &= E^{-1}C_1 + E^{-1}(2eE^{-1}C_1 + R)z + \ldots. \\ \epsilon_1{}^2 &= G^{-1}C_1 + G^{-1}(2gG^{-1}C_1 + R)z + \ldots. \end{aligned}\right\} \ldots [39]$$

These equations are of the form

$$\left.\begin{aligned} \epsilon_1{}^1 &= E^{-1}(A_1 + A_2 z + \ldots.) \\ \epsilon_2{}^2 &= G^{-1}(B_1 + B_2 z + \ldots.) \\ \epsilon_2{}^1 &= E^{-1}(C_1 + C_2 z + \ldots.) \\ \epsilon_1{}^2 &= G^{-1}(C_1 + C_2' z + \ldots.) \end{aligned}\right\} \ldots\ldots\ldots [40]$$

When Equations [38] and [7] are substituted in Equations [39] and the results are compared with Equations [40], it is seen that A_2, B_2, C_2, and C_2' are given by Equations [8].

Equations [7], [8], and [40] determine completely the mixed form of the strain tensor. The extensions, per unit length, (physical strains), in the x and y-directions are

$$\epsilon_x = \epsilon_1{}^1, \quad \epsilon_y = \epsilon_2{}^2 \ldots\ldots\ldots\ldots\ldots\ldots [41]$$

This is seen from the fact that the extension, per unit length, in any direction ξ^i is $\epsilon_{ij}\xi^i\xi^j$. If the direction ξ^i is tangent to the x co-ordinate line

$$\xi^1 = 1/\sqrt{g_{11}} = \sqrt{g^{11}}, \quad \xi^2 = \xi^3 = 0$$

Then

$$\epsilon_x = \epsilon_{11}\, g^{11} = \epsilon_1{}^1$$

A similar derivation applies for $\epsilon_2{}^2$.

It is assumed, as in the theories of plates and beams, that the normal stress on any surface, z = const, may be neglected. It then follows from the stress-strain relations of classical elasticity

$$\epsilon_z = -\frac{\nu(\epsilon_x + \epsilon_y)}{1 - \nu}$$

in which ϵ_z is the extension, per unit length, in the z-direction, and ν is Poisson's ratio. Consequently, by Equations [41]

$$\epsilon_3{}^3 = \frac{-\nu(\epsilon_1{}^1 + \epsilon_2{}^2)}{1 - \nu} \ldots\ldots\ldots\ldots\ldots [42]$$

The angular decrement between the x and y-directions (physical shearing strain) is

$$\gamma_{xy} = 2\sqrt{\epsilon_2{}^1\epsilon_1{}^2} \ldots\ldots\ldots\ldots\ldots [43]$$

For, if ξ^i and η^j are unit vectors, respectively, in the x and y-directions

$$\gamma_{xy} = 2\epsilon_{ij}\xi^i\eta^j = \frac{2\epsilon_{12}}{\sqrt{g_{11}g_{22}}} = 2\sqrt{g^{11}g^{22}}\,\epsilon_{12}$$

$$= 2\sqrt{g^{11}\epsilon_{12}}\sqrt{g^{22}\epsilon_{12}} = 2\sqrt{\epsilon_2{}^1\epsilon_1{}^2}$$

It follows from Equations [40] and [43]

$$\gamma_{xy} = 2\,(EG)^{-1/2}\sqrt{(C_1 + C_2 z)(C_1 + C_2' z)}$$

This relation has been given in Equation [11].

Strain Energy

The classical theory of elasticity provides the following invariant formula (1b) for the strain energy per unit volume of the material

$$V = \mu(\epsilon_i{}^k\epsilon_k{}^i + \frac{\nu}{1 - 2\nu}\epsilon_k{}^k\epsilon_i{}^i) \ldots\ldots\ldots\ldots [44]$$

Here μ represents the shear modulus, and ν is Poisson's ratio.

By Equation [28] $\epsilon_3{}^1 = \epsilon_3{}^2 = 0$. Hence with the aid of Equation [42], Equation [44] reduces to

$$V = \frac{\mu}{1 - \nu}\left[\epsilon_1{}^1\epsilon_1{}^1 + \epsilon_2{}^2\epsilon_2{}^2 + 2\nu\,\epsilon_1{}^1\epsilon_2{}^2 + 2(1 - \nu)\epsilon_2{}^1\epsilon_1{}^2\right]. \quad [45]$$

Substitution of Equations [40] in Equation [45] yields

$$V = \frac{\mu}{1 - \nu}\left[\frac{A_1{}^2}{E^2} + \frac{B_1{}^2}{G^2} + 2\nu\frac{A_1B_1}{EG} + 2(1 - \nu)\frac{C_1{}^2}{EG}\right] + \frac{\mu}{1 - \nu}\left[\frac{A_2{}^2}{E^2} + \frac{B_2{}^2}{G^2} + 2\nu\frac{A_2B_2}{EG} + 2(1 - \nu)\frac{C_2C_2'}{EG}\right]z^2 + \text{a linear term in } z. \ldots\ldots [46]$$

The linear term in z is irrelevant, since it cancels out of the subsequent equations. The quadratic term in z is important, for it accounts for the energy of bending. This term is approximate, since it is derived only from the products of the linear z-terms in the strain tensor. Quadratic z-terms in the strain tensor, which have been neglected for the sake of simplicity, would also give a small contribution to the quadratic z-term in Equation [46]. However, the nonlinearity of the strain distribution throughout the thickness of the shell will have a negligible effect upon the strain energy, if the radii of curvature are large compared to the thickness.

The element of area of the middle surface of the shell is $\sqrt{EG}\,dx\,dy$. Hence the total strain energy of the shell is approximately

$$U = \int\int \sqrt{EG}\,dx\,dy \int_{-h/2}^{h/2} V\,dz \ldots\ldots [47]$$

in which h is the thickness of the shell. If Equation [46] is substituted in Equation [47], integration with respect to z may be carried out, and the linear term in z disappears. In view of the form of Equation [46], the strain energy splits into a sum of two terms, U_1 and U_2, in which U_1 contains h to the first power, and U_2 contains h to the third power. When integration with respect to z is performed, Equations [9] and [10] are obtained.

The Use of the Centrifugal Pendulum Absorber for the Reduction of Linear Vibration

By F. E. REED,[1] CAMBRIDGE, MASS.

A machine, consisting of rotating tuned pendulums free to oscillate in planes containing the axis of rotation, is proposed as a dynamic absorber for linear vibrations. The influences of size, exactness of tuning, and damping are investigated and curves for evaluating the effectiveness of the machine are shown.

Introduction

THE use of centrifugal pendulum vibration absorbers for the elimination of torsional vibrations in internal-combustion engines has been very successful.[2] Not only have they been useful in the reduction of torsional vibration stresses in engines of the conventional type but their use has permitted the design of gear systems which could not be expected to be reliable were the torsional vibrations not reduced. These benefits have been obtained with a relatively simple attachment which does not add appreciably to the cost and weight of the power plant.

Since the torsional pendulum absorbers have proved so successful, the question naturally arises as to whether the same principle could not be applied to the reduction of linear vibrations. Since most objectionable linear vibrations are set up by some machine, it might be possible to drive some type of pendulum absorber by the machine which would by the action neutralize the forces which the machine generates.

It is the purpose of this study to investigate the characteristics and the effectiveness of such an absorber.

Development of Characteristics of Linear Pendulum Absorber

The device proposed is expected to absorb vibrations acting in the direction of the axis of rotation. It is mounted on some structure which is subjected to a harmonic force generated by a machine which will allow the absorber to be rotated at a speed which bears an exact predetermined ratio to the frequency of the force. This study will show that the absorber will behave as a large mass which, if rigidly attached to the point of action of the force, will by its movement absorb a large portion of the exciting force; or, if located at a point remote from the exciting force, will tend to reduce the vibratory motion at the point of attachment to zero.

The absorber consists of two or more pendulums, each free to oscillate in a plane containing the axis of rotation. The pendulums are identical and are so disposed about the axis that the centrifugal forces will cancel. The shaft with its attached pendulums rotates at some multiple n of the frequency of the vibrating force.

In order to analyze the behavior of the absorber it is necessary to define quantities which characterize the elements of the system. A diagram of this is shown in Fig. 1.

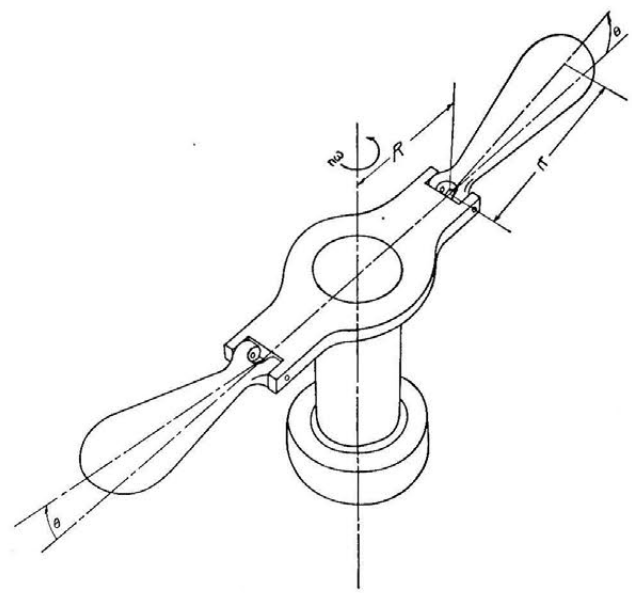

Fig. 1 Elements of the Absorber System

Let each pendulum be characterized by the following:

m = mass of pendulum
r = distance of center of gravity of pendulum from pivot axis
I_1 = moment of inertia about axis 1 parallel to pivot axis through center of gravity
I_2 = moment of inertia about axis 2 which passes through center of gravity and pivot axis and is perpendicular to pivot axis
I_3 = moment of inertia about axis 3 which is perpendicular to axes 1 and 2
R = distance of pivot axis of pendulum from axis of rotation

Choose a cylindrical co-ordinate system, letting x be the motion of the center of gravity of the pendulum in the direction of the axis of rotation, taking the positive direction downward, and the base $x = 0$ corresponding to the position of the pivot axis when the time $t = 0$. Let θ be the angular motion of the pendulum measured from the plane of rotation of the pivot axis, with the positive direction giving a displacement of the center of gravity

---

[1] Assistant Professor of Mechanical Engineering, Massachusetts Institute of Technology. Mem. ASME.

[2] "Mechanical Vibrations," by I. D. Den Hartog, McGraw-Hill Book Company, Inc., New York, N. Y., third edition, 1947, pp. 272–280.

Contributed by the Applied Mechanics Division and presented at the Annual Meeting, New York, N. Y., November 28–December 3, 1948, of The American Society of Mechanical Engineers.

Discussion of this paper should be addressed to the Secretary, ASME, 29 West 39th Street, New York, N. Y., and will be accepted until July 11, 1949, for publication at a later date. Discussion received after the closing date will be returned.

Note: Statements and opinions advanced in papers are to be understood as individual expressions of their authors and not those of the Society. Paper No. 48—A-25.

opposite to x. Equation $x_1 = x_0 \sin \omega t$ represents the motion of the plane of the pivot axes.

Fig. 2 illustrates the co-ordinate systems. The co-ordinates of the center of gravity of the pendulum are as follows

$$x = x_1 - r \sin \theta \quad \ldots\ldots\ldots\ldots\ldots\ldots [1]$$

$$\rho = R + r \cos \theta \quad \ldots\ldots\ldots\ldots\ldots\ldots [2]$$

$$\varphi = n\omega t \quad \ldots\ldots\ldots\ldots\ldots\ldots [3]$$

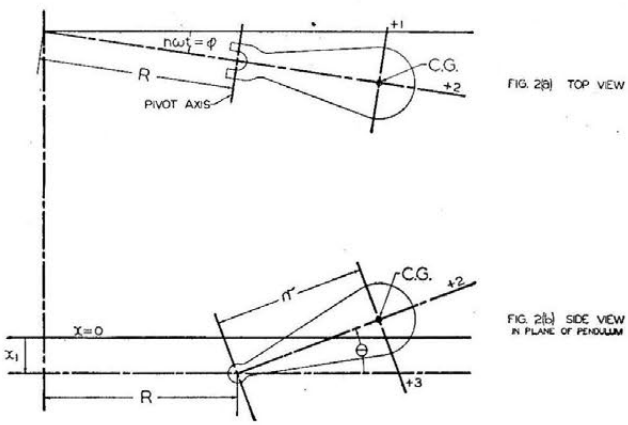

FIG. 2 CO-ORDINATE SYSTEM
(*a*, Top view. *b*, Side view in plane of pendulum.)

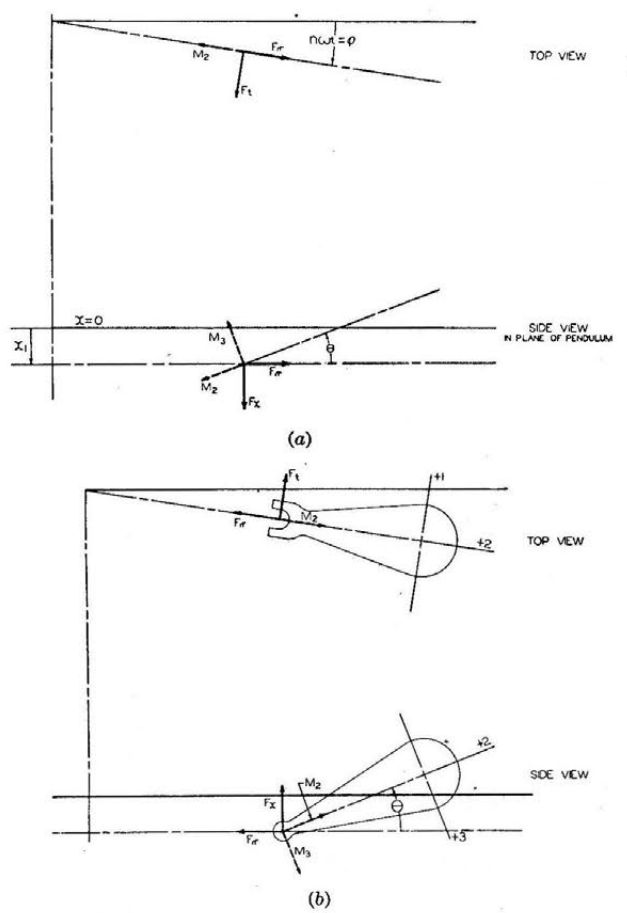

FIG. 3 REACTIONS AT PENDULUM PIVOT
(*a*, Forces and torques on pendulum carrier. *b*, Forces and torques on pendulum.)

Let a set of pairs of forces and moments represent the reactions at the pendulum pivot; F_x the forces in the x-direction, F_r the radial forces, F_t the tangential forces, and M_2 and M_3 the torque reactions. These reactions are shown in Fig. 3.

Applying dynamical laws to the pendulum gives the following equations for translation

$$-F_x = m\,(\ddot{x}_1 + r \sin \theta\dot{\theta}^2 - r \cos \theta\ddot{\theta}) \quad \ldots\ldots [4]$$

$$-F_r = m[-r \sin \theta\ddot{\theta} - r \cos \theta\dot{\theta}^2 - (R + r \cos \theta)n^2\omega^2] \quad \ldots [5]$$

$$-F_t = m(-2r \sin \theta\dot{\theta}n\omega) \quad \ldots\ldots\ldots\ldots [6]$$

The following are equations for rotation

$$-I_1\ddot{\theta} - (I_3 - I_2)n^2\omega^2 \sin \theta \cos \theta = F_x r \cos \theta + F_r r \sin \theta \ldots [7]$$

$$-I_2\, n\omega\dot{\theta} \cos \theta - (I_1 - I_3)n\omega\dot{\theta} \cos \theta = M_2 \quad \ldots\ldots [8]$$

$$-I_3\, n\omega\, \dot{\theta} \sin \theta + (I_2 - I_1)n\omega\dot{\theta} \sin \theta = M_3 + F_t r \quad \ldots\ldots [9]$$

Equations [6], [8], [9] would be used for determining the bearing reactions and would not be of particular interest in this study. Eliminating F_x and F_r from Equation [7] by use of Equations [4] and [5] results in the equation

$$(I_1 + mr^2)\ddot{\theta} + (I_3 - I_2)n^2\omega^2 \sin \theta \cos \theta + mr^2\left(\frac{R}{r} + \cos \theta\right) n^2\omega^2 \sin \theta = mr\ddot{x}_1 \cos \theta \ldots [10]$$

This equation is difficult to integrate as it stands. By restricting θ to small values (i.e., $\theta < 10$ deg), the equation simplifies to

$$\left(\frac{I_1}{mr^2} + 1\right)\ddot{\theta} + n^2\omega^2\left[\frac{I_3 - I_2}{mr^2} + \frac{R}{r} + 1\right]\theta = \frac{\ddot{x}_1}{r} \ldots [11]$$

Since x_1 has a circular frequency of ω, the solution of this equation is

$$x_1 = r\left[\frac{I_1}{mr^2} + 1 - n^2\left(\frac{I_3 - I_2}{mr^2} + \frac{R}{r} + 1\right)\right]\theta \ldots [12]$$

If now the element in the brackets be made equal to zero, then x_1 should be zero for any finite value of θ, and the device under the conditions assumed will prevent any longitudinal movement of the rotating axis.

There is a definite relationship between θ and F_x, the force acting on the absorber, which may be determined from Equation [4] which, since $x_1 = 0$, may for small angles be written as

$$F_x = mr\ddot{\theta} \quad \ldots\ldots\ldots\ldots\ldots\ldots [13]$$

or

$$\theta = \theta_{\max} \sin \omega t$$

It is proper to say that the force exerted by a perfectly tuned absorber in the absence of damping is

$$F_{\max} = mr\omega^2\, \theta_{\max} \quad \ldots\ldots\ldots\ldots\ldots\ldots [14]$$

acting in a direction opposite to x_1.

EFFECTS OF DAMPING AND OF INEXACT TUNING ON ABSORBER

The practical absorber could not be perfectly tuned and would contain some damping. The practical effects of each should be considered.

Damping may be considered to exist as a torque proportional to the angular velocity of the pendulum. Considering this proportionality factor to be c, Equation [7] would be modified to include the damping torque

$$-I_1\ddot{\theta} - (I_3 - I_2)n^2\omega^2 \sin \theta \cos \theta = F\, r \cos \theta + F_r r \sin \theta + c\dot{\theta} \quad \ldots\ldots\ldots\ldots [15]$$

Substituting the values of F_x and F_r and restricting the motion to small angles, this develops to

$$\left(\frac{I_1}{mr^2}+1\right)\ddot{\theta}+\frac{c\dot{\theta}}{mr^2}+n^2\omega^2\left[\frac{I_3-I_2}{mr^2}+\frac{R}{r}+1\right]\theta=\frac{\ddot{x}_1}{r} \quad [16]$$

By Equation [4], the force exerted by the absorber, being equal and opposite to that exerted on it, is in the direction of minus x and is equal to

$$F = m(\ddot{x}_1 + r\sin\theta\dot{\theta}^2 - r\cos\theta\ddot{\theta})$$

or for small angles

$$F = m(\ddot{x}_1 - r\ddot{\theta}) \quad [17]$$

To ascertain the value of F it is necessary to find θ in terms of x_1 by solving Equation [16]. To simplify the development consider two nondimensional quantities

$$T = \text{a tuning function} = -\left(\frac{I_1}{mr^2}+1\right)+n^2\left[\frac{I_3-I_2}{mr^2}+\frac{R}{r}+1\right] \quad [18]$$

$$C = \text{a damping function} = \frac{c}{mr^2\omega} \quad [19]$$

Letting

$$\theta = \theta_0\sin(\omega t-\varphi) \quad \text{and} \quad x_1 = x_0\sin\omega t$$

Equation [16] becomes

$$\theta_0\sqrt{T^2+C^2} = -\frac{x_0}{r} \qquad \tan\varphi = \frac{C}{T}$$

$$F = -m\omega^2\left[x_0\sin\omega t+\frac{x_0}{\sqrt{T^2+C^2}}\sin(\omega t-\varphi)\right]$$

It is apparent from this that the neutralizing force is not in phase with the displacement when there is damping present. Therefore it is necessary to consider the response of a more complete system to the stimulus of an imposed force when it is fitted with the absorber.

Consider therefore a mass M, connected to a fixed point by a spring of stiffness K, which is fitted with an absorber of the characteristics considered and is subjected to a harmonic force $P_0\sin(\omega t+\gamma)$ of such amplitude and phase that the resulting motion of the mass is $x_0\sin\omega t$, as shown in Fig. 4.

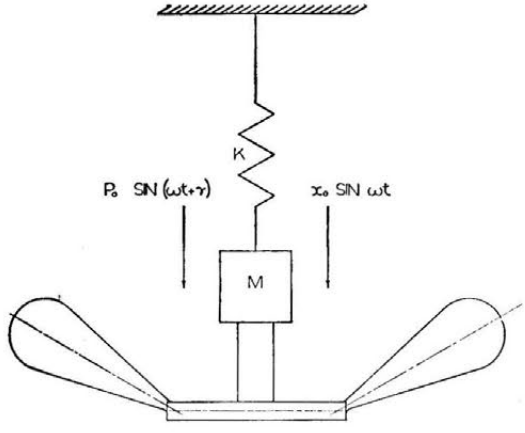

FIG. 4

The equation of motion of the mass is

$$P_0\sin(\omega t+\gamma) - F - kx = m\ddot{x} \quad [20]$$

Upon substitution of the force from the absorber and the amplitude of motion this becomes

$$P_0\sin(\omega t+\gamma)+m\omega^2\left[x_0\sin\omega t+\frac{x_0}{\sqrt{T^2+C^2}}\sin(\omega t-\varphi)\right]-kx_0\sin\omega t = -M\omega^2x_0\sin\omega t \quad [21]$$

When this equation is solved for x_0, the following value is obtained

$$x_0 = \frac{P_0}{\sqrt{\left[(M+m)\omega^2-k+\frac{mT\omega^2}{T^2+C^2}\right]^2+\left[\frac{mC\omega^2}{T^2+C^2}\right]^2}} \quad [22]$$

To simplify the considerations of this equation, introduce two more nondimensional quantities

$$\beta = \text{frequency ratio} = \frac{\omega}{\omega_n} = \omega\sqrt{\frac{M+m}{k}} \quad [23]$$

$$S = \text{a size function} = \frac{m}{M+m} \quad [24]$$

Then

$$x_0 = \frac{P_0}{(M+m)\omega^2}\cdot\frac{1}{\sqrt{\left[1-\frac{1}{\beta^2}+\frac{ST}{T^2+C^2}\right]^2+\left[\frac{SC}{T^2+C^2}\right]^2}} \quad [25]$$

The maximum value of x_0 will occur at a value of β such that the first bracket in the denominator is equal to zero

$$\beta = \sqrt{\frac{T^2+C^2}{T^2+C^2+ST}} \quad [26]$$

and will have an amplitude

$$x_0 = \frac{P_0}{(M+m)\omega^2}\cdot\frac{T^2+C^2}{SC} = \frac{P_0(T^2+C^2)}{m\omega^2C} \quad [27]$$

This indicates that in the absence of any other damping, some damping is necessary in the absorber to secure a finite amplitude in the mass. However, if the tuning is perfect ($T=0$), this resonance would occur at $\beta = 0$; if not perfect, the resonance will occur at a value of

$$\beta = \sqrt{\frac{T}{T+S}}$$

The minimum value of x_0 at a given value of T will be secured where $C_{opt} = T$ at which point

$$x_0 = \frac{2P_0}{m\omega^2}C_{opt} = \frac{2P_0}{m\omega^2}T \quad [28]$$

$$\beta = \sqrt{\frac{T}{T+S/2}} \quad [29]$$

The significance of these equations is most easily shown by the plots in Figs. 5, 6, 7, 8, 9, and 10.

It is necessary in designing an absorber of this type to have some concept of the magnitudes of the tuning and damping functions which it is possible to obtain. Consider first the tuning function

$$T = -\left(\frac{I_1}{mr^2}+1\right)+n^2\left[\frac{I_3-I_2}{mr^2}+\frac{R}{r}+1\right]$$

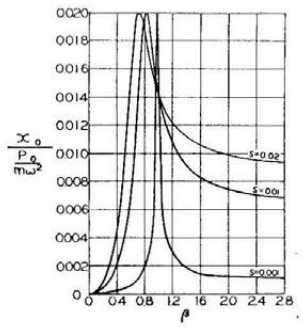

FIG. 5 VARIATION OF AMPLITUDE OF VIBRATION WITH FREQUENCY AND SIZE
$T = 0.01$
$C = 0.01$

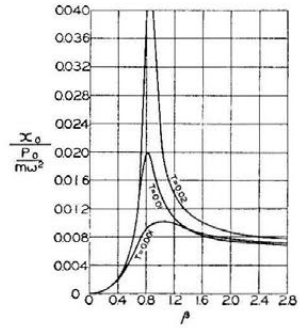

FIG. 6 VARIATION OF AMPLITUDE OF VIBRATION WITH FREQUENCY AND TUNING
$S = 0.01$
$C = 0.01$

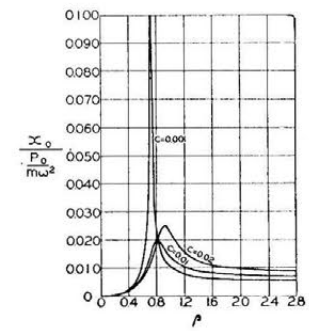

FIG. 7 VARIATION OF AMPLITUDE OF VIBRATION WITH FREQUENCY AND DAMPING
$S = 0.01$
$T = 0.01$

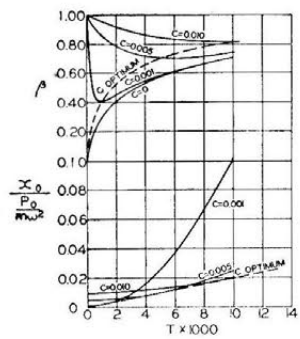

FIG. 8 VARIATION IN MAXIMUM AMPLITUDE WITH TUNING AND DAMPING FUNCTIONS WITH THE CORRESPONDING FREQUENCIES FOR
$S = 0.01$

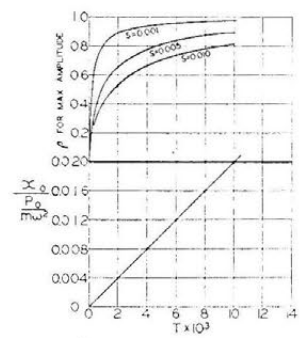

FIG. 9 VARIATION IN MAXIMUM AMPLITUDE WITH TUNING FUNCTION FOR AN ABSORBER HAVING OPTIMUM DAMPING WITH THE CORRESPONDING FREQUENCIES AS A FUNCTION OF SIZE RATIO

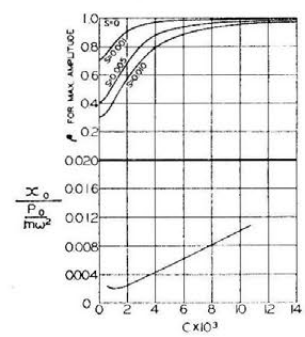

FIG. 10 VARIATION IN MAXIMUM AMPLITUDE WITH DAMPING FUNCTION FOR AN ABSORBER HAVING CONSTANT TUNING $T = 0.001$ AND THE CORRESPONDING FREQUENCIES AS A FUNCTION OF THE SIZE RATIO

Of the quantities involved in this function, n is exact as set by the speed ratio between the absorber and the source of the disturbance; m and r may be obtained by careful weighing of the completed pendulum; I_1 may be obtained by finding the period of the pendulum in a gravity field; I_2 and I_3 in the actual application would be approximately equal and could be calculated with reasonable accuracy; R is a measured value which should also be obtainable with a high degree of accuracy. Furthermore, it should be possible to tune the pendulum to a specific application by the addition or subtraction of small weights. A pendulum carried by antifriction bearings, if once accurately tuned, should remain in tune indefinitely.

The same degree of control is not available for the damping constant

$$C = \frac{c}{mr^2\omega} = \frac{\text{Friction torque}}{mr^2\omega^2}$$

By loading a facsimile of the pivot bearing with loads corresponding to the centrifugal force of the pendulum and rotating the bearing at different speeds, it should be possible to obtain an accurate value of c and hence of C.

Another estimate of the value of C can be obtained by a comparison with the pendulum acting in a gravity field. In this case it can be shown that

$$C = \frac{\rho^2}{r^2\pi} \log_e \frac{\theta_n}{\theta_{n+1}}$$

where ρ is the radius of gyration about the pivot; r is the distance of the center of gravity from the pivot, as before; θ_n is the amplitude of vibration at the nth swing.

Since ρ is probably not very different from r, it will be seen that if the amplitude of vibration is reduced to $^1/_2$ of its original amplitude in 50 cycles, C would be approximately 0.0044; if 100 cycles were required to cut the amplitude in half, C would be approximately 0.0022. A simple experiment will show that a relatively light pendulum fitted with ball bearings will oscillate 50 times for a 50 per cent reduction, and that the number of cycles will increase appreciably as the size is increased. Damping functions C of from 0.0050 to 0.0005 seem quite within the region of probability, and experience may indicate that lower values are possible.

APPLICATIONS

If an absorber of this type is to have any application, some estimates of the size and complexity of the mechanism, as applied to actual applications, should be made. In general, the details of the absorber will be set by considerations of particular design application, but it is possible to outline briefly what might be determined by the first considerations of particular applications. The applications are applied to a ship, since the ship vibrations excited by the propeller are difficult to reduce.

Case I. A large passenger ship is subjected to an undesirable vibration excited by the propellers. Let it be assumed that each of the two propellers puts a harmonic force into the ship of

100,000 lb, having a frequency of 500 vibrations per min., and the amplitude over the propellers due to the action of each is 0.10 in. (or a total in-phase amplitude over the propellers due to the action of both is 0.20 in.) when at a natural frequency of the hull. It is desired to reduce this vibration to $^1/_4$ of its present value by the use of a pendulum absorber located over each propeller.

Let it be assumed that a damping constant of $C = 0.001$ can be obtained. Tuning the absorber to $T = 0.001$ results in a value of

$$x_{0\,\max} = \frac{P_0}{m\omega_2} \times 0.002$$

$$= 0.73 \times 10^{-6} \frac{P_0}{m}$$

For a value of $x_{0\,\max} = \frac{0.10}{4}$ and $P_0 = 100{,}000$ lb

$$m = 2.82 \text{ lb-sec/in.}$$

$$w = 1090 \text{ lb}$$

Check for amplitude of θ_0

$$\theta_0 = -\frac{x_0}{r\sqrt{T^2 + C^2}} = -70.7\frac{x_0}{r}$$

Limiting max θ to 10 deg gives

$$r_{\min} = 105 \text{ in.}$$

This radius would appear large for the weight, and so design considerations would probably act to reduce the radius to, say, 60 in. Then, with the same damping factor, the amplitude of x_0 would be reduced to 0.143 in., and the total weight of the pendulums would be increased to 1900 lb. This would be divided among at least two pendulums and probably three or four or even more, depending upon the details of the design. It is difficult to estimate the total weight and space requirements of such an absorber, but a rough estimate might give a weight of from 5 to 10 tons and a space requirement of 300 to 500 cu ft. Hull stiffening and connecting shafting should be added to these figures. The advantage of this type of absorber would lie in its ability to neutralize the propeller forces at all speeds and thus the amplitude of vibration at every resonant speed. However, the forces involved in an absorber of this size become of such magnitude that a much more complete study would be required to ascertain whether an application such as this is practical. One element which should be considered is the reduction in P_0, which is caused by the lowering of the resonant frequency.

Case II. The towers on a battleship being remote from the hull are found to vibrate excessively, making it difficult to use the range finders and other sensitive apparatus.

The amplitude of motion is measured and is found at the worst location in the operating range to be 0.15 in. at a frequency of 600 vibrations per min and is found to be composed of the propeller-blade frequencies from the two propellers, i.e., at times it adds up and then cancels as the blade forces come in and out of phase. By tests with a vibration generator it is found that a harmonic force of 1000 lb with a frequency of 600 vibrations per min at one of the uppermost points on the tower will give a similar vibration pattern having an amplitude of 0.07 in. It is desired to reduce the maximum vibration amplitude to 0.02 in. using pendulum absorbers.

Two absorbers would be required, one connected to each shaft through an alternating-current motor and generator. Since the absorber would not be very large take $C = T = 0.003$.

$$x_{0\,\max} = \frac{P_0}{m\omega^2} \times 0.006$$

$$m = \frac{1000 \times 0.006}{\left(\frac{600}{60} \times 2\pi\right)^2 \times 0.02} = 0.0762$$

$$w = 29.4 \text{ lb}$$

$$r\theta_0 = \frac{0.02}{0.003\sqrt{2}} = 4.71 \text{ in.}$$

If θ is limited to 10 deg = 0.169 radians, then r would be

$$r = \frac{4.71}{0.169} = 27.9 \text{ in.}$$

This would indicate an absorber some 6 ft diam, whose weights are only 30 lb. A more practical design would have a larger pendulum weight and a smaller size. If the tuning and damping constants be kept the same, and the weight increased to 50 lb, then $x_{0\,\max}$ would be lowered to 0.0118 in., providing a steadier support and the necessary radius would be decreased to 16.5 in. The optimum weight-size ratio would be determined by the over-all design characteristics. It would appear that the weight of the absorbers and their equipment, particularly topside weight, would be appreciably less than the stiffening which might otherwise be used. The pendulum absorber would seem to be admirably suited to an application of this type. Another advantage would arise from the characteristic of the absorber which reduces the resonant frequency. It is not possible to calculate the new resonant frequency without an elaborate consideration of the particular system, but the drop in resonant frequency alone should be of great value.

Supersonic Diffusers for Wind Tunnels

By E. P. NEUMANN[1] and F. LUSTWERK,[2] CAMBRIDGE, MASS.

An investigation of supersonic diffusers was conducted for conditions wherein a boundary layer was present at the diffuser entrance. The pressure rise obtained from a shock in a constant-area tube was measured, and the measurements compared with values computed from a simple one-dimensional analysis. For the range of Mach numbers covered (1.8 to 4.2), separation of the stream from the tube wall was always induced by the shock. The length of the separated region was from 8 to 12 tube diameters. The results of the tests on shocks in a constant-area tube were utilized in the design of several types of diffusers for which test data are reported at Mach numbers ranging from 2 to 3. The most efficient diffuser tested consisted of a contraction to a minimum starting area followed by a constant-area tube approximately 10 diam long. The tube was in turn followed by a subsonic diffuser. Only diffusers of constant geometry were considered.

Nomenclature

The following nomenclature is used in the paper:

a = cross-sectional area, sq ft
c_p = specific heat at constant pressure, 0.240 Btu/(deg F) (lb)
D = diameter of test section
g = acceleration given to unit mass by unit force, fps^2
h = enthalpy, ft-lb per lb
J = number of ft-lb in 1 Btu = 778.3
k = ratio of specific heats, 1.4
L = length of test section
M = Mach number = $V/\sqrt{gc_p(k-1)TJ}$
p = pressure, psia
T = temperature, deg F abs
V = mean velocity of fluid stream at given cross section of test section, fps
η = diffuser efficiency, work of isentropic and adiabatic compression between initial condition and final pressure divided by kinetic energy expended (see Appendix)

Subscripts:

$_1$ refers to state of fluid stream upstream of a "transverse" shock where velocity is supersonic, and sometimes refers to diffuser entrance
$_2$ refers to state of fluid stream downstream of "transverse" shock where stream is subsonic
$_3$ refers to state of fluid stream after diffuser where velocity is approximately zero.
$_0$ refers to stagnation state of fluid stream at entrance of accelerating nozzle
$_*$ refers to state of fluid stream at Mach number of unity

Superscripts:

$'$ (prime) refers to minimum cross section or throat of supersonic diffuser
$''$ (double prime) refers to minimum cross section or throat of supersonic diffuser when this section is elongated and of constant area

Introduction

The most important single factor contributing to the large power requirement of a supersonic wind tunnel is the irreversibility encountered in the wind-tunnel diffuser. For example, if the diffuser efficiency of a tunnel operating at a Mach number of 2 is increased from 80 to 85 per cent, the power required to drive the tunnel is reduced by 30 per cent.

The primary object of the investigation reported in this paper was to use simple small-scale apparatus to obtain information that would aid in the design of an efficient diffuser for a wind tunnel. A secondary object was to obtain information that would make possible the design of diffusers for air intakes on missiles or on aircraft traveling at supersonic speeds, and of diffusers for rotating machinery.

In the case of supersonic intakes, air usually enters the diffuser passage with little or no boundary layer. Under these conditions, the analytical design of the passageways is reasonably satisfactory since here the assumption of no boundary layer is more tenable than in the case of a wind-tunnel diffuser.

However, as a first step in the design of a wind-tunnel diffuser, the assumption can be made that no boundary layer is present, and a simple one-dimensional analysis can then be undertaken. For a wind tunnel of the steady-flow type, the design of an efficient accelerator or nozzle of the Laval type is practicable. The pressure drop across this nozzle is not much different from that computed if reversible flow is assumed, that is, the irreversibility introduced in the accelerator is small. Although this might seem to indicate that a similar passage introduced in the reverse direction would serve as a satisfactory diffuser, such is not the case because of the effect of the transverse pressure shock that is formed at the accelerator throat when the tunnel is started. As the downstream pressure is reduced, this shock will move downstream to higher Mach numbers. The process involved in the shock is irreversible, the degree of irreversibility increasing as the Mach number at which the shock occurs increases. It can be shown readily that the minimum possible cross-sectional area of the stream after the shock must be greater than the minimum cross-sectional area in the accelerator. Since the area of the diffuser throat must be greater than that of the accelerator, a reversed accelerator, identical with the first, will not function as a diffuser. In other words, if an irreversible effect between the accelerator and diffuser (i.e., the transverse shock) must accompany the starting process, the state at the accelerator entrance cannot be re-established. If, however, it were possible to devise a mechanism that decreased the area of the diffuser throat after the shock had passed by, a reversed Laval nozzle would function as a diffuser. Should such a device be used, it would still be necessary to provide a pressure ratio for starting, equivalent to the total pressure loss that would be obtained if the only irreversibility during deceleration occurred in a shock at the Mach number present at the diffuser entrance.

If a transverse shock during the starting process is assumed to

---

[1] Assistant Professor of Mechanical Engineering, Gas Turbine Laboratory, Massachusetts Institute of Technology. Jun. ASME.
[2] Research Associate, Department of Mechanical Engineering, Gas Turbine Laboratory, Massachusetts Institute of Technology. Jun. ASME.

Contributed by the Applied Mechanics Division and presented at the Annual Meeting, New York, N. Y., November 28–December 3, 1948, of The American Society of Mechanical Engineers.
Discussion of this paper should be addressed to the Secretary, ASME, 29 West 39th Street, New York, N. Y., and will be accepted until July 11, 1949, for publication at a later date. Discussion received after the closing date will be returned.
Note: Statements and opinions advanced in papers are to be understood as individual expressions of their authors and not those of the Society. Paper No. 48—A-14.

be inevitable, the pressure ratio at which a wind tunnel will start can be computed. These computed values, subject to the limitations imposed by a one-dimensional analysis that neglects friction, are presented in Fig. 8 for Mach numbers from 1.0 to 3.0.

The results of the one-dimensional analysis may be summarized as follows:[3]

(*a*) For starting conditions, the minimum pressure across a wind tunnel (nozzle plus diffuser) must be equal to the loss in stagnation pressure across a shock at the test-section Mach number.

(*b*) For operating conditions, the minimum pressure across a wind tunnel must be equal to the loss in stagnation pressure across a shock at the Mach number in the diffuser throat.

These conclusions must be accepted with reservations since it has been assumed that no boundary layer is present and that the only possible transition from supersonic to subsonic flow during the starting operation is a transverse shock. The assumption of no boundary layer, i.e., no wall friction, ignores irreversibilities which are actually present, whereas the assumption of a transverse shock may assume greater irreversibilities than are actually necessary. In addition, the expedient of decreasing the area of the diffuser throat after the shock has passed through would permit reversible operation in the absence of friction.

The Transverse Shock

Transverse shocks, which seemed to be inevitable in a supersonic diffuser, were studied experimentally in a constant-area tube by means of pressure measurements and also by schlieren observations. The arrangement of the test apparatus is shown in Fig. 1.

Figs. 2(*a*) and (*b*) are schlieren plates of a shock in a constant-area passageway. Note in Fig. 2(*a*) that the influence of shock extends some distance downstream from its point of inception.

[3] See Appendix for formulas used.

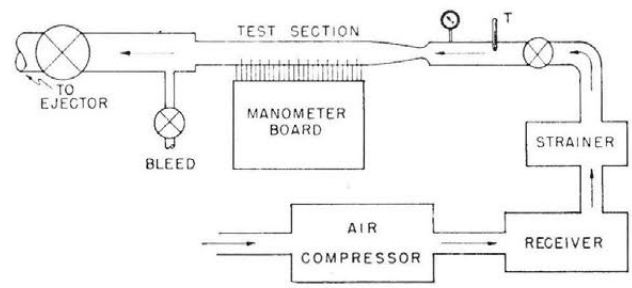

Fig. 1 Schematic Plan of Test Apparatus

Fig. 2(*b*) shows a transverse shock in the constant-area section which follows the contraction in a supersonic diffuser.

Figs. 3 and 4 show pressure measurements taken at the wall of a constant-area passage. The lower curves sloping gradually upward and to the right represent the conditions when supersonic flow fills the entire tube. The steeper curves represent pressure measurements for different positions of the shock region in the constant-area passageway. The curves at the top part of the diagram sloping downward and to the right represent pressure measurements for the case where the stream again filled the passageway and friction causes a pressure drop in the direction of flow. In Fig. 3 are shown runs A and B. These runs are for identical pressure and temperature at the entrance to the accelerating nozzle. The slight discrepancy between runs A and B can probably be ascribed to the fact that humidity of the air supplied to the compressor varied between these two runs.

The pressure measurements, Figs. 3 and 4, and schlieren plates, Figs. 2(*a*) and (*b*), indicated that the idealized transverse shock assumed in the one-dimensional analysis was never obtained. Instead, the interaction of the shock and boundary layer caused separation of the stream from the tube wall. Once separation

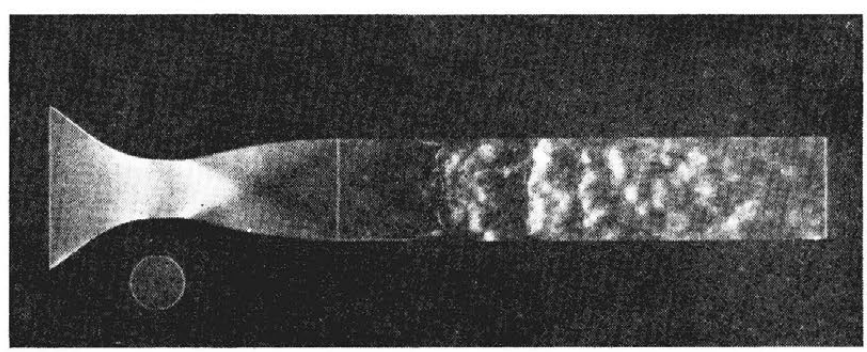

Fig. 2(*a*) Schlieren Plate of Shock Region in Constant-Area Tube
(Light vertical line shows end of nozzle. Flow is from left to right. Mach number = 2.06; depth of passage perpendicular to plane of view = 0.919 in.; width of constant-area section = 0.919 in.; exposure time, 5 microsec.)

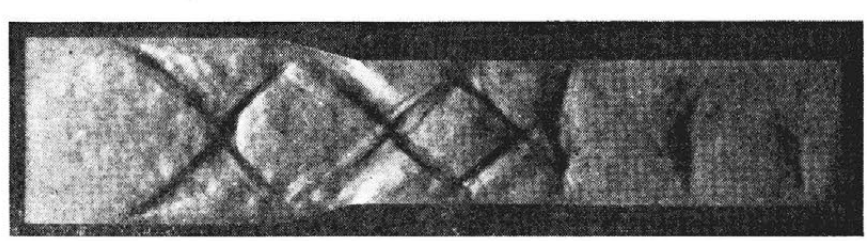

Fig. 2(*b*) Schlieren Plate of Shock in Constant-Area Throat Section of Diffuser
(Note repetition of transverse shock. Flow is from left to right. Mach number = 2.55 before diffuser; 15-deg wedge angle; width of passage before diffuser = 1.292 in.; depth of passage perpendicular to plane of view = 1.292 in.; exposure time, 5 microsec.)

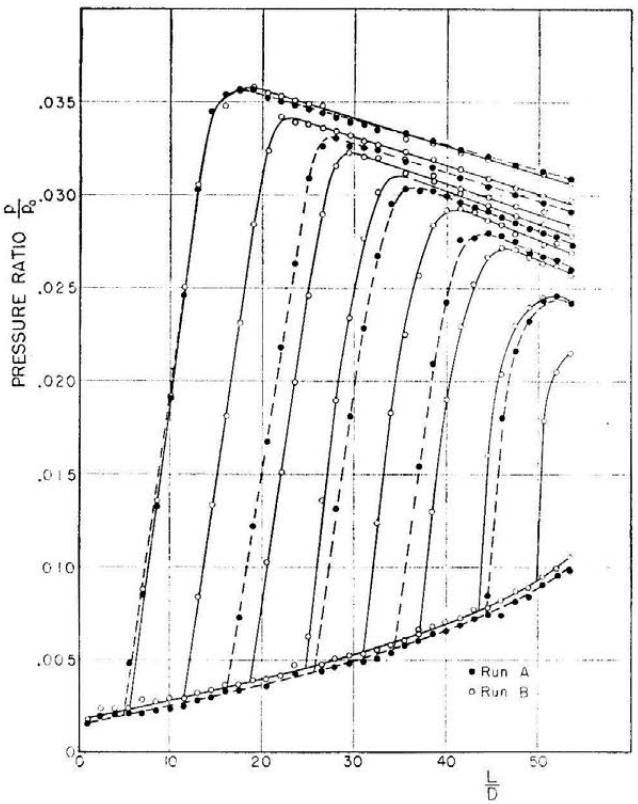

FIG. 3 PRESSURE DISTRIBUTION ALONG 1.000-IN-DIAM TUBE FOR NOZZLE WITH 0.170-IN-DIAM THROAT
(L/D is measured from the nozzle exit.)

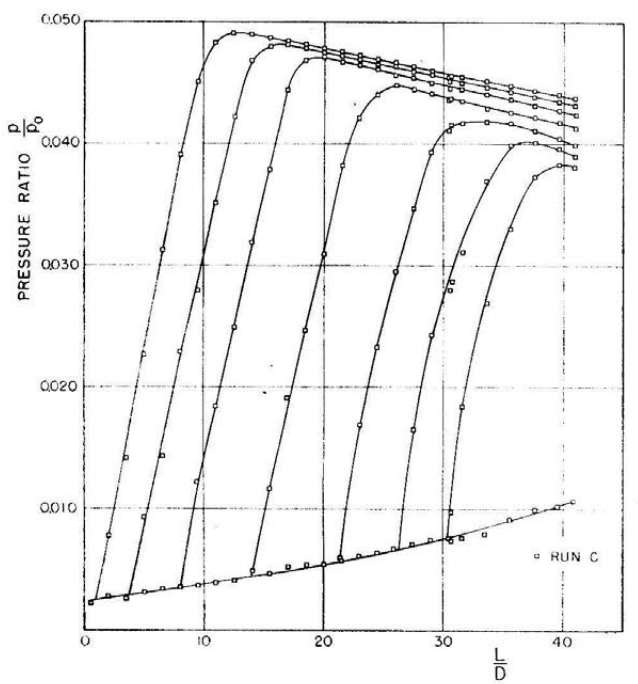

FIG. 4 PRESSURE DISTRIBUTION ALONG 1.000-IN-DIAM TUBE FOR NOZZLE WITH 0.200-IN-DIAM THROAT
(L/D is measured from the nozzle exit.)

occurred, the stream did not again fill the passage for a distance equal to 8 to 12 diam of the tube. Fig. 5 shows the length of shock region in terms of tube diameters for Mach numbers ranging from 1.8 to 4.2. The length of shock region is defined as the distance from the point of inception of the shock to the point downstream at which the maximum pressure was recorded. The value of this length, as determined from Figs. 3 and 4, agrees reasonably well with measurements obtained from high-speed ($^1/_{200,000}$ sec) photographs taken in conjunction with a schlieren apparatus. For the schlieren photographs, the test section had a rectangular cross section (see, for example, Fig. 2*a*).

Fig. 6 compares the measured values of the efficiency and pressure rise across a shock with the corresponding values computed from a one-dimensional analysis. The good agreement between measured and calculated values, a maximum departure of 5 per cent, indicates that the wall forces in the separated region are small.

Some measure of the effect of boundary layer on length of shock region may be obtained by comparing runs A and B with

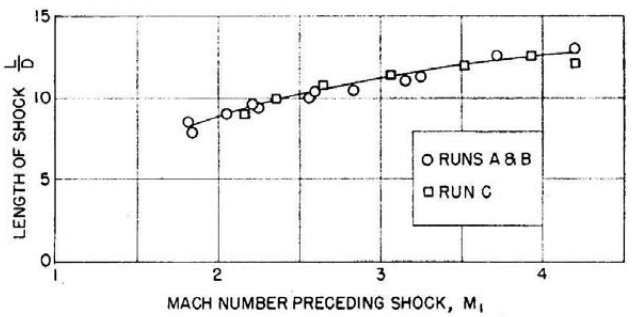

FIG. 5 LENGTH OF SHOCK VERSUS MACH NUMBER PRECEDING SHOCK

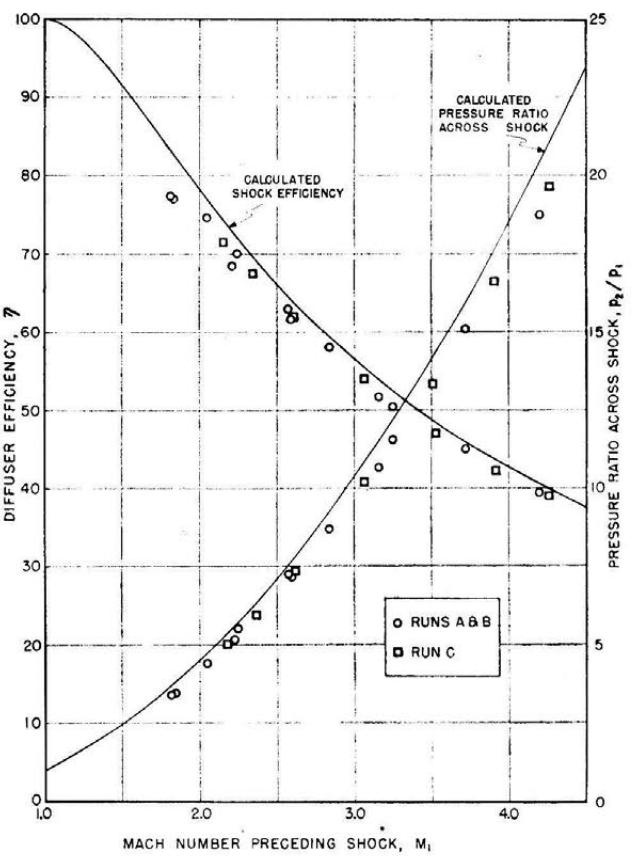

FIG. 6 DIFFUSER EFFICIENCY VERSUS MACH NUMBER PRECEDING SHOCK

run C. In runs A and B, for example, 26 diameters of straight tube preceded the shock at a Mach number of 2.6; whereas, in run C, 21 diameters preceded the shock at the same Mach number. The length of shock was the same for both cases. Keenan and Neumann[4] indicate that it is necessary that a distance of between 30 and 50 tube diameters precede the shock before a developed velocity distribution is obtained.

Supersonic Diffuser

In order to establish a standard of comparison between the various diffusers to be studied, the diffuser in Fig. 7 labeled type I, a type commonly used for supersonic wind tunnels, was tested. The efficiency of this diffuser is appreciably lower than is predicted by one-dimensional analysis.

When it was observed that separation accompanied a shock, but that the change in state across the separated region was approximately the same as that predicted by a one-dimensional analysis, the diffuser shown as type II in Fig. 7 was designed and tested. In the same illustration, measured and calculated values of the diffuser efficiency are shown. For the type II diffuser, the ratio of measured to calculated value of efficiency is approximately 0.97 for a range of Mach numbers from 2 to 3. This efficiency (η) is defined as the ratio of the isentropic increase in enthalpy to the change in kinetic energy in the diffuser. The isentropic increase in enthalpy is computed between the state preceding the diffuser entrance and the pressure after the exit to the subsonic diffuser. The change in kinetic energy is computed between the entrance and exit states. The efficiency may be expressed in terms of symbols as follows:

$$\eta = \frac{\frac{2}{k-1}\left[\left(\frac{p_3}{p_1}\right)^{\frac{k-1}{k}} - 1\right]}{M_1^2 - \frac{V_3^2}{gkRT_1}}$$

In order to measure the effect of cross section on performance, a type II diffuser with a square cross section was tested at a Mach number of 2.46. As is shown in Fig. 7, there is little difference in efficiency between the square and the circular-cross-section diffusers. Note also that the diffuser with the square cross section was preceded by a scale model of a supersonic wind tunnel.

To obtain the maximum operating efficiency predicted by one-dimensional analysis, it is necessary to have a contraction to minimum area in the supersonic diffuser. The type III diffuser of Fig. 7 was designed with this minimum starting area, i.e., $\pi(D')^2/4$. The experimental results obtained with this diffuser indicate a slightly better operating efficiency than that obtained for the type II diffuser. However, schlieren observations indicated that the shock at the minimum-area section was separating from the passage wall much in the same fashion as in the type I diffuser, except that the point of separation occurs at a lower Mach number for a given entrance Mach number.

To increase the operating efficiency, a diffuser, shown as type IV in Fig. 7, was designed and tested. The only departure from a design indicated by a one-dimensional analysis was an elongated throat or minimum-area section, which should permit the separated region to again fill the passageway before it is introduced into the subsonic diffuser. The ratio of measured to computed efficiency for stable operation was 0.92 at Mach numbers of 2.32 and 2.99. A higher efficiency, indicated by the solid dot in Fig. 7, could be obtained with this type of diffuser under unstable conditions. For this less stable case, the ratio of measured to computed efficiency was 0.94.

In the case of this diffuser, the minimum area for starting is greater than the minimum value computed from a one-dimensional analysis which does not take into account friction in the elongated throat during the starting process. For example, the experimental value of the ratio of the diffuser-entrance area to the throat area for a type IV diffuser was 0.757 at a Mach number of 2.99; whereas, a computed value of 0.719 was obtained when reversible conditions from entrance to throat were assumed. If friction in the 10.9 diam of straight section is taken into account, a computed value of 0.761 is obtained. The friction coefficient was computed from the Kármán-Nikuradse relation between friction coefficient and Reynolds number. The computed value of diffuser efficiency used in obtaining the ratio of measured to calculated efficiency was based upon the actual minimum starting-area ratio of 0.757, rather than on the computed minimum value of 0.719. For the types III and V diffusers, the value of the throat area for starting which was computed when reversible conditions from entrance to throat were assumed, agreed with the measured value within the precision of measurement of the throat area.

Consideration of Starting Conditions

The comparison between measurement and theory has been made on the basis of conditions obtaining after the diffuser has started, that is, after supersonic flow has been established at the throat or minimum-area section. Often, the maximum pressure ratio available, rather than the power available, is the determining factor in defining the Mach number possible for a given supersonic tunnel. A better criterion than the operating efficiency is then the minimum efficiency during starting, or the maximum pressure ratio p_6/p_3 needed to establish supersonic flow at the diffuser throat.

Again, simple one-dimensional considerations indicate that the pressure ratio necessary for starting is that obtained across a shock at the test-section Mach number and a reversible subsonic diffuser after the shock. This condition appears to be present even if a variable geometry type of diffuser is used.

In the case of the types I and II diffusers, the starting and operating conditions are identical. The type IV diffuser has a higher operating efficiency and a lower starting efficiency than does the type II. For example, the pressure ratio (p_3/p_1) obtained during starting is 10.6 for the type IV diffuser and 11.0 for the type II diffuser.

In an effort to improve the starting characteristics of the type IV diffuser and at the same time to maintain high operating efficiencies, the constant-area throat section was given a slight divergence in order to compensate for the effect of friction when subsonic flow is present during starting. A type V diffuser, designed in this manner, was built and tested. As indicated in Table 1, the starting characteristics were improved at the expense of a small decrease in the operating efficiency over that obtained with the type IV diffuser.

TABLE 1 DIFFUSER STARTING CONDITIONS AT $M = 2.99$[a]

Diffuser type	Pressure ratio p_3/p_1 obtained across Diffuser — Starting	Diffuser — Operating
I	8.53	8.53
II	10.99	10.99
III	11.07	11.51
IV	10.63	13.02—Stable 13.66—Unstable
V	10.99	12.82

[a] Fifteen diameters of straight tube preceded the diffuser entrance for the conditions tabulated.

Diffuser Entrance Shape[5]

An investigation was conducted to determine the best inlet

[4] "Measurement of Friction in a Pipe for Subsonic and Supersonic Flow of Air," by J. H. Keenan and E. P. Neumann, Journal of Applied Mechanics, Trans. ASME, vol. 68, 1946, p. A-91.

[5] The test results presented here were obtained by Angus N. MacDonald in a thesis submitted to the Department of Mechanical Engineering, Massachusetts Institute of Technology, June, 1947, "An Investigation of Supersonic Diffusers for Wind Tunnels."

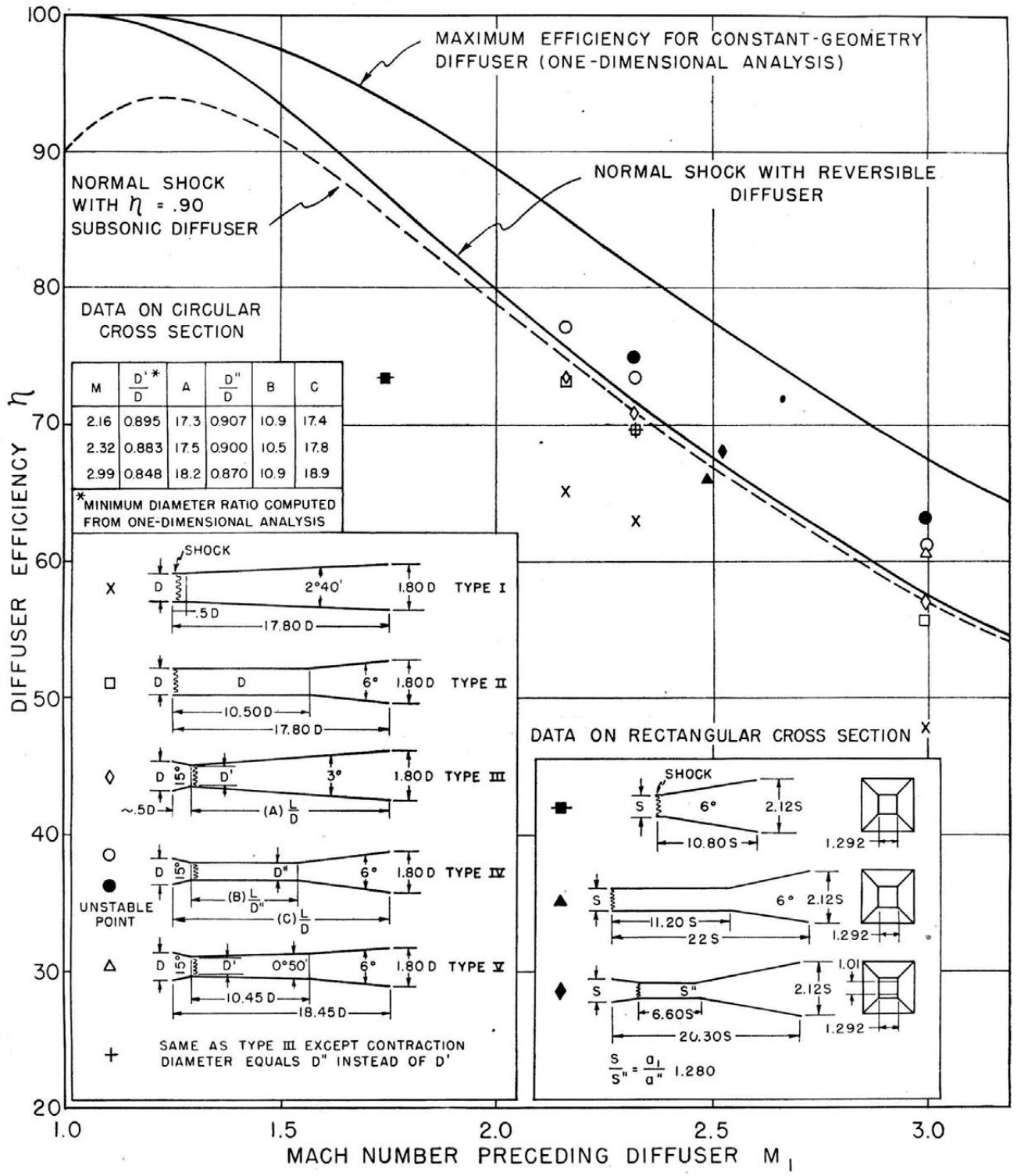

M	D'/D *	A	D"/D	B	C
2.16	0.895	17.3	0.907	10.9	17.4
2.32	0.883	17.5	0.900	10.5	17.8
2.99	0.848	18.2	0.870	10.9	18.9

*MINIMUM DIAMETER RATIO COMPUTED FROM ONE-DIMENSIONAL ANALYSIS

Fig. 7 Efficiency Curves for Various Diffusers

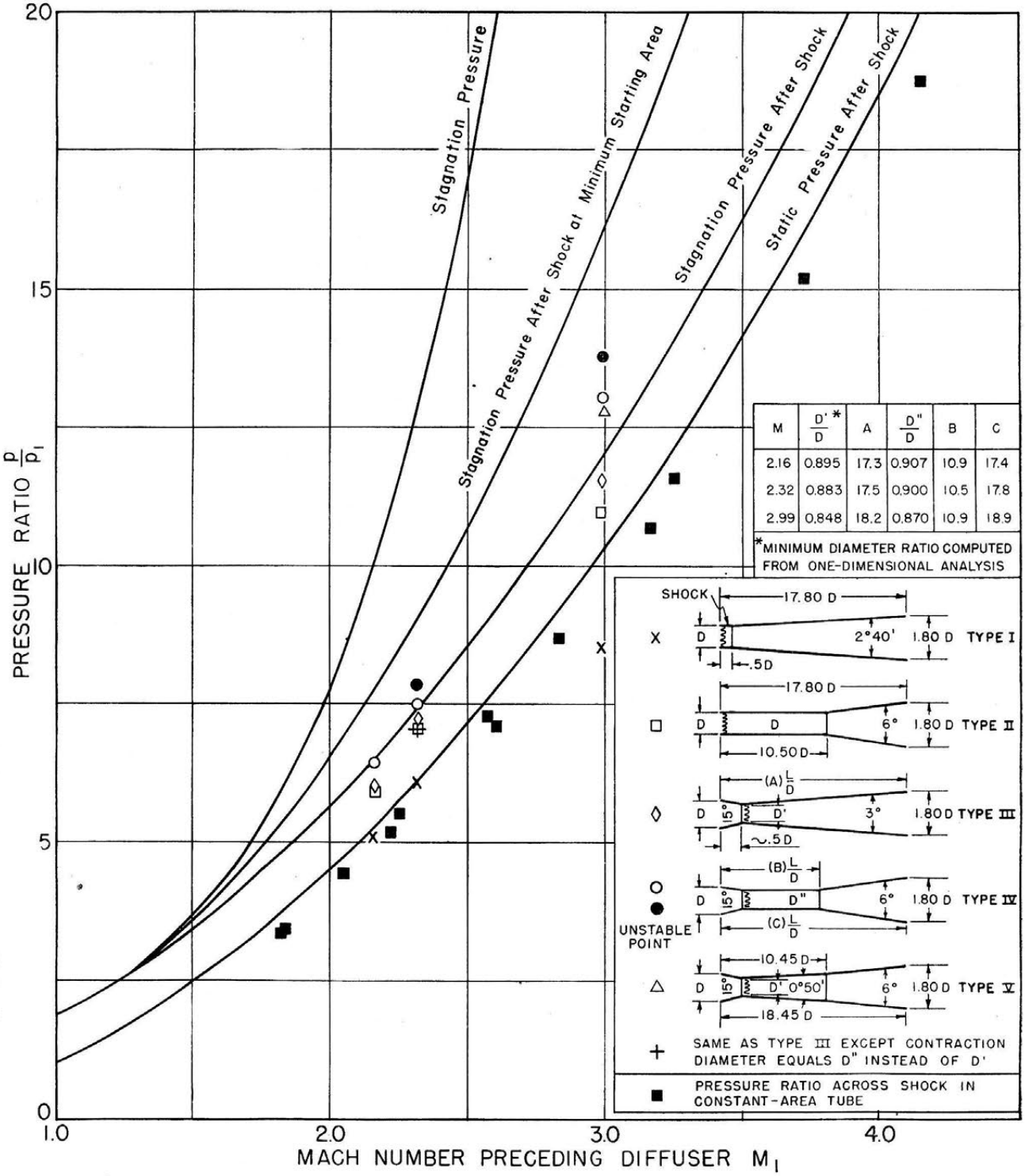

FIG. 8 PRESSURE RATIOS FOR VARIOUS DIFFUSERS

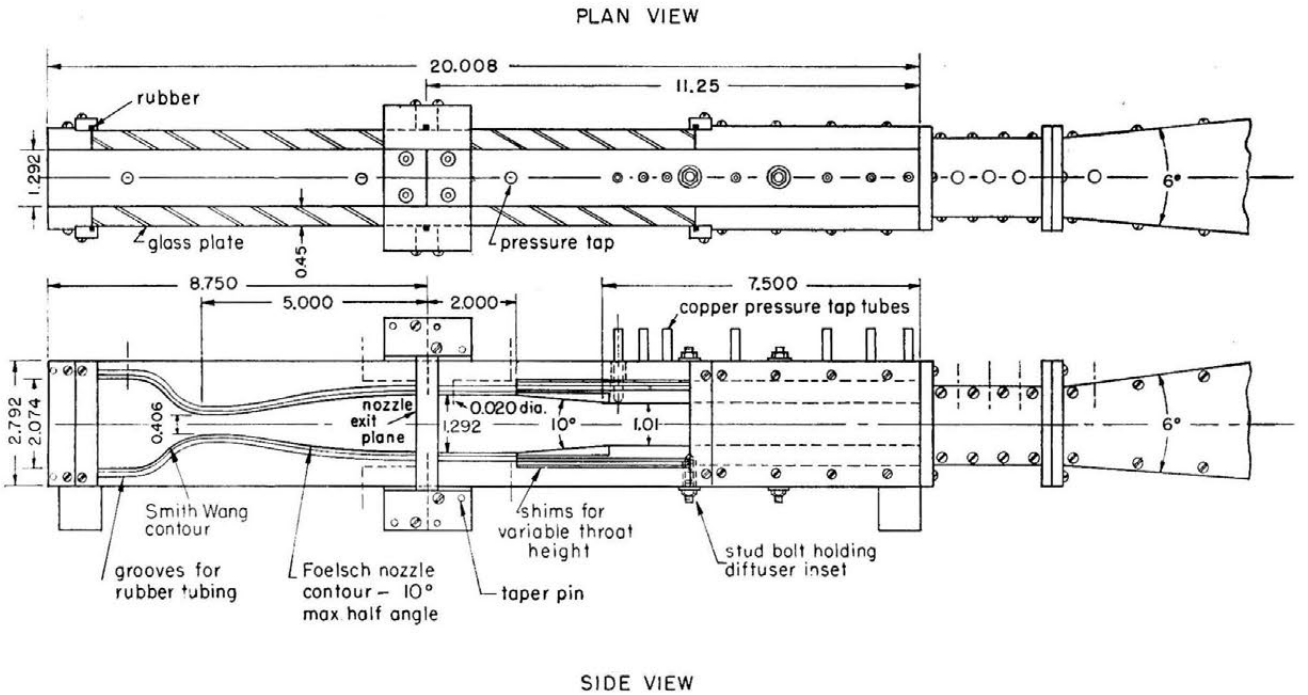

FIG. 9 APPARATUS USED TO STUDY VARIATION IN ENTRANCE ANGLE OF DIFFUSER

included angle for the convergent portion of the diffuser. These tests covered only diffusers with a rectangular cross section. The apparatus used to study this variation in entrance angle is shown in Fig. 9. The entrance angle was varied between 10 and 50 deg at a Mach number of 2.55, and the effect on efficiency was measured.

In all of the tests, the contraction to minimum starting area was followed by a constant-area passage approximately 7 hydraulic diameters in length, and a subsonic diffuser of square cross section with walls at a 6-deg included divergence angle.

The test results are shown in Fig. 10. The best diffuser efficiency was obtained with the smallest entrance angle tested, namely, $\omega = 10$ deg. A smaller inlet angle might have shown a slight additional improvement in efficiency. However, tests at smaller angles were not attempted because an increase in length of the apparatus would have been necessary, and the resultant increase in frictional area would probably have offset the gain obtained by the smaller wedge angles.

ACKNOWLEDGMENT

This work was carried out as part of the Guided Missiles Program at the Massachusetts Institute of Technology and was sponsored by the Navy Department, Bureau of Ordnance. Fig. 10 was obtained from MacDonald[5] and Fig. 3 from Newberg.[6]

Appendix

All calculations used in this report were based upon a one-dimensional analysis of the flow. The velocity and pressure were assumed to be uniform across any cross section in the tube. The energy, momentum, and continuity equations were used to obtain the state of the fluid from pressure measurements made at the walls of the tube. Air was assumed to be a perfect gas with $k = 1.400$ and $R = 53.35$ ft/deg F.

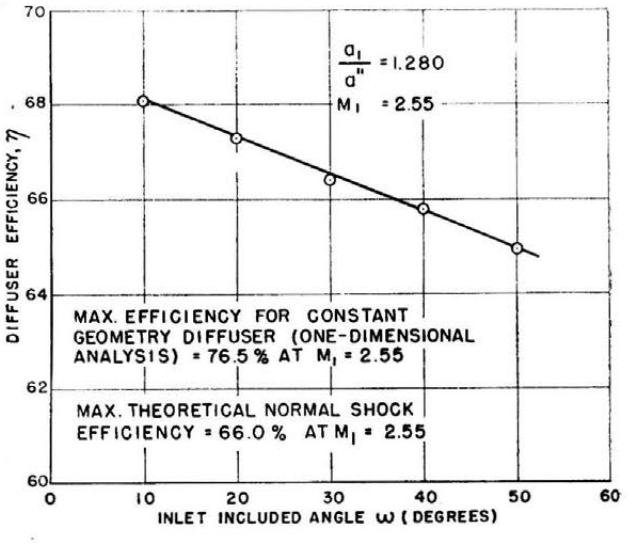

FIG. 10 TEST RESULTS

The pressure rise across a transverse shock was computed from the following equations

$$M_2 = \frac{M_1^2 + \frac{2}{k-1}}{\frac{2k}{k-1} M_1^2 - 1} \quad \ldots\ldots [1]$$

$$\frac{p_2}{p_1} = \frac{1 + kM_1^2}{1 + kM_2^2} \quad \ldots\ldots [2]$$

The efficiency, as used in this paper, is defined as the work of

[5] Measurements of Diffuser Efficiency of Supersonic Pressure Shocks," by Eric G. Newberg, Jr., S. M. Thesis, Department of Mechanical Engineering, Massachusetts Institute of Technology, February, 1946.

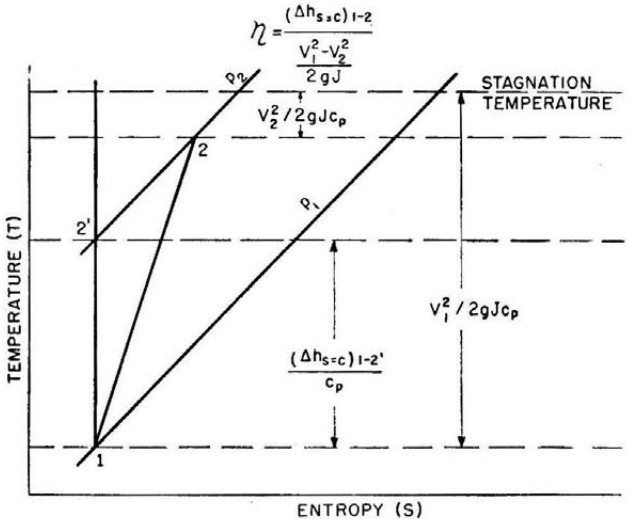

FIG. 11

isentropic compression between the initial condition and the final pressure divided by the kinetic energy expended

$$\eta = \frac{(h_{s=c})_{1-2'}}{\frac{V_1^2}{2g} - \frac{V_2^2}{2g}} \quad \ldots\ldots [3]$$

This is illustrated in Fig. 11.

Substituting

$$h = c_p T \quad \ldots\ldots [4]$$

$$\frac{T_{2'}}{T_1} = \left(\frac{p_2}{p_1}\right)^{\frac{k-1}{k}} \quad \ldots\ldots [5]$$

and the definition of Mach number into Equation [3], we obtain

$$\eta = \frac{\frac{2}{k-1}\left[\left(\frac{p_2}{p_1}\right)^{\frac{k-1}{k}} - 1\right]}{\mathbf{M}_1^2 - \frac{V_2^2}{gkRT_1}}$$

The calculations for the minimum diffuser throat area for starting were made assuming an isentropic expansion to $\mathbf{M} = 1$ after a shock at the entrance to the diffuser. The contraction ratio a_1/a' can be found from the stagnation pressure after the shock by means of the usual isentropic flow equations

$$\frac{a_1}{a'} = \frac{\left(\frac{p_{2s}}{p_{20}}\right)^{\frac{1}{k}}\left[\left(\frac{p_{2s}}{p_{20}}\right)^{-\frac{k-1}{k}} - 1\right]}{\left(\frac{p_2}{p_{20}}\right)^{\frac{1}{k}}\left[\left(\frac{p_2}{p_0}\right)^{-\frac{k-1}{k}} - 1\right]}$$

where p_{20} is the stagnation pressure after the shock and p_{2s} is the pressure obtained if the fluid after the shock is accelerated reversibly to $\mathbf{M} = 1.0$. Since k equals 1.400

$$\frac{a_1}{a'} = \frac{0.255804}{\left(\frac{p_2}{p_{20}}\right)^{\frac{1}{k}}\left[\left(\frac{p_2}{p_0}\right)^{-\frac{k-1}{k}} - 1\right]}$$

The pressure ratio and efficiency for the minimum-throat diffuser were calculated by assuming an isentropic compression from conditions before the diffuser to the diffuser throat, followed by a transverse shock at that point and a reversible subsonic diffuser after the shock. For the theoretical calculations, the exit velocity was assumed to be zero. In the actual cases the kinetic energy at the exit was between 0.5 to 1.2 per cent of the initial kinetic energy.

Vibration of Slender Bars With Discontinuities in Stiffness

By W. T. THOMSON,[1] MADISON, WIS.

Vibrational characteristics of elastic bodies are altered by discontinuities in stiffness resulting from narrow grooves or cracks. This paper presents a theoretical method for determining the effect of such discontinuities on the flexural, longitudinal, and torsional vibration of slender bars.

Nomenclature

The following nomenclature is used in the paper:

A = cross-sectional area
A' = reduced cross-sectional area
I_0 = moment of inertia in bending
I_0' = reduced moment of inertia
I_p = polar moment of inertia
I_p' = reduced polar moment of inertia
$\alpha = \frac{A'}{A}, \frac{I_0'}{I_0}, \frac{I_p'}{I_p}$
E = modulus of elasticity
G = shear modulus of elasticity
ρ = density, lb/unit volume
U = longitudinal strain
y = flexural displacement
M_a = moment at a
P_a = axial force at a
T_a = torque at a
a = position of slot
c = width of slot
$\mathfrak{L}$ = Laplace transform
$\beta = \left(\frac{m\omega^2}{EI_0}\right)^{1/4}, \left(\frac{\rho\omega^2}{Eg}\right)^{1/2}, \left(\frac{\rho\omega^2}{Gg}\right)^{1/2}$
l = length of bar
m = mass per unit length of beam

Introduction

Hetényi[2] has shown that the statical deflection of beams of varying cross section can be determined by considering the beam to be uniform with a modified load. The fundamental equation for such problems can be written as

$$\frac{d^2y}{dx^2} = -\frac{1}{EI_0}\frac{M}{\alpha} \quad \text{.....[1]}$$

where EI_0 is the stiffness of the equivalent uniform beam, and $M/\alpha = MI_0/I$ the new moment which can be obtained by modifying the original loading.

This concept can be extended to vibration problems where the change in stiffness is due to a narrow slot of width c a distance a from one end of the bar, as shown in Fig. 1(*a*).

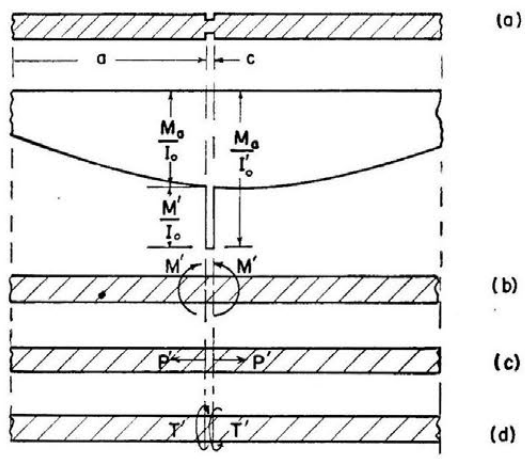

Fig. 1 Modified Loads for an Equivalent Uniform Bar in Flexure, Tension, and Torsion

Letting A, I_0, and I_p be, respectively, the cross-sectional area, and moment of inertia in bending and torsion with corresponding primed symbols for the reduced section, the slotted bar can be replaced by a uniform bar with the following modified loads as shown in Fig. 1(*b*, *c*, and *d*):

Flexural vibration

$$M' = M_a\left(\frac{1}{\alpha} - 1\right) \quad \text{.....[2]}$$

$$\alpha = \frac{I_0'}{I_0}$$

Longitudinal vibration

$$P' = P_a\left(\frac{1}{\alpha} - 1\right) \quad \text{.....[3]}$$

$$\alpha = \frac{A'}{A}$$

Torsional vibration

$$T' = T_a\left(\frac{1}{\alpha} - 1\right) \quad \text{.....[4]}$$

$$\alpha = \frac{I_p'}{I_p}$$

Actually, this simple concept is an idealization, since much of the material adjacent to the slot is ineffective in carrying the load, and just how the equivalent slot varies with the width and

[1] Associate Professor of Mechanics, University of Wisconsin.

[2] "Deflection of Beams of Varying Cross Section," by M. Hetenyi, Journal of Applied Mechanics, Trans. ASME, vol. 59, 1937, p. A-49.

Contributed by the Applied Mechanics Division and presented at the Annual Meeting, New York, N. Y., November 28–December 3, 1948, of The American Society of Mechanical Engineers.

Discussion of this paper should be addressed to the Secretary, ASME, 29 West 39th Street, New York, N. Y., and will be accepted until July 11, 1949, for publication at a later date. Discussion received after the closing date will be returned.

Note: Statements and opinions advanced in papers are to be understood as individual expressions of their authors and not those the Society. Paper No. 48—A-17.

depth of cut must be established by experimentation. Kirmser,[3] using a static curve and Rayleigh's method, has found for the flexural problem that the computed natural frequencies of a beam with a slot at mid-span agreed with the experimental values when an equivalent slot width of 5 times the actual width was used. However, even a casual inspection of the problem would indicate that, in general, such a simple relationship could not exist as the amount of ineffective material adjacent to the slot must vary with the depth of the slot, with the width of the slot having little influence.

Fundamental Concepts

The operational method based on Laplace transformations offers a convenient approach to problems with concentrated forces and moments, and hence some basic concepts of the method will be briefly reviewed.

The Laplace transform $F(s)$ of a function $f(x)$ is defined as follows

$$F(s) = \mathcal{L}f(x) = \int_0^\infty f(x)e^{-sx}\,dx \quad \ldots\ldots [5]$$

Of particular interest to this problem are the transforms of the following types of functions:

Unit Function. The unit function $u(x - a)$ is the basic building block for other functions. As shown in Fig. 2, it is equal

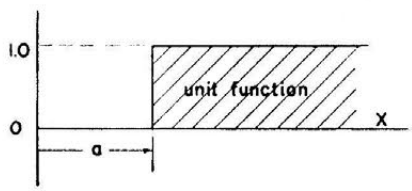

Fig. 2 Graphical Representation of a Unit Function

to unity for x greater than a and zero everywhere else. The Laplace transform for such a function is

$$\mathcal{L}u(x - a) = \int_0^a 0\cdot e^{-sx}\,dx + \int^\infty 1\cdot e^{-sx}\,dx = \frac{e^{-as}}{s} \quad \ldots [6]$$

Unit Impulse. The unit impulse $u_i(x - a)$, shown in Fig. 3,

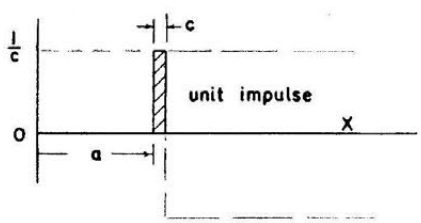

Fig. 3 Graphical Representation of a Unit Impulse

is defined by the following limit

$$u_i(x - a) = \lim_{c\to 0} \frac{u(x - a) - u(x - a - c)}{c} \quad \ldots\ldots [7]$$

with the added restriction that

$$\int_0^\infty u_i(x - a)\,dx = 1$$

[3] "The Effect of Discontinuities on the Natural Frequency of Beams," by P. G. Kirmser, Proceedings of the ASTM, vol. 44, 1944, p. 897.

Its transform can be obtained by substituting the transform of each term in the foregoing relation and using L'Hospital's rule

$$\mathcal{L}u_i(x - a) = \lim_{c\to 0} \frac{e^{-as} - e^{-(a+c)s}}{cs} = e^{-as} \quad \ldots\ldots [8]$$

Unit Doublet. The unit doublet $u_d(x - a)$ shown in Fig. 4

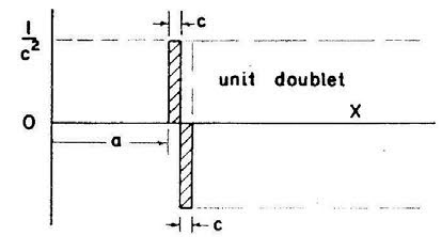

Fig. 4 Graphical Representation of a Unit Doublet

is obtained from the limit

$$u_d(x - a) = \lim_{c\to 0} \frac{u(x - a) - 2u(x - a - c) + u(x - a - 2c)}{c^2} \quad \ldots\ldots [9]$$

For determining its transform, we use the same procedure as for the unit impulse, the indeterminate form after two applications of L'Hospital's rule becoming

$$\mathcal{L}u_d(x - a) = \lim_{c\to 0} \frac{e^{-as} - 2e^{-(a+c)s} + e^{-(a+2c)s}}{c^2 s} = se^{-as} \quad \ldots\ldots [10]$$

The Statical Problem

Consider the problem of determining the statical deflection of the beam in Fig. 5, with a crack at a distance a from the left end. The beam can be treated as a uniform beam with a positive doublet $M'u_d(x - a)$ and a negative doublet $-M'u_d(x - a - c)$

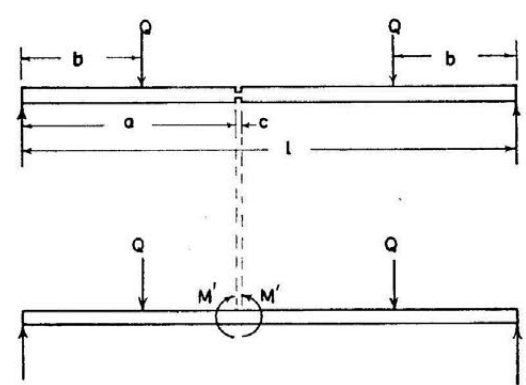

Fig. 5 Beam With Slot Reduced to Uniform Beam With Modified Load

as the modified loading. The differential equation for the loading can then be written as

$$EI_0 \frac{d^4y}{dx^4} = -Q[u_i(x - b) + u_i(x - l + b)] + M'[u_d(x - a) - u_d(x - a - c)] \quad \ldots\ldots [11]$$

Letting Y be the Laplace transform of y, the transformed equation becomes

$$EI_0Y = EI_0\left[\frac{y'(0)}{s^2} + \frac{y'''(0)}{s^4}\right] - Q\left[\frac{e^{-bs} + e^{-(l-b)s}}{s^4}\right] + M'\left[\frac{e^{-as} - e^{-(a+c)s}}{s^3}\right] \quad [12]$$

where $y(0)$ and $y''(0)$, representing the deflection and moment at $x = 0$, are zero. Taking the inverse transformation of Equation [12], we obtain

$$EI_0y = EI_0\left[y'(0)x + y'''(0)\frac{x^3}{6}\right] - \frac{Q}{6}[(x-b)^3u(x-b) + (x-l+b)^3u(x-l+b)] + \frac{M'}{2}[(x-a)^2u(x-a) - (x-a-c)^2u(x-a-c)] \quad [13]$$

Evaluating $y'(0)$ and $y'''(0)$ from the boundary conditions $y(l) = y'''(l) = 0$

$$\left.\begin{aligned} EI_0y'''(0) &= Q \\ EI_0y'(0) &= -\frac{Q}{2}b(l-b) - \frac{M'}{2l}[2c(l-a) - c^2] \end{aligned}\right\} \quad [14]$$

and the final equation for the deflection becomes

$$y = -\frac{Q}{EI_0}\left[\frac{b}{2}(l-b)x - \frac{x^3}{6} + \frac{1}{6}(x-b)^3u(x-b) + \frac{1}{6}(x-l+b)^3u(x-l+b)\right] - \frac{M_a}{2EI_0}\left(\frac{1}{\alpha} - 1\right)\left[[2c(l-a) - c^2]\frac{x}{l} - (x-a)^2u(x-a) + (x-a-c)^2u(x-a-c)\right] \quad [15]$$

The first part of Equation [15] is the deflection of the beam without the crack, and it will depend on the type of loading. The second part represents the contribution due to the crack, and it will have the same form regardless of the type of loading, provided the boundary conditions are the same as that of this problem. Thus the statical deflection of the beam for any type of loading can be written as

$$y = y_Q + y_c \quad [16]$$

where y_c is given by the second part of Equation [15].

Substitution of Equation [16] into the expression for the strain energy, results in the relation

$$U = \frac{1}{2EI_0}\int M_Q^2dx + \frac{M_a^2c}{2EI_0}\left(\frac{1}{\alpha} - 1\right) \quad [17]$$

where the second part is the contribution of the crack to the total strain energy of the beam. This relation can also be obtained by inspection of the $M/(EI)$ diagram and the moment-area consideration.

Vibration of Beams With a Crack

We will consider here the vibration of the free-free beam with a crack at a distance a from one end. The differential equation for the loading then becomes

$$EI_0\frac{d^4y}{dx^4} = m\omega^2y + M'[u_d(x-a) - u_d(x-a-c)] \quad [18]$$

Letting

$$\beta^4 = \frac{m\omega^2}{EI_0}$$

the transform of this equation is

$$Y = \frac{M'}{EI_0}\left[\frac{se^{-as} - se^{-(a+c)s}}{s^4 - \beta^4}\right] + \left[\frac{s^3y(0) + s^2y'(0)}{s^4 - \beta^4}\right] \quad [19]$$

where $y''(0) = y'''(0) = 0$. Applying the inverse transformation, we obtain the deflection equation

$$y = \frac{M'}{2\beta^2EI_0}\{[\cosh\beta(x-a) - \cos\beta(x-a)]u(x-a) - [\cosh\beta(x-a-c) - \cos\beta(x-a-c)]u(x-a-c)\} + \frac{y(0)}{2}[\cosh\beta x + \cos\beta x] + \frac{y'(0)}{2\beta}[\sinh\beta x + \sin\beta x] \quad [20]$$

Letting $y(0) = 1$, and eliminating $y'(0)$ from the two equations resulting from the boundary conditions $y''(l) = y'''(l) = 0$, we obtain the frequency equation

$$[\cosh\beta l\cos\beta l - 1] = \frac{M'}{2\beta^2EI_0}\{[\cosh\beta(l-a) - \cosh\beta(l-a-c) + \cos\beta(l-a) - \cos\beta(l-a-c)][\cosh\beta l - \cos\beta l] + [\sinh\beta(l-a-c) - \sinh\beta(l-a) + \sin\beta(l-a) - \sin\beta(l-a-c)][\sinh\beta l - \sin\beta l]\} \quad [21]$$

Substituting

$$M' = M_a\left(\frac{1}{\alpha} - 1\right)$$

where

$$\frac{M_a}{\beta^2EI_0} = \frac{1}{\beta^2}\left(\frac{d^2y}{dx^2}\right)_{x=a}$$

and assuming c to be small, the frequency equation can be simplified to the final form

$$[\cosh\beta l\cdot\cos\beta l - 1] = \frac{1}{4}\left(\frac{1}{\alpha} - 1\right)\left(\frac{c}{l}\right)(\beta l)\left\{[\cosh\beta a - \cos\beta a] - \left[\frac{\sinh\beta l + \sin\beta l}{\cosh\beta l - \cos\beta l}\right][\sinh\beta a - \sin\beta a]\right\} \times \{[\sinh\beta(l-a) - \sin\beta(l-a)][\cosh\beta l - \cos\beta l] + [-\cosh\beta(l-a) + \cos\beta(l-a)][\sinh\beta l - \sin\beta l]\} \quad [22]$$

Equation [22] is a function of three dimensionless parameters, namely, βl, βa, and $[(1/\alpha) - 1](c/l)$. The depth and width of the slot is described by the quantity $[(1/\alpha) - 1](c/l)$, while its position along the beam is specified by βa.

Equation [22] must reduce to the frequency equation for a uniform beam, $\cosh\beta l\cos\beta l - 1 = 0$, when the discontinuity is reduced to zero. Examination of the equation shows that this condition is satisfied when

$c = 0$ (width of slot $= 0$)
$\alpha = 1$ (depth of slot $= 0$)
$a = 0$, or l (position of slot is at either end of beam)

Numerical computations for a slot at mid-span ($a = l/2$) were carried out and each side of Equation [22] was plotted as function of βl in Fig. 6 for various values of the slot parameter $[(1/\alpha) - 1](c/l)$. Since this quantity appears only as a factor in the right side of the frequency equation, the variation in the slot dimensions for any given position a can be obtained from a single curve with different values of the multiplier $[(1/\alpha) - 1](c/l)$.

Examination of Fig. 6 indicates that minute cracks in beams

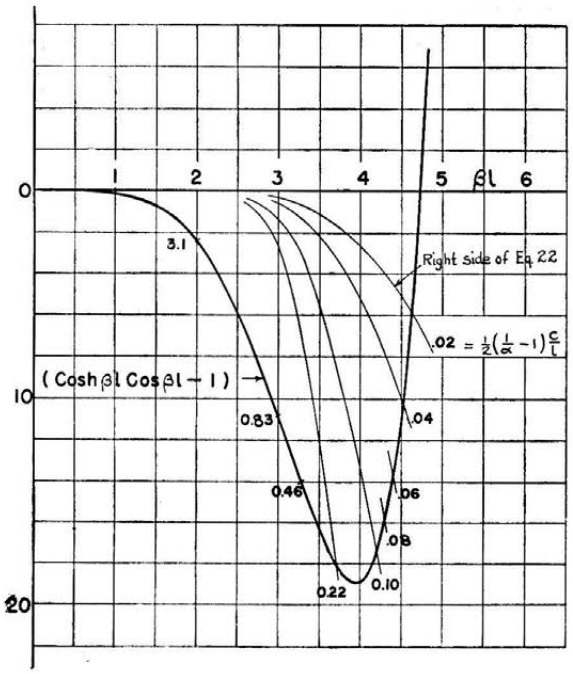

FIG. 6 FLEXURAL VIBRATION: PLOT OF FREQUENCY EQUATION [22] FOR $a = l/2$, AND VARYING VALUES OF THE SLOT PARAMETER $[(1/\alpha) - 1](c/l)$

have only a small influence on the natural frequencies. For deeper slots, the quantity

$$\left(\frac{1}{\alpha} - 1\right) = \left(\frac{I_0}{I_0'} - 1\right)$$

increases quite rapidly and the change in the natural frequency due to a change in the slot dimensions becomes considerably larger. For higher modes, the trigonometric terms become negligible compared to the hyperbolic terms and

$$\cosh \beta l \cong \sinh \beta l \cong \frac{1}{2} e^{\beta l}$$

The right side of Equation [22] then approaches zero while the curve for the left side is nearly vertical. It is evident then that the effect of the slot on higher modes is negligible.

LONGITUDINAL AND TORSIONAL VIBRATION OF BARS

For the longitudinal vibration of a bar with a narrow slot of width c, a distance a from one end, the equivalent uniform bar must be loaded with axial loads

$$P' = P_a\left(\frac{1}{\alpha} - 1\right)$$

at $x = a$ and $x = a + c$. Assuming harmonic motion, the differential equation for this case becomes

$$AE\frac{d^2U}{dx^2} + \left(\frac{\omega^2 A\rho}{g}\right)U = -P'[u_i(x - a) - u_i(x - a - c)] \quad \ldots\ldots[23]$$

where the concentrated loads are represented by the unit impulse.

The transform of Equation [23] is

$$U(s) = -\frac{P'}{AE}\left\{\frac{e^{-as} - e^{-(a+c)s}}{s^2 + \beta^2}\right\} + \frac{sU(0)}{s^2 + \beta^2} + \frac{U'(0)}{s^2 + \beta^2} \quad \ldots\ldots[24]$$

where

$$\beta^2 = \left(\frac{\omega^2\rho}{Eg}\right)$$

Performing the inverse transformation, we obtain the following equation

$$U(x) = -\frac{P'}{AE\beta}[\sin \beta(x - a)u(x - a) - \sin \beta (x - a - c)\, u(x - a - c)] + U(0)\cos \beta x + \frac{U'(0)}{\beta}\sin \beta x \ldots\ldots[25]$$

For a free-free bar $U'(0) = U'(l) = 0$, and letting $U(0) = 1$, the frequency equation from the second boundary conditions becomes

$$\sin \beta l = \frac{-P_a\left(\frac{1}{\alpha} - 1\right)}{AE\beta}[\cos \beta, (l - a) - \cos \beta(l - a - c] \quad \ldots\ldots[26]$$

Since P_a is the axial tension just to the left of the crack, we have

$$P_a = AE\left(\frac{\partial U}{\partial x}\right)_{x=a} = -AE\beta \sin \beta a \ldots\ldots[27]$$

Substituting Equation [27] in [26], and assuming c to be small, the final form of the frequency equation becomes

$$\sin \beta l = \left(\frac{1}{\alpha} - 1\right)\left(\frac{c}{l}\right)(\beta l)\sin \beta a \sin \beta(l - a) \ldots[28]$$

Equation [28] also reduces to that of the uniform rod, when the slot dimensions approach zero, or when its position approaches either end of the rod. If the depth of cut is extended completely through the rod, $1/\alpha = \infty$, and we obtain the frequency equation $\sin \beta a = 0$ and $\sin \beta(l - a) = 0$, corresponding to the natural modes of the two severed rods.

Numerical computations from Equation [28] are again carried out for a slot at mid-length ($a = l/2$), and the plotted curve in Fig. 7 shows that the natural frequencies are lowered by the slot as expected. Modes of vibration with a node at the center are of course not affected by the slot at $a = l/2$. Unlike the flexural case, the influence of the slot on the higher modes is greater than for the lower modes.

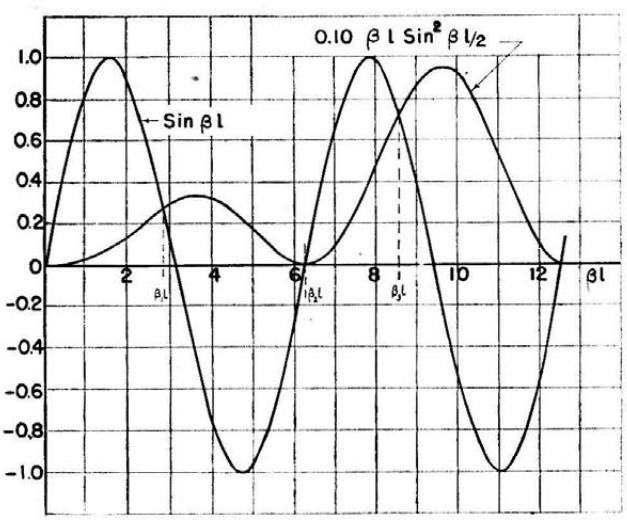

FIG. 7 LONGITUDINAL OR TORSIONAL VIBRATION: PLOT OF FREQUENCY EQUATION [28] FOR $a = l/2$, AND SLOT PARAMETER $[(1/\alpha) - 1](c/l) = 0.10$

Since the differential equation for the torsional vibration is the same as that of the longitudinal vibration, Equation [28] also applies for the torsional case with free ends provided

$$\beta^2 = \left(\frac{\omega^2\rho}{Gg}\right)$$

Conclusion

A procedure is developed for the determination of the vibrational characteristics of slender bars with discontinuities in stiffness due to a narrow slot or crack. Interpretation of the results is illustrated by the numerical computation of the natural frequencies for a special case of $a = l/2$. No attempt is made to determine the equivalent slot accounting for the ineffective material adjacent to the slot. This the author believes can be carried out experimentally by vibrating bars in flexure, torsion, and longitudinally with various width and depth of slot at various positions a along the beam. It would also be of interest to obtain the same reduction in cross section by different means such as drilling holes instead of cutting slots.

Correlation of Tension Creep Tests With Relaxation Tests

By IRVING ROBERTS,[1] JEANNETTE, PA.

This paper shows that analytical solutions to the bolt relaxation problem, based upon empirical creep-data equations may be obtained by direct substitution, rather than by differentiation and integration, as was done by Soderberg, Popov, and Housner.

IN order to predict relaxation rates from tension creep data, Soderberg[2] has presented the following analysis of the problem: The bolt is assumed to be originally tightened on rigid flanges, so that

$$\epsilon_e + \epsilon_p = \epsilon^* = \text{const} \quad [1]$$

where ϵ^* is the initial elastic strain. The elastic strain at any time ϵ_e, is given by

$$\epsilon_e = \frac{\sigma}{E} \quad [2]$$

where E, the elastic modulus, is assumed constant. The plastic strain ϵ_p, is assumed from creep data to be a continuous function of stress σ, and of time t, of the form

$$\epsilon_p = \frac{s_1}{E}\left(e^{\sigma/s_1} - 1\right) T \quad [3]$$

where T is a time function, one form of which may be

$$T = ct^m \quad [4]$$

but which is handled as a single variable.

Equation [1] is differentiated to give

$$\frac{d\epsilon_e}{dt} + \frac{d\epsilon_p}{dt} = 0 \quad [5]$$

Equations [2] and [3] are then differentiated and substituted into Equation [5], giving

$$d\sigma = -s_1 \frac{e^{\sigma/s_1} - 1}{1 + Te^{\sigma/s_1}} dT \quad [6]$$

Soderberg states that this differential equation cannot be integrated readily, and numerical integration is suggested.

In a recent paper,[3] Popov has made a thorough comparison of the methods which have been proposed for solution of the relaxation problem, including not only Soderberg's analytical method, but also arithmetical and graphical methods based upon various assumptions, notably that of strain-hardening. In using Soderberg's method, Popov also states that Equation [6] cannot be integrated readily, and he uses numerical integration for his comparison. It is of interest that the numerical integration of Equation [6] is found to be in good agreement with the results given by the strain-hardening method.

In his discussion of the Popov paper, Housner[4] states that he has integrated Equation [6] obtaining

$$T = \frac{1}{s_1} \frac{(\sigma_0 - \sigma)}{(e^{\sigma/s_1} - 1)} \quad [7]$$

where σ_0 is the stress at $T = 0$. Housner also integrates a differential equation given by Popov for the case of relaxation with elastic follow-up.

The author wishes to point out that it is not necessary to proceed through differentiation and integration to obtain a solution to this problem. Since both ϵ_e and ϵ_p are assumed to be continuous functions of σ and t (or T), Equations [2] and [3] may be substituted directly into Equation [1], giving

$$\frac{\sigma}{E} + \frac{s_1}{E}(e^{\sigma/s_1} - 1)\, T = \epsilon^* \quad [8]$$

Remembering that

$$\epsilon^* E = \sigma_0 \quad [9]$$

Equation [7] is obtained directly. The other solutions given by Housner may be obtained also by simple substitution in the same manner.

With this simplification, it is possible that Soderberg's analytical method may find wider application in the solution of problems of a similar nature.

---

[1] Division Engineer, Process Division, Research and Development Department, Elliott Company. Mem. ASME.

[2] "The Interpretation of Creep Tests for Machine Design," by C. R. Soderberg, Trans. ASME, vol. 58, 1936, pp. 733–743.

[3] "Correlation of Tension Creep Tests With Relaxation Tests," by E. P. Popov, JOURNAL OF APPLIED MECHANICS, Trans. ASME, vol. 69, 1947, p. A-135.

[4] Ibid., discussion by G. W. Housner, p. A-352.

Note on the Bending of Circular Plates of Variable Thickness

By H. D. CONWAY,[1] ITHACA, N. Y.

In a recent paper[2] a solution was given to the problem of a symmetrically loaded circular plate with a central hole, the thickness of the plate at any section being proportional to the distance of the section from the center of the plate. A very simple solution can be obtained for another variation of thickness of which the foregoing is a special case.

IN this problem, making the usual assumptions, the differential equation to be solved is

$$D\frac{d}{dr}\left(\frac{d\phi}{dr}+\frac{\phi}{r}\right)+\frac{dD}{dr}\left(\frac{d\phi}{dr}+\nu\frac{\phi}{r}\right)=-Q \quad \ldots\ldots [1]$$

where D is the flexural rigidity, ϕ the slope of the middle surface at radius r, and Q is the shearing force per unit circumferential length of plate. Many variations of thickness can be represented approximately in the form $D = D_0 r^m$ where D_0 and m are constants. Using this variation of flexural rigidity, Equation [1] becomes

$$r^2\frac{d^2\phi}{dr^2}+(m+1)r\frac{d\phi}{dr}-(1-m\nu)\phi=-\frac{Q}{D_0 r^{m-2}} \quad \ldots [2]$$

For a load P uniformly distributed around a central hole, this equation becomes

$$r^2\frac{d^2\phi}{dr^2}+(m+1)r\frac{d\phi}{dr}-(1-m\nu)\phi=-\frac{P}{2\pi D_0 r^{m-1}} \quad \ldots [3]$$

the general solution of which is

$$\phi = Ar^{\frac{2\alpha-m}{2}}+Br^{-\left(\frac{2\alpha+m}{2}\right)}+\frac{P}{2\pi D_0 m r^{m-1}(1-\nu)} \quad \ldots [4]$$

where $4\alpha^2 = 4 - 4m\nu + m^2$. The constants A and B are then obtained from the boundary conditions in the usual manner, and the stresses and deflections found.

As an example, the case of a plate with the external edge clamped and supported and the internal edge clamped, may be considered. Denoting by a and b the external and internal radii, respectively, the constants A and B are

$$A=\frac{Pa^{1-p}}{2\pi D_0 m(1-\nu)}\left\{\frac{n^{p-1}-n^{2\alpha}}{n^{2\alpha}-1}\right\}$$

$$B=\frac{-Pa^{1+q}}{2\pi D_0 m(1-\nu)}\left\{\frac{n^{p-1}-1}{n^{2\alpha}-1}\right\}$$

where $2p = 2\alpha + m$, $2q = 2\alpha - m$, and $n = a/b$.
Hence

$$\phi=\frac{P}{2\pi D_0 m(1-\nu)}\left\{r^{1-m}-\frac{a^{1-p}r^{-p}}{n^{2\alpha}-1}[a^{2\alpha}(n^{p-1}-1)-r^{2\alpha}(n^{p-1}-n^{2\alpha})]\right\}$$

$$\frac{d\phi}{dr}=\frac{P}{2\pi D_0 m(1-\nu)}\left\{(1-m)r^{-m}+\frac{a^{1-p}r^{-1-p}}{n^{2\alpha}-1}[pa^{2\alpha}(n^{p-1}-1)+qr^{2\alpha}(n^{p-1}-n^{2\alpha})]\right\}$$

The bending moments calculated from the well-known equations

$$M_r = D\left(\frac{d\phi}{dr}+\nu\frac{\phi}{r}\right)$$

$$M_\theta = D\left(\frac{\phi}{r}+\nu\frac{d\phi}{dr}\right)$$

are then given by

$$M_r=\frac{P}{2\pi m(1-\nu)}\left\{1-m+\nu+\frac{1}{r^{q+1}a^{p-1}(n^{2\alpha}-1)}[(p-\nu)a^{2\alpha}(n^{p-1}-1)+(q+\nu)r^{2\alpha}(n^{p-1}-n^{2\alpha})]\right\}$$

$$M_\theta=\frac{P}{2\pi m(1-\nu)}\left\{1-m\nu+\nu+\frac{1}{r^{q+1}a^{p-1}(n^{2\alpha}-1)}[(\nu p+1)a^{2\alpha}(n^{p-1}-1)+(\nu q-1)r^{2\alpha}(n^{p-1}-n^{2\alpha})]\right\} \quad \ldots [5]$$

The positions of the maximum stresses calculated by the use of Equations [5] will vary with the value of the constant m and are best found by graphical methods.

For a linear variation of thickness, $m = 3$. Assuming that Poisson's ratio is $1/3$, Equation [5] becomes

$$M_r=\frac{P}{12\pi}\frac{a^2(n+1)(8a-5nr)-r(5a^2+n^2r^2)}{a^2r(n^2+n+1)}$$

$$M_\theta=\frac{P}{12\pi}\frac{2a^2(n+1)(3a+2nr)+r(4a^2+3n^2r^2)}{a^2r(n^2+n+1)} \quad \ldots [6]$$

Integrating Equation [4] and finding the new constant of integration from the condition of zero deflection at the outer edge of the plate, the maximum deflection is

$$\omega_{max}=\frac{Pa^{2-m}}{2\pi D_0 m(1-\nu)}\left\{\frac{n^{m-2}-1}{m-2}-\frac{1}{n^{2\alpha}-1}\left[\frac{(n^{p-1}-n^{2\alpha})(n^{-1-q}-1)}{q+1}+\frac{(n^{p-1}-1)^2}{p-1}\right]\right\} \quad \ldots\ldots [7]$$

Placing $m = 3$ in this equation and assuming that Poisson's ratio

[1] Professor of Mechanics, Cornell University. Jun. ASME.

[2] "The Bending of Symmetrically Loaded Circular Plates of Variable Thickness," by H. D. Conway, JOURNAL OF APPLIED MECHANICS, Trans. ASME, vol. 70, March, 1948, pp. 1–6.

Contributed by the Applied Mechanics Division and presented at the Annual Meeting, New York, N. Y., November 28–December 3, 1948, of THE AMERICAN SOCIETY OF MECHANICAL ENGINEERS.

Discussion of this paper should be addressed to the Secretary, ASME, 29 West 39th Street, New York, N. Y., and will be accepted until July 11, 1949, for publication at a later date. Discussion received after the closing date will be returned.

NOTE: Statements and opinions advanced in papers are to be understood as individual expressions of their authors and not those of the Society. Paper No. 48—A-6.

is $^1/_3$ and that the thickness at the outer edge is H, the maximum deflection is

$$\omega_{max} = \frac{4Pa^2}{3\pi EH^3} \frac{(n-1)^3}{n^2+n+1} \quad [8]$$

For the case of a plate subjected to a uniformly distributed load w per unit area

$$Q = \frac{1}{r} \int_b^r wrdr$$

and Equation [1] becomes

$$r^2 \frac{d^2\phi}{dr^2} + (m+1)r \frac{d\phi}{dr} - (1-m\nu)\phi = \frac{-w(r^2-b^2)}{2D_0 r^{m-1}} \quad [9]$$

The general solution of this equation is

$$\phi = Ar^{\frac{2\alpha-m}{2}} + Br^{-\left(\frac{2\alpha+m}{2}\right)} - \frac{W}{2D_0 r^{m-1}} \left\{ \frac{r^2}{8-3m+m\nu} + \frac{b^2}{m(1-\nu)} \right\} \quad [10]$$

The expressions are seen to be rather cumbersome, and there is no particular value in obtaining expressions for the deflections and stresses with other boundary conditions.

Stresses and Displacements in a Semi-Infinite Elastic Body With Parabolic Cross Section Acted on by Its Own Weight Only

By R. J. HANK[1] and F. H. SCRIVNER,[2] AUSTIN, TEXAS

The earlier solution for the stress distribution in a semi-infinite elastic wedge is compared with the solution for a cross section of parabolic shape. Displacement diagrams for two extreme values of Poisson's ratio are given for the parabolic section.

Introduction

In 1898, Levy,[3] and in 1912, Fillunger[4] published the solution for the stress distribution in a semi-infinite elastic wedge. The solution was discussed at length by Terzaghi.[5]

The present solution is similar to the wedge solution but applies to cross sections of parabolic shape.

Statement of the Problem

Fig. 1 represents the cross section of the body, taken perpendicular to the z-axis. All cross sections taken from $z = -\infty$ to $z = +\infty$ are assumed identical, and the problem of stress determination is one of plane deformation. Gravity acts in the positive direction of the y-axis, and no other forces act on the body.

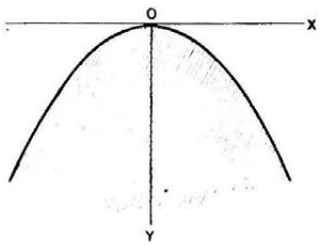

Fig. 1 Semi-Infinite Body With Boundary Equation, $y = ax^2$

The equation of the boundary is

$$y = ax^2 \quad \ldots\ldots [1]$$

where a is an arbitrary constant.

The Stress Function

Employing the methods outlined by Timoshenko,[6] it can be shown that the boundary and all other conditions required by the theory of elasticity are satisfied if the Airy stress function ϕ, is taken in the form

$$\phi = -\frac{w}{3}x^2y - \frac{1}{12}\frac{w}{a}y^2 \quad \ldots\ldots [2]$$

where w = weight per unit of volume of the material.

Stress and Displacement Equations

The components of stress corresponding to Equation [2] are

$$\left.\begin{aligned} \sigma_x &= -\frac{w}{6a}y \\ \sigma_y &= -\frac{2w}{3}y \\ \tau_{xy} &= -\frac{w}{3}x \end{aligned}\right\} \quad \ldots\ldots [3]$$

and the associated displacements are

$$\left.\begin{aligned} u &= \frac{-w(1+\mu)}{3E}\left[\frac{(1-\mu)}{2a}x - 2\mu xy\right] \\ v &= \frac{-w(1+\mu)}{3E}\left[(1-\mu)y^2 - \frac{\mu}{2a}y + (1+\mu)x^2\right] \end{aligned}\right\} \quad .[4]$$

where

σ_x = horizontal normal stress
σ_y = vertical normal stress
τ_{xy} = shear stress in xz- and yz-planes
u = displacement parallel to the x-axis
v = displacement parallel to the y-axis
μ = Poisson's ratio
E = Young's modulus

Displacements at Certain Locations Within Cross Section

Equations [4] lead to the following conclusions:

1 A plane surface containing points of zero horizontal displacement passes through the body. Its equation is

$$y = \frac{1-\mu}{4a\mu} \quad \ldots\ldots [5]$$

Horizontal lines located above this plane are shortened; those below it are lengthened.

2 A curved closed surface, containing points of zero vertical

---

[1] Materials and Tests Engineer, Texas Highway Department.

[2] Senior Research Engineer, Texas Highway Department.

[3] "Sur la Légitimité de la Regle Dite du Trapeze dans l'étude de la Resistance des Barrages en Maconnerie," by M. Levy, Académic des Science, Paris, France, Comptes Rendus hebdomadaires des séances, vol. 126, 1898, pp. 1235–1240.

[4] "Drei wichtige ebene Spannungszustände des keilformigen Körpers," by P. Fillunger, *Zeit. fur Mathematik und Physik*, Leipzig, Germany, vol. 60, 1912, pp. 275–285.

[5] "Theoretical Soil Mechanics," by K. Terzaghi, John Wiley & Sons, Inc., New York, N. Y., 1943, pp. 406–409 and 429–430.

Contributed by the Applied Mechanics Division and presented at the Annual Meeting, New York, N. Y., November 28–December 3, 1948, of The American Society of Mechanical Engineers.

Discussion of this paper should be addressed to the Secretary, ASME, 29 West 39th Street, New York, N. Y., and will be accepted until July 11, 1949 for publication at a later date. Discussion received after the closing date will be returned.

Note: Statements and opinions advanced in papers are to be understood as individual expressions of their authors and not those of the Society. Paper No. 48—A-27.

[6] "Theory of Elasticity," by S. Timoshenko, McGraw-Hill Book Company, Inc., New York, N. Y., and London, first edition, 1934, pp. 12–51.

displacement, lies within the upper portion of the body. It is given by

$$y = \frac{\mu \pm \sqrt{\mu^2 - 16a^2(1-\mu^2)x^2}}{4a(1-\mu)} \quad [6]$$

All points enclosed by this surface move downward during deformation. All points outside the surface move upward.

3 A plane surface of zero vertical strain passes through the body. Its equation is

$$y = \frac{\mu}{4a(1-\mu)} \quad [7]$$

Vertical lines above this plane are elongated; below it, they are shortened. It can be seen by comparing Equation [7] with Equation [5] that the planes represented by these two equations coincide when Poisson's ratio is $1/2$.

For Poisson's ratio $\mu = 0$, surface, Equation [6], becomes imaginary; surface, Equation [7], ceases to exist; and surface, Equation [5], exists only at an infinite distance below the origin.

Displacement Diagrams

Fig. 2 illustrates the displacements in the upper portion of the body when the value of Poisson's ratio is $1/2$. The length of each arrow in the figure is proportional to the magnitude of the displacement of a point located at the feather of the arrow, while the direction of the arrow is the direction of the displacement.

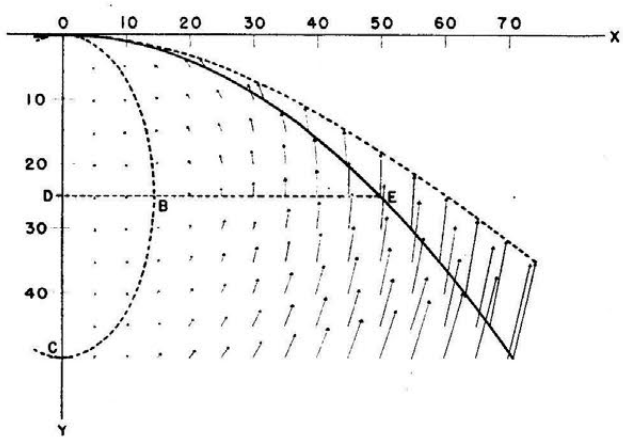

Fig. 2 Displacements for Poisson's Ratio = $1/2$
(*OBC* is surface of zero vertical displacement; *DE* is surface of zero horizontal displacement and zero vertical strain.)

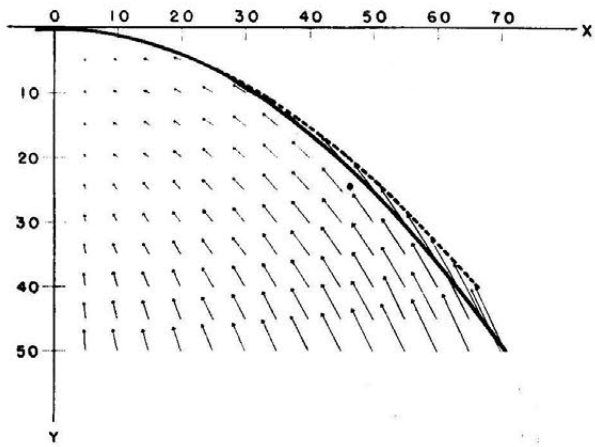

Fig. 3 Displacements for Poisson's Ratio = 0

Fig. 3 shows displacements when Poisson's ratio is zero.

For both figures, the factor w/E, in the displacement Equations [4], was set equal to 0.004, while the constant a, in the boundary equation was assigned a value of 0.01. Thus the differences in magnitude and direction of arrows, representing corresponding points in the two diagrams, result solely from the differences in the assigned values of Poisson's ratio.

Application—Conditions at Foundation

Conditions at a rough rigid boundary, parallel to the xz-plane, would require that $(\partial v)/(\partial x) = 0$ and that $u = 0$ for all points on this boundary. From the second of Equations [4]

$$\frac{\partial v}{\partial x} = \frac{-2w(1+\mu)^2 x}{3E} \quad [8]$$

From Equation [5]

$$u = 0 \text{ at } y = \frac{1-\mu}{4a\mu} \quad [9]$$

Equation [8] precludes the existence of the exact conditions necessary for a rigid boundary, as might have been expected. Also, from the principle of the uniqueness of the solution, it may be concluded that the conditions necessary for the existence of a horizontal elastic foundation are absent.

From these considerations, and according to the principle of Saint Venant, it may be concluded that the solution could be legitimately applied only to a limited region in a cross section having a large height-to-base ratio. The same restriction of course applies to the solution for the triangular cross section, Fig. 4.

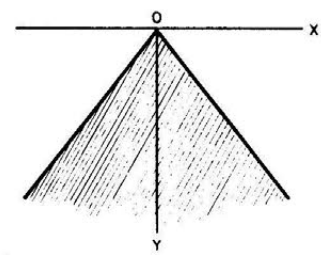

Fig. 4 Semi-Infinite Body With Boundary Equation, $y = \pm ax$

Comparison With Solution for Elastic Wedge

The similarity of the foregoing solution to that for the elastic wedge may be seen by comparing Equations [2] and [3] with the following equations which apply to the wedge, Fig. 4

$$\phi = -\frac{w}{4}x^2 y - \frac{w}{12a^2}y^3 \quad [10]$$

$$\left.\begin{aligned} \sigma_x &= -\frac{w}{2a^2}y \\ \sigma_y &= -\frac{w}{2}y \\ \tau_{xy} &= -\frac{w}{2}x \end{aligned}\right\} \quad [11]$$

where the equation of the boundary is

$$y = \pm ax \quad [12]$$

Acknowledgment

The authors wish to thank Dr. Dana Young of the University of Texas, who read the manuscript and at whose suggestion the paper was prepared.

Discussion

Vibration of a Cantilever Beam With Prescribed End Motion[1]

R. V. Churchill.[2] The author presents an interesting and accurate analysis of the transverse forces occurring at the movable end of a cantilever beam when that end is made to move in certain prescribed ways. The three types of end motions which are considered are simple ones related to physical applications. His examination of conditions under which the end force undergoes a reversal in sign is especially pertinent. The details of his mathematical analysis are presented clearly and concisely. Readers not familiar with the modern form of Heaviside's operational calculus will need to do some collateral reading to follow the steps; but, to some degree, this situation is bound to be unavoidable. The assumption in problem D that $2\pi/d \neq q_n$[2] was not explicitly pointed out. In case $2\pi/d$ is equal to one of the numbers q_n, a new type of term is involved in the series which represents the end force; but this special case seems to have no very great significance.

Author's Closure

Professor Churchill's comments are appreciated. In problem D, the inequality to which he refers is indeed necessary for the solution as presented. However, the values of d for which the curves of Fig. 8 are plotted are such that $\frac{2\pi}{d} < q_1$ so that the inequality is satisfied.

Centrifugal and Thermal Stresses in Rotating Disks[1]

Florence F. Buckland.[2] The method described in this paper seems to be a handy scheme for calculating stresses, but certain parts of the paper need to be clarified.

In the introduction it is stated that the radial temperature gradient may be expressed as kr^n. Radial temperature distribution is what is meant.

The nomenclature lacks several important symbols, including s and t. Also t is used for temperature as well. Y and Z do not need to be included, except for saying Y, Z, M, F, h, p, w, and y are defined where they occur.

The tabular form sheet starts with 25,000 psi radial rim stress which may be assumed to mean only two significant figures. The numerical operations performed end up with five and six significant figures. This is an example of the unnecessary precision of a calculating machine giving results which are by no means justified by the primary data.

It would be helpful to know the constants in the equation for temperature distribution given in Fig. 3.

R. A. Strub.[3] The method of calculating thermal stresses in disks presented in this paper has the advantage of being simple but is limited to a given type of temperature distributions. However, this limitation is wide enough to permit the calculation of thermal stresses in most cases encountered in turbine disks. A generalization can, however, be reached if the temperature gradient of each elementary ring is taken as a constant. The radial temperature distribution in the disk can then be split up into elements of straight lines. The true temperature distribution is thus approximated by a polygonal line. When proceeding thus, the functions Y and Z will have a discontinuity each time the temperature gradient changes. The graphical method for the computation of s and t developed by R. Grammel can still be used, and the condition $\Delta\sigma_t = \mu\Delta\sigma_r$ remains unchanged.

Such a procedure will give a sufficiently accurate result for the field of thermal stress due to any temperature distribution.

A somewhat similar method can be used in introducing the radial and tangential thermal stresses due to a constant gradient of temperature, and for the following boundary condition at the inner radius of each elementary ring $\sigma_r = 0$; $\sigma_t = 0$. The corresponding stresses at any radius of the elementary ring are given by

$$\sigma_r = t_0 \cdot \alpha \cdot E\left[-\frac{1}{6}\frac{1}{\rho^2} + \frac{1}{2} - \frac{1}{3}\rho\right]$$

$$\sigma_t = t_0 \cdot \alpha \cdot E\left[\frac{1}{6}\frac{1}{\rho^2} + \frac{1}{2} - \frac{2}{3}\rho\right]$$

in which ρ is the ratio of any radius to the inner radius of an elementary ring and t_0 the temperature at the inner radius, the elementary distribution of temperature being given by $t = t_0\rho$. The method described by R. Grammel for centrifugal forces only can be used for determining s and t and the stresses given by the foregoing relations are added at the outer diameter of the elementary ring. The boundary conditions at the inner diameter are unaffected.

A somewhat similar method has been developed by the writer in an unpublished work, "A General Method of Calculating Mechanical and Thermal Stresses in Disks and Tubes." The method is semigraphical and makes use of elements consisting of conical convergent and divergent disks and introduces the variation of the modulus of elasticity and of the coefficient of linear thermal expansion with temperature.

J. T. Wang.[4] This is a brilliant paper except that a revision is necessary in the viewpoint of the distribution of temperatures in the disk. Neglecting the variation of the temperatures along the axis of the disk, the differential equation of temperature distribution symmetrical with respect to the axis is

$$\frac{\partial^2 t}{\partial r^2} + \frac{1}{r}\frac{\partial t}{\partial r} = 0$$

The solution of the differential equation is

$$t = \frac{1}{\log\frac{b}{a}}\left[(t_b - t_a)\log r - (t_b \log a - t_a \log b)\right]$$

---

[1] By G. A. Nothmann, published in the December, 1948, issue of the Journal of Applied Mechanics, Trans. ASME, vol. 70, pp. 327–334.

[2] Professor of Mathematics, University of Michigan, Ann Arbor, Mich.

[1] By W. R. Leopold, published in the December, 1948, issue of the Journal of Applied Mechanics, Trans. ASME, vol. 70, pp. 322–326.

[2] General Engineering and Consulting Laboratory, General Electric Company, Schenectady, N. Y.

[3] Research Mechanical Engineer, E. I. du Pont de Nemours & Company, Inc., Belle Works, W. Va.

[4] Professor of Machine Design, University of Chekiang, China; Visiting Consulting Engineer, Allis-Chalmers Manufacturing Company, Milwaukee, Wis.

TABLE 1 ANALYTICAL RESULTS OF AUTHOR'S PROBLEM

1		3	4	5	6	7	8	9	10	11	12	13	14	15	16
Sect.	r	r^2	$10^3 w$	$\beta_1\omega^2 r^2$	$\beta_2\omega^2 r^4$	Y	Z	y	$\frac{-\Delta y}{y+\Delta y}$	σ_r	Δs	Δt	σ_t	$\sigma_{t\theta}$	$\sigma_{r\theta}$
1	12.5	156	6.41	35100	20200	0	−33800		.....	25000	.....	.....	6900	6560	25000
								1.2		0			2000		
2	11	121	8.26	27200	15700	4080	−27800		0.200	36980	7400	2220	16600	17320	40735
								1.0		−290			2290		
3	9	81	12.35	18250	10500	10100	−17850		−0.167	60640	−10100	−3030	32680	30660	55740
								1.2		−987			2913		
4	7	49	20.4	11000	6350	16200	−3980		−0.250	64117	−16000	−4800	47473	44340	56430
								1.6		−2063			4197		
5	4.5	20.25	49.4	4550	2620	20000	27400		−0.200	51195	−10240	−3072	84925	81900	47000
								2.0		−5720			8520		
6	2.75	7.58	132	1705	983	0	87000			−2716	.....	.....	169600	166150	0
										−15810			20110		

By using this expression of temperature instead of $t = t_a + kr^n$ as proposed by the author, we have, instead of his expressions of Y and Z, the new expressions

$$Y = \frac{E\alpha(t_b - t_a)}{2\log\frac{b}{a}}\left[\frac{\log b - \left(\frac{a}{b}\right)^2 \log a - \left(\frac{a}{r}\right)^2 \log\frac{b}{a}}{1 - \left(\frac{a}{b}\right)^2} - \log r\right]$$

$$Z = \frac{E\alpha(t_b - t_a)}{2\log\frac{b}{a}}\left[\frac{\log b - \left(\frac{a}{b}\right)^2 \log a + \left(\frac{a}{r}\right)^2 \log\frac{b}{a}}{1 - \left(\frac{a}{b}\right)^2} - (\log r + 1)\right]$$

By this rational method, the results of analysis of the same problem illustrated at the end of the paper is shown in Table 1 herewith. Comparing it with the author's original solution, the difference in the maximum stress is about 25 per cent. The representation of the temperature gradient by the author's formula is, in fact, impossible. A better form of the equation is $t = t_a + K(r - r_a)^n$. Nevertheless, the rational formula is no more complicated than the empirical. The use of the latter is therefore not justified particularly with the view that the values of n and k will vary with each particular case. The rational formula will give a completely determined temperature gradient as soon as the boundary temperatures are known.

Author's Closure

In the preparation of this paper, the terms "gradient" and "distribution" were both considered for the expression kr^n. Both appeared correct from dictionary definitions, but the term gradient was chosen since it seemed to connote more accurately the author's intended significance of the expression. Inasmuch as the choice of words does not affect the meaning or the method proposed in the paper, the choice remains with the reader. Since the temperature curve in the sample calculation was an arbitrary assumption for purposes of illustration, the values of the constants were not given. Any one of several well-known methods of determining such constants will show that $n = 5$ and $k = 0.001805$.

The author agrees with the assumptions that Mr. R. A. Strub suggests. However, it is believed that the method proposed in the paper is more accurate without the addition of serious complication of computations, especially in the case of a rapidly changing temperature curve. The method proposed by the author is limited to temperature curves which continually increase or decrease for exact analysis. However, in the case of rotating disks, this type of temperature curve is a generalized case rather than a limited one. If however, a temperature curve which does not continually increase or decrease is encountered, several fairly accurate methods are available which transform these curves to the type of expression used by the author. The resulting expression is of course approximate, although a high degree of accuracy still exists. This type of transformation allows the method proposed to be used in almost any problem encountered.

The comments of Professor Wang are interesting, although quite misleading. The differential equation proposed by Professor Wang is obtained by neglecting several terms from the following differential equation

$$\frac{\partial t}{\partial T} = K\left[\frac{\partial^2 t}{\partial r^2} + \frac{1}{r^2}\frac{\partial t}{\partial r} + \frac{1}{r^2}\frac{\partial^2 t}{\partial \theta^2} + \frac{\partial^2 t}{\partial Z^2}\right]$$

where

T = time
Z = axial axis
θ = angular displacement of a point on disk

Since a steady-state condition is assumed $\partial t/\partial T = 0$. Further, since the disk is subjected to a uniform temperature distribution circumferentially

$$\frac{1}{r^2}\frac{\partial^2 t}{\partial \theta^2} = 0$$

However, by neglecting the term $\partial^2 t/\partial Z^2$, Professor Wang assumes that no heat transfer takes place through the sides of the disk, which of course makes his expression very limited in application. The method proposed by the author assumes that transfer can exist through the sides of the disk, but assumes that, since the axial dimension is small, the stress resulting from a gradient in that direction is negligible.

The author has taken the liberty of plotting the temperature gradient obtained from the equation proposed by Professor Wang. Fig. 1 of this closure shows the resulting temperature curve, as well as the one used by the author in the sample problem. The difference between the two curves results in the 25 per cent increase in maximum stress as reported by Professor Wang. The versatility of the method proposed by the author is again illustrated since, by using a value of $n = 0.156$, $k = 1730$, Professor Wang's curve is duplicated, and the stresses Professor Wang predicts with his temperature-curve result.

In defining temperature gradient in the paper, the gradient was stated to exist from the absolute center of the disk to the rim and

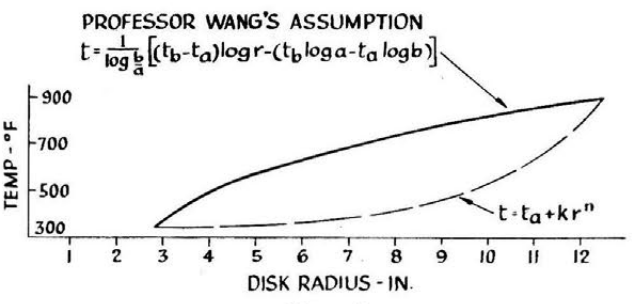

Fig. 1

hence the equation $t = t_i + kr^n$ does exist. Since the temperature gradients in a disk with a central hole have a small change of slope at the hole, the error introduced by neglecting the r_a term proposed by Professor Wang is negligible.

It is evident from Professor Wang's comments that the fact of this method's, being general for any temperature gradient actually existing in the disk was not clearly presented. These various gradients can exist from heat transfer through the sides of the disk, various types of cooling, predictions from previously measured data or calculated by other means. For these reasons, a theoretical expression as suggested by Professor Wang was not used as it is too limited in scope. It is hoped that the foregoing has clarified this point.

Stress-Strain Laws of the Mathematical Theory of Plasticity—A Survey of Recent Progress[1]

R. Hill.[2] The author has given a comprehensive and admirably lucid survey of the stress-strain relations which have been suggested by various writers for a plastically deforming metal. As he has mentioned, there are, broadly speaking, two main types of stress-strain relations, which have been designated by Ilyushin flow and deformation theories, respectively. It would be preferable to speak rather of differential and finite strain theories, since "flow" has a special significance in metal physics, connoting deformation brought about by thermal activation under constant external stress. It appears inappropriate to apply it to describe a theory for a work-hardening metal in which plastic deformation under constant stress is not possible, and where the element of time is absent.

In the differential-strain theory (typified by the Reuss equations) the ratios of the components of the plastic-strain increment (or velocity strain) are directly related to the ratios of the components of the current stress, while the increment of stress enters only in determining the magnitude of the strain increment (through the rate of work-hardening). The differential relations between the plastic-strain increment, stress, and stress increment are nonintegrable, and there is no unique relation between the current stress and the total strain (which may be of any magnitude). In the finite-strain theory, typified by the Hencky equations, the total strain (always assumed small and defined as in elasticity) is directly related to the current stress. The finite strain theories, in their present form, are not applicable to problems where the strains are large, for example, in most mechanical working processes.

It is easy to see that a finite-strain law is inappropriate for representing the observed behavior of a metal. Suppose an element of metal has been plastically deformed in some way, and then unloaded. If the element is now reloaded, under a different system of combined stresses, until it is again on the point of yielding, the change in strain during the unloading and reloading is purely elastic (secondary effects such as the hysteresis loop are disregarded in present theories). However, according to the finite-strain theory, a different plastic state of stress implies a different state of plastic strain. Consequently the finite-strain theory is not in agreement with observation.

The author refers to a similar objection raised by Handelman, Lin, and Prager with regard to neutral changes of stress, where the stress is changed in such a way that the element is kept just on the point of yielding. Differential-strain laws are free from these objections, as the author mentions. In the special case when the loading is such that the deviatoric stress components are increased proportionately, it is easy to show (as remarked in particular by Ilyushin) that the Hencky and Reuss laws agree in predicting the same process of deformation. In general, however, the finite- and differential-strain theories lead to different conclusions, especially when the change of stress tends to be nearly neutral.

A rather interesting comparison of the Hencky and Reuss equations is provided by the behavior of a thick-walled closed tube, expanded under internal pressure. Both theories agree in predicting that, with increasing plastic distortion, the axial stress tends to the mean of the radial and circumferential stresses, everywhere throughout the wall. Hence the Reuss theory implies that the successive increments of axial plastic strain tend to zero, so that the total axial plastic strain (of elastic order of magnitude) tends steadily to a maximum value. The Hencky theory, on the other hand, implies that the total axial plastic strain itself is finally zero, and thus that it reaches a maximum and then diminishes. It would be interesting to test this experimentally, the axial strain being measured of course between two sections well away from the ends.

In view of the shortcoming of finite-strain theories, it is a little surprising that they have been so much used in applications. There seem to be three possible reasons for this: (1) their mathematical convenience in small-strain problems, (2) their approximate agreement with experiment when the material is never unloaded and the stress changes are far from neutral, and (3) the lack of experiments specifically designed to discriminate between the two theories. It is, in a sense, unnecessary to perform such experiments, since the outcome of the unloading and reloading process mentioned previously is of course known. On the other hand it is not surprising that for certain loading paths the Hencky equations may give results more in agreement with observation than the Reuss equations. This was so, for example, in the experiment of Hohenemser, where a tube was twisted and then extended, while the twist was held constant. Since the theories can be compared only when the strains are small, a significant comparison is largely prevented by secondary effects (anisotropy, rounding of yield point, creep, and elastic after-effect), disregarded in both theories. The significance of Hohenemser's or similar experiments lies much more in a test of the Reuss equations. These are known not to be strictly accurate when the stress increment is negligible, owing to the deviations from the Lévy-Mises relation observed by Lode, and by Taylor and Quinney.

The author has discussed more general differential-strain theories which take these deviations into account. However, there is also the possibility that the stress increment may affect the ratios of the components of the plastic-strain increment. This possibility is not taken into account in present differential-strain theories. Its effect would be most pronounced where the elastic- and plastic-strain increments are comparable in magnitude.

On the general question as to what theory is best suited for practical applications, there seems no doubt that when the strains are large the Reuss theory is satisfactory. The error due to neglecting deviations from the Lévy-Mises relation is probably smaller than the accuracy required in most practical applications, particularly in view of random variations in the material itself. The inclusion of work-hardening within the framework of the Reuss equations, either by the concept of a generalized stress-strain curve, or by the equivalent assumption that the hardening is a function only of the plastic work, appears reasonably well confirmed so long as appreciable anisotropy is not developed during the straining. When an especially high

[1] By W. Prager, published in the September, 1948, issue of the Journal of Applied Mechanics, Trans. ASME, vol. 70, pp. 226–233.

[2] Cavendish Laboratory, Cambridge, England.

accuracy is required, and is justified by experimental technique, the Reuss equations will have to be replaced by some more general differential-strain theory of the type mentioned by the author. At the moment, however, theory has here outstripped experiment.

W. P. Roop.[3] The papers on the flow and fracture and the theory of plasticity of metals which were brought together at the Applied Mechanics Conference of June, 1948, were even more significant as a group than singly. Taken together they offer a stimulating résumé of the subject at its present stage. The author[1] referred to two ways in which progress is to be made: by (*a*) critical discussion of the laws and their general consequences, and (*b*) the solution of concrete problems. The question of priority between these is that around which the main contrasts of thought turned, and the writer wishes to offer herewith some detailed comment bearing upon this question.

The separation of these two points of view is only for convenience in thinking about them. Even the most refined theories cannot cut loose entirely from the background of experience, and not even the grossest empiricism can get along without ideas which have at least some shred of truth. The octahedral theory takes a middle path: it is assuredly inadequate in generality, but it is also regarded by certain men able to build excellent structures as too theoretical for any use. Both of these objections are valid, but instead of condemning this theory for both of two opposite reasons, the writer prefers to extract from it all the guidance it can give in practical design, without ignoring the limitations which the philosophers see so clearly.

Let us consider four reports referring mainly to experimental work, i.e., those of S. J. Fraenkel,[4] of Julius Miklowitz,[5] of H. E. Davis and E. R. Parker,[6] and A. Gleyzal.[7] All four relate to phenomena of flow in simple geometries, all make use of grids, and give more or less attention to questions of strain distribution, all use medium steel in the ductile mode, all took data pertinent to the validity of octahedral theory. Yet in addition to the difference in geometries, each exhibits a different attitude with respect to the purposes for which the data were taken and the conclusions to be drawn from them.

In Fraenkel's work,[4] a specific effort was made to explore the effects on strain of varying the intermediate principal stress σ_2 from equality with σ_1 to equality with σ_3. Octahedral theory is an approximation which assumes that the Mohr circles of stress and of strain are similar in form,[8] ignoring the position of the origin of co-ordinates on the stress circles, or otherwise stated, using the Mohr circles of the stress deviators. What will be called the "eccentricity" of the circles of stress is the departure of σ_2 from the mean value $(\sigma_1 + \sigma_3)/2$. To make this difference dimensionless, it is divided by the semidiameter of the outer circle $(\sigma_1 - \sigma_3)/2$ to give a coefficient of eccentricity of stress μ as defined by the author. This also may be expressed as the difference between the two minor shear intensities, $\tau_1 - \tau_3$, measured by the semidiameters of the inner circles, divided by the major shear τ_2, measured by the semidiameter of the outer circle. In dealing with these shear intensities it is better to think in terms of absolute values and ignore sign.

Now plastic flow is the response of a ductile metal to shear stress, and in a polycrystalline material with random orientations enough single crystals will have their planes of weakness near the plane of maximum shear τ_2 to cause slip in a zone including this plane, regardless of what happens in the planes of minor shear τ_1 and τ_3. These minor shear-stress intensities vary in such a way that one is at least and the other at most equal to half τ_2, and at the limit both have this same value, and the stress eccentricity μ is zero. In this case the shear strain is in fact greatest in the plane of τ_2, but since by symmetry the two minor shear strains will be equal, and their sum equals the major strain, the eccentricity of strain ν must also be zero. For similar reasons, when one of the minor circles has shrunk to zero and the other has expanded to coincide with the major circle, the index of eccentricity for stress μ, and also that for strain ν, both will reach the value unity, and thus again equal each other.

Octahedral theory assumes that this equality of eccentricity of strain with that of stress holds also for all other values of μ. If the ratio of τ_2 to γ_2 be regarded as a plastic modulus λ, varying with the stress level τ_{oct}, then at any given τ_{oct} it will also be true that $\tau_1/\gamma_1 = \tau_3/\gamma_3 = \lambda$, regardless of the value of τ_{oct}. The modulus λ is in effect the ratio of any dimension on the stress circles to the same dimension on the strain circles, and thus also the ratio of octahedral stress to strain.

It comes now to a question of the nature of the error in inferences from the octahedral theory if this assumption of equality is incorrect. Some evidence exists in this paper and in its references, to show that the index of strain eccentricity is reluctant to follow the stress eccentricity as it departs from the zero value at which the two are in any case equal. Only as τ_1 (or τ_3) approaches τ_2 in intensity does γ_1 (or γ_3) follow it in the assumed ratio. It is possible that in some geometries or patterns of load this might make a decisive difference, although no such case occurs to the writer.

Similar comment may be made on the data relating to the significance of path. The example, shown in Fig. 11 of the Fraenkel paper,[4] is not strictly one of neutral loading in the author's (Prager)[1] sense, which would require σ_z to diminish as σ_t increases, so as to maintain constant octahedral value. However, there is no reason to suppose that the result would have been notably different if this condition had been exactly satisfied.

In the Miklowitz paper on the flat tensile bar,[5] the descriptive data relating to the highly nonuniform action of the later stages of flow marks a start along a path which has already been followed much further in connection with the round bar. With notable differences, this case has some interesting similarities to that of a meridional slab cut from the round bar. A point of resemblance lies in the combination, in transverse sections, of concavity toward mid-length near mid-length, with convexity at greater distances. In no other way can the presence of greater axial strains at mid-width than at the edges in the sections near mid-length be reconciled with the greater over-all length of the sinuous line at the edge as compared with the straight line at the axis. A point of difference lies in the absence in the flat bar of the counterpart of the hoop components of stress in the round bar. A significant query may be made whether the crossed regions of high strain shown in Fig. 16 of the paper,[5] have analogs in the round bar.

[3] Structural Research Laboratory, Swarthmore College, Swarthmore, Pa.

[4] "Experimental Studies of Biaxially Stressed Mild Steel in the Plastic Range," by S. J. Fraenkel, published in the September, 1948, issue of the JOURNAL OF APPLIED MECHANICS, Trans. ASME, vol. 70, pp. 193–200.

[5] "The Influence of the Dimensional Factors on the Mode of Yielding and Fracture in Medium-Carbon Steel—I," by Julius Miklowitz, published in the September, 1948, issue of the JOURNAL OF APPLIED MECHANICS, Trans. ASME, vol. 70, pp. 274–287.

[6] "Behavior of Steel Under Biaxial Stress as Determined by Tests on Tubes," by H. E. Davis and E. R. Parker, published in the September, 1948, issue of the JOURNAL OF APPLIED MECHANICS, Trans. ASME, vol. 70, pp. 201–215.

[7] "Plastic Deformation of a Circular Diaphragm Under Pressure," by A. Gleyzal, published in the September, 1948, issue of the JOURNAL OF APPLIED MECHANICS, Trans. ASME, vol. 70, pp. 288–296.

[8] "Stress and Strain in Plastic Flow," by W. P. Roop, *The Welding Journal*, vol. 25, September, 1946, pp. 799–823.

The flat tensile bar, however, has an importance of its own.[9] The dimple which develops at the center of the cross is in effect a plastic notch, and the fact that ϵ_3 at this point has a maximum value which depends not at all on the width of the plate and only a little on thickness, Fig. 15,[5] is new evidence that the ductile behavior of a flat plate in tension has a stable character of the sort that makes this type of specimen a good indicator of how a given material will act in an assembled structure. By placing a machined notch at the point where the plastic notch would otherwise develop, we come closer to the conditions of service without losing the advantage of this stability.

Fig. 15[5] also shows that the octahedral strain at fracture in the dimple rises with decreasing thickness and (below about five thicknesses) with decreasing width. The additional data on distribution of residual strain in Figs. 17 to 21 of the same paper, if brought together in a contour chart like that in Fig. 20, but in terms of octahedral strain, would come close to giving a true picture of energy distribution. To carry through such a reduction, even on a single specimen, would be a big job, and for all 18 of them hardly practicable. However, the average of the unit energy absorption, in inch-pounds per cubic inch, taken over the whole of a region, say, two widths long, could be taken out at moderate cost; comparison with the maximum values in the dimple could then be made. The writer is of the opinion that this ratio of maximum to average unit energy may be greater in these unnotched plates than in those with notches. Might we infer from such a conclusion that to increase the gross energy absorption of an extended structure we should put holes in it?

More nearly amenable to analytical study is the question of strain ratios in the range of uniform straining, as in Fig. 10.[5] It is usual to assure that a length of not more than 10 widths is needed to obtain a uniform distribution in the mid-section of a tensile specimen. The ratio of 5 in this case, combined with generous fillets in both width and thickness, should have come near the mark. A further assumption widely accepted is that even in a long specimen a high ratio of width to thickness increases transverse constraint, reducing ϵ_2 from equality with ϵ_3 in narrow widths toward zero in great widths, the condition of plane strain in the length-thickness section. Fig. 10 shows the stages through which this transition passes. Even at the low strain level at which the effect is the greatest, and at the highest width-thickness ratio tested, namely, 10, the ratio ϵ_2/ϵ_3 has hardly more than a good start toward the zero value. On the reason for such a state of affairs the theory of plasticity seems thus far to be silent.

Easier to theorize about are the two remaining cases, of tubes and diaphragms. The tube tests are considered by Davis and Parker[6] to give general confirmation to octahedral theory. Even in the single case in which stress ratios were varied, the octahedral stress strain reasonably falls in with the curves at constant ratio. Predictions of strain ratios drawn from similarity of strain with stress circles are reasonably confirmed and this occurs also in the one case at low temperatures in which a ductile strain of 50 per cent was followed by cleavage fracture. In addition, these authors give, with almost no comment, some distribution data. In specimens 1, 2, and 3, a condition like that of plane strain in the peripheral-radial section was achieved over a fair part of the length, with hoop strain of about 25 per cent and near-zero axial strain. The inverse condition of load which would produce zero hoop strain was not used.

In the case of the diaphragm, with its polar symmetry, Dr. Gleyzal[7] offers a complete analytical solution in open form for the two components of stress not zero, for the two independent components of strain, both as functions of the radius; and also a series of deflection profiles at a series of assigned pressure values; all by direct inference from octahedral theory with appeal to experiment only for the functional relation between octahedral stress and strain. Agreement with observation lies within the limits with which the stress-strain curve is defined.

It would be difficult to trace the details of this calculation or to paraphrase the processes of thought by which the ten different relations between the ten independent quantities as listed were established. Dr. Gleyzal states, in notes to Figs. 6 to 10, that his solution is based only on the "equilibrium conditions, strain-displacement relations, and plastic stress-strain laws." It would be useful to follow more closely the process by which the form of the stress-strain curve acts in controlling the radial displacements u which, in turn, are associated with the radial distribution of thickness h.

For a simple numerical check of Fig. 5,[7] the writer has evaluated t/h_0 at the center point, where $\epsilon_r = \epsilon_\theta$, for the stress-strain curve $\tau = 48.4\ \gamma^{1/4}$, and finds the numbers reasonably confirmed. However, since ϵ_θ falls away from equality with ϵ_r at the center to zero at the rim, is not the upper half of Fig. 5 in which $\epsilon_\theta > \epsilon_r$ superfluous?

It is noted that although the strains in Fig. 5 are carried only to values of 0.05, the calculated strains in Figs. 6 and 7 of the same paper,[7] go up to 0.09 and the rupture point in Fig. 1 is at a strain of not less than 0.40 octahedral value, or 0.14 linear value. If the stress-strain exponent is $^1/_4$, differentiating Dr. Gleyzal's formulas gives a maximum of t/h_0 at $\epsilon = 0.10$, and of σ at about $\epsilon = 0.18$, where $\epsilon = \epsilon_r = \epsilon_\theta$.

So far as the writer is aware, this is the first complete solution proposed for the circular diaphragm. It is hoped that it can be reduced to somewhat more tractable form and especially that questions of stability may be studied further. In any case, however, it offers a good example of what the octahedral theory can do for us.

To balance our discussion, take now the three papers presented in quick succession by J. E. Dorn and A. J. Latter,[10] E. A. Davis,[11] and Professor Prager.[1] The intent of all three of these, again is the same, to find a middle path between the nominal formulas which have the merit of giving useful numerical predictions in special cases and a more generalized analysis whose merit lies in complying more rigorously with basic requirements. All three make use of the concepts and nomenclatures of the theory of elasticity, moving thence toward broadened ranges of application.

In the ordinary elastic case the stress-strain relation is that of simple proportion, the strains are infinitesimal, the action is reversible. Between load and deformation the correspondence is unique regardless of path of loading, a condition which is described[12] by referring to the existence of a valid "deformation theory." Whether or not it is possible to imagine exceptions axes of elastic strain are usually parallel to those of stress, and when load patterns are held constant, with changes only in intensity, ratios of principal stress deviators to each other and to principal strains remain constant, and their axes remain fixed in the body. The distributions, i.e., the variations from point to point in the body of intensity, orientation, and ratios of components, are determined uniquely by the geometric condition of "com-

[9] "Tests of Ductility in Ship Structure," by W. P. Roop, ASTM Symposium, June, 1948.

[10] "Stress-Strain Relations for Finite Elastoplastic Deformations," by J. E. Dorn and A. J. Latter, published in the September, 1948, issue of the JOURNAL OF APPLIED MECHANICS, Trans. ASME, vol. 70, pp. 234–236.

[11] "A Generalized Deformation Law," by E. A. Davis, published in the September, 1948, issue of the JOURNAL OF APPLIED MECHANICS, Trans. ASME, vol. 70, pp. 237–240.

[12] "General Stress-Strain Laws of Elasticity and Plasticity," by A. Gleyzal, JOURNAL OF APPLIED MECHANICS, Trans. ASME, vol. 69, June, 1947, p. A-167; comment by William Prager.

patibility," the dynamic condition of equilibrium, applicable throughout the interior of the body, and the restraints or "surface tractions" applied at the boundaries.

Given ingenuity and patience enough to follow through the necessary process of search and confirmation, every specific problem in elasticity is soluble, and examples of success are found in other parts of the program of the conference.

With such precedents it is natural to wish for a correspondingly complete theory of plastic behavior. It is clear that under given conditions the problem still has a unique solution, namely, that found by the metal itself, which shows no signs of doubt as to patterns of deformation. But it is equally clear that none of the three conditions used in calculations in the elastic range is now applicable. The stress-strain relation is discontinuous, the strains finite, and loading and unloading must be handled separately. How can we make assumptions of a more intricate nature that will lead to calculated results reasonably corresponding with the facts?

One such assumption is so naïve that it is not even mentioned by any of our four authors,[1,10,11] although it underlies work which has been prolific in solutions of practical value. It is that after the elastic limit has been left behind locally, for moderate further advances in load level the strain pattern persists, with only the change in stress, its local peak values are cut down to yield point intensity. Whether or not this violates conditions of equilibrium and compatibility, it does lead to approximations for observed values of load-bearing capacity which are useful in design (van den Broek, Hrennikoff, Wang), and these have led to efforts to provide for it a more rigorous basis (Osgood, Shanley). Ductility does not come in question since the method at best is still limited to small strains.

Such a direct treatment of plastic as an extension of elastic behavior is not contemplated by Professor Dorn,[10] although the word "elastoplastic" occurs in his title. He is seeking principles of more general validity and the question with him is: What concessions are to be made for what benefits? The benefits are those of a more specific recognition of the difficulties in principle, and for this we must give up the hope of early solution of specific problems on the more rigorous basis proposed.

The difficulty in principle which is chiefly discussed is that caused by strain being no longer infinitesimal, and the remedy proposed is that of proceeding by a series of increments $\frac{\partial \epsilon}{\partial t}\,dt$ as in his Equation [10].[10] In addition to integration with respect to space co-ordinates, solution of a particular problem will also require integration with respect to t. This variable might, in a simple case, be time, but more generally it represents "the extent of the deformation." However, like time, presumably, it is independent of the space co-ordinates, so that any particular value of t applies equally to all parts of a body.

To make such a procedure at all feasible, further concessions are necessary. Professor Dorn,[10] in Equation [12] accepts the idea that elastic and plastic strains can be separated and superposed. It is noted, however, that the step from superscript E to superscript P will occur at different values of t in different parts of the body. He also accepts in the plastic range the constancy of volume and the sufficiency of the second invariants, σ_{II} and ϵ_{II}. His Equation [15] makes the ratio of the strain increment to the stress deviator the same for each of the principal axes.

The writer ventures to describe this as octahedralism, coupled with the reservation that plastic strain must be taken in increments. Thus is it not a suitable compromise between pure deformationism and the flow theory?

What worries Mr. Davis[11] is something quite different, not deformationism, with which he is quite content, but the perverseness of eccentricity of strain in not always equaling that of stress. He proposes to allow for this by introducing into his otherwise purely geometrical Equation [5] the quantity f, which refers to the stress components. Quantity f is called a distribution function; not that it has anything to do with space co-ordinates, but because, as in Equation [23], it determines the partition between γ_1 and γ_3 of their sum γ_2. If $\mu = \nu$, this follows the proportion of the shear stresses, but if not, then it is no longer true that $\tau_1/\gamma_1 = \tau_2/\gamma_2 = \tau_3/\gamma_3$, and the value of γ_{oct} as in his Equation [8] is changed in consequence. Quantities f and $\mathfrak{F}$ can then be independent of each other only if the change is such as to leave $\mathfrak{F}$ unchanged by the shift of f to something different from simple equality with μ. Substitution of the values in Equation [18] in Equations [3] and [8] seems to indicate that this condition is met, since f drops out of the expression for $\mathfrak{F}$. Whether in fact this is true or not, the formulas are useful if they permit prediction of the change in principal strains caused by a given deviation of ν from μ.

Professor Prager's broad résumé[1] speaks for itself. The writer is sure he would not like to be called an octahedralist but it is also sure that Professor Prager has a clear idea of the conditions under which octahedral theory forms a valid approximation. Isotropic incompressible material monotonically loaded is all that was assumed by Mr. Davis,[11] the avowed octahedralist. Professor Prager's Equation [19] excludes strain-hardening, but this restriction is lifted in his Equation [30]. Neutral changes of load, in which the ratios of the principal stresses change without affecting the octahedral value, are related to variations in path of loading. The question as to what then really happens is still unanswered, but octahedral theory claims nothing more than that octahedral strain also remains unchanged. Parallelism of the axes of principal strain with those of stress and the equality of the ratios of the principal strains to the corresponding stress deviators are conditions which are satisfied approximately in a wide variety of practical cases.

It has often been observed that it is not easy to design experiments which will furnish conclusive data on the effect of departures from the assumptions mentioned in actual materials, ordinary geometries, and common load configurations. As a designer the writer is quite willing to wait for such errors to make themselves felt; so long as he retains a mind open enough to recognize them when they do appear, he does not feel obligated to go in search of them.

Author's Closure

The author greatly appreciates the interest which the discussers have shown in his paper. The objection which Dr. Hill raises against Ilyushin's terminology ("flow" and "deformation" theory) is doubtless a valid one. On the other hand, Dr. Hill's term "finite-strain law" might prove somewhat confusing because these theories are not necessarily concerned with finite (as opposed to infinitesimal) strains. Moreover, any finite stress-strain relation can be written in differential form. The important fact is that a differential law in the sense used by Dr. Hill, cannot be integrated to yield a finite law. It seems to the author that a really adequate terminology suggesting all these facts is missing as yet.

The Propagation of Plasticity in Uniaxial Compression[1]

D. S. Clark.[2] The authors in their paper state, "No experimental data exist on compression impact, at least in cases where the type of behavior is expected to differ fundamentally from that observed in tension." The authors are referred to an investigation on compression impact by P. E. Duwez, D. S. Clark, and H. E. Martens.[3]

In these studies of compression impact, static stress-strain curves for several materials were determined on specimens for which the l/d ratio was 2. These results are shown in Figs. 1 and 2 of this discussion. In comparing these curves with Fig. 1 of the paper, it is to be observed that there is no well-delineated inflection point, and that the slope of the stress-strain curves is

[1] By M. P. White and LeVan Griffis, published in the September, 1948, issue of the Journal of Applied Mechanics, Trans. ASME, vol. 70, pp. 256–260.

[2] Associate Professor of Mechanical Engineering, California Institute of Technology, Pasadena, Calif.

[3] "The Propagation of Plastic Strain in Compression," by P. E. Duwez, D. S. Clark, and H. E. Martens, NDRC Report No. M-302, OSRD No. 3886, 1944.

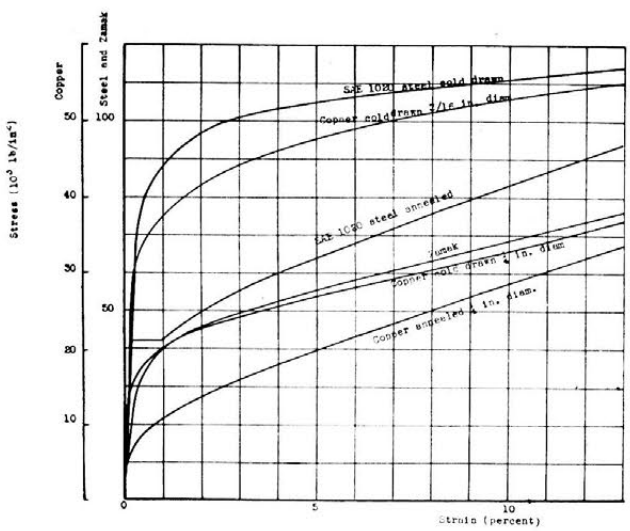

Fig. 1 Static Compression Stress-Strain Curves $l/d = 2$

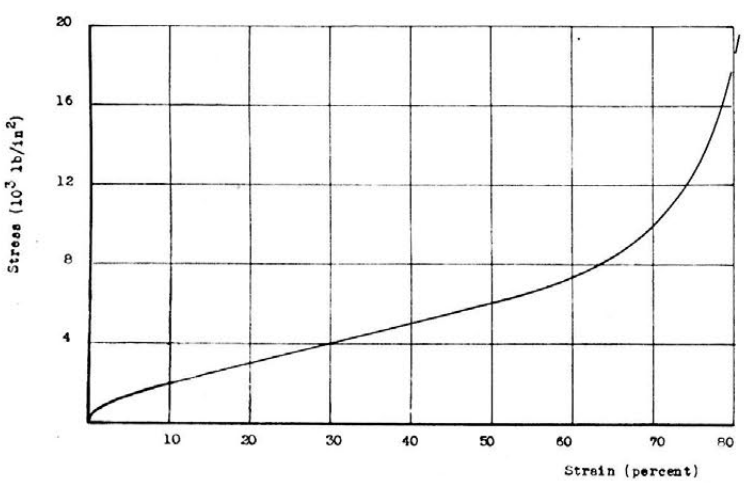

Fig. 2 Static Compression Stress-Strain Curve for Lead Specimen 3/8 In. in Diam, 3/4 In. Long

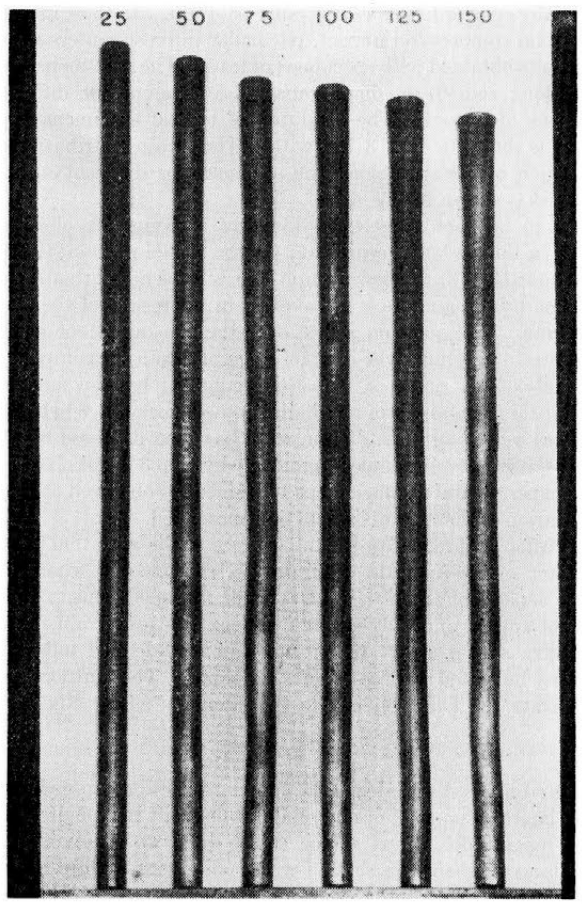

Fig. 3 Lead Specimens After Compression Impact at Velocities Indicated (Ft. per Sec). Original Length 12 In.

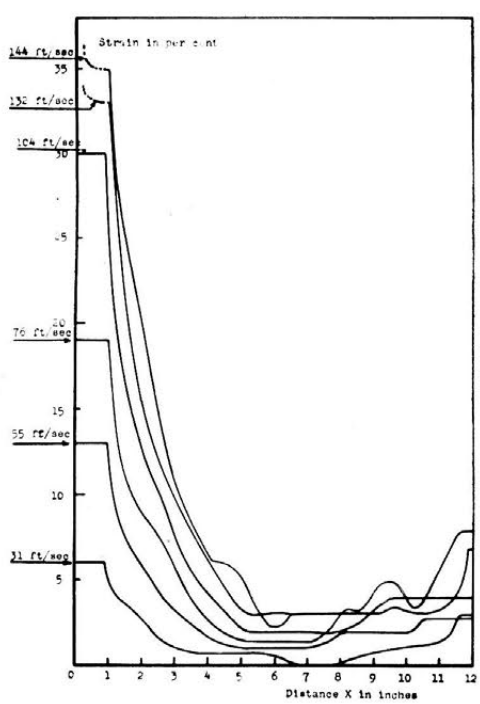

Fig. 4 Strain Distribution Curves. Compression Impact on Lead Specimens 12 In. Long, 3/8 In. in Diam

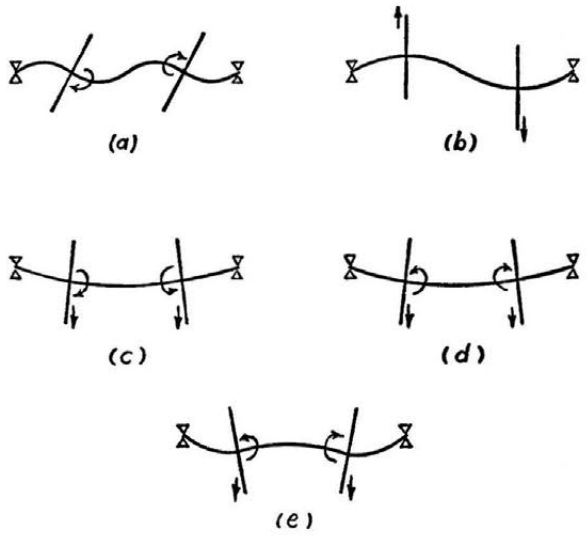

FIG. 1

(*b*) All precessions. K_3^2 equals 8, Fig. 9; lines three and eight, Fig. 11.

(*c*) Lower negative precession. K_3^2 below 1, Fig. 9; line five, Fig. 11.

(*d*) Positive precession. K_3^2 between 1 and 4, Fig. 9; line four, Fig. 11.

(*e*) Higher negative precession. K_3^2 above 4, Fig. 9; lines one and seven, Fig. 11.

The mode shapes of the other systems are not too difficult to visualize, once those of the two systems described are understood.

Investigations of the Flow in Curved Ducts at Large Reynolds Numbers[1]

W. E. TRUMPLER.[2] The paper is very instructive in conveying the exact nature of flow in curved passages. Such presentations are of great help to engineers in hydraulic machines, where flow losses generally are lumped together in a percentage and little is known of its real nature. It would be of further advantage if such an investigation could be extended to curved channels in rotating elements, such as centrifugal-pump or compressor wheels.

[1] By J. R. Weske, published in the December, 1948, issue of the JOURNAL OF APPLIED MECHANICS, Trans. ASME, vol. 70, pp. 344–348.

[2] Chief Engineer, Centrifugal Compressors, Clark Bros. Company, Inc., Olean, N. Y. Mem. ASME.

AUTHOR'S CLOSURE

Certain aspects of secondary flows in rotor wheels of turbomachines have been studied by the author and a paper, "Secondary Flows in Rotating Passages at High Reynolds Numbers" presented at the VII Congress of Applied Mechanics in London, England, in September, 1948, which will be published in the Proceedings of that Congress.

Theory of the Damped Dynamic Vibration Absorber for Inertial Disturbances[1]

C. F. GARLAND[2] AND F. M. SAUER.[3] The results of a similar analysis of the dynamical vibration absorber, together with experimental data, are included in a paper by the writers.[4] A comparison of the writers' analysis with that of the author indicates a discrepancy in the expressions for the optimum damping in the "Lancaster-type" absorber. It is believed that the author's Equation [34*b*] is incorrect and that the optimum damping for this case should be

$$h_{opt}^2 = \frac{1}{2(2 + \mu)}$$

The author's Equation [34*b*] leads to a corresponding distortion of curve 3, Fig. 6 of the paper. It is noted that curve 1 in Fig. 6, is not in agreement with Equation [34].

AUTHOR'S CLOSURE

Professor Garland and Mr. Sauer give the correct form of Equation [34*b*] and note that curves 1 and 3 of Fig. 6 are not consistent with the correct formulas [34] and [34*b*] which they are supposed to represent. I am grateful to them for correcting the record.

Also the author would like to point out that the expression $\pi c\omega\xi^*$ appearing in Equation [45] of the paper and two lines earlier should read $\pi c\omega\xi^{*2}$. This oversight does not affect later results.

[1] By J. E. Brock, published in the March, 1949, issue of the JOURNAL OF APPLIED MECHANICS, Trans. ASME, vol. 71, pp. 86–92.

[2] Associate Professor, Department of Mechanical Engineering, University of California, Berkeley, Calif. Mem. ASME.

[3] Instructor, Department of Mechanical Engineering, University of California, Berkeley, Calif. Jun. ASME.

[4] "Performance of the Viscously Damped Vibration Absorber Applied to Systems Having Frequency-Squared Excitation," by C. F. Garland and F. M. Sauer, published in this issue of the JOURNAL OF APPLIED MECHANICS, pp. 109–116.

Book Reviews

Applied Scientific Research

APPLIED SCIENTIFIC RESEARCH. Reports published under the auspices of three societies for applied science and engineering in Holland. Vol. 1A, No. 2, Mechanics, Heat. Paper, 6 1/4 × 9 1/2 in., 168 pp., figs.; Vol. 1B, No. 2, Electrophysics, Acoustics, Optics. Paper, 6 1/4 × 9 1/2 in., 148 pp., figs. Published by Martinus Nyhoff, The Hague, Holland, 1948.

REVIEWED BY J. P. DEN HARTOG[1]

THIS new publication, entirely in the English language, appears in two series: A, mechanics, heat; and B, electrophysics, acoustics, optics; so that series A is of particular interest to readers of this JOURNAL. It appears in sections of about 80 pages each, to form a volume of 480 pages, which is estimated to take about one and one-half years, and the subscription price is about $8 per volume. The printing, illustrations, and quality of paper are excellent.

We have before us the second issue, pages 81 to 168, containing 8 articles on a variety of subjects. The first article is on the flow of a viscous fluid through a porous mass with application to oil cracking, where oil or gas passes through a bed of porous catalyst. The second article deals with abrasive action of various tooth powders and pastes on teeth, reporting on an interferometer method whereby very small changes in the tooth surface can be clearly demonstrated. There are two articles on thermodynamic properties of substances under high pressure and temperatures. There is one article in soil mechanics on the resistance of a steam roller when rolling down a roadbed, and on the energy dissipated in the process. Another paper deals with the buckling of pipes standing vertically in water or in another fluid medium with application to a mine shaft and still another with the vibration of a beam on elastic foundation with damping, subjected to an arbitrary force. The last paper deals with a near vector theory of involute gearing. Judging from the range and quality of the papers in this issue the new publication deserves the serious attention of workers in the field.

Historical Appraisal of Mechanics

A HISTORICAL APPRAISAL OF MECHANICS. By Harvey F. Girvin. International Textbook Company, Scranton, Pa., 1948. Cloth, 6 1/4 × 9 1/4 in., ix and 275 pp., $3.25.

REVIEWED BY H. O. FUCHS[2]

THIS compact volume will be welcomed by all those who see in mechanics a branch of human thought and growth, rather than just a collection of recipes. Interest in history is a necessary part of our urge to seek understanding of the world; the history of mechanics will be more interesting than any other to readers of this JOURNAL, because here we are best equipped to see each development in perspective, in its relation with others, its contrast with current views, and its effect on applications.

Too many libraries have no books on the history of mechanics; Professor Girvin's book can, and should, fill this gap where it exists. It can be recommended to all students curious to see whether knowledge was developed as logically as it is deduced in the textbooks (it was not). Engineers interested in the development of their profession will also want to read this historical appraisal.

In this brief volume the author gives the dates of the most important discoveries in mechanics, sketches of the lives of outstanding men, some reflections on the philosophy of the subject, a brief history of engineering education, and a bibliography. No deductions or explanations of mechanical theorems are given; the reader is assumed to be familiar with elementary mechanics.

The text is divided into three parts: Part 1 includes, among others, sections on Aristotle, Archimedes, the Moors, and Roger Bacon. Part 2 is mainly concerned with the development of classical dynamics from Leonardo da Vinci to D'Alembert. One chapter of this part is devoted to Galileo, another to Newton. Part 3 is titled Mechanics of Materials; it takes us from Galileo and his theory of cantilever beams on to current literature such as, for instance, Van Den Broek's Theory of Limit Design. On the way we find such interesting items as the very slow development of the concept of "neutral axis" by Hooke, Mariotte, Coulomb, and Young, and the purely mathematical derivation of beam deflections by Bernoulli and of column stability by Euler—both without benefit of neutral axis or Young's modulus. Part 3 also includes a chapter on the history of engineering education with data on the earliest schools, on early textbooks, and on the organization of engineering courses.

Obviously so brief a volume on so large a subject is bound to be uneven. Professor Girvin probably is receiving scores of letters from readers who have suggestions for improvements. By publishing the volume as it is, the author has performed a valuable service. If the book has the circulation which it deserves, a second edition will become necessary, and the author will no doubt be able to refine his work with each edition.

Combustion Engines

COMBUSTION ENGINES. By Arthur P. Fraas. McGraw-Hill Book Company, New York, N. Y., 1948. Cloth, 6 × 9 in., vii and 428 pp. $5.50.

REVIEWED BY A. R. ROGOWSKI[3]

THIS book is a general college text on internal combustion engines and as such must touch upon the theoretical and practical as well as the purely descriptive aspects of a wide range of subject matter. To achieve a balance between these categories which will satisfy all readers is obviously impossible. My personal feeling is that Mr. Fraas has done particularly well in his treatment of the practical and descriptive aspects of the internal-combustion engine and its accessories, but that he leaves something to be desired in his development of basic theory, and in bringing out its direct application to the calculation of engine performance.

The book starts with a chapter on engine types and construction. This is brief but well done with many fine illustrations. In fact, the photographic reproductions throughout the book are of exceptional clarity with none of the usual loss of detail. There follows the usual chapter on the theoretical air cycle with a short discussion of other approximate cycles. Mean effective pressure

[1] Professor of Mechanical Engineering, Massachusetts Institute of Technology, Cambridge, Mass. Mem. ASME

[2] Assistant Chief Engineer, Preco, Inc., Los Angeles, Calif. Mem. ASME.

[3] Associate Professor of Aeronautical Engineering, Massachusetts Institute of Technology, Cambridge, Mass.

is introduced as a constant hypothetical pressure, but the more useful concept of mean effective pressure as the number of inch-pounds of work done per cycle per cubic inch of displacement volume, is not used. In the next chapter, the use of the air tables of Keenan and Kaye is explained, and about ten pages are devoted to the use of the thermodynamic charts of Hottel. The Hottel charts are probably the most useful tool we have for estimating the effects of engine variables on cyclic pressures, temperatures, and efficiency. The discussion of these charts seems to me totally inadequate and confusing. I would recommend going back to the original charts and discussion of Hershey, Eberhardt and Hottel. (Reference 5).

There follows a chapter on combustion which contains the excellent schlieren photographs of normal combustion and detonation taken by Mr. C. D. Miller at NACA.

Actual cycles and the effect of various engine variables are then covered in some detail. Carburetors are discussed fairly well, with the aid of one page of simple theory. Fuel injection is covered in a general way with some fine spray photographs and pictures of injection pumps and nozzles.

The chapters on Ignition, Fuels, and Lubricants are excellent and contain much up-to-date material. The chapter on lubrication would be improved by the inclusion of the simple Petroff relationships for plain bearings.

The chapter on cooling has much useful information. The cooling theory might have started with the effect of Reynolds number; leading to Equation [15] and following through to the same end results without using Campbell's semirational formula.

Supercharging is covered briefly, and there is a good chapter on performance.

Chapters on the gas turbine, overhaul, and maintenance complete the book.

There is almost no discussion of the two-stroke engine, although this type is widely used in large sizes for marine and stationary power plants. There is no mention of the application of the principles of similitude to engines, so that the effect of size and inlet Mach number are not considered.

The lists of references and the problems at the end of each chapter add greatly to the value of the book.

The author has apparently had wide practical experience and keeps up with American developments. He is usually 100 per cent right about what an engine will do, but sometimes wrong about why it does it. Some examples are the discussions of the "Ricardo" head, the effect of residual gas on volumetric efficiency, and the best economy fuel-air ratio at part load.

I would say that this is a better than average engine book whose place is somewhere between the books on maintenance and construction and the more scholarly texts such as Taylor and Taylor or Lichty.

Flight of Birds

THE FLIGHT OF BIRDS. By John H. Storer. Bulletin No. 28, Cranbrook Institute of Science, Bloomfield Hills, Mich., 1948. Cloth, 6 × 9 in., xv and 94 pp., illustrated. $2.50.

REVIEWED BY G. S. CHERNIAK[4]

IT becomes evident after reading this book, that the engineering tasks attempted with varying degrees of success by Icarus, da Vinci, and other pioneers (legendary or otherwise) in the field of aeronautics would have been furthered had they studied the problem of bird flight with the thoroughness of Mr. Storer. Man's earliest attempts to fly have been based on efforts at simulating the mechanism and equipment of birds. Until fairly recent times, aeronautical engineers have looked down upon this early approach in the belief that the modern airplane bore but a slight and exceedingly fundamental relationship to a bird. Mr. Storer's book indicates that this is far from being correct.

By dint of painstaking observation and some first-rate photographic records of birds in flight, the author has succeeded in producing a technically plausible analysis of the bird as a flying machine. The book is divided into three main sections dealing with the aerodynamics of flight, the flying equipment of birds, and an analysis of various aspects of bird flight such as control, take-off, landing, soaring, manueverability, etc. The technical reader will probably be irked by the occasionally awkward or inaccurate terminology; however, this does not appear to detract materially from the data presented, as for example in tables of speed and wing loading where the latter for various species is expressed in sq cm per gram.

The author brings out the fact that in general a bird combines the features of the fixed wing, rotary wing, and cycloidally propelled wing. Specialized types have evolved such as gliders and soarers (condor, albatross), helicopters (humming bird), speed fliers (duck hawk, eagle), formation fliers (pelican, goose), as well as birds adapted for special take-off and landing conditions (egret, ibis). It is shown that the basic wing comprises a relatively fixed inboard lifting surface and an oscillating outboard section which serves as the propeller and one of the control surfaces. The aerodynamic properties of these two elements can be controlled through a wide range by varying the thickness, angle of attack, and also by introducing such scientific sophistications as slots, flaps, tabs and automatic pitch controls. Wing contours and aspect ratios have been evolved to enable these unmotorized flying machines to take full advantage of environment, and in this connection the author presents a very interesting discussion of the difference in wing form between the albatross which is an ocean glider, and the California condor which is a land glider.

Any engineer who has on occasion given some thought to biomechanics will find this book a stimulating and informative addition to his library.

Fluid Dynamics

FLUID DYNAMICS. Victor L. Streeter. McGraw-Hill Publications in Aeronautical Science. McGraw-Hill Book Company, New York, 1948. Cloth, 6 × 9 in., illustrated, $5.

REVIEWED BY ASCHER H. SHAPIRO[5]

PARADOXICALLY, modern developments in the understanding of the mechanics of real fluids have, through widespread use of the boundary-layer concept, served to increase rather than diminish the importance of the classical theory of frictionless fluids. This new work, although it refers almost exclusively to concepts and methods which were in the main known at the turn of the century, will therefore be welcomed by many.

Lamb's great treatise, "Hydrodynamics," has long been an invaluable source book, but it is generally felt to be unsuitable for purposes of instruction. Professor Streeter's book, on the other hand, is primarily a textbook designed to promote an understanding of methods rather than to collect the fruits of these methods.

It is stated in the preface that "every effort has been made to clarify the concepts and to include those exasperating steps in derivations which are usually omitted." For this many students (and their professors) will be grateful, as they will be also for the many refreshers in mathematics preceding and accompanying each section where advanced mathematics is necessary.

[4] Chief Engineer, Lessells and Associates Inc., Boston, Mass. Jun. ASME.

[5] Associate Professor of Mechanical Engineering, Massachusetts Institute of Technology, Cambridge, Mass. Mem. ASME.

Chapters 1, 2, and 3 provide the fundamental concepts by which the motions of incompressible, frictionless fluids are studied. After introducing the ideas of the continuum, stresses at a point, and the ideal fluid, there are discussed in detail Euler's equations, the equation of continuity, the nature of boundary conditions, irrotational flow and the velocity potential, the stream function, circulation and vortices, the Laplace equation, and uniqueness theorems for ideal motion.

In chapter 4 we find the application of these fundamentals to problems of three-dimensional flow, comprising combinations of sources, sinks, doublets, and uniform flows, and leading to solutions for flow past Rankine ovoids, spheres, etc.

An introduction to the algebra of complex numbers, and a demonstration of how two-dimensional problems are greatly simplified through the special properties of analytic functions of a complex variable, are presented in chapter 5. Numerous examples are given in chapter 6. In chapter 7 are the special applications to airfoils, particularly the line of development leading to the Joukowski airfoils. The treatment of flows with free streamlines with the aid of the Schwarz-Christoffel Theorem is outlined in chapter 8, together with a detailed development of the theorem itself.

The fundamentals of vortex motion and such examples as vortex rings and rows of vortices are given in chapter 9.

The book is concluded with three brief chapters on the Navier-Stokes equations, examples of laminar flow, and the boundary layer.

There are many well-selected examples throughout the entire book. However, the practical usefulness or range of validity of these examples is seldom discussed. This reviewer is of the opinion that the potential usefulness of these examples was not fully exploited, largely because the results are not interpreted in terms of the mechanics of the boundary layer.

The concluding three chapters, on real fluids, are not well integrated into the remainder of the book, and are in fact too brief to survey the many modern developments on the boundary layer, viscous flow, and turbulence. Professor Streeter's real contribution lies in a lucid introductory exposition of the mathematical methods for dealing with the flow of an ideal, incompressible fluid.

Thermodynamics

THERMODYNAMICS. By Edward F. Obert. McGraw-Hill Book Company, New York, N. Y., 1948. Cloth, 6 × 9 in., xiv and 471 pp., illus. $5.50.

REVIEWED BY JOSEPH KAYE[6]

THIS volume is intended as a fundamental text in the fields of thermodynamics and heat power. The first quarter of the book begins with a survey of dimensions and units, then proceeds with a discussion of fundamental concepts, the First Law, the reversible process, and ends with a chapter on the Second Law. The remainder of the book deals mainly with properties of fluids, and with applications to the heat-power field. In this latter section, much space is devoted to characteristics of real and perfect gases, flow of fluids, processes using mixtures of air and water vapor, thermochemistry, power cycles, and refrigeration. A brief description of the Third Law is given in the chapter on thermochemistry.

The many sketches and drawings in the book are excellent and serve to give the reader a quick picture of the process or piece of machinery under discussion.

One of the basic objectives of a text which introduces thermodynamics to undergraduate students should be a clear and concise presentation of the simple concepts, definitions, and principles. The present text makes many attempts to achieve this objective but falls far short of this goal. A careful examination shows that whereas the introduction of some of the concepts and definitions is above standard, there are many instances where the student is given tools which he can neither understand nor use until he has studied some later chapters in the book. There appear to be many cases where the organization of the basic material has been poorly accomplished. As an illustration, we note that heat is defined excellently on pages 30 and 31, its transitional nature clarified, and yet on page 121, under the discussion of entropy, we find the following sentence: "One simple answer to these questions is found in the singular fact that heat has only one measurable property, temperature." Certainly such a statement has no place in the art of teaching thermodynamics, or even in metaphysics. Again consider the following definition of "available energy" (on page 83) which is used to introduce the concept of reversibility: "Available energy in the broadest sense of the term is the maximum amount of work that can be obtained from a quantity of energy in a specified state." No method of measuring this "available energy" is given in the discussion which follows, yet the student is asked on page 85 "to remember that reversibility is merely a test to ensure that neither work nor available energy is misused." The number of such examples is large. Since thermodynamics is a quantitative science, one cannot justify the use of such ambiguous concepts in any course on this subject.

The greater part of the book covers the properties of fluids and applications in the heat-power field. The description of these applications with the aid of many clear diagrams will help the reader considerably. Many numerical examples are included for purposes of illustration. At the end of the book is found a collection of numerical constants and of properties of common fluids. In addition, a collection of diagrams such as specific heats, compressibility factors, temperature-entropy charts, etc., is given after the index.

Advanced Dynamics

ADVANCED DYNAMICS. By S. Timoshenko and D. H. Young. McGraw-Hill Book Co., New York, N. Y., Toronto, Can., London, England, 1948. Cloth, 6 × 9¼ in., diagrams, charts, tables, 400 pp., $5.50.

REVIEWED BY MARTIN GOLAND[7]

A HIGHLY controversial topic relating to modern trends in applied mechanics is whether too many current contributions place undue emphasis on mathematical elegance, to the detriment of physical clarity. An opinion to the effect that advanced mathematical techniques should not be used whenever more elementary methods will suffice draws the accusation "reactionary" and "shortsighted" from some quarters, while a statement to the contrary is inevitably the cue for the counter-argument that unnecessary analytic sophistication serves but to obscure the physical mechanism being studied.

Professors Timoshenko and Young have long been associated with the philosophy that the most direct path between a problem and its solution is the best, and that the impressive aspects of an investigation are in the results deduced, rather than the methods employed. Continuing along these lines they have now come forth with a new text on advanced dynamics which has wide breadth, and which does not have a solitary printed "matrix" or "tensor" in evidence.

In their characteristic style which we have come to know so

[6] Assistant Professor of Mechanical Engineering, Massachusetts, Institute of Technology, Cambridge, Mass. Mem. ASME.

[7] Chairman, Engineering Mechanics Division, Midwest Research Institute, Kansas City, Mo. Mem. ASME.

well from their previous writings, the authors conduct the reader on a disarmingly smooth excursion into the various phases of dynamics. Far from constituting a classical treatment of the subject, the approaches to the theoretic developments are informal, with free use being made of problem illustrations drawn from practice to break ground for new proofs, or to point up significant high lights. For the research student this text forms an invaluable engineering link between elementary and classical dynamics; for the practicing engineer it permits a discriminating use of advanced techniques without the encumbrance of unnecessary generalization.

The scope of the text is suitably broad. Chapter one deals with the dynamics of a particle and provides the occasion to investigate various approximate numerical and graphical methods for the solution of the total differential equations of dynamics, tools which so often must be used in practice. The chapter includes a concise but adequate treatment of particle dynamics techniques in ballistics, and a similarly satisfactory discussion of one degree-of-freedom vibrating systems. The remarks dealing with nonlinear oscillating systems are refreshingly to the point. It seems to this reviewer that this first chapter should certainly be made required reading for all students of engineering dynamics.

The second chapter develops the usual theorems with regard to systems of particles and investigates the theory of engine balancing in some detail. Chapter three introduces the concept of generalized co-ordinates and then proceeds to the derivation and discussion of the Lagrangian equations, which have become an essential part of the equipment of the present-day dynamics engineer. Hamilton's principle is also dealt with briefly.

Chapter four is devoted to the theory of small vibrations and approaches the general problem in a series of gradual steps. In addition to touching on the usual facets of the subject a typical iterative procedure for extracting the normal mode frequencies from the characteristic determinant is described. While the treatment of general vibrating systems is entirely adequate for the purposes of the text, the student specifically interested in this branch of the subject will probably feel the need to consult a more extended treatise. (Professor Timoshenko already has provided a text entirely devoted to vibration theory.)

The final chapter of the book is concerned with gyroscopic theory and its applications, and an appendix provides a brief but useful account of dimensional analysis and the theory of models. Approximately 150 well-chosen problems, together with answers, are included to test the skill and understanding of the reader. The style and format of the text are uniformly excellent.

With this new book Professors Timoshenko and Young have added a powerful tool for advanced engineering education. A forthright text, such as they have written, has long been needed in the field of dynamics. In view of the extreme scarcity of competent dynamists in the profession today, the authors' efforts are both timely and significant.

Gas Tables

GAS TABLES. By Joseph H. Keenan and Joseph Kaye. John Wiley and Sons, Inc., New York, 1948. Cloth, 10 × 7 in., 237 pp., $5.

REVIEWED BY NEWMAN A. HALL[8]

AMONG current developments in the field of applied thermodynamics, one of the more dominant has been the demand for working data on the thermodynamic properties of the various media of practical importance. The developments in steam power and refrigeration required the ultimate preparation of tables of the thermodynamic properties of steam and the several refrigerants.

The much simpler thermodynamic structure of the simpler gases has enabled the engineer to get along with approximate data with reasonable success. Recent advances in thermodynamic systems, particularly those associated with flight propulsion have demanded, however, much more extensive and much more accurate information.

In the "Gas Tables," Professors Keenan and Kaye have made a further step in meeting these expanding needs of the development engineer. Briefly, this new publication represents a revision and a major expansion of the authors' earlier publication "Thermodynamic Properties of Air."

The collection of tables falls into two categories: Tables 1 through 23 pertain to the thermodynamic properties of air, basic gases, and products of combustion of hydrocarbon fuels. Tables 24 through 59 pertain to fluid-dynamic analysis, including items relative to one dimensional accelerated steady fluid, one and two-dimensional supersonic shock phenomena, and isentropic supersonic two-dimensional expansion fields.

The thermodynamic tables give enthalpy, internal energy, constant-pressure entropy, pressure and volume ratios for isentropic processes, specific heats, specific-heat ratio and sonic velocity for air, nitrogen, oxygen, water vapor, carbon dioxide, carbon monoxide, and combustion products of hydrocarbon fuels with 200 and 400 per cent of theoretical air, all at zero pressure.

The fluid-dynamic tables are largely reprinted from two sources: M.I.T. Meteor Report 14 "The Mechanics and Thermodynamics of Steady One-Dimensional Gas Flow With Tables for Numerical Solution," by A. H. Shapiro, W. R. Hawthorne, and S. M. Edelman and J.H.U. A.P.L. Bumblebee Report 26, "The Theory and Practice of Two-Dimensional Supersonic Pressure Calculations," by N. Edmonson, F. D. Mornaghon, and R. M. Snow.

The zero-pressure thermodynamic properties are based on the early calculations of Johnston, Geauque, Gordon, and Kassel as interpolated by Heck[9] and adjusted to accomodate revisions in fundamental constants in accord with practice of the Bureau of Standards.[10] The accuracy is similar to that of the earlier air tables and is wholly sufficient for engineering purposes. The tables of products of hydrocarbon-fuel combustion are presented in a form suitable for convenient interpolation to any lean mixture combustion analysis as described recently by Kaye.[11]

It is clearly stated that the thermodynamic tables apply strictly only for zero pressure and an extended discussion is given to indicate in general that only at unusually high pressures is the accuracy too poor for engineering analysis. It seems unfortunate, however, that in view of many applications where these high pressures do occur that the authors did not include more adequate quantitative data on the pressure limitations as well as suitable high-pressure correction factors.

This reference handbook will find its major use among two groups of development and research engineers. Those concerned with power plants and propulsion will use the thermodynamic data while those concerned with performance and design involving fluid dynamics will use the corresponding tables. While these two groups and their problems overlap to some extent, it is

[8] Professor of Thermodynamics, Institute of Technology, University of Minnesota, Minneapolis, Minn. Mem. ASME.

[9] "The New Specific Heats," by R. C. H. Heck, *Mechanical Engineering*, vol. 62, 1940, pp. 9–12; vol. 63, 1941, pp. 126–135.

[10] "Heats, Free Energies, and Equilibrium Constants of Some Reactions Involving O_2, H_2, H_2O, C, CO, CO_2, and CH_4," by D. D. Wagman, J. E. Kilpatrick, W. J. Taylor, K. S. Pitzer, and F. D. Rossini, J. Res. National Bureau of Standards, vol. 34, 1945, pp. 143–161.

[11] Thermodynamic Properties of Gas Mixtures Encountered in Gas-Turbine and Jet-Propulsion Processes, by Joseph Kaye, JOURNAL OF APPLIED MECHANICS, Trans. ASME, vol. 70, 1948, pp. 349–361.

possible that their needs might have been met more conveniently had the two sets of tables appeared separately.

The authors have organized and explained their tables skillfully and the reproduction is an example of clarity. There is no doubt that this publication will become an essential addition to the library of many engineers.

Scientific Foundations of Vacuum Technique

SCIENTIFIC FOUNDATIONS OF VACUUM TECHNIQUE. By Saul Dushman. John Wiley and Sons, Inc., New York, N. Y., Chapman and Hall, London, England, 1949. Cloth, 6 × 9¼ in., illus., diagrams, charts, tables, xi and 882 pp., $15.

REVIEWED BY RICHARD S. MORSE[12]

IN GENERAL books on the subject of high vacuum have to date tended to fall into two categories: those which describe the techniques of a particular laboratory or author, and those which review the work of others from a historical and bibliographical viewpoint. The title of Dr. Dushman's book is in keeping with the contents. Here in one volume we now have a very thorough treatment of the scientific foundations of high-vacuum practice. The book is written to be of maximum value to the worker concerned with research and development where vacuum phenomena are encountered with less emphasis on the engineering and economic aspects of industrial processes.

Complete data are given for computing the flow of gases and vapors as may be required by the vacuum engineer. The theory of flow and gas viscosity is treated with great clarity and thoroughness, based on fundamental concepts of kinetic theory.

An excellent review of the development of the diffusion pump also includes typical operating data for the most recent commercial units. All possible methods for the production and measurement of low pressures are described in detail with specific information concerning the most recently developed instruments as currently employed by research workers and industry. Here for the first time is given a review of modern developments in leak detection.

A substantial portion of the book is devoted to three chapters totaling 266 pages, describing the interaction of gases and vapors with solids. Here is a very exhaustive review of the theory with available data on gas and vapor adsorption and absorption under varying conditions of pressure, temperature, etc., and with a variety of materials such as glass, cellulose, charcoal, powders, and metals. Problems of gas evolution and diffusion of gases in solids under vacuum conditions are discussed in detail. In the metals field questions of gas content are again covered with particular emphasis on gas diffusion and occlusion and the influence of such problems on vacuum melting and degassing.

Problems of evaporating metals and alloys are particularly well covered from a theoretical viewpoint, although the development of such operations on an industrial scale is omitted. A brief review of problems of free-energy calculations is included together with a discussion of typical reactions of metals, including data on thermal reduction of compounds and oxidation rates.

With the exception of patent references Dr. Dushman's book contains by far the most complete and up-to-date review of all prior art in the field that has yet been published. The most valid criticism of the book is probably the extent to which the work of others has been included without the elimination of the more obsolete or less important information.

Certainly no library can afford to be without this publication, even based on its value as a reference manual alone; and it is a most welcome and long awaited addition to the desks of all research men or engineers engaged in the growing field of high vacuum.

[12] President, National Research Corp., Cambridge, Mass.

Cours De Mécanique

COURS DE MÉCANIQUE. Volume II. Dynamique des Corps Solides Rigides. By Henry Favre. Published in French by Dunod, Paris, France, and Leemann Frères, Zurich, Switzerland, 1947. Paper, 6¼ × 9½ in., 434 pp., illus. (No price)

REVIEWED BY J. P. DEN HARTOG[13]

THIS is the second volume in a series of three volumes, covering the regular (French language) course on engineering machanics at the famous bilingual Federal Polytechnic of Zurich, Switzerland. The first volume in the series, reviewed previously in this JOURNAL (March, 1948, Vol. 15, No. 1, p. 93), covered statics and elementary strength of materials, the present second volume is on dynamics, while the third and concluding volume is to treat the theory of elasticity.

The book comprises 13 chapters, of which the first four are on particle dynamics, including a fairly elaborate theory of linear vibration, free and forced, with damping and with consideration of transient conditions. The next four chapters deal with the dynamics of a single rigid body, with a rather complete exposition of the slowly rotating gyroscope. The last five chapters treat the dynamics of systems in a general way with the theorems of Lagrange and Hamilton.

After each chapter a number of exercises is listed, totaling 173 in the book, of which some are problems in the usual sense (without answers) and some ask for proofs of general theorems.

The book is well written and the subject matter treated is of considerably greater completeness than is usual in courses in our schools, although it does not go quite as far as Webster's treatise. It is clearly and beautifully printed and well illustrated and will be very valuable as a reference work.

Yankee Science in the Making

YANKEE SCIENCE IN THE MAKING. By Dirk J. Struik. Little Brown & Co., Boston, 1948. Cloth, 5¾ × 8½ in., 430 pp. $5.00

REVIEWED BY J. P. DEN HARTOG[13]

ONCE in a blue moon a book is written that equally well deserves to be reviewed in the JOURNAL OF APPLIED MECHANICS as in the *Saturday Review of Literature*, and this is it. It is a delightful history of scientific and engineering development in the United States, particularly in New England, up to the period of the Civil War. Some years ago Van Wyck Brooks published "The Flowering of New England" and "New England: Indian Summer" with the literary and artistic history. What Van Wyck Brooks did for the poets and writers, Struik did for the scientists, engineers, and manufacturers. The book is divided into three parts: "Beginnings," covering prerevolutionary days, the "Federalist Period" and the "Jacksonian Period." It contains a wealth of most interesting details. There is the story of Benjamin Thompson, the poor boy from Boston, who became a schoolteacher in the town of Rumford, N. H., which is now Concord, N. H. He married the richest widow in town and associated only with the best, which gave him the reputation of being a Tory. To show that this was correct, he left New Hampshire during the revolution and went to England. Being a good scientist he was of great service to King George, who made him a

[13] Professor of Mechanical Engineering, Massachusetts Institute of Technology, Cambridge, Mass. Mem. ASME.

knight. Later he entered the employ of the King of Bavaria and laid out improvements in the City of Munich, for which the King made him a count, and Benjamin called himself henceforth Count Rumford. He published many important scientific papers, among which is a rough calculation of the mechanical equivalent of heat, deduced from the heat produced in boring cannon for the Bavarian King. This was fifty years before Joule.

Then there is the story of Bowditch, the eminent Practical Navigator, whose name is known to every sailor and who was one of the founders of the first scientific academy in this country: the American Academy of Arts and Sciences in Boston.

A very interesting and large chapter deals with the development of turnpikes, canals, and later railroads, of water power and the water-supply system of Boston. The most prominent name mentioned here is Laommi Baldwin, the first civil engineer of great reputation in this country.

Among the many inventors is Eli Whitney, who invented the cotton gin, (while he was teaching Latin for a spell to the sons of a rich planter down South), and with it revolutionized the economy of the South. This invention gave him little money and many law suits, and he turned around and made a fortune manufacturing rifles in a plant which eventually became the Winchester Arms Company. Similar stories are told of Colt, the inventor of the revolver, Slater, who started the still existing firm making textile machinery, the various members of the Brown family, who founded the Brown and Sharpe Company and Brown University, and of many others.

Another chapter deals with the founding of the various schools of science, medicine, and engineering. Science, as such, in the beginning was mostly "natural science," geology and biology, and many interesting details are given of Audubon, Agassiz, and others. A story is told of a great comet which appeared in 1843 and aroused much public interest in astronomy, leading to a large bequest to Harvard for an observatory. The "great telescope" was installed in 1847 but had to be imported from Europe.

This book should be of intense interest to historically inclined scientists and engineers, and to all economists and historians. Logically it should have been written by a native New Englander; historian or engineer, but it was not: the author of all things is a mathematician and a Dutchman, although he has lived in Boston for twenty years. It is rumored that he has plans to write a second volume on the developments after the Civil War and the reviewer hopes that the rumor comes true and that the second volume will be as interesting as the first.

NOTICE TO AUTHORS ON PREPARATION OF MANUSCRIPTS FOR THE JOURNAL OF APPLIED MECHANICS

In order to do a more economical job in the printing of papers for the JOURNAL OF APPLIED MECHANICS the following rules have been drawn up to serve as a guide for intending authors. We invite co-operation in seeing that they are observed.

Length: Due to the present difficulty of publishing all of the papers it is found necessary to restrict the length of most manuscripts to six printed pages of the JOURNAL. Solid type runs 1200 words per page and due allowance must be made for title, footnotes, bibliography, illustrations, and mathematical work.

Manuscripts: These should be typewritten, double or triple space, on one side of standard-sized paper with ample margins. Cut captions (on a separate sheet), illustrations, and tables should accompany the manuscript.

Bibliography: Footnotes and bibliographical references should be complete and thoroughly checked. They should not be abbreviated and should be in the A.S.M.E. style: namely, title, author, name of periodical, volume and number, date, page. If this refers to a book the order should be: title, author, publisher, place of publication, date, page referred to.

Mathematical Work: Symbols should be in accordance with ASA-Z10.3 "Letter Symbols for Mechanics of Solid Bodies." May be obtained from The American Society of Mechanical Engineers, 29 W. 39th Street, New York 18, N. Y. All symbols should be clearly written and carefully checked. The difference between capital and lower-case letters should be clearly distinguished and care taken to avoid confusion between zero (0) and the letter (O), between numeral (1) and letter (l) and prime ('), between alpha (α) and a, and between kappa (κ) and k. All subscripts and exponents should be clearly marked, and dots and bars over letters should be avoided.

Illustrations: All photographs should be clear, so as to produce good half tones, and should be black and white photographic prints, not lantern slides or other copy. All drawings, graphs, and diagrams should be as simple as possible, with explanatory notes in captions rather than on the graphs. They should be in black ink on white paper or tracing cloth, the latter being preferred. The average drawing is reduced to column width ($3\frac{1}{4}$ inches), or less, and the lettering should be of a size that will be at least $\frac{1}{16}$ inch high when the drawing is reduced. All drawings should be carefully checked since it is expensive to make changes on the cuts.

A.S.M.E. Publications Committee